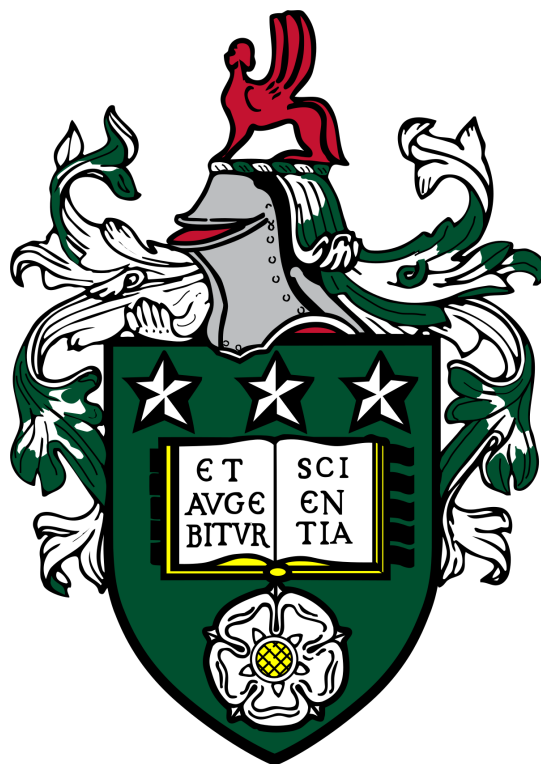


PhD Thesis

The Role of Hydrothermal Treatment in the Biorefining of Macroalgae



Gillian Finnerty

School of Chemical and Process Engineering
University of Leeds

Dr. A. B. Ross
Prof. C. Rayner

August 2020

I would like to dedicate this thesis to my late father, Graham William Finnerty.

Also, to all those who lost their lives during the ongoing Covid-19 pandemic.

Declaration

This thesis is an account of research undertaken between June 2015 and April 2020 at the School of Chemical and Process Engineering and the School of Chemistry, at The University of Leeds, UK.

I, Gillian Louise Finnerty, declare that this thesis titled, ‘The Role of Hydrothermal Treatment in the Biorefining of Macroalgae’ and the work presented in it are my own. I confirm that:

- This work was done wholly or mainly while in candidature for a research degree at this University.
- Where any part of this thesis has previously been submitted for a degree or any other qualification at this University or any other institution, this has been clearly stated.
- Where I have consulted the published work of others, this is always clearly attributed.
- Where I have quoted from the work of others, the source is always given. With the exception of such quotations, this thesis is entirely my own work.
- I have acknowledged all main sources of help.
- Where the thesis is based on work done by myself jointly with others, I have made clear exactly what was done by others and what I have contributed myself.

Signed:

Gillian. L. Finnerty

Date:

30th April 2020

Acknowledgements

I would like to thank first and foremost my late father, Graham Finnerty, for his encouragement to push through and carry on with the PhD when I was considering leaving. This was one of the last times I chatted to him before he fell into a coma, and I hope he's proud of me for listening to him and fulfilling his wishes to finish my PhD. Thanks also to my lovely mum, Glynis Finnerty, for always being supportive of me. My mum and dad helped me significantly when I suffered a broken arm halfway through my PhD as well, caring for me in every way they could. My older sister, Samantha Goodwin was extremely helpful in helping encourage me and inspiring me to finish. She helped me with typo checking, grammatical errors and editing pointers. Thank you, also, to my twin sister, Kelly, and older sister, Sam Goodwin, for keeping me motivated and helping me get through this whilst dealing with family illness. My extended family, Chris Goodwin, Kevin Crabb and Pam Haram were great throughout the last few years, by encouraging me and always being there to talk to if I needed some advice. Thank you to them for their relentless support. Thank you also to my awesome little nephew, Jack Goodwin, for providing some much needed stress relief and happiness in my time spent with him in the past two years.

Thank you to The University of Leeds for the opportunity given to me to complete a PhD and become a Doctor of Philosophy, and to the Engineering and Physical Sciences Research Council (EPSRC) for providing the funding for this research. Thanks to SINTEF in Trondheim and Judit Sandquist and Hans Fredrik for hosting me during my industrial placement and funding me for an extra month, - this was a brilliant experience. For help in the labs, ranging from helping prepare samples, setting up methods to use on the analytical machines, advice, training and help running my samples, I would like to thank the following people: Iram Razaq, Aaron Brown, Aidan Smith, James Hammerton, Jeanine Williams, David Elliott, Meryem Benhoud, Mark Howard, Adrian Cunliffe, Karine Thorne, Lauren Ford, James Wheatley, Andy Price-Allison, Simon Lloyd, Kiran Parmar, Harriet Fletcher, Haya Mahfouz, Patrick Biller, Jenny Jones, Ed Woodhouse, Surjit Singh and Bijal Gudka. Also thank you to Paul Williams who helped me resolve

some items on my Transfer Report. Faizan thank you for helping me computerise the HTC Biorefinery concept diagram. To the people who helped me overcome issues with my LaTeX code, a huge thank you; Hana Mandova, Luke Higgins, Ulrike Fischer and Flora Brocza. My work colleagues from my Bioenergy CDT 2014 cohort, and later cohorts, thanks for helping me retain a good work-life balance and being there to brighten up any late nights in the office. Richard Birley thanks for giving me some great advice when needed, and Ollie Grasham, Hana Mandova, Lee Roberts, Nicola Wood and Iram Razaq for your helpful and motivational chats and good company.

A huge thank you and massive respect for my amazing supervisors, Professor Chris Rayner and Dr Andrew Ross, who somehow put up with me and my many issues over the years with family problems, snowboarding accidents and mindset barriers. I could not have managed this PhD without them both, sincerely, thank you so much for all your help, feedback and advice. Thank you also to Victoria Masters and her colleagues from the Graduate Student Office, who helped with the admin side of things to help get my PhD over the line.

Last but not least, thank you to my amazing boyfriend, Pete Winterbottom, for always believing in me and knowing the right thing to say, and for making me realise that no matter what happens, I'll always know I have a fantastic future waiting for me with him. Thank you Pete for putting up with me, helping with chores while I've been busy writing up and giving me something to look forward to, a shoulder to cry on and providing a nice bright light at the end of this long dark tunnel. Thanks Pete also for your help with the typo checking in the final days. Thanks to everyone that's helped me, I've probably missed some people out as there's so many people in my life that have helped me during my PhD in some way or another. You know who you are and I'm eternally grateful for all your help, friendship and guidance. I'm so happy I've managed to overcome all the issues I've encountered and come out the other side with no regrets.

Abstract

Bioenergy is a key part of the renewable energy sector which has yet to reach its full potential. Macroalgae as a biomass feedstock has many benefits over the first and second generation biofuels. The organic-rich aqueous phase resulting from the hydrothermal processing of macroalgae could additionally provide a means of supplying commodity chemicals or feedstock for anaerobic digestion (AD) as a by-product from the biofuel production. The work for this PhD has focussed on the hydrothermal carbonisation of some key species of seaweed: *Saccharina latissima* (SL) and *Fucus serratus* as well as *Miscanthus giganteus*. Hydrothermal Carbonisation (HTC) was performed on the samples along with some key model compounds and co-processed mixes of the terrestrial and algal biomass/model compounds in a 80:20 ratio, respectively. HTC was performed at 150°C, 200°C or 250°C, for one hour. The hydrochars and aqueous phase products were characterised via ultimate and proximate analysis and XRF analysis along with mass balance calculations. The aqueous phase samples were also analysed via NMR, TOC, HPLC, pH, and GC-FID analysis. Anaerobic Digestion (AD) was also performed for the two 100% seaweed samples using a AMPTS(II) digester. A higher heating value of 24.2 MJ/kg was achieved for the co-processed mix at 250°C, and the effect of co-processing was promotive in increasing the hydrochar yield up 4% at this temperature. The main findings indicate that the sugars in the pure biomass feedstock tend to decompose more at higher temperatures, as expected due to the hydrolysis of the polysaccharides, and produce more shorter chain acids at higher temperatures, eventually degrading into more gases at the 250°C temperature. The abundance of VFAs increases with temperature, due to acidogenesis and degradation of the amino acids and fatty acids. The co-processed hydrochars shows significantly reduced heavy metals content compared to the 100% seaweed hydrochars, due to the lower proportion of seaweed feedstock. However, the hydrochar from the co-processed mix falls remains just short of the slagging and fouling limits. It is recommended that further research on co-processing uses a 85:15 *Miscanthus:Saccharina latissima* ratio to increase the likelihood that the hydrochar produced adheres to slagging and fouling limits. Anaerobic digestion tests of the seaweed aqueous phase feedstocks yielded successful BMP production levels, achieving 160 ml

CH₄/gCOD for the SL 250°C sample. The proposed biorefinery concept involving AD post-HTC treatment is therefore possible with the qualities of the aqueous phase suitable for anaerobic digestion, in addition to other potential further uses. The relatively new technology of Hydrothermal carbonisation, coupled with the use of seaweed as part of the feedstock mix, is hence shown to be an important consideration for further development, to help bridge the gap between our current renewable energy capacity and the UK's future renewable energy targets, to enable a more sustainable future.

Table of contents

Declaration of Authorship	iv
List of figures	xiii
List of tables	xvii
Abbreviations	xix
1 Introduction	1
1.1 Background and Justification	1
1.2 Research Gap	7
1.3 Aims and Objectives	11
1.4 Thesis Plan	13
2 Literature Review	15
2.1 Biomass Feedstock Options	15
2.1.1 First and Second Generation Biomass	15
2.1.2 Third Generation Biomass	16
2.2 Seaweed as a Potential Biomass Feedstock	18
2.2.1 International Seaweed Cultivation	18
2.2.2 The Seaweed Industry in the UK	20
2.2.3 Chemical Composition of Macroalgae and Current Uses in Industry	24
2.3 Different Techniques for Producing Energy from Seaweed	28
2.3.1 Direct Combustion	29
2.3.2 Bioethanol and Biobutanol	29
2.3.3 Pyrolysis	30
2.3.4 Gasification	31
2.3.5 Hydrothermal Liquefaction	32
2.3.6 Hydrothermal Carbonisation	34

2.3.7	Anaerobic Digestion of Macroalgae	39
3	Methodology	43
3.1	Introduction	43
3.2	Sample Collection and Preparation	44
3.2.1	Sample Size Reduction	44
3.3	Characterisation of Feedstocks	45
3.3.1	Ultimate Analysis and HHV	45
3.3.2	Proximate Analysis	46
3.3.3	XRF Analysis	47
3.4	Hydrothermal Processing	49
3.4.1	Mass Balances and Yields	50
3.5	Analysis of the HTC Hydrochar	52
3.5.1	Ultimate Analysis of the Hydrochar	52
3.5.2	Proximate Analysis of the Hydrochar	52
3.5.3	Inorganic Analysis of the Hydrochar	53
3.6	Analysis of the HTC Aqueous Phase	55
3.6.1	Ultimate Analysis of the Aqueous Phase	55
3.6.2	Proximate Analysis of Aqueous Phase	55
3.6.3	Liquid XRF of the Aqueous Phase	55
3.6.4	pH	56
3.6.5	Nuclear Magnetic Resonance	56
3.6.6	High Pressure Liquid Chromatography	58
3.6.7	Gas Chromatography Flame Ionisation Detector	58
3.6.8	Total Organic Content	59
3.6.9	Biochemical Methane Potential	61
3.7	Energy Balance Calculations	66
4	Hydrothermal Processing - Mass Balances	69
4.1	Introduction	69
4.2	Preliminary Data	71
4.3	Lignocellulosic Model Compounds	72
4.4	Seaweed Model Compounds	77
4.5	100% Biomass Feedstocks	82
4.6	Co-Processed Feedstocks	85
4.7	Conclusions	89

5	Composition of Hydrochar following Hydrothermal Carbonisation	91
5.1	Introduction	91
5.2	Lignocellulosic Model Compounds	94
5.2.1	Ultimate and Proximate Analysis	94
5.2.2	Fate of Inorganics: Pressed Pellet X-Ray Florescence	98
5.3	Seaweed Model Compounds	102
5.3.1	Ultimate and Proximate Analysis	102
5.3.2	Fate of Inorganics: Pressed Pellet X-Ray Florescence	106
5.4	100% Biomass Feedstock	108
5.4.1	Ultimate and Proximate Analysis	108
5.4.2	Fate of Inorganics: Pressed Pellet X-Ray Florescence	111
5.5	Co-Processed Feedstock	114
5.5.1	Ultimate and Proximate Analysis	114
5.5.2	Fate of Inorganics: Pressed Pellet X-Ray Florescence	118
5.5.3	Slagging and Fouling Indices	122
5.6	Conclusions	126
6	Composition of Aqueous Phase following Hydrothermal Carbonisation	129
6.1	Introduction	129
6.2	Lignocellulosic Model Compounds	132
6.2.1	Ultimate and Proximate Analysis	132
6.2.2	Total Organic Content	135
6.2.3	Nuclear Magnetic Resonance	137
6.2.4	High Pressure Liquid Chromatography	140
6.2.5	Gas Chromatography FID	142
6.2.6	Fate of Inorganics: Liquid X-Ray Florescence & pH	144
6.3	Seaweed Model Compounds	146
6.3.1	Ultimate and Proximate Analysis	146
6.3.2	Total Organic Content	149
6.3.3	Nuclear Magnetic Resonance	150
6.3.4	High Pressure Liquid Chromatography	152
6.3.5	Gas Chromatography FID	153
6.3.6	Fate of Inorganics: Liquid X-Ray Florescence & pH	155
6.4	100% Biomass Feedstock	156
6.4.1	Ultimate and Proximate Analysis	156
6.4.2	Total Organic Content	159
6.4.3	Nuclear Magnetic Resonance	160

6.4.4	High Pressure Liquid Chromatography	165
6.4.5	Gas Chromatography FID	170
6.4.6	Fate of Inorganics: Liquid X-Ray Florescence & pH	172
6.5	Co-Processed Feedstock	173
6.5.1	Ultimate and Proximate Analysis	173
6.5.2	Total Organic Content	175
6.5.3	Nuclear Magnetic Resonance	177
6.5.4	High Pressure Liquid Chromatography	180
6.5.5	Gas Chromatography FID	185
6.5.6	Fate of Inorganics: Liquid X-Ray Florescence & pH	193
6.6	Conclusions	194
7	Potential Biochemical Methane Production from Macroalgae following HTC	197
7.1	Introduction	197
7.2	Theoretical BMP Analysis	201
7.3	Experimental BMP Analysis	203
7.3.1	Saccharina latissima BMP_{ex}	203
7.3.2	Fucus serratus BMP_{ex}	206
7.3.3	Comparison of Seaweed BMP_{ex} Results	208
7.4	Biodegradability Index	210
7.5	Energy Balance Analysis	211
7.6	Conclusions	212
8	Conclusions	213
8.0.1	Further Work	216
	References	219
	Appendix A Appendix	235
A.1	Sample Size Reduction	235
A.2	XRF Raw Data	235
A.3	NMR Spectra	240
A.4	HPLC Chromatographs	245

List of figures

1.1	Carbon Dioxide levels and Temperature Anomalies in the Earth's Atmosphere	2
1.2	Britain's Electricity Generation Mix	5
1.3	HTC Biorefinery Concept	10
2.1	The Three Generations of Biomass	16
2.2	Microalgae vs Macroalgae	17
2.3	Red, Brown and Green Seaweed group variations.	20
2.4	Maps of <i>Saccharina latissima</i> on European Coastlines.	22
2.5	Seaweed Cultivation Concept	22
2.6	Diagram of Cellulose, Hemicellulose and Lignin.	24
2.7	Phase Diagram for Water	33
2.8	Three different Hydrothermal Processing Techniques	34
2.9	Primary and Secondary Hydrochar Production from Cellulose	35
2.10	HMF Unit Flow Diagram	35
2.11	Reaction Mechanisms for Hydrochar Production: A Schematic	36
2.12	HMF Chemical Structure	37
2.13	Anaerobic Digestion Diagram	40
3.1	Analytical Methods Flow Chart	43
3.2	Specac Presser	48
3.3	Parr Reactor 4540 Schematic	50
3.4	The AMPTS II system loaded with samples	64
4.1	HTC Biorefinery Concept - HTC Processing	70
4.2	Saccharina Latissima Triplicate HTC Runs	72
4.3	The Mass Balances as received of the Lignocellulosic Model Compounds	73
4.4	The HTC yields of the Lignocellulosic Model Compounds	74
4.5	The Mass Balances as received of the Seaweed Model Compounds	78
4.6	The HTC yields of the Seaweed Model Compounds	79

4.7	The Mass Balances as received of the 100% Biomass feedstocks	82
4.8	The HTC yields of the 100% Biomass Feedstocks	83
4.9	The Mass Balances as received of the Co-Processed Biomass feedstocks . .	86
4.10	The HTC yields of the Co-Processed Feedstocks	87
5.1	HTC Biorefinery Concept - Hydrochar	92
5.2	The CHNO values from the Hydrochar of the Lignocellulosic Model Com- pounds	95
5.3	VK Diagram for the Lignocellulosic Model Compounds solid phase	96
5.4	HHV values for the Lignocellulosic Model Compounds solid phase	97
5.5	Cellulose Pressed Pellet XRF Analysis	99
5.6	Protein Pressed Pellet XRF Analysis	99
5.7	Lignin Pressed Pellet XRF Analysis	100
5.8	ACL Pressed Pellet XRF Analysis	100
5.9	The CHNO values from the Hydrochar of the Seaweed Model Compounds	103
5.10	VK Diagram for the Seaweed Model Compounds solid phase	104
5.11	HHV values for the Seaweed Model Compounds solid phase	105
5.12	Sodium Alginate Pressed Pellet XRF Analysis	106
5.13	Calcium Alginate Pressed Pellet XRF Analysis	106
5.14	Alginic Acid Pressed Pellet XRF Analysis	107
5.15	The CHNO values from the Hydrochar of the 100% Biomass Feedstock .	109
5.16	VK Diagram for the 100% biomass feedstocks solid phase	110
5.17	HHV values for the 100% Biomass Feedstocks solid phase	111
5.18	<i>Saccharina latissima</i> Pressed Pellet XRF Analysis	111
5.19	<i>Fucus serratus</i> Pressed Pellet XRF Analysis	112
5.20	<i>Miscanthus</i> Pressed Pellet XRF Analysis	113
5.21	The CHNO values from the Hydrochar of the Co-Processed Feedstock . .	115
5.22	VK Diagram for the Co-processed Biomass Feedstocks solid phase	117
5.23	HHV values for the Co-processed Biomass Feedstocks solid phase	118
5.24	<i>Miscanthus:Saccharina latissima</i> Pressed Pellet XRF Analysis	119
5.25	<i>Miscanthus:Sodium Alginate (Misc:NA)</i> Pressed Pellet XRF Analysis . .	120
5.26	<i>Miscanthus:Mannitol</i> Pressed Pellet XRF Analysis	121
6.1	HTC Biorefinery Concept - Aqueous Phase	130
6.2	The CHNO values from the process waters of the Lignocellulosic Model Compounds	134
6.3	VK Diagram for the Lignocellulosic Model Compounds aqueous phase . .	135

6.4	HHV values for the Lignocellulosic Model Compounds aqueous phase . . .	136
6.5	TOC - Lignocellulosic Model Compounds Aqueous Phase	136
6.6	GC-FID results for the Lignocellulosic Model Compounds aqueous phase	143
6.7	The CHNO values from the process waters of the Seaweed Model Compounds	147
6.8	VK Diagram for the Seaweed Model Compounds aqueous phase	148
6.9	HHV values for the Seaweed Model Compounds aqueous phase	148
6.10	TOC - Seaweed Model Compounds Aqueous Phase	149
6.11	GC-FID results for the Seaweed Model Compounds aqueous phase	154
6.12	The CHNO values from the process waters of the 100% Biomass Feedstock	157
6.13	VK Diagram for the 100% biomass feedstocks aqueous phase	158
6.14	HHV values for the 100% Biomass Feedstocks aqueous phase	158
6.15	TOC - 100% Biomass Feedstock Aqueous Phase	160
6.16	NMR Spectra - <i>Saccharina latissima</i>	162
6.17	NMR Spectra - <i>Miscanthus</i>	164
6.18	<i>Saccharina latissima</i> Aqueous Phase HPLC Chromatographs	167
6.19	<i>Miscanthus</i> Aqueous Phase HPLC Chromatographs	168
6.20	GC-FID results for the 100% Biomass Feedstocks aqueous phase	171
6.21	The CHNO values from the process waters of the Co-Processed Feedstock	174
6.22	VK Diagram for the Co-processed Biomass Feedstocks aqueous phase . .	175
6.23	HHV values for the Co-processed Biomass Feedstocks aqueous phase . . .	176
6.24	TOC - Co-processed Feedstock Aqueous Phase	176
6.25	NMR Spectra - <i>Miscanthus:Saccharina latissima</i>	178
6.26	<i>Miscanthus:Saccharina latissima</i> Aqueous Phase HPLC Chromatographs	183
6.27	GC-FID results for the Co-processed Biomass Feedstocks aqueous phase .	186
7.1	HTC Biorefinery Concept - Anaerobic Digestion	198
7.2	<i>Saccharina latissima</i> - BMP Experimental Results	204
7.3	<i>Saccharina latissima</i> - BMP Experimental Flow Rate	204
7.4	<i>Fucus serratus</i> - BMP Experimental Results	206
7.5	<i>Fucus serratus</i> - BMP Experimental Flow Rate	207
7.6	Total BMP _{ex} Results for SL and FS	208
A.1	NMR Spectra - Lignocellulosic Model Compounds Aqueous Phase	241
A.2	NMR Spectra - Seaweed Model Compounds Aqueous Phase	242
A.3	NMR Spectra - 100% Biomass Feedstock Aqueous Phase (<i>Fucus serratus</i> only)	243
A.4	NMR Spectra - Co-processed Feedstock Aqueous Phase	244

A.5	Cellulose Aqueous Phase HPLC Chromatographs	246
A.6	Protein Aqueous Phase HPLC Chromatographs	247
A.7	Lignin Aqueous Phase HPLC Chromatographs	248
A.8	ACL Aqueous Phase HPLC Chromatographs	249
A.9	Sodium Alginate Aqueous Phase HPLC Chromatographs	250
A.10	Calcium Alginate Aqueous Phase HPLC Chromatographs	251
A.11	Alginic Acid Aqueous Phase HPLC Chromatographs	252
A.12	Mannitol Aqueous Phase HPLC Chromatographs	253
A.13	Fucus serratus Aqueous Phase HPLC Chromatographs	254
A.14		
	Miscanthus:Sodium Alginate Aqueous Phase HPLC Chromatographs	255
A.15		
	Miscanthus:Mannitol Aqueous Phase HPLC Chromatographs	256

List of tables

1.1	Thesis Plan	14
2.1	Chemical Structures in Brown Macroalgae	26
3.1	Slagging and Fouling Indices limits	54
3.2	GC-FID Methodology	59
4.1	Experimental and Theoretical MSL Mass Balances and yields	88
5.1	Lignocellulosic Model Compound Hydrochar Ultimate and Proximate results	94
5.2	Seaweed Model Compound Ultimate and Proximate results	102
5.3	100% Biomass Feedstock Hydrochar Ultimate and Proximate results . . .	108
5.4	Co-processed Biomass Feedstock Hydrochar Ultimate and Proximate results	115
5.5	Slagging and Fouling Indices for the 100% Biomass Feedstocks	123
5.6	Slagging and Fouling Indices for the Co-processed Feedstocks	124
6.1	Lignocellulosic Model Compound Aq. Phase Ultimate and Proximate results	133
6.2	NMR (¹ H) Integrated Values - Lignocellulosic Model Compounds	138
6.3	HPLC Sugars - Lignocellulosic Model Compounds	141
6.4	HPLC VFAs - Lignocellulosic Model Compounds	141
6.5	GC-FID data for the Lignocellulosic Model Compounds	143
6.6	pH Results - Lignocellulosic Model Compounds	145
6.7	Liquid XRF Results - Lignocellulosic Model Compounds	145
6.8	Seaweed Model Compound Aq. Phase Ultimate and Proximate results . .	146
6.9	NMR Integrated Values - Seaweed Model Compounds	151
6.10	HPLC Sugars - Seaweed Model Compounds	152
6.11	HPLC VFAd - Seaweed Model Compounds	153
6.12	GC-FID data for the Seaweed Model Compounds	154
6.13	pH Results - Seaweed Model Compounds	155
6.14	100% Biomass Feedstock Aq. Phase Ultimate and Proximate results . . .	157

6.15	NMR Integrated Values - 100% Biomass Feedstock	161
6.16	HPLC Sugars - 100% Biomass Feedstock	165
6.17	HPLC VFAs - 100% Biomass Feedstock	165
6.18	GC-FID data for the 100% Biomass Feedstocks	170
6.19	pH Results - 100% Biomass Feedstock	172
6.20	Liquid XRF Results - 100% Biomass Feedstock	172
6.21	Co-Processed Feedstocks Aq. Phase Ultimate and Proximate results . . .	173
6.22	NMR Integrated Values - Co-processed Feedstock	177
6.23	HPLC Sugars - Co-processed Feedstock	180
6.24	HPLC VFAs - Co-processed Feedstock	181
6.25	GC-FID data for the Co-processed Biomass Feedstocks	185
6.26	pH Results - Co-Processed Feedstock	193
6.27	Liquid XRF Results - Co-Processed Feedstock	193
7.1	BMP Theoretical Values	202
7.2	BMP - Biodegradability Index Values	210
7.3	Overall Energy Balance Table	211
A.1	Sample Size Reduction - Milling Techniques	236
A.2	XRF Pressed Pellet Results for all the Hydrochar Samples	237
A.3	Metal Oxide values and Slagging and Fouling Indices for all samples. . .	238
A.4	Liquid XRF Results	239

Abbreviations

AA Alginic Acid

$R\frac{b}{a}$ Acid Base Ratio

ACL, A/C/L 20% Sodium Alginate/ 40% Cellulose/ 40% Lignin Feedstock mix

AD Anaerobic Digestion

AI Alkali Index

AMPTS II BioprocessTM Automatic Methane potential Test System

BAI Bed Agglomeration Index

BECCS BioEnergy with Carbon Capture and Storage

BEIS Department for Business, Energy and Industrial Strategy

BI Biodegradability Index

BMP Biochemical Methane Potential

BMP_{ex} Experimental Biochemical Methane Potential

BMP_{th} Theoretical Biochemical Methane Potential

CA Calcium Alginate

CCS Carbon Capture and Storage

Cell, C Cellulose

CHNO Carbon, Hydrogen, Nitrogen, Oxygen contents

CHNOS Carbon, Hydrogen, Nitrogen, Oxygen, Sulphur contents

CHNS Carbon, Hydrogen, Nitrogen, Sulphur contents

COD Chemical Oxygen Demand

COP25 United Nations Climate Change Conference (Conference Of the Parties) 25

daf dry ash free

db dry basis

DEFRA Department for Environment, Food and Rural Affairs

EA The Environment Agency

EB Energy Balance

EI Energy Input

EO Energy Output

EU The European Union

EPSRC Engineering and Physical Sciences Research Council

FC (%) Fixed Carbon (%)

FI Fouling Index

FS *Fucus serratus*

GC-FID Gas Chromatography-Flame Ionisation Detection

GHG Greenhouse Gas

HHV Higher Heating Value

HPLC High Pressure Liquid Chromatography

HTC Hydrothermal Carbonisation

HTP Hydrothermal Processing

IPCC Intergovernmental Panel on Climate Change

L Lignin

M (%) Moisture (%)

Man D-Mannitol

Misc, M *Miscanthus giganteus*

MMan 80% Miscanthus 20% Mannitol Feedstock

MNA 80% Miscanthus 20% Sodium Alginate Feedstock

MSL 80% Miscanthus 20% Saccharina latissima

NA Sodium Alginate

NMR Nuclear Magnetic Resonance

NNFCC National Non-Food Crops Centre

P Protein

ppm Parts Per Million

PM2.5, PM10 Particulate Matter, 2.5 μ m, 10 μ m in diameter

PW Process Water, the Aqueous Phase after HTC

RED II Renewable Energy Directive II

SAMS The Scottish Association of Marine Science

SI Slagging Index

SINTEF The Foundation for Scientific and Industrial Research at the Norwegian Institute of Technology

SL, Sac Lat *Saccharina latissima*

SLR Solid Loading Ratio

SVI Slag Viscosity Index

TGA Thermogravimetric Analysis

TOC Total Organic Carbon

TS Total Solids

UK RES UK Renewable Energy Strategy

UN United Nations

UNFCCC United Nations Framework of Climate Change

V_{CH_{4s}} Volume of *CH*₄ from the sample (ml)

VFA Volatile Fatty Acid(s)

VK Van-Krevelen

VM (%) Volatile Matter (%)

VS Volatile Solids

%wt % weight

XRF X-Ray Fluorescence

§ Section or Chapter

Chapter 1

Introduction

1.1 Background and Justification

The climate is changing at an unprecedented rate in human history. Urgent and drastic changes must be made in order to limit the amount of carbon dioxide (CO₂) and other greenhouse gas (GHG) levels in the atmosphere to within safe limits (considered to be 1.5-2°C, IPCC 2007) [1]), in order to avoid the catastrophic effects of increased global warming including global sea level rise and the increased likelihood of more frequent and severe extreme weather events. Such extreme weather events may include severe droughts, flooding, heatwaves, more intense storms and hurricanes, and worsening wildfires, in addition to millions more species becoming extinct, a loss of biodiversity and ocean acidification [1].

We have the burden of responsibility on our shoulders, as the first country in the world to start burning coal in the 1880's for power generation [2]. With the UK's history of innovative and large scale infrastructure projects such as the building of the canals and railways, coupled with our in-depth scientific knowledge, it is not unforeseen and unthinkable that such large scale changes can be made. The political willpower, and financial incentives must create an environment in which solving the various environmental issues facing us can be done both successfully and profitably. It is essential that the UK takes a leading role in this fight against climate change.

Global CO₂ levels have risen in the last 100 years faster than any other time in history, due to human activity and the burning of fossil fuels. It is estimated by experts that levels may reach 550 parts per million (ppm) by the year 2100, resulting in a 6°C temperature rise [3]. Figure 1.1 shows the trends and relation between the levels of CO₂ in the atmosphere and global average temperatures, from 800,000 years ago until 2018 [4].

Recorded CO₂ levels as of February 2020 stands at 407.4 ± 0.1 ppm [5].

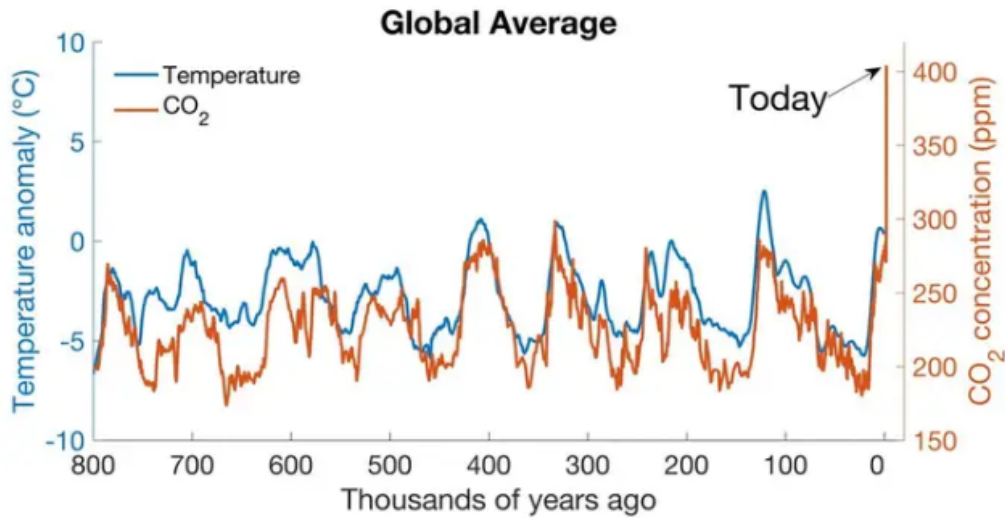


Fig. 1.1 Carbon Dioxide levels and temperature anomalies in the Earth's atmosphere over the last 800,000 years [4].

Due to the ongoing Covid-19 pandemic this monthly average carbon dioxide ppm may drop significantly over the next year, as there is a significant reduction in transport usage (especially flights), less overall electricity usage, and less manufacturing happening worldwide [6], [7]. It is hoped that yearly average carbon dioxide ppm and nitrate concentrations will continue to be reduced going forward and that the current coronavirus lock-down situation may have a catalytic affect on increasing the capacity of employees to work from home, reducing transport usage in the long term, and more food manufacturing would be within local areas, further reducing GHG emissions [8], [7]. Other more sustainable practises may be adopted by more of the world's population as a direct or indirect result of the Covid-19 outbreak, however it is too early to say exactly how this situation may play out regarding climate change. Nonetheless it is certainly proving to have a positive effect on global warming and the environment in the short term [6].

With the advent of renewable technologies and the widely held recognition that climate change is the biggest threat to humanity at present, it is hoped that steps will be made by international organisations such as the United Nations (UN) and European Union (EU) to incentivise and implement stricter policies and regulations on pollution and the use of fossil fuels in industry. Certain targets have been agreed thus far to aim for, with financial penalties for those countries that miss targets. For example, there could be

finer for those exceeding their CO₂ targets. In 2006, for the first time, the Environment Agency (EA) fined four companies in the UK £750,000 each, under the European Union's emissions trading scheme to limit their carbon emissions, for non-compliance [9].

For the UK to meet its agreed targets on reducing its greenhouse gas (GHG) emissions, wide-ranging and greater use of both established and new renewable technology with an increased focus on bioenergy must be part of the plan. The UK has agreed to reduce the GHG emissions in 2008 by at least 80% as compared to levels in 1990 (UK's Climate Change Act [10]). This aim also notes that significant progress must be achieved by 2020 [10].

More recently, the Renewable Energy Directive II - Recast to 2030 (RED II), which was revised in December 2018, sets out the EU's target of generating 32% of all its energy needs from renewable technology by 2030 [11], 5% higher than the previous target [12]. Individual nations must all adhere to this target in addition to the revised 14% target of sourcing their transport fuels from renewable sources [11]. It is as yet unclear whether the UK will adhere to these EU targets upon leaving the EU due to the result of the Brexit vote (June, 2016). Regardless, urgent and significant steps need to be made in the UK and worldwide to re-prioritise the mitigation of anthropogenic climate change, in order for sustainable development, future-proofing the planet and for both manageable and feasible adaptation of the effects caused by climate change [13].

More recently, in December 2019 the COP25 Madrid Chile conference, by the United Nations Framework on Climate Change (UNFCCC), aimed to finalise the 'rulebook' of the Paris Agreement from UNFCCC (2016). The Paris Agreement states that global warming should stay below 2°C, and be limited to 1.5°C [14]. The Intergovernmental Panel on Climate Change (IPCC) reported in 2014 that the world is on track to warm on average between 3 and 4 °C by 2100 [15], [13].

The COP25 conference was widely regarded as a missed opportunity to address the worryingly widening gap between goals and progress made, something which did not go unnoticed by the world's media. The UN's Secretary General, Antonio Guterres, said he was disappointed, and that 'the international community lost an important opportunity to show increased ambition on mitigation, adaptation and finance to tackle the climate crisis' [16] and upon opening the conference asked 'Do we really want to be remembered as the generation that buried its head in the sand?' [17]. Just before the COP25 conference, the UN Emissions Programme (UNEP) published an emissions gap

report. They concluded that the 1.5°C goal agreed in the Paris Agreement was ‘slipping out of reach’ and that GHG emissions by mid-century would amount to 38% higher than the levels required to achieve that aim [18].

It has become increasingly clear that the changes that need to be made on a large scale are more difficult to implement than first thought. It is therefore more essential than ever that scientifically proven renewable technologies become more widely established and potential newer methods of producing sustainably sourced fuels considered on a large scale. Bioenergy is a key component of the world’s potential future source of energy and is currently underutilised.

In the UK especially, Drax power station have identified the potential for bioenergy to produce significantly more of the UK’s annual electricity needs, from 100% biomass use from the Drax power station alone, after discontinuing the use of coal by March 2021 [19]. This new target to produce all their electricity from biomass by 2021 is four years earlier than the governmental target of 2025 [19]. Figure 1.2 demonstrates how the Bioenergy from Drax would provide a growing proportion of the UK’s electricity needs [20]. The vertical black line in the figure specifies the point at which the largest change occurred in the electricity generation mix, which was found to be ‘more in the 2010s than in the previous ninety years combined’ [21]. Drax has a ‘world-leading’ target to become carbon-neutral by 2030, utilising Bioenergy with Carbon Capture and Storage (BECCS) technologies, and could potentially play a big role in the UK’s current target of achieving net-zero by 2050 [22]. However, a large proportion of the biomass pellets used for energy production at Drax are imported from the US and Canada, which contributes significantly to the total carbon dioxide emissions of their process. Hence, more local biomass supplies would help to further reduce the overall carbon footprint of energy production from biomass within the UK. With Drax currently being the biggest decarbonisation project in Europe [19], the UK is in a good position to demonstrate to other countries how to reinvent traditional coal fired power stations to cater for more sustainable fuel sources, to rapidly facilitate the reduction of burning fossil fuels.

Due to existing pre-treatment methods of biomass to increase its energy efficiency, it is possible to fairly easily convert old coal-fired power stations to use hydrochar as a fuel source instead of the unsustainable, sulphur-rich coal. Hydrochar is the term used to describe the resultant solid material product from hydrothermal carbonisation of biomass. It is a black carbonaceous solid product, easily friable and contains rich oxygen-containing

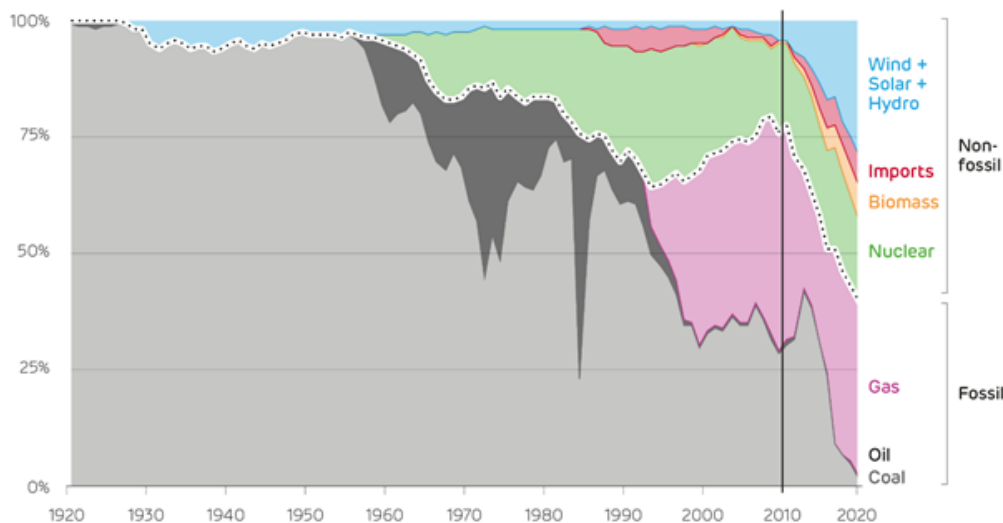


Fig. 1.2 Britain's electricity generation mix over the last 100 years[21]. Plotted using data from BEIS, Digest of UK Energy Statistics, BP [20].

functional groups and has a high heating value (HHV), giving it suitable properties for use as a fuel, once its separated from the process water from the hydrothermal carbonisation process.. Drax's conversion from coal to biomass has been proof of the ability to adapt traditional power stations for a new type of fuel. Therefore, it is feasible to consider that future adaptations in similar historically coal-based power plants can be made to sufficiently adapt their systems and processes to enable incorporation of hydrochar as a source of fuel, either mixed in with the coal powder, or as a full replacement in the long term. Coupled with Carbon Capture and Storage (CCS) technology, this electricity generation technique would result in negative carbon emissions and has the advantageous effect of reducing the carbon dioxide levels in the atmosphere [23]. Different pre-treatment processes and a variety of feedstocks eligible for production within the UK must be evaluated for future large-scale usage, at sites such as Drax. More research, development and life-cycle analysis evaluations of potential biomass feedstocks and technologies and pre-treatment methods must be performed, with increasing necessity.

The Department for Environment, Food and Rural Affairs (DEFRA) has collaborated with various agencies to establish maps to aid the identification of opportunities and optimal areas for the cultivation of Short Rotation Willow Coppice (SRC) and *Miscanthus* in the UK [24]. Of the five maps produced for England, these maps show areas where *Miscanthus* yields could be high, low or average [24]. This information solidifies *Miscanthus* as a key biomass resource able to be grown around the UK, with established

advice readily available for farmers to consult. Miscanthus has been identified as the second generation terrestrial biomass feedstock chosen for this research, due also to the numerous research conducted on this feedstock for biomass potential thus far.

In 2003 the UK government set up the National Non-Food Crops Centre (NNFCC) in York, as an ‘independent authority on plant-based renewable materials and technologies’. The NNFCC provides advice on biomass production for UK farmers, evaluates and analyses potential suitable renewable technologies, analyses suitable feedstocks and publishes the annual report on Anaerobic Digestion Deployment in the UK, [25], [26]. Information can be provided from the NNFCC for consumers and manufacturers in addition to biomass producers [25], [26]. With the UK becoming more reliant on renewable technology in order to meet its 2050 net zero targets, the NNFCC could provide an invaluable role in suggesting appropriate technologies to be implemented on a local and national scale, and the most sustainable feedstock choices to use. In addition to assessments by similar UK-based environmental consultancies, businesses and organisations and therefore the UK can be held to account with regards to reducing their carbon footprint and meeting international renewable energy targets. It is therefore in their economic interest for industry to take climate change seriously and invest strategically to actively reduce their dependence on fossil fuel, to avoid fines or other penalties.

Along with the recently established and widely successful technologies of solar, wind, tidal and hydroelectric energy, bioenergy certainly has its place in the UK market as a leading potential sustainable source of heat and electricity. The UK’s Renewable Energy Strategy (UK RES, 2009) estimates that of the 15% energy from renewables target, biomass heat and power can supply more than 30% of this (or 50% if biomass for transport is included) [27]. Energy from biomass has the particular advantage of utilising existing power stations and agricultural infrastructure, transitioning them to cultivate and process pre-treated or raw biomass feedstocks with comparatively simple and feasible adaptations to the infrastructure, as evident by the successful conversion of Drax power station. The unique advantages of hydrothermal carbonisation as a pre-treatment for biomass creates significant potential for use within the energy sector. The ability to use wet feedstocks enables to utilisation of such underused resources such as seaweed from around the UK coastline, potentially reducing our future reliance on biomass products imported from as far away as North America and Canada. In addition, use of algal based biomass from our extensive coastline and sea-beds could help fill the gap in local biomass production without the issue of driving up food prices.

The added potential for the extraction of bio-based chemicals from seaweed is also part of the appeal for using specific pre-treatment methods such as hydrothermal carbonisation, as these may provide a secondary, profitable product stream and in effect improve the sustainability of our cosmetics, food additives, soil amendments and fertilisers if used downstream within these industries [28], [29]. Anaerobic digestion of the aqueous phase is also possible before or after extraction of high value chemicals, with the benefit of producing biomethane from renewable sources [30]. Natural gas (methane, CH₄) is another widely used fuel source in the UK which requires more environmentally friendly, sustainable replacement options to be implemented to reduce the UK's GHG emissions and adhere to the RED targets.

Taking all these issues into account whilst considering the current research in biomass pre-treatment methods, it was identified that biochar (or 'hydrochar') production from biomass, with the use of a mix of second and third generation biomass, could bridge a key gap in the needs of the UK's electricity generation needs in the near future. This would be possible whilst also being profitable via the multiple product streams from the HTC process, with the added benefit of not requiring the energy intensive drying stage prior to HTC processing [30], [31]. Therefore, the wet process of hydrothermal carbonisation coupled with the *Miscanthus* and seaweed co-processed feedstock will be evaluated for its feasibility and best options in this study. It is hoped that the co-processed mix will have improved fuel efficiency and quality compared to the raw mix, have the potential for further use of the organically rich aqueous phase, coupled with the further extraction of biomethane from the aqueous phase.

1.2 Research Gap

Interest in carbon neutral biofuels has increased recently due to concern regarding the effects which burning fossil fuels have on the climate [32]. The growing population in both developed and developing nations, alongside ambitious international climate and carbon targets, demonstrates that reducing our dependence of non-renewable fuel sources as quickly as possible is imperative for maintaining our current way of life, whilst adhering to various CO₂ targets. The OECD forecast a 90% growth in energy demand by 2035 [33]. Biofuels provide a promising alternative to fossil fuels, which has the potential to dramatically decrease our carbon footprint. Unlike the food supply, there is no predicted increase in the amount of fluctuations in the seaweed demand due to

overpopulation, as it does not require arable land or a supply of freshwater to be grown, and it appears readily in the wild. In the UK especially, the abundant coastlines and access to the surrounding ocean allows for the possibility of seaweed to be a sustainable source of biomass feedstock for local fuel production.

There is potential for this overlooked, abundant, natural resource to provide a fuel source which can contribute to the transition to a renewable, sustainable energy spectrum in the years to come. This could be produced, for example, by hydrothermally processing (HTP) the wet macroalgae to produce a hydrochar, as well as an organically rich aqueous phase. Utilising the by-products from HTP of seaweed for further use or to sell to the food or cosmetic industry would maximise the economic feasibility of a bio-refinery based on the hydrothermal treatment of seaweed. Research into the use of seaweed as a biofuel has become more abundant in the last decade, although the potential uses for the different HTP by-products has not been researched in much detail at present.

The extraction processes for various chemicals from seaweed, such as alginate, are well understood and are not expected to be improved upon by the hydrothermal treatment of the algae prior to extraction. Use of seaweed as a potential source of biofuel has been studied at an increasing rate in recent years. However, integration of the potential use of the aqueous phase streams from the hydrothermal processing of the seaweed has not been studied in much detail. There is a gap in the knowledge about the different characteristics of the product streams for the hydrothermal processing of seaweeds and their potential usage, and in the understanding of the chemical pathways. The inherent catalysts within the seaweed due to its high metal content are likely to be of value in the biofuel industry, as this would be an excellent way of catalysing the lignocellulosic biomass. This would be achieved by adding not only a natural source of the catalysts, but a readily available (or quickly grown) biomass that in itself will produce biofuel. This research in particular addresses the potential for seaweed to maximise overall biofuel production and efficiency by co-processing seaweeds with lignocellulosic biomass via hydrothermal processing.

The bridge between these two topics of the hydrothermal processing of seaweeds, and its properties being used with the well established, second and third generation biomass is under-explored in current research. Incorporating the two may improve the economic attraction for industry to develop their techniques on the hydrothermal processing of biomass, resulting in their biofuel production becoming more efficient, and more econom-

ically viable.

As an overall concept for the biorefinery system proposed by this work, figure 1.3 was produced to aid visualisation and understanding of how the different processes would fit together on a large scale. The HTC on a large scale would likely be cylindrical with an Archimedes screw to allow for continual processing, rather than batch processing, which would require energy-intensive repeated heating of the reactor.

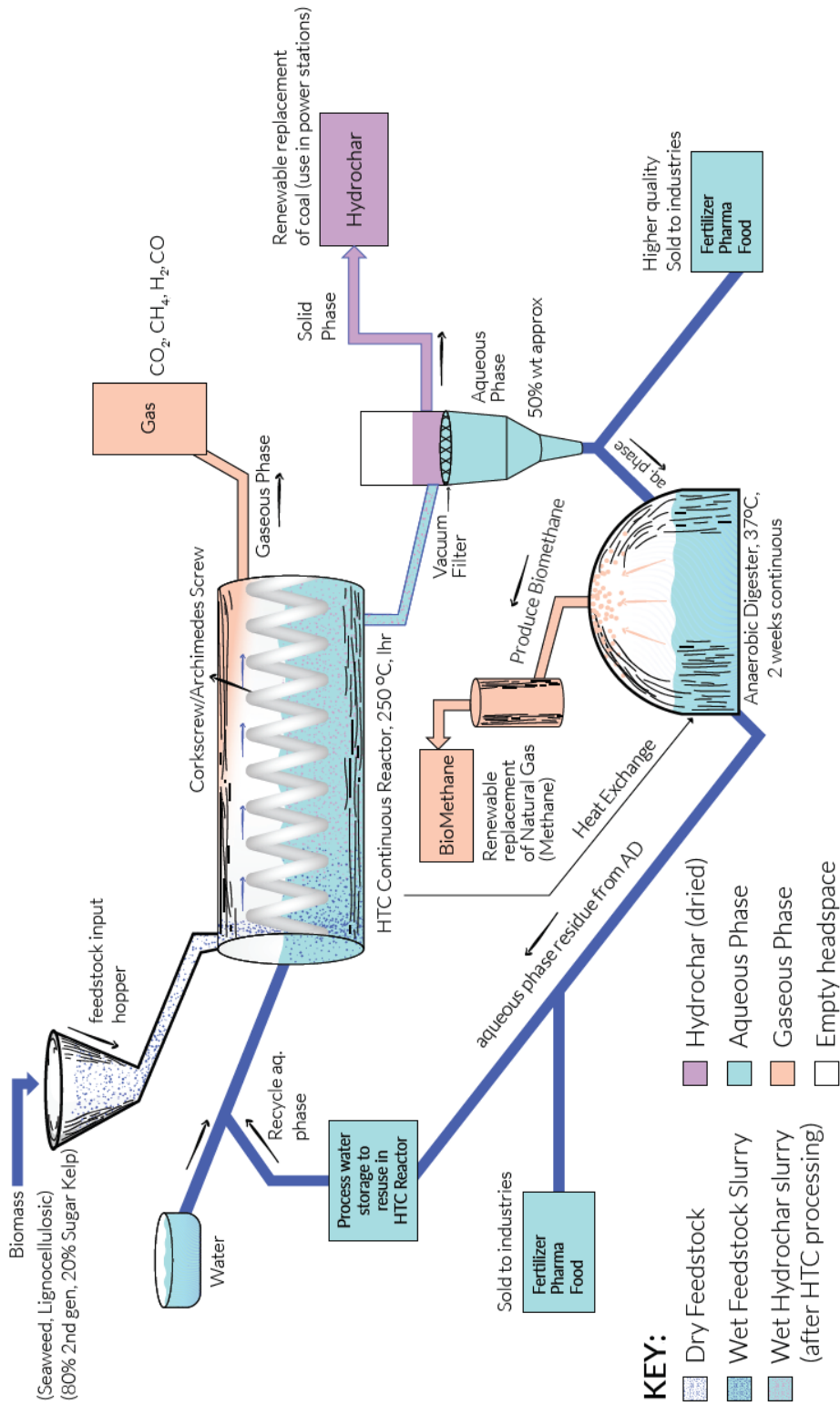


Fig. 1.3 The Biorefinery Concept of a continuous Hydrothermal Carbonisation Reactor, focussing on maximum renewable energy output from the different products with scope for profits from some by-products. For the purpose of this work and brevity of the diagram, a condenser has been omitted between the HTC reactor cylinder and the storage of the gaseous phase. In a real biorefinery a condenser would be necessary to condense any evaporated aqueous phase, which can then be dripped down into the liquid processing stream.

The proposed anaerobic digester would use bacteria with an optimum working temperature of 37°C. This could use any residual heat from the reactor, however high quality insulation would minimise heat loss. The additional potential use of heat exchange pipes within the biorefinery could also reduce heating costs to a minimum. The slurry containing about half and half aqueous phase and hydrochar is separated after HTC processing using a vacuum filter. The hydrochar can then be dried at a low heat, using residual from the reactor heat, to reduce the energy requirements. This can then be stored and used as a replacement for coal in traditional coal-fired power stations, or similar modern boilers geared for burning dry feedstocks, if the fuel quality is indeed within industry guidelines.

The aqueous phase, depending on the chemical content, could be further utilised either as sold to industries for profit, for extraction of chemicals or used as a fertiliser, for example. However, the greater potential of the process water usage lies within the ability to anaerobically digest (AD) the process water. If enough sugars remain within this aqueous phase from the initial biomass feedstocks, then AD could provide a very useful source of sustainably produced methane. The aqueous phase left after the AD process may be then sold as fertiliser, with the trace metal content remaining within the liquid, or as another useful source of chemicals that may be extracted. Therefore, the incorporation of AD could be a worthwhile step in the process between HTC processing and selling on the by-product of the aqueous phase.

Figure 1.3 shows the different processes involved in such a HTC biorefinery as is proposed for consideration at a large scale. This research will evaluate the feasibility of this concept and thus will approach each of the main processes and determine their feasibility and overall suitability as part of the proposed biorefinery process. Hence, for each of the results chapters, the relevant section of the process discussed from this schematic will be highlighted in a variation of this figure in the introduction sections of the respective chapters. This will aid in the overall understanding of the purposes of the work performed in each chapter and revisit the main aims of this research.

1.3 Aims and Objectives

The main aim of this research is to determine the suitability of Hydrothermal Processing (HTP) macroalgae for the production of biofuel and potential incorporation into the current biofuel industry, taking advantage of some of the key properties of seaweed.

The project will develop an understanding of the different chemical pathways involved in the hydrolysis and hydrothermal carbonisation of seaweed, and how it reacts when co-processed with a terrestrial biomass.

This research will focus on a temperature range of hydrothermal processing between 150°C and 250°C of different feedstocks. These include macroalgae feedstocks, several of the main lignocellulosic and seaweed model compounds, a second generation feedstock (*Miscanthus giganteus*), a co-processed mix of two biomass feedstocks, and some co-processed biomass and model compound mixes. The analysis will focus on the behaviour of some key components of macroalgae after undergoing HTC in order to determine the most suitable methodology and initial feedstock mix for the production of quality bio-char, alongside a chemically rich aqueous phase suitable for further AD processing, or further by-product options within a biorefinery scenario.

The product streams from HTP will be analysed, with particular attention paid to the aqueous phase and its different chemical components. Model compounds such as mannitol, cellulose and alginic acid will be compared to a series of macroalgae with different biochemical compositions, and HTP runs of a seaweed and lignocellulosic mix. This will hence develop an understanding of the different chemical pathways involved in the degradation of algae and its effects on the other biomass feedstocks.

The overall aim of the PhD is to understand the chemical pathways involved in the degradation of seaweed when undergoing hydrothermal processing, and its potential for co-processing with lignocellulosic biomass for hydrothermal processing, to produce a quality biofuel resource.

The specific objectives of the research are outlined in the following six objectives:

1. Selection of suitable species of macroalgae with different biochemical content, including a kelp (*Saccharina latissima*) and a wrack (*Fucus serratus*).
2. Characterisation of the raw feedstocks including but not limited to proximate and ultimate analysis and XRF analysis.
3. Processing of seaweeds by hydrothermal processing at a range of operating conditions, with three variations in HTC temperatures.

4. Detailed analysis of product streams, including process waters and hydrochars following hydrothermal processing. This will include ultimate and proximate analysis, HPLC, GC-FID, NMR, XRF, pH, TOC and BMP analysis.
5. Assessment of the potential for co-processing of seaweed with established biomass feedstocks via overall energy balance calculations. The overall aim of this objective is to understand the benefits of blending macroalgae with highly available biomass such as lignocellulosic biomass to assess the potential for promotive reactions in the degradation of cellulose, hemi-cellulose or lignin, and any reductions in the slugging and fouling propensity compared to the pure seaweed feedstocks.
6. Help understand the role of macroalgae in a future hydrothermal based biorefinery.

1.4 Thesis Plan

The thesis plan and its structure is detailed in numerical order in table 1.1 below. The individual chapters are given with their titles and their respective page count. This helps to give an indication of the relative proportion each chapter contributes to the overall thesis. In addition, details of the chapter contents are given on the far right column along with the numerical Objectives identified in §1.3 approached within each chapter, where applicable.

There are four results chapters. For chapters four, five and six, these chapters contain four subgroups of samples analysed. These are, in order; Lignocellulosic Model Compounds (LMC), Seaweed Model Compounds (SMC), 100% Biomass Feedstocks and the Co-Processed feedstocks. Each of these subgroups are analysed in order throughout these three key results chapters. The final results chapter, chapter seven, focuses on the potential for using the HTC aqueous phase of the two 100% seaweed samples to produce biomethane, using bench scale anaerobic digestion texts and theoretical calculations.

All four of the results chapters have an introduction section before the main results and discussion sections. Each results chapter are also summarised with an individual conclusion section at the end of each chapter. The final chapter before the References and the Appendix is the Conclusions chapter. In this chapter all the key findings will be addressed and contextualised, any suggestions for further work given, as well as the overall biorefinery concept shown in figure 1.3 evaluated and assessed, as per objective number six.

Table 1.1 The Thesis Plan and Structure for this research.

Chapter Number	Chapter Title	Pages	Objectives Met	Chapter Content
1	Introduction	13	-	<ul style="list-style-type: none"> - Context for Bioenergy in the UK - Research Gap - Research Justification - Aims and Objectives Specified - Thesis Plan and Structure
2	Literature Review	25	1	<ul style="list-style-type: none"> - Background on Biomass Feedstocks - Seaweed as a Biomass Source - The Current UK Seaweed Industry - Different Techniques for Energy Production from Macroalgae - Hydrothermal Carbonisation Detailed Overview - Anaerobic Digestion Detailed Overview
3	Methodology	26	-	<p>Describes the Different Methodologies:</p> <ul style="list-style-type: none"> - Sample Collection and Preparation - Hydrothermal Processing - Raw Feedstock Characterisation - Hydrochar Characterisation after HTC Processing - Aqueous Phase Characterisation after HTC Processing - Aqueous Phase Wet Analytical Techniques - BioMethane Production (Theoretical and Experimental)
4	Hydrothermal Processing - Mass Balances	21	1, 2, 3	<ul style="list-style-type: none"> - Mass Balances as-received analysis - HTC Yields (Fate of the Feedstock)
5	Composition of Hydrochar following Hydrothermal Carbonisation	36	2, 4, 5	<ul style="list-style-type: none"> - Characterisation of Hydrochars and Fuel Suitability Analysis - Fate of Inorganics in Hydrochars - Slagging and Fouling Propensity of Hydrochars
6	Composition of Aqueous Phase following Hydrothermal Carbonisation	64	4, 5	<ul style="list-style-type: none"> - Characterisation of Aqueous Phase - TOC and NMR Analysis - HPLC (Sugars and VFAs) Analysis - GC-FID (Organic Acids) Analysis - Fate of Inorganics: XRF and pH Analysis
7	Potential Biochemical Methane Production from Macroalgae following HTC	16	4, 5	<ul style="list-style-type: none"> - Theoretical BioMethane Potential Analysis - Experimental BioMethane Potential Analysis - Biodegradability Analysis - Energy Balance Calculations
8	Conclusions	4	6	<ul style="list-style-type: none"> - Summerisation of Results and Key Findings - Aims and Objectives Revisited - Macroalgae use in HTC based Biorefinery - Improve understanding of a HTC biorefinery concept - Context and Meaning of Results and Bigger Picture

Chapter 2

Literature Review

2.1 Biomass Feedstock Options

2.1.1 First and Second Generation Biomass

The first generation of biofuels consists of crops that were already familiar for farmers to grow on fertile land, consisting of crops such as wheat, straw and sugarcane. However, cultivating such crops at a large scale it may have an adverse affect on food prices if grown on fertile land, as this would reduce the overall amount of food able to be cultivated [34], as the biomass crops are grown specifically for energy generation. These crops are high in sugars and/or starch and can be converted into biofuel using well understood technologies, and have an established commercial market [35]. Fertilisers and pesticides are required to ensure a reasonable yield of the crops, in addition to plenty of water usage. These factors resulted in concerns over the true long term environmental benefits and sustainability of first generation biofuels, as well as presenting an economic barrier for this fuel source. The food vs fuel debate was addressed by the advent of second generation biofuels [35]. Figure 2.1 shows the evolution of the different types of biomass feedstocks, with some key examples for each category.

Second generation biofuels are terrestrial crops which are not typically grown on arable or fertile land, and can be grown on marginal land, thus alleviating the issue that arises for the first generation biofuels, which use up vital land space that could otherwise be used to grow food crops. These consist of woody crops, agricultural residues or waste. These plants can be grown on marginal land; land which is not suitable for cultivating food crops. These lignocellulosic based crops therefore have the advantage of not competing for land space with food crops, in addition to minimal fertiliser/pesticide

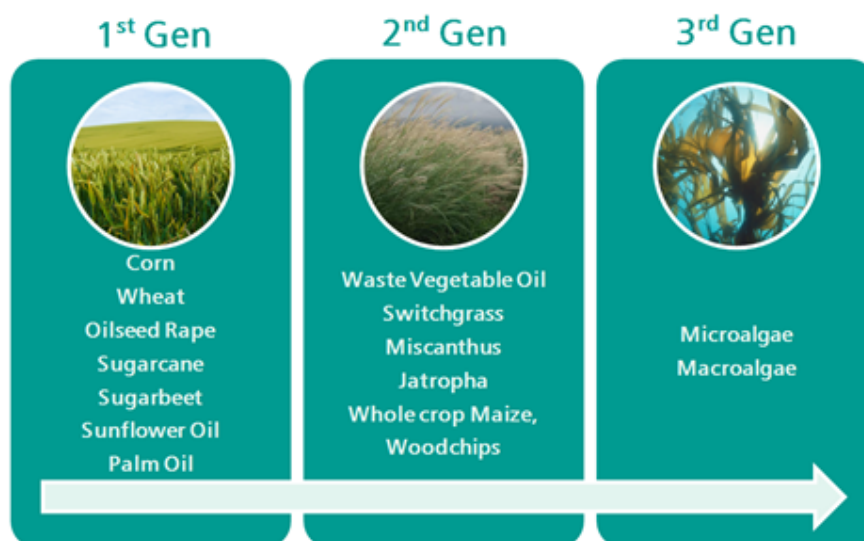


Fig. 2.1 A summary of the different feedstocks from the first generation through to the third generation of biomass. Data taken from R. Lee et al. [36].

requirements [34], [35], [37]. However, it was found that only on arable land most of these crops were able to produce high enough yields to be economically viable [38]. Waste vegetable oil has proven to be a valuable resource of renewable transport fuel [38]. The lignocellulosic biomass in the second generation biofuels required developments to be made in extraction technologies. Due to the lignocellulosic nature of most second generation biomass, several processing steps are needed prior to fermentation [38]. Ultimately, the lack of profitability of second generation biofuels when grown on non-arable land led to the development of biofuels from aquatic environments: third generation biofuels.

2.1.2 Third Generation Biomass

This group of biomass feedstock refers to plants that grow in an aquatic environment; algae. Algae can grow in a variety of aqueous habitats, both freshwater or saltwater species exist, as well as algae that grow in industrial wastewater or brackish water. These photoautotrophic organisms have a wide range of physical and chemical properties. Microalgae are unicellular and tend to grow where there are plenty of nitrogen and phosphorus, whereas seaweed, or macroalgae, can grow as long as tens of metres, and have a variety of shapes and sizes, usually taking the form of a main stem and blades. Therefore methods of cultivation between these two types are vastly different. Microalgae tend to be harvested by growing them in nutrient rich shallow man-made ponds, or in

a system of plastic bags or tubes. In contrast, macroalgae can be grown in lakes or in the ocean by sowing spores in ropes, with no nutrients or water supply required [39]. The figure 2.2 sums up the main differences and similarities between microalgae and macroalgae and compares them to each other for use as a biomass feedstock.

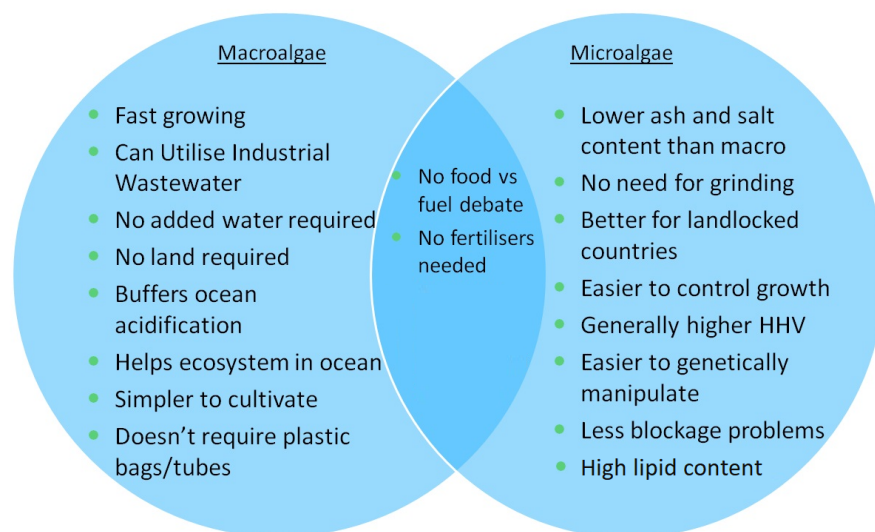


Fig. 2.2 A Venn diagram comparing the advantages of using macroalgae versus microalgae as a feedstock for bioenergy.

Compared to more traditional, first and second generation feedstock, the production and use of algae as a biomass has numerous advantages. The solar to chemical energy conversion and the CO₂ fixation potential is about 1.7kg/kg on a dry basis for microalgae, which is higher than land-based biomass [40]. More practical reasons to use such feedstocks as a biomass source include its rapid growth. Macroalgae can reach its full size after about six months [41], and can grow to over six metres long [42].

Growing kelps for cultivation purposes involves sewing 'spores' onto ropes. The life-cycle of seaweed is complex and has several stages. These involve the fertilisation of the egg with the sperm to form a *Zygote*, there follows the *Developing sporophyte* stage, which matures into a *Sporophyte*, with roots and blades. The *Sporangia* that develops on the surface of the blades will eventually create female and male gametophytes through *Meiosis*, in order to reproduce again [43]. No extra fresh water, fertiliser, pesticides or any land space is needed for it to grow. This means it is also very cheap to harvest, and it does not have to compete for food crops for any land space. The nutrients and carbon dioxide required for maximal yield of the macroalgae can be provided by growing the seaweed in an underwater plantation in close proximity to any wastewater streams into the sea, or in

a wastewater fed open reactor [44] or via using industrial wastewater and waste CO₂ [45]. These methods prevent the carbon dioxide from entering the atmosphere before it is absorbed by the seawater, which is approximately a forty year cycle, in which time it would play a part in warming the climate [46]. The nutrients from industrial waste water (such as calcium, potassium, magnesium and phosphorous [47]) help the macroalgae to grow, reducing their pollutant effects on the local marine ecosystem. The seaweed acts like a mop in the seawater; absorbing the excess nutrients in the sea [41]. Another benefit of large scale cultivation of macroalgae include its potential to buffer the ocean to minimise the effects of ocean acidification; one of the major problems caused by climate change [48].

One such seaweed species that appears very apt for large scale use within a biorefinery is *Saccharina latissima*. This species is from the *Phyllum heterokontophyta*, is of the class *Phaeophyceae*, and order: *Laminariales*. It is a *Saccharina* genus from the family of *Laminariaceae* [49]. Its fast growth, natural abundance and high sugar content make it ideal as a source of biomass. *Saccharina latissima* is a brown sugar kelp which grows up to between 2m and 4m long blades, with growth rates recorded to be 4.87cm/day in Summer [50]. This seaweed is found in large quantities off semi-exposed and unexposed coasts like Western Ireland, some coasts around England, Scotland and around Scandinavian countries, from the Barents Sea to Galicia on the coast of Spain [49]. It is the high value chemical compounds found within this seaweed that deems it particularly attractive for cultivation, for use within a variety of industries ranging from medical, food and now emerging interest in the renewable energy industry [51], [52].

2.2 Seaweed as a Potential Biomass Feedstock

2.2.1 International Seaweed Cultivation

There are over 10,000 known species of macroalgae, which are divided into three broad groups; green, red and brown. Over two hundred of these macroalgae species are harvested worldwide for a variety of purposes [53], [54]. Six different genres; *Porphyra*, *Saccharina*, *Euclima*, *Kappaphycus*, *Undaria* and *Gracilaria* make up 95% of the seaweed biomass [54]. Almost all (99.8%) of the 15.8 million tonnes of seaweed cultivated annually comes from Asian countries: China, Japan, Korea, Indonesia, and the Philippines [54]. The seaweed market is estimated to be worth £9.6bn worldwide [52].

Wild seaweed could be collected to use as a source of bioenergy. Seaweed is often

regarded as a troublesome plant, as the ‘weed’ part of its name suggests. However, to provide a sustainable and carbon neutral source of macroalgae-based biofuel, large scale cultivation of macroalgae is required. Seaweed can be grown almost anywhere, so long as there is enough sunlight, carbon dioxide and water [41], although some species can grow in deep waters with little sunlight penetration, due to different pigments in the chemical composition of the algae [55].

Large scale cultivation of seaweed has been going on for over three hundred years [56], so the methods already implemented have been proven to be feasible in the long term, however, the cost still may be high. Cultivation of seaweed in an Integrated Multitrophic Aquaculture environment would maximise the benefits of harvesting seaweed. Its ability to recapture dissolved inorganic nutrients in the seawater benefits the nearby fish and invertebrates also harvested within the same aquaculture [54].

The three different groups of macroalgae; red, green and brown, differ in composition, with further variation in compositions within these groups also. The three groupings are so called due to the type of light they most readily absorb, which is dependent on how deep (or close to the surface) they normally grow. There are considerable variations in the biochemical features including the photosynthesis pigments, storage compounds and the cell wall composition within these groups [57], and figure 2.3 shows the main differences between these three seaweed groups.

The species chosen for the experiments in this study both are of the brown macroalgae species, although show variation within the phyla. The *Saccharina latissima*, or sugar kelp, and the *Fucus serratus*, an intertidal wrack, were chosen as they both have rapid growth rates, which is important for suitability as a potential third generation energy crop, and are both found around the UK coastlines, as conditions are suitable for growth around the sheltered, rocky shores found around the UK. Both species therefore have the capacity to produce large quantities of biomass every year. The terrestrial biomass chosen for co-processing with the macroalgae biomass was *Miscanthus × giganteus*.

Miscanthus

Miscanthus × giganteus is an Asian perennial rhizomatous grass grown as an energy crop throughout Europe due to its high yield and low fertiliser demands [61]. It can therefore grow on sub-optimal land, that wouldn’t be suitable for most food crops. It also has the advantage of having a low moisture content at harvesting time [61]. *Miscanthus* can

Red Algae <i>Rhodopyhta</i>	Brown Algae <i>Phaeophyceae</i>	Green Algae <i>Chlorophyta</i>
<ul style="list-style-type: none"> •Red colour from phycoerythrin and phycocyanin pigments. •Contains chlorophyll a (no b) and beta-carotene. •Also contains several unique xanthophylls. •Main food reserves are floridean starch and floridoside (true starch not present). •Walls made from cellulose, agars and carrageenans, the latter two are long chain polysaccharides. •High in vitamins and minerals •High in antioxidants •Rich in Calcium and Magnesium •Some unicellular examples of diverse origin. •Most species of seaweed are Red (6,500 out of about 10,000). •Majority are marine, intertidal and subtidal. •Most diverse group of the seaweeds. •Found at greater depths than other seaweeds. 	<ul style="list-style-type: none"> •Brown due to dominant xanthophyll pigment fucoxanthin. •contains chlorophyll a and c (no b). •contains beta-carotene. •contains other xanthophylls. •Food reserves usually complex polysaccharides, sugars and higher alcohols. •Main carbohydrate reserve is laminarin. •Walls made from cellulose and alginic acid. •All are multicellular, and all are found in marine habitats. •Abundant in intertidal and subtidal zones in cold temperate waters. •High in Iodine •Contains Iron and Magnesium •Contains vitamins B-2, B9, B-12 •No known unicellular or colonial brown seaweeds. •Kelps are the largest, most structurally complex, only algae known to have internal tissue differentiation. 	<ul style="list-style-type: none"> •Green due to dominant chlorophyll a and b and beta-carotene pigments. •Food reserves are starch, with some fats or oils. •Have membrane-bound chloroplasts and nuclei. •May be unicellular, multicellular, colonial or coenocytic. •Most are aquatic, can be in freshwater or marine habitats. •Like high levels of sunlight, usually found in shallow waters. •Some are terrestrial, some are symbiotic with lichens or animals. •Two phyla of green algae; Chlorophyta and Charophyta. •Diverse in morphology and habitat.

Fig. 2.3 Differences within the Red [58], Brown [59] and Green [60] seaweed groups.

provide a storable, portable energy source, and at present is mainly used in Europe as a combustion material for electricity generation, but is also suitable for biochemical conversion technologies due to its fast growth rate, high yield and low-nutrient requirements.

This C4 sterile energy crop changes in composition throughout the year. Variations in certain biomass composition traits have been shown to be influenced by factors such as geographical area, climate conditions, crop management practices and harvesting time [62]. As the *Miscanthus* becomes senesced, it dries out, losing the green colour in its leaves, and the moisture content is reduced. Harvesting miscanthus during different senescence times can cause variations in N, P, K, moisture, ash, Cl and Si contents [63]. It is normally harvested in late Winter or early Spring, so *Miscanthus* samples harvested during this period (April) was used for this research to allow for suitable comparisons [61] [64].

2.2.2 The Seaweed Industry in the UK

As the UK is an island nation, to make use of the vast seawaters surrounding this country for energy utilisation would be a sensible step to take. With over 30,000 km of coastline [65], and much of it sheltered, there is a wide variety of macroalgae species

living in the UK waters in the wild. In terms of the mass of seaweed potentially available around the UK; from Scotland's shores alone, it has been estimated that 10 million tonnes of seaweed are present [65]. If seaweed were to be cultivated on a larger scale, the correct species, location and method must be considered. Seaweed usually grows rapidly and is known to have some seasonal variation, so harvesting time may be determined based on the preferred percentage contents of some key organic compounds and some inorganics for the seaweed's end usage. Due to its fast growth, the estimated yield per year of this feedstock is likely to be higher than the terrestrial feedstocks [65].

R.M.Araujo et al. [66] mapped the existence of four types of macroalgae in 2015-2016 (via an expert consultation with local experts) on the coastlines of Europe, and how their presence have changed over time. The four species studied were: *Alaria esculenta*, *Saccharina latissima*, *Laminaria digitata* and *Laminaria hyperborea*. The results of this study for the *Saccharina* species are shown in figure 2.4 [66]. The colour coding along the UK coastline shown in this figure indicates a large presence around the UK coast, in addition to presence around the Scandinavian, French and Spanish coastlines. Therefore this species is a suitable feedstock to be considered for potential large scale utilisation in UK or European based Biorefineries.

However, in order to scale up the usage of seaweed, seaweed must be cultivated, so it is not just wild seaweed that is harvested, which if done incorrectly or too much may lead to the extinction of species in the area. Therefore, research at organisations such as SINTEF (Norwegian Seaweed Technology Center) in Norway and SAMS (Scottish Association of Marine Science) in Oban, Scotland are cultivating macroalgae species such as *Saccharina latissima* and *Laminaria digitata* to determine best methods [67], [68]. At SINTEF, their Trondheim lab are using spores on ropes attached to buoys located around local fish farms in the sheltered fjords off the coast of Norway [67] [69]. This is so the seaweed can uptake any excess nutrients from the fish feed and the fish droppings, in order to accelerate growth and improve nutrient contents [67]. Figure 2.5 shows the rope and buoy set-up of cultivating seaweed, which is common practise and used by SINTEF [69], [70].

It has been shown that seaweed growth adjacent to fish farm cages of the species *Saccharina latissima* and *Palmaria pamata* can reduce the pollution caused by fish farming, with an improved rate of production, and an enhanced rate of up to 61% and 48% during Summer, respectively [71]. SAMS have recently began trials on using fabric

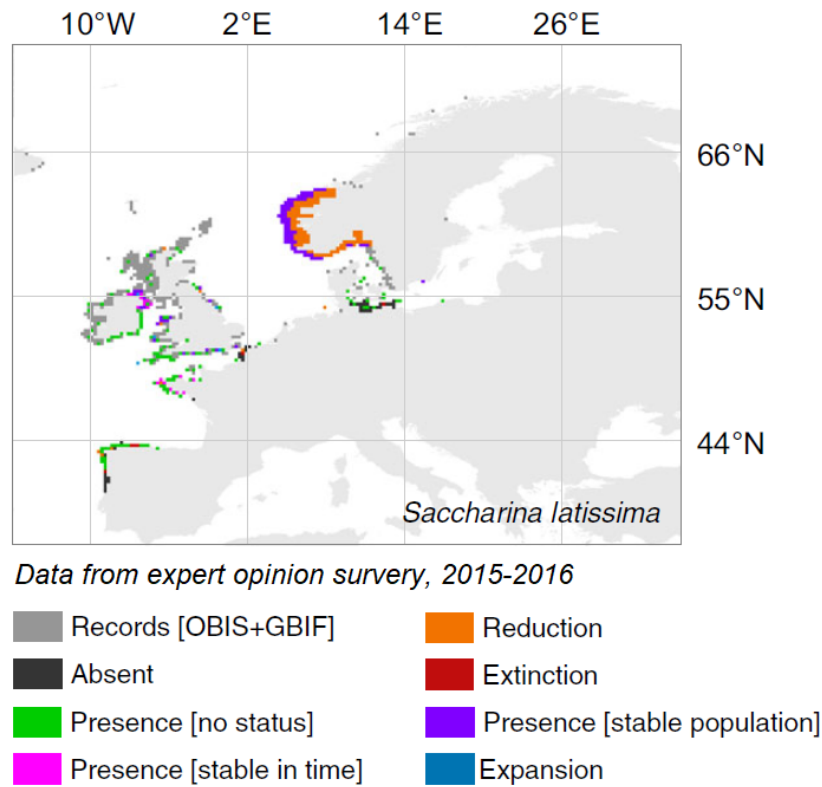


Fig. 2.4 A map showing the locations of *Saccharina latissima* at the European coastlines. Adapted from R. M. Araujo et al [66].

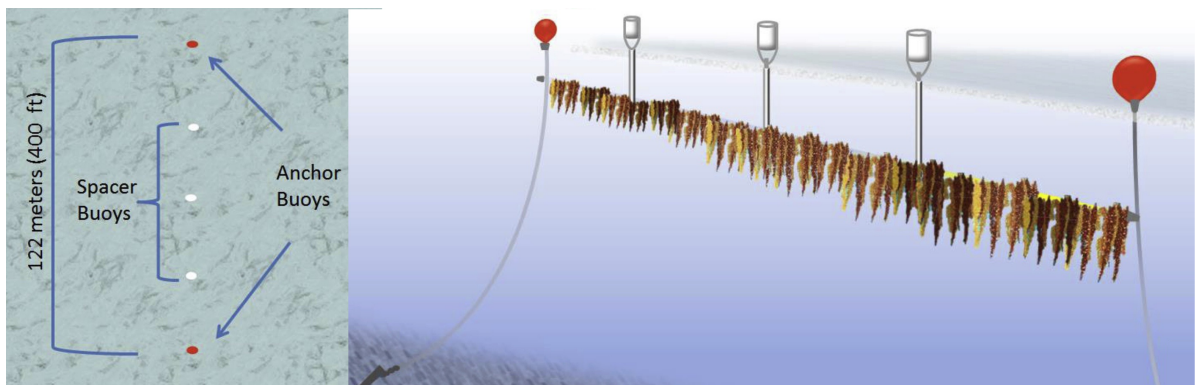


Fig. 2.5 Seaweed cultivation method used extensively by industry [70].

sheets and even carpet as a medium to grow seaweed from spores, in order to produce a higher yield [72].

More interest is developing in the seaweed industry in the UK and Europe in recent years. Dr. Adam Hughes from SAMS notes that “The interest in the Scottish seaweed industry has grown massively and this means we need to consider the various implications and the stakeholders involved, alongside the potential for expansion and sustainability [51].” In order for seaweed farming to really take off in the UK, the main barrier to overcome is keeping the costs low [72]. The versatile nature of seaweed and its many potential uses in the cosmetics, plastics, animal feed and food additive industries mean that perhaps post extraction of the high-value chemicals, the residual biomass made be used as biofuel [72]. This would improve commercial viability of seaweed farming in the UK, and allow the market to compete with cheaper imports.

To this end, it has been recently announced that a new seaweed farm, ‘SeaGrown’ based off the coast of Scarborough has been backed by the local authority and plans to open for business in 2021 [52], [73]. They have a 25 hectare site licensed, and if successful, would be the first UK company to produce bioplastics, biotextiles and pharmaceuticals from cultivated seaweeds [52]. They have adopted the buoys and chains method, with the macroalgae growing on the submerged lines, three miles into the North Sea [52], [73]. After harvesting, the macroalgae would be taken to Scarborough harbour and onwards to a proposed new facility in Eastfield Business Park, if approved [52].

Although initial plans don’t mention the use of seaweed as a biofuel, the economic and practical proof of concept of seaweed cultivation on an English coastline may make this idea a more feasible prospect for future investors and business start-ups. Perhaps, if successful, SeaGrown could partner with Drax power station in the future (which lies 57 miles to the South-West), to further utilise any residual seaweed biomass for bioenergy production via co-processing with their woody biomass pellets, thereby reducing any waste from the end of the SeaGrown production line.

Overall, the UK has a wide range of macroalgae species growing in abundance on its coastline and has the potential to cultivate these to increase capacity. However, the overall energy needs of the UK population is at a large and ever-increasing scale. Although seaweed on its own may not meet the needs of renewable energy generation, it can play a part in the renewable energy industry. Cultivation and wild harvesting of seaweed are not feasible at such a scale that power plants may be reliably ran on this feedstock type alone, but the increased utilisation of seaweed as a biomass source will increase local feedstock capacity and reduce the need for imports. The nature of the algae feedstock would also enable renewable energy production facilities to reduce their reliance on crop-based

biomass feedstock and hence reduce the key issue over the use of fertile land for growing biomass for fuel instead of food, which is a growing concern of the UK government and industry [74]. Therefore, co-processing of the seaweeds with lignocellulosic biomass forms an integral part of this research.

2.2.3 Chemical Composition of Macroalgae and Current Uses in Industry

Algae are at the base of the aquatic food chain, using photosynthesis to convert sunlight into sugars. This process is done in the chloroplasts, and produces oxygen as a by-product. In this way, seaweed recycles carbon dioxide and oxygen within their ecosystems. Seaweed also absorbs nitrogen and accumulates high quantities of metals, removing these pollutants from the seawater [75]. On average, the photosynthetic efficiency of algal biomass is 6-8%, over three times higher than that of terrestrial biomass (1.8-2.2%) [76]. This is one of the reasons why algal-based biofuels appear to be very promising; yields of between 7 and 31 times the oil yield of terrestrial biomass have been found [41].

Terrestrial plants retain their physical structure due to their high content of cellulose, hemicellulose and lignin. These are shown in figure 2.6, with the different localities of cellulose, hemicellulose and lignin labelled.

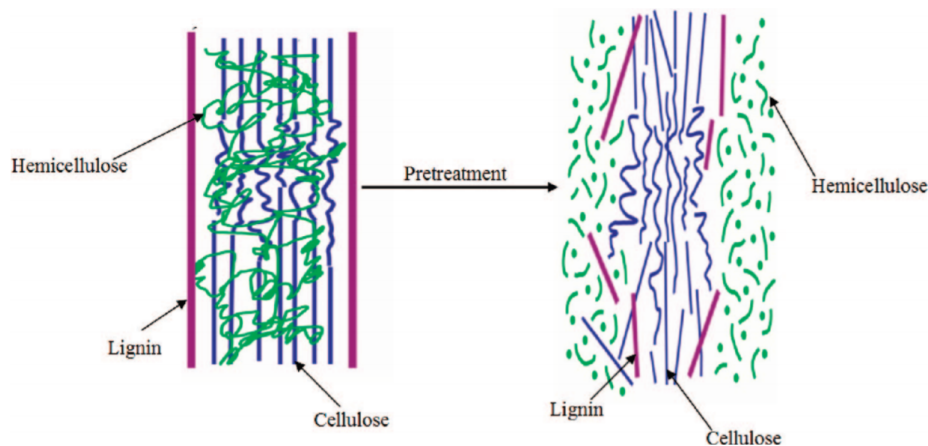


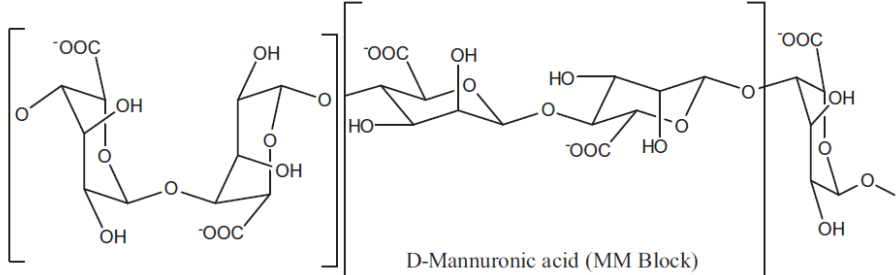
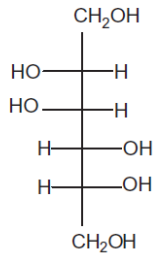
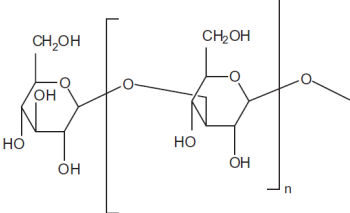
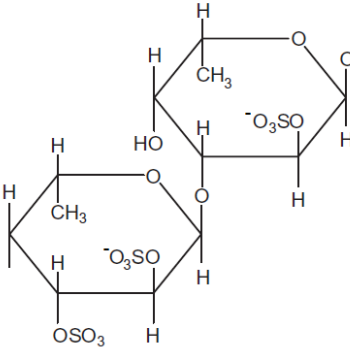
Fig. 2.6 Diagram showing cellulose, hemicellulose and lignin inside a plant structure and demonstrating how the cell walls break up during the initial HTC heating stages [77], [78].

Their distinct uses within the plant can be explained with visual aid from this diagram. Lignin helps keep the plant upright, with its fibrous and strong properties, therefore the plant would not suffer too much in windy conditions. Cellulose is a large polymeric structure comprised from the glucose monomers, which is difficult to break down to release energy. The phloem inside the plant's stem provide sugars to the plant, which can then hydrolyse the sugars to produce energy where it's required. This energy is then used for plant growth or stored in the starch and hemicellulose within the plant [79]. These three compounds can become easier to extract due to the HTC process, as the cell walls break down during the initial heating stages.

Seaweed is able to grow rapidly due to the surface of the entire plant being able to uptake nutrients in the growing medium, and the reduction in the energy-intensive lignin content (which acts as a supporting tissue) compared to terrestrial biomass [65]. Macroalgae keep their structure due to the presence of insoluble polysaccharides. This is dependant on various factors such as time of year collected or depth grown in the water, for example. On average, for a dry basis, brown macroalgae has the following proportions [80], [81];

- Alginic Acid - 10-40%
- Laminarin - 2-34%
- Mannitol - 5-25%
- Fucoidan - 5-20%

Table 2.1 A table showing the structural units of the four main carbohydrates found in brown macroalgae. Adopted from Anastasakis (2011) [55].

Carbohydrate	Structural Unit
Alginate Acid	 <p>The structure shows a repeating unit of alginate acid, consisting of two blocks: an L-Guluronic acid (GG) block and a D-Mannuronic acid (MM) block. The GG block is a cyclic structure with a carboxylate group (-COO⁻) at C5 and hydroxyl groups at C2, C3, and C6. The MM block is a cyclic structure with a carboxylate group (-COO⁻) at C5 and hydroxyl groups at C2, C3, and C6. The two blocks are linked by a 1,3-glycosidic bond between the C3 of the GG block and the C1 of the MM block.</p> <p>L-Guluronic acid (GG Block) D-Mannuronic acid (MM Block)</p>
Mannitol	 <p>The structure is the Fischer projection of mannitol, a six-carbon polyol. It has hydroxyl groups on the second and third carbons on the left side, and hydroxyl groups on the fourth and fifth carbons on the right side. The top and bottom carbons are CH₂OH groups.</p>
Laminarin	 <p>The structure shows a repeating unit of laminarin, which is a cyclic structure consisting of two glucose units linked by a 1,4-glycosidic bond. The units are shown in a chair conformation with hydroxyl groups at C2, C3, and C6.</p>
Fucoidan	 <p>The structure shows a repeating unit of fucoidan, which is a cyclic structure consisting of two fucose units linked by a 1,4-glycosidic bond. The units are shown in a chair conformation with a methyl group at C5 and a sulfonate group (-OSO₃⁻) at C2.</p>

The structures of these carbohydrates which dominate the brown algae are shown in table 2.1. The relative amounts of each type depends on the species. For brown algae, alginic acid is the main polysaccharide [82]. The average molecular weight for the alginate is roughly 260kDa, and the laminarin found in kelps is usually 20 -25 degrees of polymerisation in length. Fucoidan are the sulphated polysaccharides, made from sugars including L-fucose, mannose, galactose, xylose and glucuronic acid. Laminarin and mannitol are the two main food reserves in brown algae [80]. Mannitol is derived from D-mannose and is a sugar alcohol [80].

Due to their rich chemical content, there are a variety of uses for macroalgae within the UK. For example, agar, carrageenan and alginate can be used as hydrocolloids, and these compounds can either be used as thickening agents in foods such as ice cream or toothpastes, or agar used for wound dressing, or gelling agents in the cosmetic industry [83]. With the decreasing use of pork gelatin in sweet production due to the increasing popularity of veganism, the use of seaweed-based hydrocolloids is potentially going to become an even higher value product in the years to come [84]. Seaweeds can also be used to make feed additives, for cow or sheep fodder, and has even been shown to cause less methane to be produced in livestock when used as a replacement animal feed, and thus has the potential to help reduce a key source of GHGs in the future by being used in this manner [85]. Seaweed is also widely eaten by humans, albeit mainly in Asian diets [86]. This versatile product is so nutritious and high in minerals and vitamins that it is also used as fertilisers, and can be used as a soil amendment or can be composted to improve fertility in growing mediums [87].

The relatively new application of macroalgae for biofuel use is still very much in the research phase and hence the most suitable methodology for its large scale implementation in the biofuel industry in the UK is yet to be evaluated to a standard whereby full-scale implementation can be successfully achieved without risk. The uses of seaweed are numerous and varied and many different chemicals found in seaweed are of interest in the food and cosmetic industries, both high-value and commodity chemicals. This provides a key opportunity for integration of seaweed into an energy focussed bioeconomy with minimal waste. This would create increased economic feasibility for using seaweed as a biofuel if some key products can be extracted from the feedstock as part of the pre or post-HTC process [88].

Determining the most suitable technique of transforming the harvested wet seaweed into something that is both energy efficient for use as a fuel and enables further utilisation

of the different chemicals found within the seaweed is paramount. The high value of seaweed in the food, medical and cosmetics industry [73], [83] due to its complex biochemical composition may otherwise mean that it is not economically sensible to burn seaweed for energy use instead. Hence, a suitable balance should be achieved with full utilisation of the key attractive properties of seaweed. The hydrothermal carbonisation technique discussed in §2.3.6 is the method used in this study to derive renewable energy from seaweed, and this relatively new hydrothermal process enables the organic chemicals within the seaweed to become captured in the process water instead of lost as gases. This therefore enables the further use of the organically rich aqueous phase as part of the overall biorefinery concept, and could supply commodity and high-value chemicals extracted from the HTC aqueous phase to these industries as a by-product [88].

2.3 Different Techniques for Producing Energy from Seaweed

There are a variety of techniques explored in current research that focus on deriving biofuels from algae. An economically viable method ready for large scale commercialisation is yet to be established. Up until recently, however, microalgae derived biofuel has been the main focus of the research. These can be categorised into two types; those which process dried microalgae, and those that can tolerate the wet processes. The processes involving dry feedstocks discussed here include; direct combustion, pyrolysis and gasification. The wet processes discussed are hydrothermal liquefaction (with an introduction to hydrothermal carbonisation), bioethanol and biobutanol production and anaerobic digestion. The wet processes (particularly the HTC method) are focussed on in more detail as they are less energy intensive overall for use with macroalgae, and hence are a much more commercially feasible option for future implementation.

In order to evaporate the water (heating 20°C to 100°C at 1 atm pressure), 2.6 MJ kg⁻¹, or 700 kWhm⁻¹, is required [89]. Hence, wet techniques such as hydrothermal liquefaction does not require any drying of the feedstock before processing, so may have some significant advantages over these more established yet energy intensive processes. This is especially a factor for third generation biofuels due to their much higher moisture content compared to the more lignocellulosic terrestrial biomass.

The main methods that are attractive for the production of biofuels from microalgae are briefly outlined below. The more conventional and understood methods of direct combustion and pyrolysis are discussed first, followed by gasification, then the hydrother-

mal methods follows, starting with the higher temperature processes. Biobutanol and bioethanol production is next studied, followed by another wet process; anaerobic digestion. Impacts of catalysts and the catalytic properties of the super-heated water are also explained in more details in the final section 2.2.8.

2.3.1 Direct Combustion

This is a more traditional method, and remains today as the principal technique used to extract energy from dry biomass feedstock, for domestic or industrial purposes [90]. Direct combustion of macroalgae has not been studied in much detail [91], [92]. The high carbohydrate content of seaweed translates to a low thermal value, at around 15 MJ kg⁻¹ for dry macroalgae [93]. The high ash content of seaweed is also a limiting factor for the industrialisation of direct combustion. The high alkali index (16-82 kg alkali GJ⁻¹) of seaweed may however be an issue when it comes to preventing slagging and fouling of the combustion/boiler systems [93]. High sulphur and nitrogen contents correlate to more corrosive SO_x and NO_x emissions, which would need to be controlled. The extra energy for drying the biomass before combustion is not favourable, and so this method is not very energy efficient. As such, more advanced methods of extracting energy from this potentially attractive natural resource need to be developed.

2.3.2 Bioethanol and Biobutanol

The production of bioethanol from first generation biofuels is now well established, predominantly in the USA (from corn), and Brazil (sugarcane) [94]. A large scale commercial production of biofuel from lignocellulosic feedstocks is yet to be realised, despite the abundance of feedstock, plenty of research and funding [95], [96], [97]. To produce the ethanol, complex sugars stored in the feedstock biodegrade into simpler sugars, and then this sugar is converted to ethanol via the use of yeast *Saccharomyces cerevisiae*. It has been found that the lignin present in terrestrial biomass feedstocks have a tenancy to inhibit this biodegradation, which is one limitation of this method. However, seaweed does not usually contain a lot of lignin, and so may be a more suitable feedstock [98].

The drawback of this third generation biomass is that the polysaccharides in the seaweed does not contain a lot of glucose, which limits the production of ethanol. The sulphated

polysaccharides, mannitol, alginate, agar and carrageenan in the macroalgae may produce ethanol as an alternative [99]. Another issue here is that the yeast does not convert the sugars produced via the breakdown of these carbohydrate components (xylose and rhamose for example) very efficiently. No ‘tractable microorganism’ that can produce ethanol from these monosaccharides has yet been identified, and hence the development of this technique for producing bioethanol is limited [100], [101]. However, the yeast *Pichia angophorae* has been shown to produce a high bioethanol yield via the fermentation of laminarin and mannitol from *Laminaria hyperborea* [102].

In addition, the need for pre-treatment (e.g. hydrolysis by acids or enzymes), saccharification and removing fermentation inhibitors add complications and cost to the bioethanol production from third generation biofuels [103]. It is unlikely that the theoretical yield of 50% ethanol from macroalgae will be achieved at scale [104].

Due to its high energy density and low vapour pressure, there is a potential for biobutanol to replace bioethanol as an additive to gasoline [105]. The ability of the bacteria used in the production of butanol to digest cellulose, as well as the sugars and starch, results in a higher energy efficiency [106]. A pilot scale has demonstrated successful butanol production from the algal sugars from *Ulva* [105] and so there is a high potential for this process to become commercially feasible on a large scale. However, there are still some improvements to be made. For example, in one study on the butanol production from *saccharina*, abundant alginates were not fermented. In order to make biobutanol production from macroalgae economically feasible, the fermentation process should be improved to utilise as much as the organic fractions of the feedstock as possible [102].

2.3.3 Pyrolysis

This is defined as the thermal decomposition of the organic components of dry biomass by heating in the absence of oxygen [107], [108], [109]. A variation in the temperature and residence time produce a range of fuel products. Slow, fast and flash pyrolysis vary in heating rate from $0.01\text{-}2^\circ\text{C s}^{-1}$ to just a few seconds to reach the high temperatures required. This difference has the effect of producing higher char yields for the slower pyrolysis, and more liquid or gaseous products for the faster rates. Temperatures for fast and/or flash pyrolysis exceed 500°C , with residence times of a few seconds [109], [110]. This variation of products allows for the process to be optimised to suit particular requirements. Bio-oil production is preferred over syngas or char generally due to its

higher energy density and its ease of transportation/storage.

For microalgae, fast pyrolysis with a heating rate of $100\text{-}200^\circ\text{C s}^{-1}$ is recommended for maximisation of liquid or gaseous products [110]. A study published in 2014 by Choi et al using *Saccharina japonica* in a simulated slow-pyrolysis system with a fixed-bed found that yields of bio-oil and bio-char production were 47% and 33% respectively, when heated to 450°C [111]. The energy balance of pyrolysis of macroalgae still requires development before commercialisation.

The metals and inorganic ions abundant in seaweed in addition to the high moisture content mean that seaweed is not an ideal feedstock for the pyrolysis technique. The main issue, apart from the high ash content, is the moisture. Pyrolysis requires a dry feedstock. In addition, the heating value range of $23.08\text{-}32.46\text{ MJ kg}^{-1}$ of the oils from seaweed pyrolysis is lower than that from lignocellulosic biomass. It has been concluded that seaweed would not be a viable option for pyrolysis feedstock on a commercial level [112].

2.3.4 Gasification

Another process involving the processing of dry biomass is gasification. This is the ‘conversion of organic matter by partial oxidation at high temperature ($800\text{-}1000^\circ\text{C}$) mainly into a combustible syngas’ [90], [107], [108], [113]. This process initially pyrolyses the feedstock, and then the resultant char is gasified to produce syngas, which has a calorific value of around 5 MJ m^{-3} [107]. This gas consists of about one third hydrogen, carbon monoxide (20-30%) and methane (10-15%), with small amounts of carbon dioxide, water vapour, ethylene and nitrogen [90], [108]. Oxygen or water is used as a gasifying agent for processing the char. High temperature pyrolysis of biomass does not produce as much char as the gasification process [114]. Gasification is the preferred technique when maximising the output of gaseous products, which can be burnt off to generate electricity from the heat produced using a combined gas turbine system [90], [107].

This process can also tolerate a wet feedstock. SuperCritical Water Gasification (SCWG) can be used to produce syngas from high moisture biomass. It is possible to recover the heat energy by using the hot effluent to preheat the feedstock. Minimising the overall energy required for SCWG [115]. With the addition of a catalyst, methane rich syngas has been produced from the SCWG of *Ulva Lactuca* [116]. *Saccharina latissima* has also been studied using the SCWG process, and the July harvests were found to produce gas with the highest calorific value (due to low ash and high carbohydrates) as compared to products from the other months of harvest [117]. Hydrogen and methane production

in the syngas was maximised by adding NaOH to the SCWG process of *Saccharina latissima*, with the added effect of minimising the C₂-C₄ yields and with no production of carbon monoxide and carbon dioxide [118].

The overall energy balance of the gasification of algae, with consideration to the drying of algae prior to heating, has yet to be evaluated fully. The gasification of wet biomass is attractive economically and energetically, plus it does not have many technical difficulties in regards to any treating and refining of the product streams, unlike anaerobic digestion and fermentation methods [119]. The fast gasification process is also an advantage, and if higher yields of syngas can be produced, a more attractive energy balance can be met.

2.3.5 Hydrothermal Liquefaction

This process is able to produce biofuels using a wet feedstock, so has great potential for the production of biofuels from algae. HydroThermal Liquefaction (HTL) involves the conversion of wet biomass into a stable liquid hydrocarbon fuel (or bio-oil) at temperatures ranging from 250°C to 350°C [90], [107]. This is similar to pyrolysis, however, it is pressurised and performed in wet conditions. This process essentially speeds up the natural process of how oil is formed; through dead algae being compressed over millions of years under at high temperature. The resultant bio-oil has an increased energy density. The biomass produces partially oxygenated hydrocarbons, which is lower in oxygen and moisture content than the bio-oil produced via pyrolysis [90], [107], [120]. This more stable product is attractive, however, the feed systems can be complex, and more expensive than pyrolysis or gasification [90], [107], [110]. The main advantage of this process is its ability to handle a wet biomass, with feedstocks of up to 90% moisture content having a favourable energy balance [121] and so this technique remains one of the most interesting methods of converting algae into biofuels.

The phase diagram for water is shown in figure 2.7 for reference. This highlights the difference in the properties of the water and the boundaries of the different types of hydrothermal processes as the temperature increases. Before the water reaches its critical point, it is said to be ‘super-heated’ water and thereafter ‘supercritical’.

Hydrothermal liquefaction of microalgae has been shown to achieve bio-oil yields of up to 41% for *Spirulina* [123], 37% for *Dunaliella* [124] and 49% for *Desmodesmus*. This translates to a conversion rate of around 75% of the energy in the microalgal feedstock. Macroalgae is yet to produce yields as high as this, with a bio-oil yield of up to 23% [125].

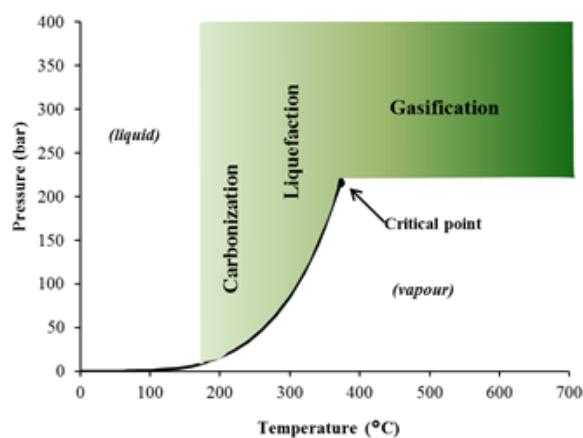


Fig. 2.7 A phase diagram showing the temperatures and pressures at the boundaries between the different phases of water, which demonstrates how these parameters determine which of the hydrothermal processes they relate to. [122]

Energy recovery from *Saccharina latissima* was 63%, and *Enteromorpha prolifera* at 56% [126], [127]. It is possible to utilise the gas and hydrochar produced via HTL treatment of biomass, as these could be burnt to produce energy, or used as fertilisers. The different residence times and heating rates of HTL can determine the mass balances of the product streams, and so can be adjusted to suit specific requirements. The bio-oil is produced in a crude form and so can be further distilled to produce a variety of chemicals [128].

Researchers at SINTEF have found that using *Saccharina latissima*, on a small scale using sealed quartz capillary reactors with a heating rate of $585^{\circ}\text{C min}^{-1}$, up to a temperature of 350°C , resulted in a dry ash free (daf) bio-oil yield of 79% [129] (retention time of 15 mins, with a substrate/water loading ratio 1/10 w/w). This high yield remains to be reached on a batch reactor scale, and hence large scale conversion of macroalgae to bio-fuel is still a long way off, but looks to be a promising method when a higher proportion of bio-oil is desired. At lower temperatures, the hydrochar production increases in proportion, as the bio-oil reduces. The three different stages of hydrothermal processing are so called due to the different temperature ranges they cover. These three types are outlined in figure 2.8. HTC is the term for the lower temperature process which favours hydrochar production, although the aqueous phase is still chemically rich, just not with many oil-based compounds.

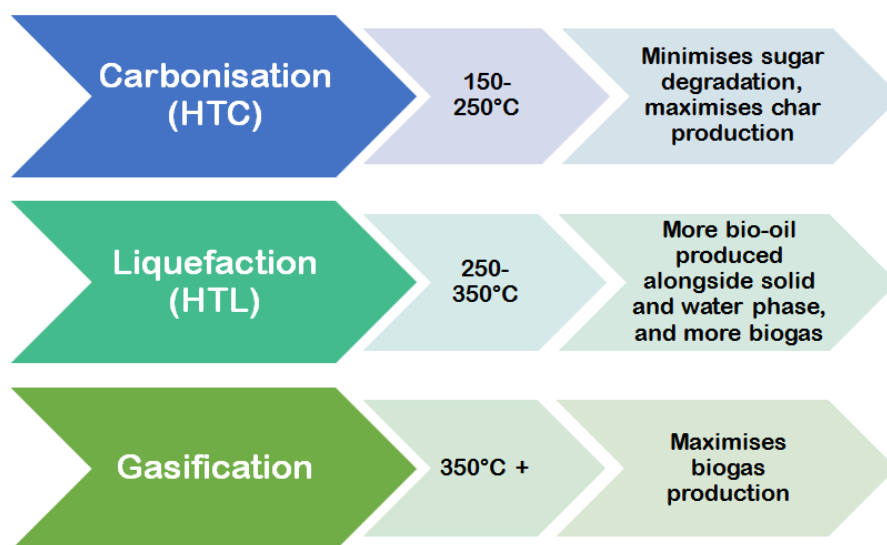


Fig. 2.8 A schematic summarising the main differences in the three different hydrothermal processes.

2.3.6 Hydrothermal Carbonisation

HydroThermal Carbonisation (HTC) is a similar hydrothermal technique to HTL, but is performed at lower temperatures and pressures. Some studies look at temperatures ranging to 290°C, although most range from about 170-250°C. Using lower temperatures and hence pressures than HTL, HTC produces a higher proportion of the solid product, hydrochar. This is due to the formation of primary and secondary char. Hydrothermal carbonisation of biomass (or alternative feedstocks) produce a more coal-like hydrochar, with high energy efficiency.

It is well known that increasing the HTC temperature improves the fuel quality, as there is more energy densification. HTC usually raises the HHV of biomass feedstocks from about 15-18 MJ kg⁻¹ to 25-30 M kg⁻¹ [130]. In addition, the physical characteristics of the feedstock change; the hydrochar is more friable and mills down more easily [128]. This would be a practical advantage for industrial pre-treatment processes prior to use within a biomass boiler, for example. The residence time used in current HTC research varies from minutes to a day. Recent studies indicate that one hour is the most preferred residence time, due to limited improvement in HHV of the products found with additional residence time, in a study looking at residence times of up to eight hours [131].

The three main steps of HTC are firstly the hydrolysis of carbohydrates and proteins, and then dehydration and fragmentation reactions occur to the dissolved hydrolysis products. Some decarboxylation reactions take place, producing carbon dioxide gas [128]. These

organic products are now in the form of solubilised monomers. Polymerisation and condensation then occurs, and then aromatisation (ring molecules are produced) [132], [133]. This is followed by the hydrochar particles rapidly nucleating (primary char, 1°). Finally, these particles grow via diffusion and accumulation of other molecular compounds to adhere to the particle's surface, becoming secondary char (2°). Hence the hydrochar is a products of both primary (1°) and secondary (2°) char [134]. The relationship between the char formation and the biomass, with mechanisms responsible are shown in figure 2.9. The breakdown of cellulose (and other similar large polymeric organic structures such as polysaccharides) into glucose, and the resultant formation of HMF and then hydrochar can be summarised by the diagram in figure 2.10.

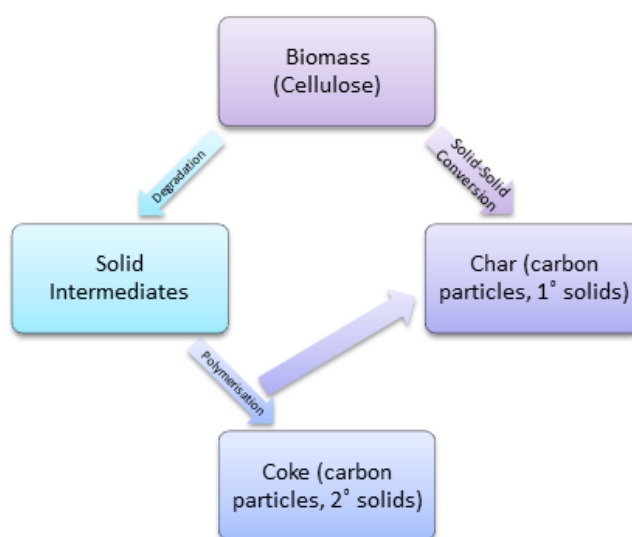


Fig. 2.9 Primary and secondary hydrochar production via the degradation and solid-solid conversion of the cellulose molecule. Adapted from Kruse et al 2019 [135].



Fig. 2.10 A simple graphic demonstrating the relationship between the glucose molecule, the HMF unit and the hydrochar product, under hydrothermal conditions. Adapted from Kruse et al 2019 [135].

The main component of the hydrochar is derived from 5-HMF. 5-Hydroxymethylfurfural(5-HMF), also 5-(hydroxymethyl)furfural. This HMF molecule is an organic compound formed by the dehydration of certain sugars. The production mechanisms responsible for producing 5-HMF is very complex. To simplify these many chemical reactions taking place

during HTC, the diagram in figure 2.11 was adapted from Shen et al 2014 [136]. These reaction mechanisms are known to occur during HTC and the production of the products are colour coordinated with the mechanisms responsible.

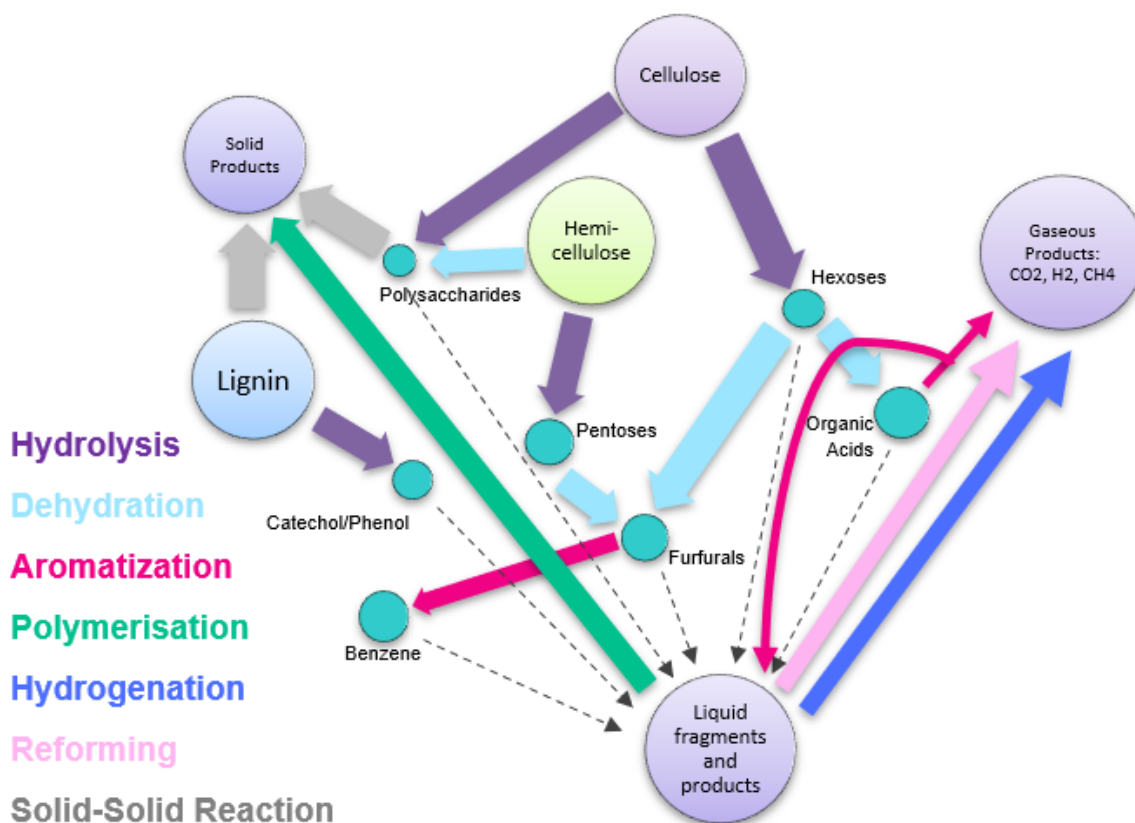


Fig. 2.11 A Schematic Diagram summarising the different reaction pathways that may lead to hydrochar production and aqueous phase compound production under hydrothermal conditions. The names of the reactions are listed on the left hand side, with the colour coding matching the relevant coloured arrows. Adapted from Shen 2014 et al [136].

The 1° part of the hydrochar is formed via solid-solid reaction mechanisms, and the 2° char is thought to be produced from the reactions happening within the liquid phase, which are then polymerised to form the char. This recent understanding of secondary char formation develops the idea that this may be due to furfural precipitation during heating and then acting as seeds of droplets of 2° char formation [135], however, this suggestion is limited due to the furfural not normally precipitating under these conditions. This co-agulation process involves the larger hydrochar particles growing from smaller particles, and hence the shape is more spherical [135].

This 2° char forms a layer around the 1° char, forming a shell around the core of

the primary char. The shell exhibits hydrophilic behaviour, whilst the core is more hydrophobic [137]. Studying the interior structure of the hydrochar in detail remains a challenge, but this field is rapidly developing due to the recent applications of X-ray spectroscopy and synchrotron radiation for hydrochar research [137]. The HMF structure has two ‘arms’ either side of a furan ring, and these can be linked together to form a longer chain polymer, which then may be processed to produce a bio-based plastic [138]. This chemical structure is shown in figure 2.12. 5-HMF is therefore a ‘platform’ chemical and is hence also of interest to the growing bio-based plastics sector [138].

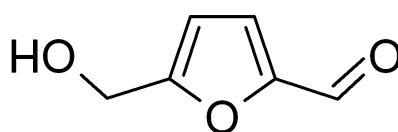


Fig. 2.12 The Chemical Structure of Hydroxymethylfurfural (HMF) [139].

It is also of note that the 2° have been shown to prevent some plant diseases in greenhouse studies [140]. However due to its high solubility in water, it has a higher tendency to leach out due to rainfall or watering, compared to the 1° char. This would hence cause more pollutions into the local environment and reduce its fertilisation capabilities [140]. The polyaromatic hydrocarbons (PAH)s are lower in hydrochars due to the lower temperatures for the process, compared to other thermal techniques, which is good as PAHs are known pollutants [140]. Although hydrochar may be considered to be a good substitute in the future for traditional peat-based growing substrates in the bioeconomy, there are some key drawbacks that may prevent this application, for example this leaching effect coupled with the presence of some toxic chemicals (furfurals and phenols mainly) within the hydrochar [141].

The process water product stream produced by HTC is another key avenue for profit or further utilisation by a biorefinery. Feedstocks that are already wet such as seaweeds benefit from the fact that HTC is a wet process, due to the discarded need for drying the feedstock, which can be energy intensive, time consuming and cause storage issues. Utilising this aqueous phase is a key consideration, as there are a variety of potential uses, depending on the feedstock and HTC parameters used. For example, for seaweeds that are generally rich in heavy metals and nutrients, sugars and polyphenols, the HTC aqueous phase may contain a variety of simple sugars derived from the polysaccharides, and also some trace metals that would make it highly suitable as a fertiliser, (e.g. for

commercial/industrial hydroponic facilities).

Alternatively, the polyphenols and other high-value chemicals dissolved in the aqueous phase may be extracted through further processing or selling onto the cosmetic or food industry. Commodity chemicals may also be extracted, such as mannitol or glucose. Another idea which would reduce the need for fresh water is that the aqueous phase may also be recirculated back into the HTC reactor. Recirculation of the aqueous phase in this way has been found to increase production of carboxylic acids in the aqueous phase (acetic, formic, levulinic or lactic acids), and produce more of the reactive intermediates of the HTC reactions; HMF and its derivatives, furfural and glucose [142]. The increase in the production of these basic chemicals makes the HTC process more useful as a source of these chemicals [142]. These chemicals polymerise to form the 2° char. Arauzo et al indeed found that by recirculating the hydrochar process water, the hydrochar yield increased due to the greater production of secondary hydrochar [142]. In addition, it was found that the increase of acetic acid by recirculation methods provides an ‘acidic milieu’ for further recirculation and results in a more stable 1° char due to a promotive effect on cellulose solvolysis [143]. Recirculation of the HTC process water may therefore be an economic and practical solution to improve the hydrochar yield whilst also reducing water intake (a key consideration for HTC development in more drought-prone locations) and remains an active point of research in the field of hydrothermal carbonisation.

The sugars in the aqueous phase may also provide a secondary stream of renewable energy source, through anaerobic digestion (AD). This approach is considered within this study and is further detailed in §2.3.7. It is important to consider the mix of chemicals contained in the aqueous phase when deciding on best uses for this product stream. The range of uses for it in general means that the HTC process is a versatile process that may create a variety of products for the bioeconomy, in addition to a source of renewable energy via hydrochar production.

During hydrothermal carbonisation, some gas is also produced by the reactions that take place in the reactor. This comprises mostly of carbon dioxide, methane, carbon monoxide and hydrogen. The potential to trap this gas and extract any methane could be a consideration, especially if an AD process is developed for post-HTC within a biorefinery.

The HTC parameters affect the ratio of the solid and liquid (and gaseous) product streams, and their chemical and physical characteristics. These parameters may be altered, as well as the feedstock chosen, to produce the desired products depending

on their respective downstream utilisation options. Most studies look at temperatures ranging from 170°C to 250°C, though some research considers temperatures up to 290°C or as low as 120°C [140]. The temperature can be adjusted, and the pressure may be either self-generated from the steam from the heated water, or can be increased before heating. Self-generated pressure results in around 40 bar at 250°C [144], [145]. The residence time may also be changed, and the feedstock to water loading ratio can be altered if required. Usually, however, a 10% or 20% dry feedstock to water loading ratio is used, and a residence time of one to two hours is the main period used in studies [144].

The HTC of seaweed is a quickly developing area of current research and is the focus of this PhD work, with attention on the potential to further utilise the abundant aqueous phase. At even lower temperatures than this, around 100°C, hydrolysis occurs. The work in this research covers a range from 100°C to 250°C and so the term used to describe the hydrothermal processing is referred to henceforth as HTP (or in some instances HTC).

2.3.7 Anaerobic Digestion of Macroalgae

Anaerobic Digestion (AD) is ‘a collection of processes by which microorganisms break down biodegradable material in the absence of oxygen’ [146]. There are different types of bacteria which digest biological matter, usually with maximum efficiency at 37°C. The overall process of organic material (for example glucose) being biochemically digested by bacteria to produce carbon dioxide and methane can be simplified by the following equation [147];



Therefore for every glucose molecule digested, three molecules of methane could be produced, assuming 100% conversion efficiency. Biomass with a high sugar content such as Miscanthus and seaweed could be a promising feedstock for AD purposes due to the high potential biomethane production. Figure 2.13 illustrates key aspects of what occurs during the anaerobic digestion of biomass. The four main steps include: hydrolysis, acidogenesis, acetogenesis and methanogenesis. ‘Genesis’ is derived from the latin to create, so it is simple to interpret that in the latter three stages, acids are formed, followed by acetic acid and finally methane is produced.

Hydrolysis, the first step, is ‘the chemical breakdown of a compound due to reaction with water’ [148], as has been introduced in §2.2.5. This step is usually the slowest

step, and therefore the limiting factor in how quickly anaerobic digestion can produce methane from the initial feedstock. This initial step can be speeded up by the use of HTC as a pre-treatment, which hydrolyses the feedstock by breaking down the complex organic matter into its constituent parts; a variety of sugars and acids. This can then be converted via the fermentation bacteria to produce VFAs, H₂, CO₂ and acetic acid. Incorporating the use of AD technology in the HTC biorefinery concept, with the aim of producing as much renewable energy as possible during the process, would be very beneficial.

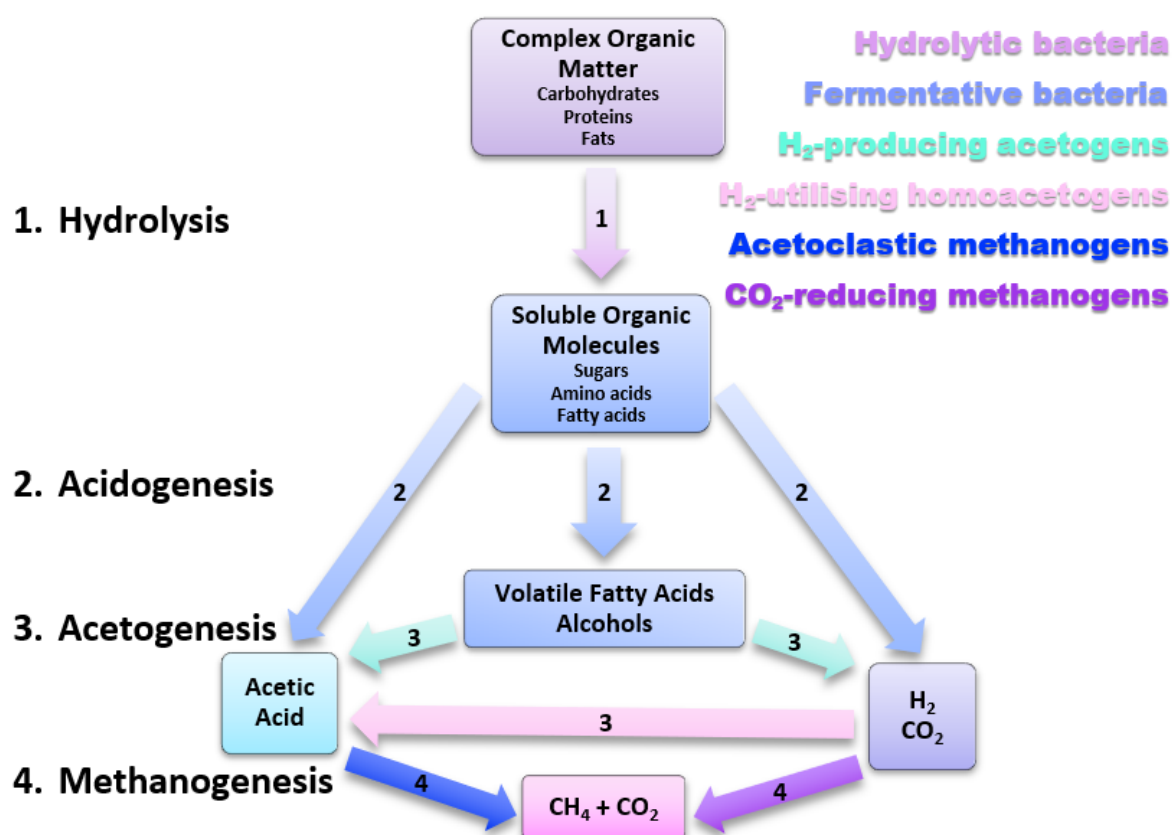


Fig. 2.13 A diagram portraying the different stages in the anaerobic digestion (AD) process. The four main stages are numbered and labelled, whilst the different types of bacteria responsible for digesting the feedstock are colour coded and listed on the right hand side of the diagram. In general, the name of the bacteria provides a good indication as to the AD stage it is responsible for. Adapted from Bibra, M. et al (2015). [149]

The whole of the feedstock can be used in this process, as the leftover material (digestate) is rich in nitrogen and phosphorus, and can therefore be used as a fertiliser or biological feedstock, creating an additional revenue[150]. The species of algae chosen for AD is

selected based on the proportions of carbohydrates, proteins and lipids. The low abundance of lipids in seaweed may result in a more suitable AD feedstock [125], [151]. The Buswell equation [152], [153] can be used to determine the theoretical yield of biogas production from AD and the chemical composition of macroalgae ($C_cH_hO_oN_nS_s$) allows for a high theoretical yield.

The methane yield from seaweeds are typically around $200\text{mm}^3 \text{CH}_4 \text{g}^{-1}$ [154]. The rate of the AD process is generally limited by the slowest step in the process, which in the case of macroalgae is thought to be the hydrolysis of seaweed-derived polysaccharides, alginates in particular [155], although this study does not use HTC as a pre-treatment before AD. One study by Sutherland et al. looked at AD with the addition of bacteria from the rumen of Ronaldsay sheep, which eat mainly seaweed. They found that the methane yield of anaerobically digested *Laminaria hyperborea* increased to $0.253 \text{L CH}_4 \text{g}^{-1} \text{VS}$ and so too did the volatile solid (VS) utilisation, to 67% [155]. A volatile solid is a ‘substance that can easily transform from its solid phase to its vapour phase without going through a liquid phase’ [156].

The high salt content in seaweeds can be an issue, however it has been demonstrated that by slowly increasing the salt content in the digester, the bacteria can adapt, instead of having ‘salt shock’ [157]. The feedstock is required to be ground to a small size in order to maximise the AD efficiency [158]. Another issue is the cost; biomethane produced via AD can be over ten times more expensive than natural gas [159]. Despite this setback, AD is currently the closest method of producing biofuels from seaweed to industrialisation.

The potential to use waste heat from the HTC reactor (150°C to 250°C) via heat exchange pipes to maintain the AD at 37°C could reduce energy requirements of the proposed biorefinery. This would best utilise the energy used for heating purposes for the HTC reactor. This heat exchange proposal is noted in the biorefinery concept shown in figure 1.3.

Extra income that may be generated from extracting commodity or high value chemicals from the chemically-rich seaweeds and other feedstocks after HTC processing would also provide economic benefits, and hence would improve the viability of attracting investors to the idea of the biorefinery, in comparison to an AD reactor as a stand-alone facility (although less biogas may be produced). Hence, although AD is a successful renewable technology, it can be improved upon via incorporation into a HTC based biorefinery. Therefore the HTC concept evaluated in this research would involve the use of AD of the HTC aqueous phase to increase the total renewable energy production and

best utilise the product streams after HTC, demonstrated in figure 1.3 in chapter 1.

Chapter 3

Methodology

3.1 Introduction

This chapter will detail the different methodologies used throughout the PhD research. The feedstock collection and milling are first discussed, followed by the HTC conditions and reactor details. The mass balance calculations are then explained thoroughly. The analysis techniques used for the characterisation of the raw feedstocks are consequently discussed, of which these techniques are replicated for the hydrochar characterisation. The aqueous phase is then discussed in terms of drying technique and the subsequent analysis of the dried aqueous phase via ultimate and proximate analysis.

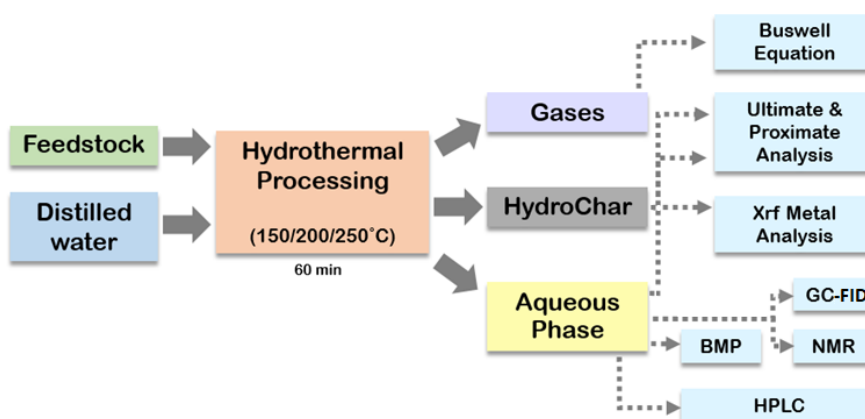


Fig. 3.1 A flow chart showing an overview of the different analytical techniques used for the different HTC product streams. Note that pH and TOC were also performed on the aqueous phase, and the raw feedstocks were also analysed via some of the techniques shown.

The wet analysis techniques are also discussed in detail, namely HPLC, GC-FID, NMR, Liquid XRF, pH, TOC and BMP. The theoretical BMP yield will also be discussed and equations given. For further clarity of the various analytical techniques performed for each product stream after HTC, please refer to figure 3.1.

3.2 Sample Collection and Preparation

The *Fucus serratus* was collected from Aberystwyth, Wales, UK in June 2015. This was subsequently air dried, milled down and then stored in a sealed plastic bag in a dark cupboard at room temperature. The *Saccharina latissima* sample was collected from Beadnell Bay, Northumberland, UK on 05/06/2017. The sugar kelp was vacuum packed and frozen for storage, then subsequently oven dried in a GenLab Drying Cabinet at 60°C. The seaweed samples were then each milled using a coffee grinder for HTP processing, and stored sealed in a plastic bag in a dark cupboard until required. The *Miscanthus × giganteus* sample was collected from Rothamsted Research, Harpenden, Hertfordshire, UK[64]. This sample was a ‘naturally occurring triploid hybrid of diploid *M. sinensis* and a tetraploid *M. sacchariflorus*’[64]. The *Miscanthus* was harvested after senescence during early Spring (April 2017), when the nutrients from the perennial energy crop have been remobilised into the rhizome in the roots. This conventional harvesting time should result in a low moisture content. The *Miscanthus* was dried and milled down to particle size smaller than 1 cm using a coffee grinder and stored in a plastic box at room temperature before hydrothermally processing as needed. The model compounds were provided from Sigma Aldrich, although the Whey Protein Isolate powder sample was purchased from an online shop (‘Piping Rock’) on 25/05/2018. The inoculum for the BMP tests was collected from an anaerobic digestion facility at Esholt wastewater treatment plant based in Bradford, UK and was stored in plastic containers in a 4°C fridge until required. Before using, the inoculum was passed through a 1mm screen to remove large particles.

3.2.1 Sample Size Reduction

In order to accurately characterise the raw feedstocks, homogenising the samples was required. The *Miscanthus* was provided already shredded to approximately 4mm in particle size, as was the *Fucus serratus* sample which has been oven dried prior. The *Saccharina latissima* was dried and reduced in size as described previously, prior to any

HTC processing. However the ultimate and proximate analysis samples were needed to be on a much smaller scale, hence further milling was performed to reduce the sample size down to $<100\mu\text{m}$ was performed on the samples.

Due to the different physical characteristic of the samples, in some cases the pestle and mortar were sufficient, which was used where possible, to minimise the heating of the sample from friction. This was the case for some of the model compounds hydrochars due to the initial small particle size. With less friable samples, particularly at the lower two temperatures and with the samples containing *Miscanthus*, a cryo-mill was used. This Retsch cryo-mill was coupled with a supply of liquid nitrogen where required to make the sample more brittle and hence easier to mill down. The samples were cryo-milled in three sets of one to two minute periods with breaks so as to avoid heating the sample via friction.

In the case of the feedstocks not containing *Miscanthus*, a Retsch Disc Mill was used to reduce the particle size. After size reduction and sieving through a $100\mu\text{m}$ sieve, the samples were ready for characterisation analysis using the CHNS, TGA and XRF techniques. For completeness and reliability of the results, the exact milling techniques used for each of the different raw biomass feedstock samples and also the hydrochars are tabulated in table A.1 in the appendix.

3.3 Characterisation of Feedstocks

3.3.1 Ultimate Analysis and HHV

Ultimate Analysis was performed on all the raw samples and the hydrochars and process waters in order to determine the elemental compositions of the samples. The raw, original feedstock samples; *Fucus serratus*, *Saccharina latissima*, and *Miscanthus giganteus* were each analysed for their carbon (C), hydrogen (H), nitrogen (N) and sulphur (S) content, with oxygen (O) calculated by difference. This was achieved using a CE Instruments Flash EA 1112 series elemental analyser. The solid phase hydrochar and dried aqueous phase samples after hydrothermal processing were also analysed using the same ultimate and proximate methodology described here, after they were each milled down to a particle size of less than $100\mu\text{m}$.

All analysis was performed in duplicate and mean values are reported. The instrument was calibrated using standards, and appropriate references used every ten samples throughout each run. The samples and standards were weighed out to be approximately

2.5mg and were crimped and sealed in tin capsules. These were then combusted in excess oxygen by the elemental analyser. Elemental compositions were automatically calculated by the CO_2 , NO_x and SO_2 concentrations in the product gas. Calibration lines from the standards were always checked and in every case fitted very well in the straight line of best fit for each component.

The as-received values were converted to a dry basis by adjusting the %H and hence the %O (by difference) values, to take into account the hydrogen associated with water present via equations 3.1 to 3.3 [160];

$$\%H_{db} = \%H_{ar} - \left(\frac{\%M}{18} \times 2 \right), \quad (3.1)$$

and for oxygen;

$$\%O_{ar} = 100\% - C_{ar} - H_{ar} - N_{ar} - S_{ar} - \%Ash_{db} \quad (3.2)$$

$$\%O_{db} = \%O_{ar} - \left(\frac{\%M}{18} \times 16 \right) \quad (3.3)$$

The resultant elemental composition was then used to calculate the HHV using the Dulong formula [160], which is expressed in equation 3.4:

$$HHV(MJkg^{-1}) = 0.3383\%C + \left(1.422 \times \left(\%H - \frac{\%O}{8} \right) \right). \quad [160] \quad (3.4)$$

The variables C, H, N, S and O are the mass percentages of carbon, hydrogen, nitrogen, sulphur and oxygen respectively. Proximate analysis was used to get the CHNOS values in terms of a dry basis (db) by using the %Moisture and %Ash contents.

3.3.2 Proximate Analysis

The three dried and milled feedstocks were analysed for Volatile Matter content (VM), moisture content (M), Fixed Carbon content (FC) and Ash content via Thermogravimetric Analysis (TGA). The hydrochar samples were also analysed using the same methodology. Approximately 10 μ g of the powdered (<100 μ m) sample were each placed into an Alumina 70 μ l ceramic crucible, tapped on the worktop to make flat, and weighed out for the initial weight. The samples were then placed into a dial for TGA analysis, with a small lid on top of the crucible. The auto sampler would remove this lid after the crucible is selected and then using the initial weight, the instrument would calculate

the difference in weight during the different burning stages, heated under a nitrogen atmosphere. These differences would be shown on the resultant pdf as a % compared with the original mass.

The instrument used for TGA analysis was a Mettler Toledo Thermogravimetric Analyser. The method used adheres to the british standard for proximate evaluation and the heating rate increases in the following five stages, with a dt of 1.00s;

1. 25°C - 105°C, 25 K min⁻¹, N₂ 50 ml min⁻¹
2. 105°C, hold 10 min, N₂ 50 ml min⁻¹
3. 100°C - 900°C, 25 K min⁻¹, N₂ 50 ml min⁻¹
4. 900°C, hold 10 min, N₂ 50 ml min⁻¹
5. 900°C, hold 15 min, Air 50 ml min⁻¹

This was performed for all three biomass feedstock samples, all the model compound samples in their raw state (before HTC) and all the hydrochar samples using the same method. The different % contents are shown to four decimal places in terms of percentile along the bottom of the chromatogram, under their relevant heating stage. The VM, Ash, FC and M content were all noted from the pdf results and tabulated. These results can then be used to produce higher heating values (HHV) along with the *CHNOS* results from the elemental analysis, as the ash content is used for equation 3.2, and the moisture content for equations 3.1 and 3.3.

3.3.3 XRF Analysis

The three main biomass feedstock samples were milled down to <100 μ m using a variety of techniques in order for the pressed pellet for XRF analysis to be prepared correctly. The hydrochars after HTP were also milled down in the same manner and analysed using the XRF pressed pellet technique.

The use of a Retsch Cryo-mill using liquid nitrogen as a coolant was required for most of the samples in order to mill it down. The Retsch RS 200 Disc Mill and PM 100 Ball Mill were also used for some samples. The model compound hydrochars (lignin, protein, A/C/L, cellulose) were ground down to size using a pestle and mortar. Once all the

hydrochars and feedstock samples could pass through a $100\mu\text{m}$ sieve, they were able to be pressed into pellets for XRF analysis.



Fig. 3.2 This Specac Presser with a maximum pressure of 15 tons was used to compress the powdered sample and wax mix into pelleted solid discs.

The pressed pellets were produced by measuring out 2.7g of powdered sample in a mixing container (FluXana MU-S Container) and then 0.3g of wax binder. The binder used was the BM-0002-1 Cereox binder from FluXana, which was labelled as ‘S-blend’ when inputting this detail into the ZSX software. Three of the FluXana MU-MB-380-1 Polyamide 9mm Mixing Balls were added to the container, stirred a little with a small spatula, then the lid was secured. The containers were then mixed using the FluXana VortexMixer for two to three minutes. The sample and binder mix was then emptied through a mini baking style sieve into a stainless steel pressed pellet vial. The steel pellet vessel was laid with a thin cellophane pellet film (PF-32-500, 32mm diameter, FluXana) on the bottom to prevent the sample sticking to the steel vessel base. Another pellet film was added to the top of the sample as well, before the steel upper cylinder was pushed into the top of the sample, and the vial added to the presser, shown in figure 3.2.

The pressure was set to a maximum pressure of fifteen tons and the samples were gradually pressed using a hand crank on the Specac instrument to push up the vial on to the clamp,

until fifteen tons was reached on the pressure gauge. The pressure was then released via a switch and the steel vessel taken out and emptied carefully. The samples were then in the form of a small cylindrical pellet ready for analysis. These were labelled accordingly.

The pellet samples were then placed into metal pellet holders with a screw top steel lid, and placed into the correct positions in the Rigaku WDXRF ZSX Primus II instrument. The format for the sample input used was 'Oxide Powder' and 'Estimate' for the balance, and both 'Metals' and 'Oxides' were calculated; this can be recalculated for either choice with the results in any case. The range chosen was B-U (Bromine to Uranium) with a 'Normal' measuring time. The sample and binder weights, pellet diameter (30mm) and height (3mm) were added into the ZSX EZ Analysis window for each sample, and the machine set to run. The results were then extracted into an excel document and manipulated using the pivot table technique. This produced an appropriately formatted table of results, - of metals or metal oxides - given in terms of a percentage concentration of the relevant species for each sample.

3.4 Hydrothermal Processing

24g of the three dried and milled algae samples were each added to the reactor for their respective runs, and mixed with 220ml of distilled water, in a 600ml Stainless Steel Parr reactor [161]. This reactor was produced by the Parr Instrument Company and is the 4540 model, used here without the use of the stirred reactor, or the glass liner. This bench top reactor, as shown in figure 3.3, had an internally placed thermocouple and was attached to a pressure gauge. The reactor was heated via a heating jacket at a rate of approximately 8°C per min. The selected temperatures the controller were set to were either 150°C, 200°C or 250°C. This was controlled using a Parr 4838 reactor controller connected to a thermocouple inserted inside the reactor.

A schematic of this reactor is shown in figure 3.3, although note that the reactor used for these experiments is double the length in the reactor chamber, without a stirring mechanism attached. These temperatures were held for a duration of 60 minutes. The maximum pressure, and the pressure and temperature before the reactor was opened for each experimental run were all recorded in addition.

After the hour was up, the reactor was left to cool to around 70°C and subsequently moved using heat proof gauntlets to a metal stand to further cool down until it reached

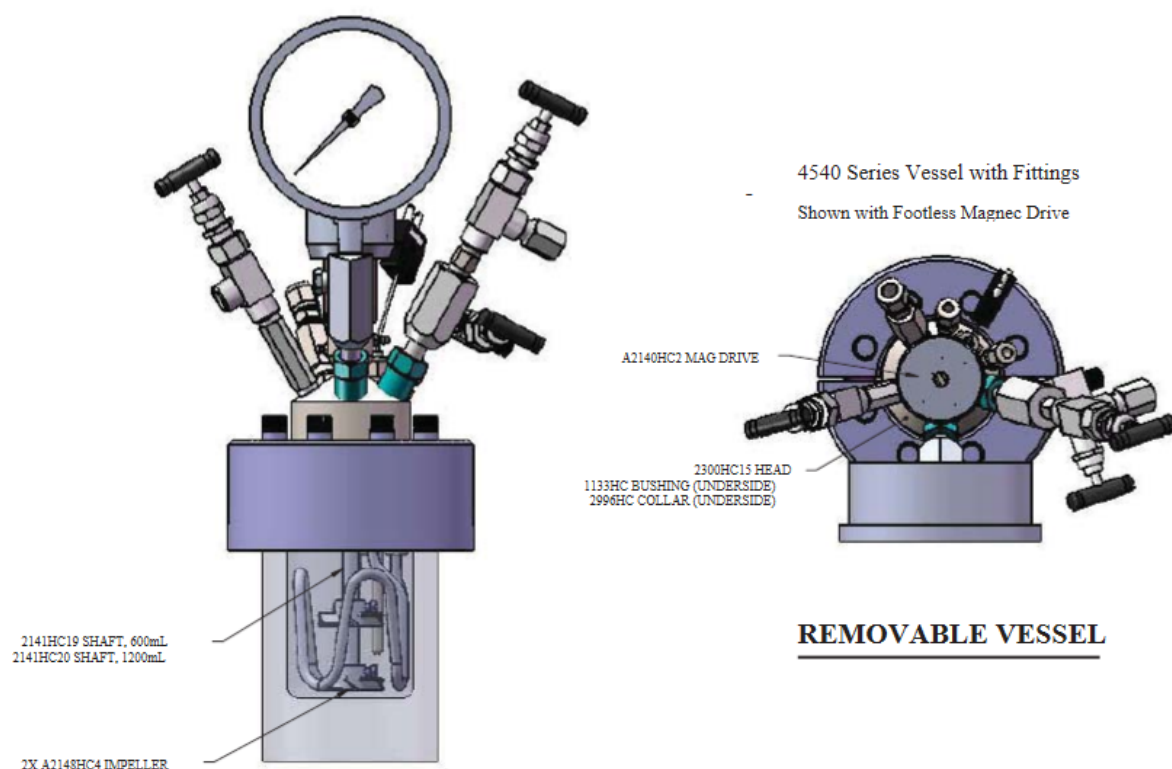


Fig. 3.3 A diagram of the 600ml Parr Reactor 4540, including the removable lid with attachments [161].

room temperature. Then the resultant slurry was passed through a filter paper. A Büchner funnel was attached to a conical flask and a vacuum was used to speed up the filtering process. This allowed for the separation and collection of the char residue and the process water yield. The process water samples were each weighed out and then stored in a plastic bottle in a chest freezer until analysed. The hydrochars dried for a few days in an oven at 65°C, then were stored in clear plastic bags and kept in a dark cupboard at room temperature until they were milled for further analysis.

3.4.1 Mass Balances and Yields

The mass balances from the HTP runs were determined by evaluating the difference in weights of both the solid and aqueous phase after hydrothermal processing. The following weights were recorded;

- Feedstock weight (initial) = $S_i = 24\text{g}$
- Water weight/volume (initial) = 220 ml

- Filter paper + evaporating dish weight (empty) = $Evap.Dish_i$
- Conical Flask (empty) = W_i
- Conical Flask (with aq. phase added) = W_f
- Filter paper + evaporating dish with added wet solids = $Evap.Dish_{full}$
- Filter paper + evaporating dish after dried in oven = $Evap.Dish_{dry}$

The total weight of the solids after hydrothermal processing (S_f) can then be deduced using the following equation;

$$S_f = Evap.Dish_{dry} - Evap.Dish_i. \quad (3.5)$$

The %Hydrochar can then be calculated by equation 3.6:

$$Hydrochar(\%) = \frac{S_f}{S_i} \times 100\% = \frac{S_f}{24(g)} \times 100\%. \quad (3.6)$$

The total weight of the aqueous phase (W_{TOT}) after hydrothermal processing can be determined similarly, using the equation below;

$$W_{TOT} = (W_f - W_i) + (Evap.Dish_{full} - Evap.Dish_{dry}). \quad (3.7)$$

In order to determine the weight of the solids dissolved in the process water, a sample of each of the process waters were added to evaporating dishes and dried in an oven at 65°C. The weights before (W_{empty}) and after (W_{full}) adding the liquid was recorded, and the weight after evaporation was measured (W_{dry}). The % yield of soluble material in the aqueous phase could then be determined using equation 3.8:

$$Yield(\%) = \left(\frac{W_{dry} - W_{empty}}{W_{full} - W_{empty}} \right) \times 100\%. \quad (3.8)$$

The yield can then be used in equation 3.9 to determine the total % amount of soluble material (% Soluble Material) in the aqueous phase, assuming that all the water has the same amount of organics dissolved in it on average.

$$SolubleMaterial(\%) = \left(\frac{yield(\%)}{100\%} \times W_{TOT} \right) \times \left(\frac{100\%}{S_i} \right). \quad (3.9)$$

Note that the values of the %Soluble Materials may be overestimated in some cases due to the assumption that both the water collected in the conical flask after filtering, and

the water lost during evaporation contain the same amount of soluble material. In reality it is unlikely that the water lost during the solids drying at 65°C (or 105°C for the smaller reactor) has as much soluble material as the water collected during the filtering process.

Therefore, when determining the mass balances, the %Hydrochar value has precedence over the %Soluble Material in any cases where the total of both exceed 100%. In which case, the %Soluble Material is reduced accordingly. For any cases in which the %Hydrochar and %Soluble Material do not add up to 100%, the %Other is calculated as follows:

$$\%Other = 100\% - \%Hydrochar - \%SolubleMaterial \quad (3.10)$$

This %Other will consist of any gases produced during the HTP process, and any organics lost during evaporation of the water when drying the solid residues (e.g. VFAs), and any residue left in the reactor after scraping out the contents for example.

In some cases there were significant losses and considering that the pressure of the reactor was not more than 4 bar before opening, as the pressure gauge was not indicating any pressure. The pressure gauge does not rise until the pressures reaches at least 4 bar. These losses may also be due an increase in the amount of organics with boiling points around or below 65°C, which were lost during the drying of the solids, for the runs in which the solids were dried in an oven.

3.5 Analysis of the HTC Hydrochar

3.5.1 Ultimate Analysis of the Hydrochar

The hydrochars were milled down to less than 100 μm and analysed using the method described in §3.3.1

3.5.2 Proximate Analysis of the Hydrochar

The hydrochars were milled down to less than 100 μm and analysed using the method described in §3.3.2.

3.5.3 Inorganic Analysis of the Hydrochar

XRF Analysis

The XRF analysis was performed on both the raw feedstocks and the hydrochars after HTP processing. The hydrochars were also milled as detailed in §3.2.1 and pressed into pellets, then analysed in a WDXRF Rigaku Primus II instrument in the same way as described in §3.3.3.

Slagging and Fouling Indices

Using the XRF data, the slagging and fouling indices of the different samples were determined and tabulated. XRF data was recalculated to give the metal oxides using the Rigaku ZSX software program. These metal oxides (as a % mass of the hydrochar) was hence used in equations 3.11 to 3.17 to determine a variety of indices. Namely, these were; Alkali Index (AI), Bed Agglomeration Index (BAI), Acid Base Ratio (R_a^b), Slagging Index (SI), Fouling Index (FI) and the Slag Viscosity Index (SVI). The medium, upper and lower limits of these values for safe and unsafe slagging and fouling for each of the indices are given in table 3.1.

The **Alkali Index (AI)** predicts how probable slagging and fouling would be if the sample analysed were to be used as a fuel source. This is determined by equation 3.11 [162].

$$AI = \frac{Kg(K_2O + Na_2O)}{GJ} \quad (3.11)$$

The **Bed Agglomeration Index (BAI)** gives an indication of whether or not the material would agglomerate at the bottom of the furnace during combustion [163]. The BAI is calculated via equation 3.12:

$$BAI = \frac{\%(Fe_2O_3)}{\%(K_2O + Na_2O)} \quad (3.12)$$

The **Acid Base Ratio (R_a^b)** is another value used to predict how inclined the material is towards slagging during biomass combustion, see equation 3.13. The SI and FI equations may be expressed in terms of (R_a^b), the acid base ratio.

$$R_a^b = \frac{\%(Fe_2O_3 + CaO + MgO + K_2O + Na_2O)}{\%(SiO_2 + TiO_2 + Al_2O_3)} \quad (3.13)$$

The **Slagging Index (SI)** (Babcock) predicts the likelihood that the material will slag during combustion. Equation 3.14 was used to calculate the SI for each of the samples.

$$SI = \left(\frac{\%(Fe_2O_3 + CaO + MgO + K_2O + Na_2O)}{\%(SiO_2 + TiO_2 + Al_2O_3)} \right) \times \%S_{dry} = R \frac{b}{a} \times \%S_{dry} \quad (3.14)$$

The **Fouling Index (FI)** is used to evaluate the probability of fouling. The equation 3.15 or 3.16 was used to determine the FI values.

$$FI = \left(\frac{\%(Fe_2O_3 + CaO + MgO + K_2O + Na_2O)}{\%(SiO_2 + TiO_2 + Al_2O_3)} \right) \times \%(K_2O + Na_2O) \quad (3.15)$$

$$FI = R \frac{b}{a} \times \%(K_2O + Na_2O) \quad (3.16)$$

Finally, the **Slag Viscosity Index (SVI)** shown in equation 3.17 shows the slagging inclination of the material.

$$SVI = \frac{\%(SiO_2 \times 100)}{\%(SiO_2 + MgO + CaO + Fe_2O_3)} \quad (3.17)$$

The limits for the slagging and fouling propensity in the UK for fuel has to adhere to strict limits due to the negative effects high values has on the boilers. These limits are set out in table 3.1 [88] [164] and are referred to in the discussion of the hydrochar characterisation using XRF analysis. Any potential fuel feedstock should remain within these limits.

Please note that these equations derive from many years of research based on minerally rich fuel sources such as coal and may not predict ash behaviour of biomass as accurately as the correlations may not fit [165]. Care should hence be taken when interpreting indices calculations for biomass samples [165]. There is significant impetus that new indices equations more suitable for feedstock containing less mineral matter be developed, to predict more accurately their ash behaviour [165].

Table 3.1 Limits of the different Slagging and Fouling indices [88] [164].

Slagging/Fouling Index	Abbreviation	Low Limit	Medium Value	Upper Limit
Alkali Index	AI	<0.17	0.17<AI<0.34	>0.34
Bed Agglomeration Index	BAI	<0.15	-	-
Acid Base Ratio	ABR	<0.5	-	-
Slagging Index	SI	<0.6	0.6<SI<2.0	>2.0
Fouling Index	FI	<0.6	0.6<FI<40.0	>40.0
Slag Viscosity Index	SVI	>72	72>SVI>63	<63

3.6 Analysis of the HTC Aqueous Phase

3.6.1 Ultimate Analysis of the Aqueous Phase

After 10ml of each of the aqueous phase samples were evaporated in an evaporating dish at 45°C, which gave the percentage yield, the dried residue left over was scraped off and stored in a glass vial. The contents were later used for ultimate analysis of the process waters, using the same method outlined in §3.3.1.

3.6.2 Proximate Analysis of Aqueous Phase

The dried residues of the aqueous phase samples were also placed in the tiny crucibles for analysis on the TGA machine, following the same methodology in §3.3.2.

3.6.3 Liquid XRF of the Aqueous Phase

With the aqueous phase samples in liquid form, the liquid XRF sample pots were analysed to determine the amount of different trace metals within the HTP process waters. The SPEX SamplePrep 3527 40mm X-CELL were used to hold the liquid samples. These were sealed on the top using the plastic rings provided to fasten a thin plastic film (3521 Polypropylene 0.2µm thick, 2.5" diameter) to the container. This was then inverted, and the liquid sample pipetted into the vial using a glass Pasteur pipette, so that any bubbles would rise to the top to be easily expelled (via manipulation with the glass pipette). Finally, small rubber bungs (RB006/S STO5005) sealed the 6mm diameter hole on the bottom edge of the underside. The pots were then turned back the right way up and the plastic film straightened out if necessary and the pot labelled.

The XRF liquid sample pots were then each placed into the XRF metal vials and into the correct sample positions. For the analysis, 'Metals' was chosen as the component type; H₂O as the balance, and the 'P.E. film' was selected for the film type, as a polypropylene film was used. The weight was entered as 10g for all the samples, as they are water based and each pot has 10ml of space for the liquid sample. The diameter for the plastic pot, for density calculations within the software, was entered as 40mm. The diameter of the mask, which was the window to be measured by the instrument, was input as 30mm, with a 'Standard' length of analysis time. A 'Liquid' sample was hence chosen, with a F-U range. These liquid XRF samples were analysed under a Helium atmosphere, so not under vacuum, unlike the XRF procedure for the pressed pellet samples. The results were then tabulated onto excel, and the picot table technique was used for further data

processing and analysis.

3.6.4 pH

A Hach pH meter was used to determine the pH of the aqueous phase samples.

3.6.5 Nuclear Magnetic Resonance

NMR was performed on each of the aqueous phase sample after HTP. Deuterium oxide was used as a solvent for the HTP aqueous phase samples. 0.05ml of HTP process water and 0.45ml of D_2O were added using a syringe to Wilmad 528-PP precision NMR tubes, which were then mixed by inverting several times, using a sonicator if necessary.

Nuclear magnetic resonance (NMR) spectra was recorded for ^{13}H NMR at 600MHz on a Japan Electro Optics Limited (JOEL) ECA600ii spectrometer, using a water suppression method ('WaterGate') by gradient tailored excitation. Chemical shifts are given in parts per million (ppm) using tetramethylsilane (TMS) as an external shift standard.

The NMR data was analysed using MestReNova. The data was cropped to show a range from 0 to 10 ppm, and a manual base line phase shift was performed for each sample. Manual integration was then used to calculate the peak area within a specified range. This consisted of selecting the peaks that lie within the following five ppm ranges; 0-2.75, 2.75-4.5 and 6-8. These three phase ranges correlate to certain groups of compounds which would be found within these values. These are respectively; VFAs (Volatile Fatty Acids), sugars and phenolic compounds. However, it is important to note that not all peaks in these areas can necessarily be attributed to these specific compound groups, though these are the most likely ranges for their respective compound to appear on the NMR spectra, if they are there. Essentially, a lack of peaks in a specified range would indeed indicate a lack of the compounds present, though peaks present in the area would need further in depth analysis before categorically stating it is present in the sample.

The first section of the NMR spectra to undergo manual integration using MestReNova, which in every case was the 0-2.75 ppm range, was always assigned a value of 1 from the software, due to it being the first reference peak area calculated. All subsequent ppm range sections of the integrated spectra were then given a value of the peak area as compared to the initial value of 1 for its first VFA range peak area. This allows for a comparison of the peak area for each sample for their different ppm range section, in

terms of relative area, not absolute.

The spectral peaks found in NMR data are caused by the number of spins in the H atom (in the ^1H method), and so the peak area under the related peaks for each compound is correlated to the concentrations of that compounds within the sample, due to the unique spin frequency of the H atoms in the chemical structure. Hence, with ranges of VFAs, sugars and phenolics given as above, it can be deduced that these integrated peak areas are directly proportional to the concentration of these group of organics within the respective samples [166], [167]. This analysis used the *relative* concentration determination, rather than the *absolute* concentration determination, as there were no samples run to quantify the peak areas with, due to the very complex nature of the aqueous phase samples [166].

To achieve a useful set of comparative values, the totals of all three integration values were totalled and used to find a % of the peak area for the three ranges analysed. This was done by dividing each integrated section by the total value of the three numbers, and hence converted into a percentage as demonstrated in equation 3.18. For example, using example numbers, for the sugar range of 2.75-4.5 that shows a peak area of 0.4 upon manual integration:

$$\%PeakArea(2.75 - 4.5) = \left(\frac{0.4}{(1 + 0.4 + 0.15)} \right) \times 100\% = 25.81\%, \quad (3.18)$$

So the relative proportion of VFAs in the sample is 26%. An example of the sections outlined on an NMR spectra is shown in the first analysis of an NMR spectra in detail, figure 6.16.

After the integration was performed, the NMR spectra for the three HTC temperatures were each stacked vertically on one figure for their respective feedstock. They were also colour coded, with darker tones correlating to higher HTC temperatures, and labelled accordingly. These spectra are shown for each feedstock in the appendix, figures 10.1 to 10.4 for reference.

The total amount of sugars in the sample cannot be determined from the NMR data alone, however, as it provides a semi-quantitative approach to how composition changes. The NMR analysis was useful when determining which mix of various chemical compounds can be found within the samples. However, further analysis is required to draw out

components of interest and quantify their amounts, using HPLC or GC-FID, for example.

NMR aids with forming the decision as to which compounds to search for in HPLC and GC-FID, helping to narrow down a methodology, and therefore the column choice and standards to be used for identification. The trends shown in the NMR for the different chemical compound groups can therefore give a greater overview as to the balance of chemical reactions happening within the HTP process waters at each temperature step. The overview of these different compounds found in the samples can tie together the trends found in the subsequent various liquid analytical techniques; HPLC for sugars and GC-FID for VFAs and to an extent the liquid XRF results. NMR analysis is therefore very helpful at helping to see a bigger picture of what the results show for each type of feedstock, and understand the general affect of HTP temperature on the different chemicals produced from the original wet feedstocks.

3.6.6 High Pressure Liquid Chromatography

HPLC analysis was performed to determine the amount of sugars and the formic and acetic acid content of the samples. The samples were prepared by first filtering 5ml of each sample through a 0.2 μ m syringe filter (VWR, 25mm) into a small beaker. A small amount of each sample was then added to HPLC glass vials and sealed with pre-slit lids. They were stored in the freezer until analysis. The HPLC instrument used is a Thermo Ultimate 3000 fitted with a Shodex RI-101 refractive index detector (for the sugar analysis) and an Ultimate 3000 photodiode array (PDA) detector set at 210 nm for detection of the acids (VFAs). The column type used for this analysis was a SUPELCOGEL C-610H (30cm \times 7.8 mm) with a guard column and a mobile phase of deionised water containing 0.1% H₃PO₄. The analysis run time was 45 minutes, with a flow rate of 0.5ml min⁻¹ and an injection volume of 10 μ l. The standards used to identify the main peaks in the chromatogram by retention times and were performed in order to calibrate the method and give concentrations for some key sugars and acids. Standards for mannitol (2g l⁻¹) and glucose (0.2g l⁻¹, 0.02g l⁻¹) were produced to run in the same batch as the samples to calculate the amount of these sugars within the samples. The values are given in units of mg/L for the VFAs and sugars. The sugar and acid concentrations in the samples were determined using calibration standards.

3.6.7 Gas Chromatography Flame Ionisation Detector

The Gas Chromatography Flame Ionisation Detector (GC-FID) analysis was performed on the aqueous phase samples using a column type DB-FFAP, of dimensions 30m in

length and 0.32mm in diameter, film thickness $0.5\mu\text{m}$. The detector was an FID (Flame Ionisation Detector), with a temperature of 200°C using N_2 as the make up gas. The auto sampler had an injection volume of $10\mu\text{l}$. The split mode was chosen, with a split ratio of 5:1, at 150°C . The carrier gas was He, with a flow rate of 10ml min^{-1} .

The heating rates used for GC-FID analysis is summarised in table 3.2. This method has been developed to best elute and hence identify the different volatile fatty acids (VFAs) within the samples. Note here that formic acid is not very well detected by FID, as the mechanism of detection is by (in short) the amount of carbon atoms in the molecule. As formic acid has only the sensitivity of the FID it is not good enough to detect formic acid at these concentrations. Hence the need for HPLC to detect formic acid, as HPLC is more sensitive for the formic acid.

Table 3.2 GC-FID methodology.

Ramp Rate ($^{\circ}\text{C}/\text{min}$)	Final Temp ($^{\circ}\text{C}$)	Hold Time (min)
-	60	4
10	140	0
40	200	5

The samples were prepared for GC-FID analysis by pipetting the aqueous phase samples into glass vials, through a $0.45\mu\text{m}$ filter, and securing the vials with a slit top lid. The results were provided in terms of the acid retention times, and the amounts of the identified acid within the samples. A table was subsequently produced with all the different samples analysed, with the amounts of the present acids given for each sample. The concentration of the acids were reported in units of $\text{ng}/\mu\text{l}$ and were tabulated as such.

3.6.8 Total Organic Content

The Total Organic Carbon (TOC) content aqueous phase samples for the first batch (TOC_{liq}) were prepared with the thawed HTP aqueous phase samples, diluted to one part in ten with distilled water. An auto-pipette was used to measure out 0.5ml of each HTP liquid sample and 4.5ml of distilled water. The TOC glass vials were then each given a small magnetic stirrer bar, in order to thoroughly mix the sample during analysis. The TOC machine used was a IL 550 TOC-TN (Hach). This was used with a high differential method, with a one in five dilution.

The carrier fluid was a 10% solution of H_3PO_4 . The TOC results were given in ppm

or mg l^{-1} . Bar charts were produced to show the different TOC content of each of the HTC aqueous phase samples for each subgroup of samples.

The errors were determined from the standard deviation of the results. This was given from the instrument as a standard deviation of the TOC results for the samples ran using the NPOC method, and calculated from the sum of the standard deviations of the TC (Total Carbon) and the IC (Inorganic Carbon) for the samples ran using the differential methodology

TOC Loss for BMP_{th} Calculations

For the *Fucus serratus*, additional TOC was performed on the dried aqueous phase after rehydrating with a known amount of distilled water, in order to compare any organics lost upon oven drying of the aqueous phase. Note that the *Fucus serratus* samples were selected for this experiment and the results utilised for both of the seaweed sample corrections as there was not enough *Saccharina latissima* aqueous phase samples left to perform this analysis. This TOC_{loss} helps to form reliable assumptions about the theoretical BMP value of the seaweeds, as the Boyle and Buswell equations used for these predictions utilises CHNS and TGA values of the *dried* aqueous phase. Therefore the actual BMP value given by these equations may be an underestimate due to the loss of volatiles upon heating the aqueous phase.

To determine the amount of organics lost upon drying of the solids, 10ml of the samples were dried in an evaporating dish in an oven set to 45°C , - the same temperature as the samples were dried at prior to CHNS and TGA analysis. 10ml of each sample was auto-pipetted into a glass evaporating dish and left to dry until the weight remained constant (48 hours at least). 10ml of distilled water was then added back to each evaporating dish using an auto-pipette. To achieve thorough mixing, an ultrasonic water bath was used, as well as manual stirring with a spatula. The TOC glass sample vials for the second batch were then prepared as the TOC_{liq} samples were prepared, again with a one in ten parts dilution.

Once reabsorbed and in a homogenous liquid state, the TOC analysis could again be performed on vials of the three TOC_{rehydr} samples and compared to the liquid TOC_{liq} value. This difference (TOC_{loss}) should give a good estimation as to how much volatile compounds are lost during the drying phase. Equation 3.19 was used to calculate the

TOC_{loss} as a % value, using the weights of the evaporating dishes before and after drying, and the initial feedstock weight of the samples (24g) before hydrothermal processing.

$$TOC_{loss}(\%) = \left(\frac{TOC_{liq} - TOC_{rehydr.}}{TOC_{liq}} \right) \times 100(\%) \quad (3.19)$$

This TOC_{loss} value was next turned into an integer between one and two via equation 3.20:

$$Corr.Factor = \frac{TOC_{loss}(\%) + 100}{100(\%)} \quad (3.20)$$

These three integers calculated for the BMP correction were assumed to be the same for the *Saccharina latissima* samples as well, during anaerobic digestion trials. The three values determined, one for each HTC temperature, were then multiplied with the Buswell and Boyle's BMP_{th} predicted values to take this into account (see §3.5.10 for this analysis). This is a useful step as in reality, the potential biomethane production from the HTC aqueous samples would rely on the organics contained in the as received aqueous phase, direct from the HTP reactor. So, any VFAs released upon drying - which occurs around 45°C for some short chain acids - would give an underestimate for the BMP_{th} .

3.6.9 Biochemical Methane Potential

Theoretical Biochemical Methane Potential (BMP_{th})

The elemental composition of the feedstock can be used to determine the theoretical amount of biomethane produced from the sample, known as the Theoretical Biochemical Methane Potential; BMP_{th} . Buswell or Boyle's equation were used to calculate the BMP_{th} of the aqueous phase samples, shown in equations 3.21 and 3.22 [152], [153], [168]:

$$BMP_{th}(Buswell) = \frac{22,400 \left(\frac{c}{2} + \frac{h}{8} - \frac{o}{4} \right)}{12c + h + 16o} \quad (3.21)$$

$$BMP_{th}(Boyle) = \frac{22,400 \left(\frac{c}{2} + \frac{h}{8} - \frac{o}{4} - \frac{3n}{8} \right)}{12c + h + 16o + 14n} \quad (3.22)$$

where the c, h, n and o values are the molar fractions. The CHNO values used in this equation were determined on a dry basis; taking into account the moisture content using

the % M from the TGA analysis.

The Volatile Solids (VS) values were derived from the % fixed carbon (FC) plus the % volatile matter (VM) of the dried aqueous phase from previous TGA results. The weight loss on evaporation of the aqueous phase in an oven was used to normalise these figures to account for any moisture content left in the dried residue. The ‘Correction Factor’ was determined using the TOC_{liq} and TOC_{dried} (after the drying and subsequent rehydration) of the three *Fucus serratus* samples and are assumed to be the same for *Saccharina latissima* for the respective HTC temperatures. The VS:COD ratio was determined using the measured COD value (g/l) using the COD Hach kit.

The BMP_{th} values were then calculated using both the Boyle and Buswell equations and converted using the VS:COD ratio for each sample, from units of VS into units of grams per COD. At this stage, the TOC_{loss} ‘Correction Factor’ was multiplied by the BMP_{th} Boyle and Buswell derived values to give a higher, more accurate estimate, to take the lost organics during drying into account. This method assumes that the same proportion of the organics lost due to the drying stage of the aqueous phase are in the same proportion as the organics measured in the CHNOS analysis, although they are made up of shorter acids and therefore have a slightly different average carbon, hydrogen, oxygen and nitrogen proportions than perhaps the whole mix of organics compounds found within the aqueous phase samples.

Due to the presence of nitrogen in the process waters, Boyle’s equation was expected to give the most accurate BMP_{th} for the samples. This calculation will, however, only produce a maximum theoretical value, most likely an over-estimate, due to it neglecting the the non-biodegradable fractions of the CHNO elements within the samples.

These Boyle and Buswell BMP_{th} values essentially give an absolute maximum value as to what the biomethane production could potentially be given a 100% conversion rate. Therefore in theory it can be deduced which feedstocks would produce more biomethane, if they have higher BMP_{th} . However the actual biomethane produced may not be as high as these BMP_{th} values calculated. The Biodegradability Index (BI) helps take this into account. First, though, the underestimation of these BMP_{th} values due to the prior drying of the aqueous phase can be considered.

Comparisons between the different BMP_{th} of the samples may indeed give an accurate representation of the BMP produced in reality, as the trend should follow the theoretical

potential given by Boyle's equation, so it is interesting to study whether or not the trend in the experimental BMP correlates with the hypothesised trends from the BMP_{th} values. However other factors affect the biodegradability of the feedstocks, such as any inhibitive phenolic compounds present, for example. Using experimental results, the theoretical values for the BMP can be compared to the actual experimental results, and hence the biodegradability of the samples can be determined.

Experimental Biochemical Methane Potential (BMP_{ex})

Using a bench scale anaerobic digester, the experimental Biochemical Methane Potential (BMP_{ex}) from the aqueous phase samples of the two 100% seaweed feedstocks could be determined. The process waters were each diluted a specific amount in distilled water depending on their Chemical Oxygen Demand (COD). These were then added to bottles with bacteria, and loaded onto the AMPTS II batch reactor. The samples were stirred periodically and kept heated to 37°C in a water bath for just over two weeks to anaerobically digest.

This two week timescale was selected for a few key reasons. The main reasoning was that in a large scale biorefinery site where the continuous HTC reactor would output some aqueous phase, having to store this liquid for much more than two weeks would cause a significant bottleneck situation in the smooth running of the biorefinery. Also, most of the sugars should have digested by that point in any case, and any residual liquid may be recirculated into the HTC, sold as fertiliser or into industry, so would not be wasted. How the aqueous phase samples react within a short period of time is within the most interest for this research, for scalability for a continuous biorefinery concept. If major changes were happening around the two week mark, the experiment would continue until any new activity settled. As it transpired, the SL samples were ran for seventeen days, and the FS samples ran for fifteen. It was expected that most of the bacteria would have finished digesting the available sugars faster than normal seaweed feedstock with no prior HTC treatment, due to the longest step in the AD process, hydrolysis, already having occurred during the HTC process.

The BioprocessTM Automatic Methane Potential Test System (AMPTS II) was used for this experiment. This small scale anaerobic digester is made up of three different parts all connected up as shown in figure 3.4. A thermostatic water bath was used to maintain the samples at the chosen temperature (37°C) and hold the batch reaction glass bottles in place, with a fitted lid to prevent any evaporation of the water. 500ml of water was

contained in the bath. Lids containing an automatic agitator to stir the sample were each added to the reactor vessels. These were programmed to mix the contents every ten minutes throughout the two weeks, on each occasion for a period of sixty seconds of continuous stirring.

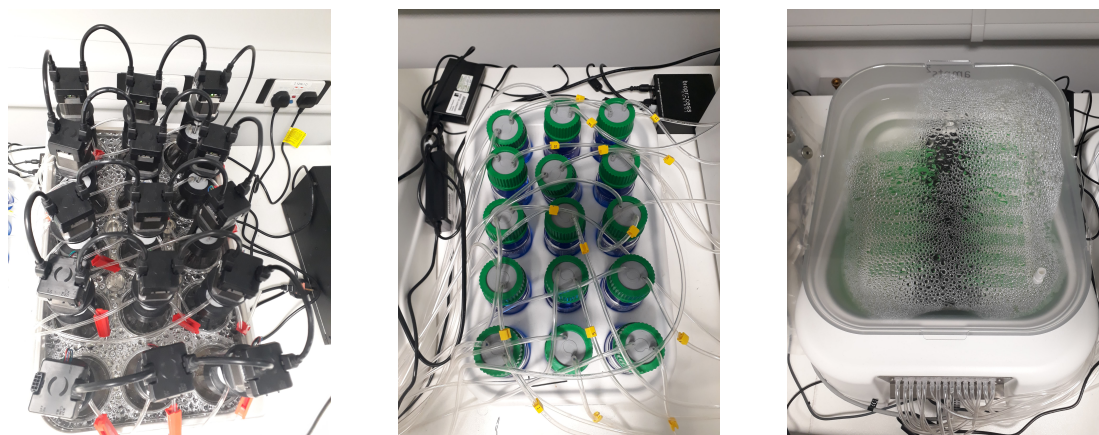


Fig. 3.4 The samples in the water bath with the automatic stirrers and tubing connected to the CO₂ fixing unit, and then onto the gas volume measuring device.

Also contained in the lid of the bottles were tubing systems for gas input and output from the headspace. These tubes were connected to the CO₂ fixing unit, containing corresponding bottles holding 80ml each of 3M NaOH solution, which absorbs the non-methane gases via diffusion. The tubes then went on to connect to the third component of the AMPTS II system; the gas volume measuring device. Any residual methane passing through the CO₂ fixing unit passes through this device, which is submerged in water. This works by using the amount of water displaced and buoyancy when the tipping cells corresponding to each sample bottle are triggered. These tipping cells, as shown in figure 3.4, release gas when they accumulate 10ml of methane. The instrument normalises the gas to be measured in standard conditions (0°C, 1 atm and 0% humidity). The information on how often each tipping cell released gas was recorded on the computer software and the biomethane production data for each sample was also shown in real-time.

The AMPTS II system had enough space for fifteen sample bottles, which with two standards required left thirteen spaces for samples. The samples were each ran in duplicate. The 500ml glass sample bottles were designed to fit 400ml of liquid sample, leaving 100ml for the headspace.

Chemical Oxygen Demand (COD)

The Chemical Oxygen Demand (COD) for each sample was calculated using a UV Spectrophotometer connected to a Hach Lange Lasa 100 heating block. The amount of COD in the sample demonstrates how much oxygen is required to oxidise completely. This correlates to the organic matter content. Hach Lange cuvettes were used to measure the COD, in which the samples become fully oxidised by potassium dichromate, sulphuric and mercury sulphate. The digestion block used for this analysis was the Hach HT200 S, and the measurements performed using 605nm wavelength UV-Vis spectrophotometry (Hach DR3900). The resultant COD values were used to determine the appropriate dilution in order to have the same COD l⁻¹ for each sample, so the results were more easily comparable. The COD per litre value was determined for each sample, the inoculum and the control cellulose, and this value was used to work out the amounts of each required to result in a 1:1 ratio of inoculum to sample (or cellulose, for the standard), in terms of their COD l⁻¹. The samples were diluted to make up to 200ml with equal COD l⁻¹. Then 200ml of distilled water was added to this, to make the total volume up to 400ml for the glass duran bottles.

The *Inoculum* was sourced from Esholt Wastewater Treatment Works, ran by Yorkshire Water and located in Esholt between Bradford and Leeds. The concentration of the diluted sample was used to quantify the volume of biomethane produced in terms of ml CH₄g⁻¹ COD. The experiment ran for at least thirty days, or until the BMP was less than 1% of the total methane already produced from the prior three consecutive days. A blank digestion of distilled water and *inoculum* (1:1 ratio) was ran alongside the samples, to determine the biomethane production for the *inoculum* on its' own. Cellulose was also ran as a standard, diluted with a 1:1 ratio with distilled water which should have produced between 300 and 500ml CH₄g⁻¹ within the two weeks. This is to ensure that the bacteria digests as normal, as if there were inactive bacteria, this would yield incorrect BMP results and the experiment would require restarting. Before the start of the experiments, the reactors were flushed with nitrogen gas in order to flush out any residual gases or air, to ensure the reactions were all anaerobic.

In order to determine the total biomethane production of the sample for any given day and the final total BMP_{ex}, the cumulative BMP amount was deduced from the data. This was calculated using equation 3.23 and given in units of ml CH₄g⁻¹ COD.

$$BMP_{ex} = \frac{V_{CH_4s} - V_{CH_4b}}{COD_{conc} \times V_{added}} \quad (3.23)$$

Where V_{CH_4s} is the Volume of CH_4 from the sample (ml), V_{CH_4b} is the Volume of CH_4 from the blank (ml), COD_{conc} is the concentration from the COD result (units of $g\ l^{-1}$) and V_{added} is the Volume of the sample added in litres (0.2l). Hence, the biodegradability index (BI) of the samples were subsequently determined using the BMP_{ex} values with relation to BMP_{th} using equation 3.24;

$$BI = \frac{BMP_{ex}}{BMP_{th}} \times 100\% \quad (3.24)$$

Therefore, the relationship between both the theoretical BMP and the experimental BMP can be further evaluated for each sample. The BMP_{ex} trends are used to help investigate the potential for the use of the seaweed HTP process waters for further biofuel production.

The BMP theoretical and experimental results are discussed in chapter 7, using the methods and calculations outlined in this section. The results from the BMP_{ex} of the *Saccharina latissima* and the *Fucus serratus* HTC aqueous phase samples are compared and contrasted, along with differences in the calculated BMP_{th} of their respective BMP yields. Overall suitability of the AD process to be incorporated within a HTC-based biorefinery is evaluated in chapter 7. In addition, the total energy balances of the HTC hydrochar HHV values and the corresponding biomethane yields from the HTC aqueous phase samples are determined and discussed.

3.7 Energy Balance Calculations

In order to comprehensively evaluate the energy efficiency of hydrothermally carbonising the feedstock and then using the process waters to produce biomethane, the hydrochar yield and process water yield and the respective energy density of the product streams need to be determined. The HHV from the hydrochar was multiplied by the hydrochar yield to give the Energy Output from Hydrochar, EO_{char} , using equation 3.25. This is based on 1kg of dried feedstock, using the same solid loading ratio used in this study of 10%.

$$EO_{char} \left(\frac{MJ}{kg} \right) = Hydrochar_{yield}(\%) \times HHV \left(\frac{MJ}{kg} \right) \quad (3.25)$$

The amount of biomethane produced from the two seaweed BMP experiments were then taken into account, with their respective process water yields, scaled up the 1kg dried feedstock representative amount. This energy output from BMP, (EO_{BMP}) was calculated using equation 3.26, using the COD/l and BMP_{exp} results, and dividing by

1,000,000 to convert to the correct MJ Kg⁻¹ units. The total Energy Output (EO_{tot}) is then determined via the addition of these two values (equation 3.27).

$$EO_{BMP} \left(\frac{MJ}{kg} \right) = \frac{PW_{yield}(\%) \times COD(g/l) \times BMP_{Exp} \left(\frac{mlCH_4}{gCOD} \right)}{1,000,000} \times 39.8(MJ/m^3) \quad (3.26)$$

$$EO_{tot} \left(\frac{MJ}{kg} \right) = EO_{char} + EO_{BMP} \quad (3.27)$$

Using 1,500 as the specific heat capacity for biomass, the overall energy input was determined, which differs for each feedstock depending on their eventual HTC temperature. This [HTC] value was either 150, 200, or 250°C for this study. The residence time was the same for all samples at 60 mins. Although the 1,500 J/kg/K specific heat capacity was an assumption based on different biomass SHC in the literature, any variation in this true value will not affect the total energy input (EI) significantly, due to most of the energy required to heat the contents of the reactor up being due to the large amount of water in the reactor. Hence, the energy input may be reduced by increasing the solid loading ratio, for example from 10% to 20%. Equation 3.28 was used to determine the different EI values for the samples, converting to the correct units of MJ kg⁻¹.

$$EI \left(\frac{MJ}{kg} \right) = \frac{((PW_{vol} \times SHC_{H_2O}) \times (Wt_{bio} \times SHC_{bio})) \times \left(\frac{(HTC_T - 25)}{SHC_{bio}} \right)}{1000} \quad (3.28)$$

Where; PW_{tot} is the total Process Water in L (10 L), SHC_{H_2O} is the specific heat capacity of water, 4.2 KJ/kgK (assuming that the process water has the same SHC as 100% water for this calculation), Wt_{bio} is the dried feedstock weight of the biomass (1kg), SHC_{bio} is the specific heat capacity of the dry biomass feedstock (assumed to be 1.5 kJ/kgK for this feedstock) and HTC_T is the maximum HTC temperature for the sample, either 150, 200 or 250 °C and the ambient temperature is assumed to be 25°C[169]. The HHV of methane is given as 39.8 MJ/m³ [170]. The overall net energy from the samples, the Energy Balance (EB), was then determined via equation 3.29;

$$EB \left(\frac{MJ}{kg} \right) = EO_{tot} - EI \quad (3.29)$$

These results are shown in table 7.3 in chapter 7. It is regretful that this cannot be calculated for the MSL feedstock due to a lack of process water left, and no more

Miscanthus feedstock left to produce more MSL process water. There are a number of assumptions that were made during the energy balance determination. These are;

- 1ml of process water weighs 1g
- The specific heat capacity of the biomass is 1,500 J/kg/K
- The energy input for heating the anaerobic digester was negligible.

Note that the energy input can be significantly reduced in practise by using a continuous HTC reactor rather than a batch reactor, and using sufficient insulation, and any residual heat to maintain the AD reactor at 37°C via heat exchange pipes for example. Lin et al found that the energy efficiency of the HTC reactor can be improved by 56.9% using pre-treatment heat recovery [169]. Also, this assumes that the seaweed is not dried prior to pre-treatment. Note that any energy required in the cultivation, harvesting, transportation, milling and processing of the feedstock is also omitted in these calculations, so the energy input may be an underestimate of the real overall life cycle analysis assessment of the energy input.

The overall energy balance is therefore an approximation, and should be treated as such. These energy balance calculations include certain values that can be changed to significantly improve or reduce the values, such as solid loading ratios. Further work may be done to improve the energy output, and other considerations included to make these values more accurate, for example determining the energy balance per day, based on a 24 hours using a continuous, heavily insulated HTC reactor using 1kg of feedstock every hour (hence no need to re-heat the reactor). The general trend in the different HTC temperature feedstock can however be viewed as accurate.

Chapter 4

Hydrothermal Processing - Mass Balances

4.1 Introduction

In this chapter, the main HTC process in the reactor of the feedstock will be evaluated. This entails the mass balances of the different solids and aqueous phase in the resultant slurry after HTC processing. The different feedstocks will have different levels of solubility and polymerisation rates, and therefore differing hydrochar yields. The most suitable feedstock for the HTC concept shown in figure 4.1 would have sufficient yields of hydrochar (roughly 50% by weight or more), yet also a suitable amount of aqueous phase left for further processing via AD. Therefore, the mass balances must be analysed and evaluated to ensure the most suitable feedstocks are identified, and their product streams more thoroughly analysed in the following chapters.

The bar charts within this section show the mass balances, as received, of the various different feedstocks after HTC processing. These mass balances are grouped in accordance with their type of feedstock; lignocellulosic model compounds, seaweed model compounds, 100% pure biomass feedstocks and finally the co-processing mixed biomass feedstocks. The two different groups of model compound mass balances are shown in §4.3 and §4.4. The third grouping is for the pure biomass samples (§4.5), which consisted of two seaweeds (*Saccharina latissima* and *Fucus serratus*) and one terrestrial biomass; *Miscanthus*. These HTC runs were 100% made up of each feedstock, unlike in the final feedstock group discussed, in which the *Miscanthus* samples were mixed before hydrothermal carbonisation, or were ‘co-processed’ in §4.6.

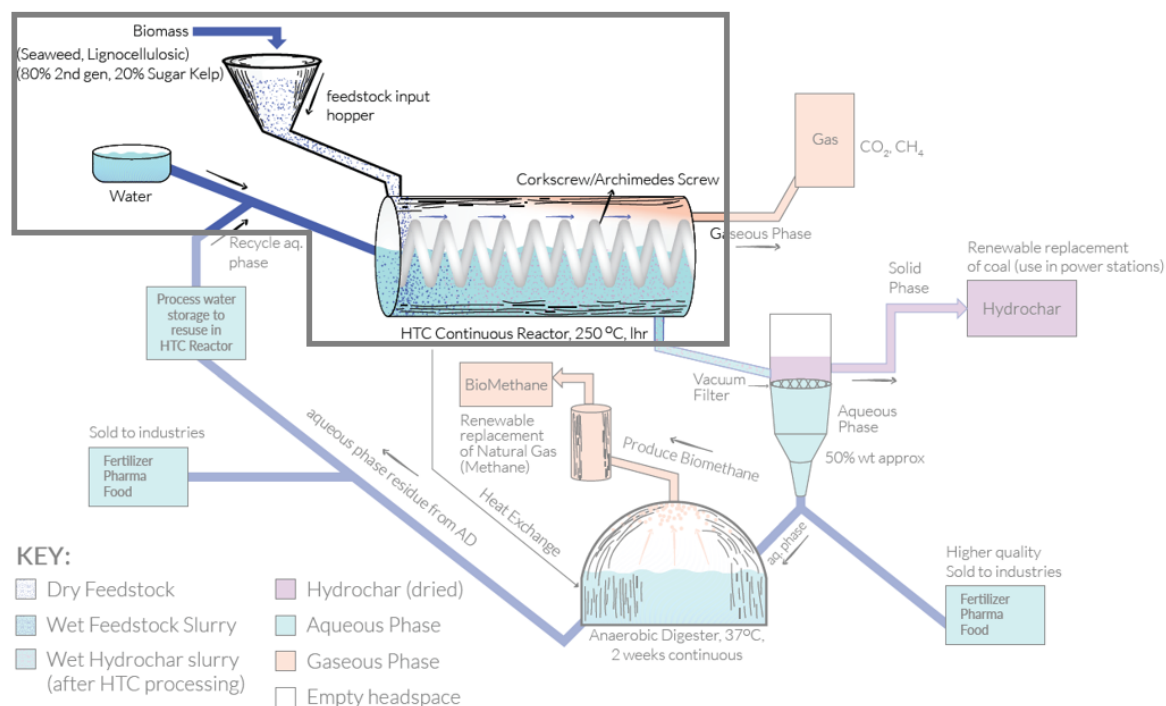


Fig. 4.1 A section of the biorefinery concept from figure 1.3, highlighted to demonstrate the aspect of the overall process focussed on in this chapter; the HTC processing of the feedstocks.

For the small scale batch HTC processing of the feedstocks, the initial weight of dry feedstock totalled 24g and was mixed with 220ml of distilled water, as described in further detail in the HTC methodology section §3.3.1. The initial solid loading ratio was: $\left(\frac{24}{24+220}\right) \times 100\% = 9.84\%$. This is in terms of the dried and milled biomass ‘as is’, and is the standard solid loading ratio for this sized reactor used in the Leeds University HTC research group. Some gas was produced, due to the reactions taking place inside the HTC reactor, as is represented by the small light blue fraction on the right hand side of the bar charts. The aqueous phase solubilises the polar organics and some of the soluble inorganic metals from the feedstock as the material breaks down, increasing the density of the water, as expected. However its overall weight fraction may be reduced. This is due to evaporative losses from the water phase, causing an apparent increase in the gaseous fraction. It is generally accepted and understood that the gaseous products during HTC of biomass consists of CO_2 , H_2 and CH_4 .

In order to aid detailed comparisons of the composition changes in the hydrochar and the process water (PW) with HTC temperature for the different feedstocks, correlations

between yields are presented as a function of HTC temperature for each of the feedstock, as shown in figure 4.4, for example. These correlations depict the mass balance in terms of the starting 24g of feedstock; how much as a fraction of the mass of this sample ends up in the solid hydrochar fraction, and how much resides in the PW fraction after HTC, due to the presence of some soluble components in the feedstock. This was determined by evaporating 10ml of the PW in an oven and using the leftover mass to calculate the % yield of the PW. This yield value was used as an average for the whole of the process water, and hence the total mass of the residual components from the feedstock dissolved within the process water was determined. Finally, this was calculated as a percentage of the initial 24g of feedstock. It is important to note here that due to the use of the drying oven at 45°C to determine the yields of the process waters, some short chain fatty acids may have evaporated at this temperature, leading to mass loss not due to H₂O loss itself. Hence, the %PW determined for these graphs may be a slight underestimate. For further details on how the mass balance in terms of the initial feedstock was calculated, see §3.3.2.

4.2 Preliminary Data

Initially, three 100% *Saccharina latissima* runs on the HTC reactor were performed for each HTC temperature, to determine reliability and repeatability of the data, in terms of mass balances and yields. The weight of the hydrochar and the aqueous phase yields were determined for these triplicate runs. The results, shown in figure 4.2 along with the error bars demonstrate that the error margin is sufficiently small, at a range of +/- 2.0% for the aqueous phase % weight at 250°C, down to +/- 0.64% for 200°C, and with a maximum standard deviation of +/- 0.07% for the solids % weights. In terms of actual weights measured, the solid phase weights did not differ more than 0.4g and the aqueous phase samples did not vary in excess of 7g, though and most weights measured were within 4 g of each other.

Therefore, the HTC runs henceforth may be performed to a sufficient level of error for this study in singlet. Running the experiments in singlet will maximise the combinations of feedstocks and temperatures able to be ran in the HTC reactor. This is due to time efficiency and also reducing the overall resources required, whilst maximising the variety of different feedstocks and model compounds that could be used for this study, - of which some key feedstocks were limited, and some model compounds were only available in limited quantities and/or expensive to purchase. Hence, the HTC runs were performed

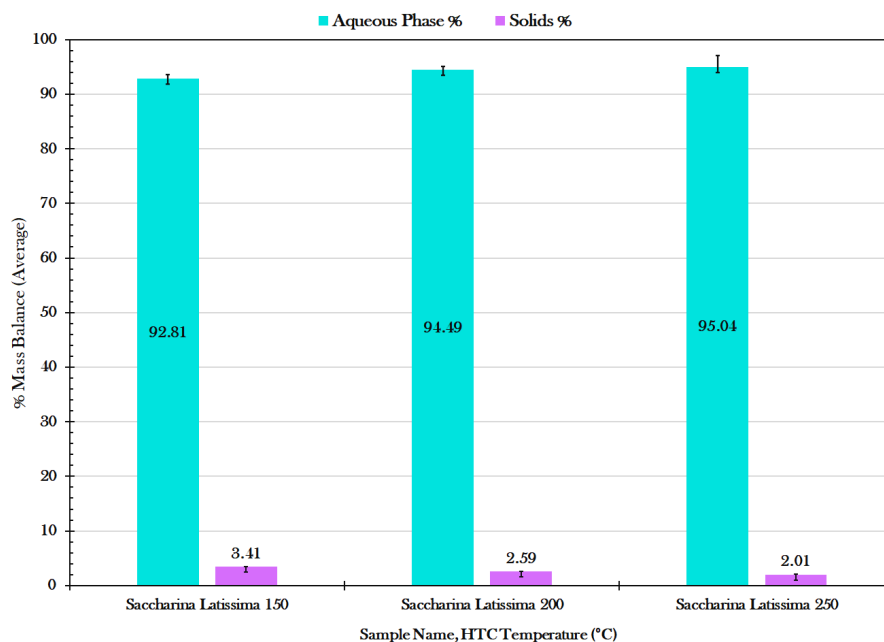


Fig. 4.2 The average percentages of the aqueous phase and solid products after HTC for three different HTC temperatures for *Saccharina latissima*, ran in triplicate. The error bars shown were determined using standard deviation.

in singlet for the remainder of the study.

In terms of the analysis of the hydrochars and the aqueous phase sample post-HTC, the CHNS was performed in duplicate, the TGA singly and the TOC, NMR, HPLC, GC-FID and XRF analysis were also performed singly. The BMP experiments were performed in duplicate.

4.3 Lignocellulosic Model Compounds

The mass balances, in terms of as received after opening the HTC reactor and weighing the contents, are shown for the lignocellulosic model compounds in figure 4.3. These results are further interpreted in terms of how much of the original 24g of the feedstock remain dissolved within the aqueous phase, or remains in solid form as hydrochar. This was calculated using the dry weights and the evaporated yields of the process water (see §3.3.2 for details). These yield values are shown as a fraction of the feedstock processed, i.e. how much by weight of the original dry feedstock remains in the solid phase or aqueous phase. It is presented respective to the HTC temperature (150°C, 200°C or

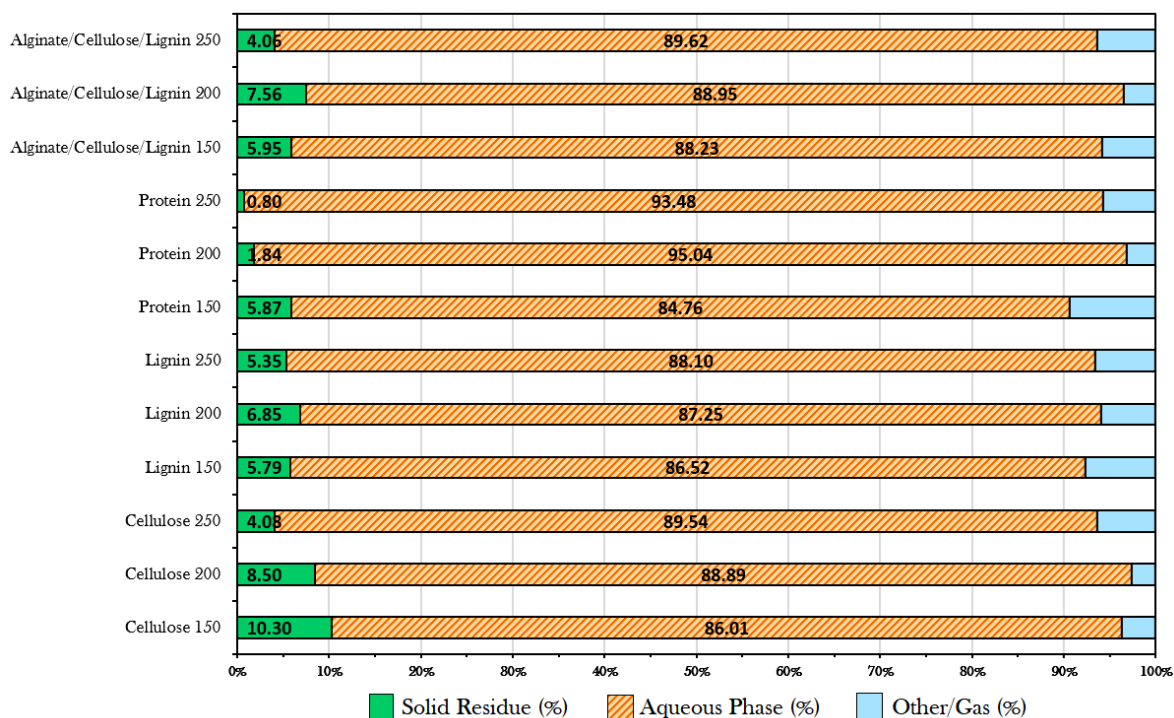
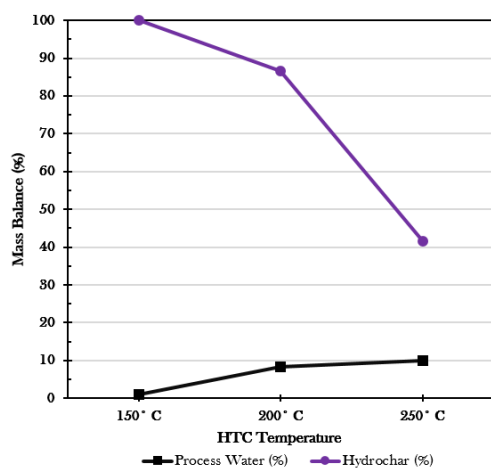


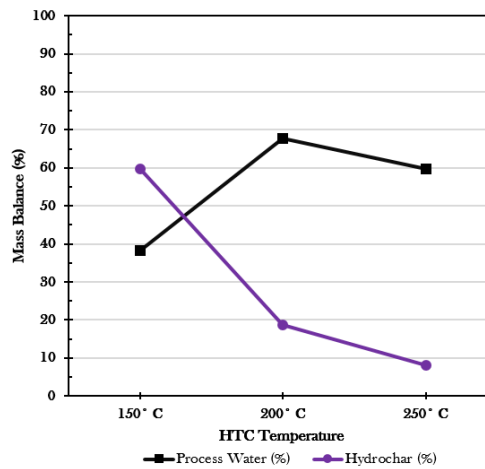
Fig. 4.3 Mass Balances as received for the lignocellulosic model compound feedstocks after hydrothermal carbonisation, for each of the three HTC temperatures, each held for one hour. This includes the 220ml of added water. The mixing ratio of the ACL mix (sodium alginate, cellulose and lignin) was 20:40:40 respectively.

250°C) in figures 4.4 (a) to (d) for each of the lignocellulosic model compound samples. This is performed for each of the four groups of feedstocks and are used to interpret the HTC yields and mass balances results.

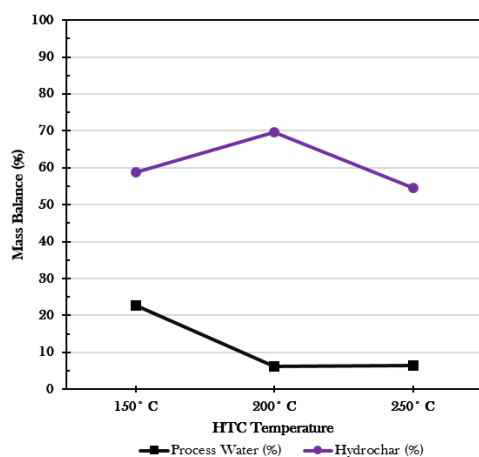
From the fraction of the feedstock that remains in the char vs the PW (figure 4.4), both cellulose and lignin have most of the feedstock remaining in the solid phase rather than becoming solubilised in the liquid phase. The only exceptions to this rule is the protein for 200°C and 250°C. For use as a coal replacement for the hydrochar end use, having most of the carbon in the feedstock remaining within the hydrochar is indeed preferred. However overall char yield and HHV must also be considered and the potential for using the process waters as an extra means of profit or as a biofuel must be considered. Hence, a good balance between organics solubilised within the aqueous phase and the feedstock remaining mostly in the solid phase as high HHV hydrochar would be the ideal post-HTC mass balance. Thus, the cellulose, lignin and the A/C/L mix all match this requirement, more so at the 250°C HTC temperature. These



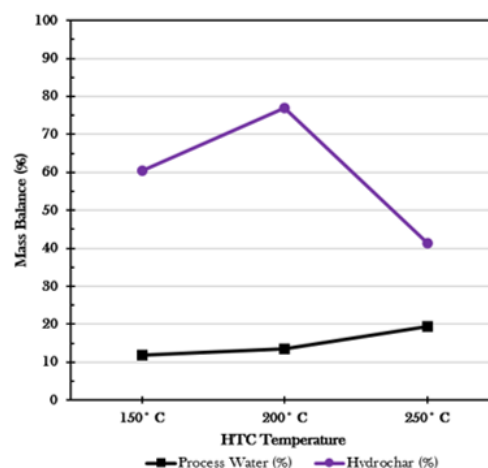
(a) Cellulose



(b) Protein



(c) Lignin



(d) ACL

Fig. 4.4 Mass Balances of where the chemical compounds from the initial feedstock end up, for the process waters and the hydrochars, for the four different lignocellulosic model compounds feedstocks. This is based on the fraction of feedstock processed. The mixing ratio of the ACL mix (sodium alginate, cellulose and lignin) was 20:40:40 respectively

results suggest that feedstocks that are rich in protein do not favour hydrochar production.

The protein structure, as evident by figure 4.4b, breaks down largely between the temperatures of 200°C to 250°C and this process produces amino acids. The protein hydrolyses into smaller peptides and individual amino acids. The kinetic energy of the molecules in the superheated water disrupts the hydrogen bonds in the protein. These amino acids usually remain stable until they exceed temperatures of 200°C. The heat from the HTC

process will have disrupted the hydrophobic interactions in the protein, meaning that as temperature increases, the more hydrophilic amino acids are present, and hence more organic compounds from the protein would become solubilised in the process water. Some of the amino acids created during the HTC process have groups that will become ionised in more acidic conditions. As the subcritical water increases in temperature, the water acts as a solvent and decreases the pH. At the temperature range studied in this research, the proteins will denature, which is what we have seen here, as the protein breaks into the amino acids [171]. This will be further investigated in the characterisation of the hydrochars and aqueous phase in the following chapters.

The way that cellulose and lignin breaks down under hydrothermal conditions is not via denaturing, but via hydrolysis. The term used for the hydrolysis of cellulose is Cellulolysis. This is the “process of breaking down cellulose into smaller polysaccharides called cellodextrins or completely into glucose units” [172]. Cellulose is quite resistant to hydrolysis, unlike other chemical compounds found in plants such as starch and hemicellulose, which generally would degrade easier. As the water becomes more ionic when it is heated under pressure during HTC, this cellulolysis would be more likely to occur, as the ions in the water can cause the strong molecular bonds within the cellulose to break and degrade into the glucose units [172]. Glucose, as a sugar, is water soluble and therefore, as expected, as the temperature of the HTC increases, the rate of cellulolysis intensifies and the proportion of the feedstock remaining in the liquid phase post-HTC increases to about 10%, whilst the fraction remaining in the hydrochar reduces significantly; from almost 100% at 150°C to just over 40% at 250°C.

As shown in figure 4.3, cellulose at 150°C has the highest amount of solid phase yield from any of the samples after hydrothermal processing, at any temperature, 10.3%. The solid phase here however, is not quite hydrochar, as it has not reacted to form the carbon-rich char at this temperature yet, - the cellulose is difficult to break down at these lower temperatures. This is also true when compared to all the feedstocks tested throughout this study. This is again caused by the strong molecular bonding in the cellulose that require ionic solvents under the right conditions to break. Hence, although the cellulose is the most stable in terms of the solid phase remaining as solid residue; with the right conditions under hydrothermal carbonisation, some of the organics can be broken down and become solubilised in the aqueous phase. However, enough of the organics remain within the solid phase, and at an even higher heating value, for the hydrochar of cellulosic materials to be considered as a suitable fuel source, with a useful sugar rich aqueous phase as a profitable by-product in addition. Cellulose is the main

component of *Miscanthus*, at a composition of around 40% (w/w) and has similar values in other terrestrial biomass feedstocks. It is this quality in fact that makes the plant or crop viable for biofuels; the high sugar content can be transformed into bioethanol, for example, and so the way cellulose reacts and breaks down in the HTC process is not something that can be ignored. This research will analyse the effects of mixing the high sugar containing seaweed species *Saccharina latissima* with *Miscanthus* and hydrothermally carbonising it, therefore it is helpful to recognise how cellulose as a sole feedstock will break down under HTC conditions.

Lignin is one of the main problems with terrestrial type biomass within the biofuels industry. Its rigidity and fibrous qualities, and its reluctance to rot, causes some feedstocks containing lignin to be unsuitable for certain techniques used to produce biofuel. It therefore would be helpful to verify that lignin molecules degrade under HTC, rendering this technology immune to the issues caused by high lignin content in terrestrial biomass. However, further analysis will see to what extent this degradation has occurred within the HTC processes here.

At 250°C, the proportion of initial lignin feedstock remaining within the hydrochar reduces to 55%, just less than the 150°C mass balance. The percentage of the feedstock remaining in the liquid phase reduces with HTC temperature, although the change in temperature from 200°C to 250°C does not seem to alter the amount, both in terms of overall PW yield, or the amount of organics solubilised within in. The degradation of lignin produces acetic acid and mainly phenolic fragments, and possibly contributes to the formation of furfural [173], which is detected in the process waters, therefore we can deduce that at least some of the lignin begins to degrade due to the higher HTC temperatures via hydrolysis. This is analysed in greater detail in §6.1.

Lignin has a large complex structure and is a polyphenolic polymer. Under normal circumstances, lignin is largely unaffected under hydrothermal conditions at the lower temperatures, however these lignin samples are pure and hence have been extracted from biomass. Therefore this breakdown seen in these HTC samples at the lower temperatures is mainly due to the fact it has been extracted. So it is important to note that Lignin might not behave in this way when processed via HTC from within a real biomass feedstock.

Lignin is not the main component of terrestrial type biomass though; it is only a component of it. So, for species with a 20% or less composition of Lignin, such as

Miscanthus, the eventual suitability of the feedstock to be used within the biofuel industry is reliant on not just the lignin's reactions during heating but its reactions within a range of other, more important, chemical components that also react in their own way. Avoiding feedstock that has bark kept on the wood (willow, for example) would reduce the overall lignin content [173], which would be helpful for bioenergy techniques such as HTC.

Although the model compounds discussed here are based on three main chemical components for lignocellulosic type biomass, the chemical components for the aquatic type biomass is somewhat different. These components will have the same job (e.g. storing energy, transporting energy), because it is grown in water, the compounds that perform these jobs differ in seaweeds. This is discussed thoroughly in the literature review and hence some model compounds from the structure of seaweeds were used for analysis.

The model compounds selected for the seaweed type feedstocks are analysed in §4.4, one of which is sodium alginate. As a mix of seaweed and terrestrial biomass is being investigated for future use as a feedstock for HTC in this research, a mix of model compounds including mostly the cellulose and lignin, were added to sodium alginate and underwent HTC. The mix contained 20% sodium alginate, 40% cellulose and 40% lignin and is referred to as the 'A/C/L mix', or 'ACL' for conciseness. It is interesting to see how these two different chemical compounds from the terrestrial and aquatic biomass types affect each other's abilities to degrade and react under HTC conditions. This mix of model compounds will hopefully help to illuminate the potential degradation mechanisms occurring during the HTC from the *Miscanthus* and *Saccharina latissima* feedstock mix as well (see §4.5).

4.4 Seaweed Model Compounds

The mass balance as received of the gas, liquid and solid phase from sodium alginate do not change notably, shown in figures 4.5 and 4.6a. There is an interesting trend to note here, as the typical yields of hydrochar and process water account for only 70%, however it is not expected to produce much gas, and therefore it appears that there is a large loss to take into account for these samples.

The fraction of the initial feedstock remaining in the hydrochar phase (figure 4.6) does not really increase from a very low amount. This is a highly soluble compound so even at room temperature, most of this compound would solubilise into the water before HTC

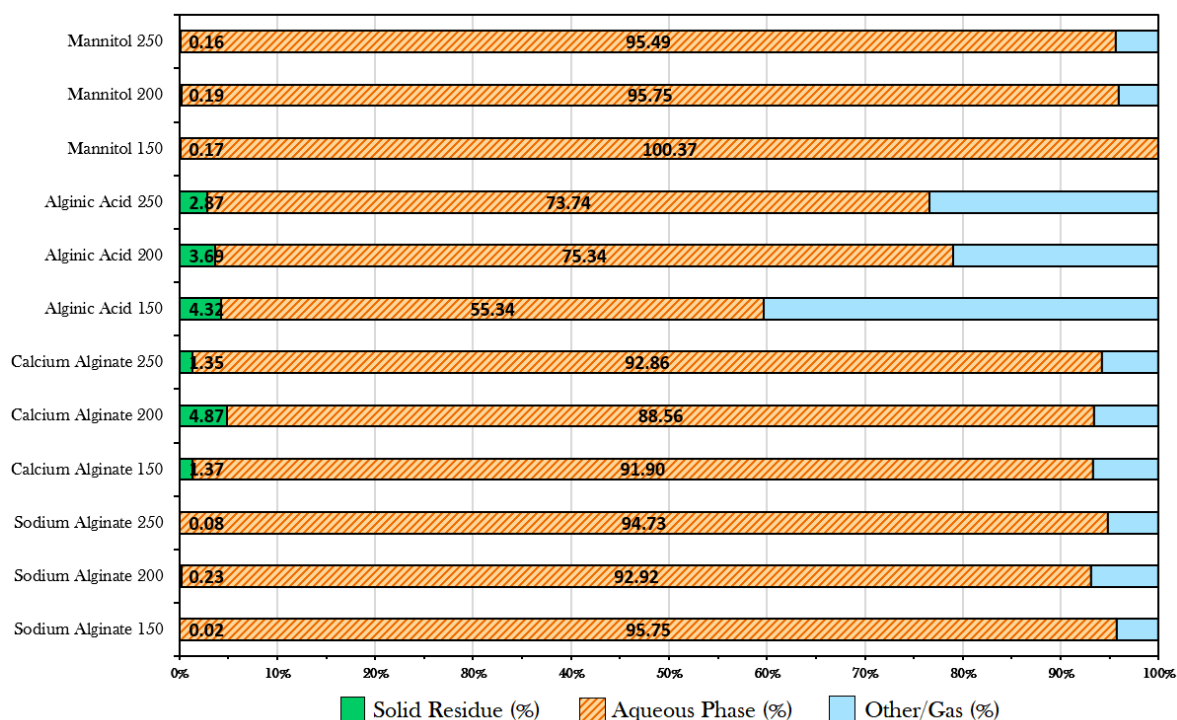
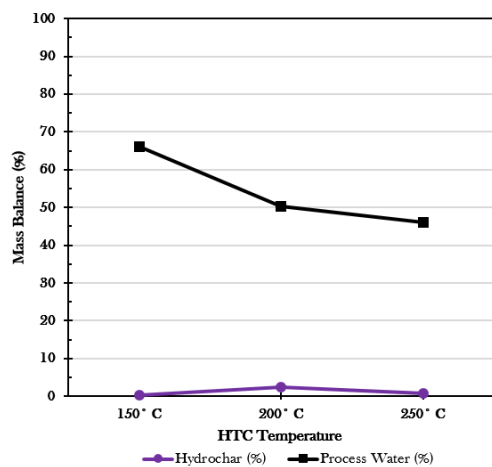
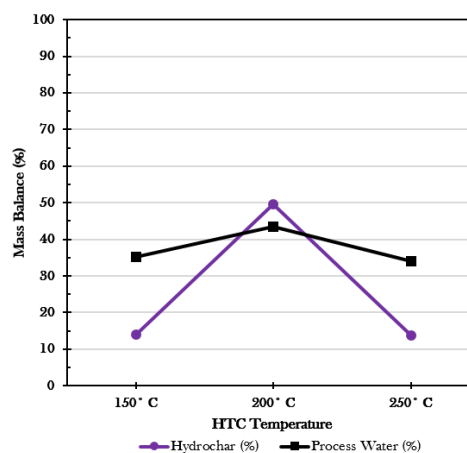


Fig. 4.5 Mass Balance as received for the seaweed model compound feedstocks after hydrothermal carbonisation, for each of the three HTC temperatures, each held for one hour. This includes the 220ml of added water.

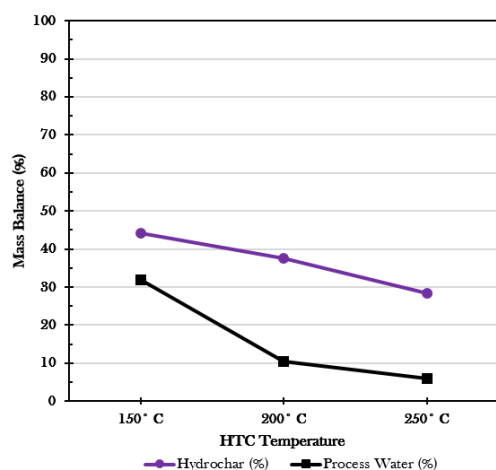
processing. After HTC it remains highly soluble, although the darkening of the process water suggest that these soluble chemicals are degradation products from the alginate as it was heated. Identification of the products found in the process waters are covered in chapter 6, but here it is the increase in solubility of the feedstock we can analyse with the yield data, compared to the char yields. As the temperature of the HTC increases, there is less solubility of the feedstock degradation products, shown by the inverse correlation of the % Process Water line in figure 4.6a. Hardly any char is produced at all from the pure sodium alginate HTC runs. The high solubility of the sodium alginate inherent in the seaweed feedstocks would have the effect of increasing the chances of having a good enough quality process water for further chemical extraction, or use as a biofuel via AD, as the PW would be sufficiently organic and nutrient rich. There are many other components of seaweed that are soluble in water, with seaweeds also containing large amount of laminarin and mannitol, which would also affect the overall solubility of the organics within the sugar kelp after HTC processing. Other model compounds found within seaweeds of course will affect this overall balance of the organic compounds from the initial biomass remaining in the hydrochar as opposed to the aqueous phase.



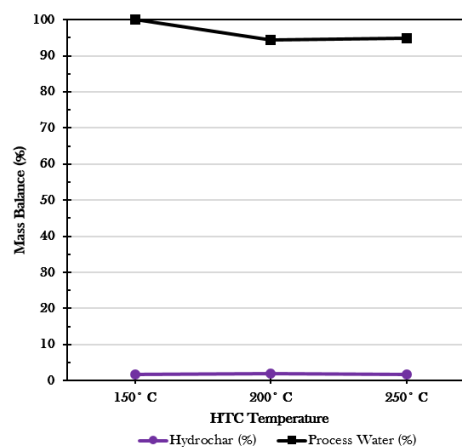
(a) Sodium Alginate



(b) Calcium Alginate



(c) Alginic Acid



(d) Mannitol

Fig. 4.6 Mass Balances of where the chemical compounds from the initial feedstock end up, for the process waters and the hydrochars, for the four different seaweed model compounds feedstocks. This is based on the fraction of feedstock processed.

In contrast to the other linear correlations, the yields from the calcium alginate HTC products has a peak in organics found within the hydrochar phase at 200°C, rising and falling from 15% to 50% of the feedstock, shown in figure 4.6b. This temperature is the only event in which a higher proportion of the feedstock ends up in the char phase rather than the process water phase. This is due to the fact that unlike the other model compounds, calcium alginate is not soluble in water. It seems that this may be caused by the polymerisation of the organics in the liquid phase below 200°C and then perhaps the solid products formed were then further degraded and broken down into smaller, more

soluble components or gaseous products at higher temperatures, residing in the aqueous phase once again at 250°C. However this requires further analysis of the process waters to understand fully.

This high char yield is mirrored in figure 4.5, where calcium alginate at 200°C has a mass balance of 4.87% hydrochar, around triple the yield for the other temperatures, and the highest of all the seaweed model compound char yields as received. The further analysis of the process water in chapter 6 will shed some light on which reactions are occurring at temperatures between 150°C and 200°C that might produce the chemicals found in the insoluble fraction, and which chemical compounds are later produced between 200°C and 250°C during HTC that are more soluble.

The fraction of the feedstock that remains in the solid phase reduces steadily with an increase in HTC temperature for the alginic acid model compound. The fraction of the feedstock that becomes solubilised into the aqueous phase also follows this downward trend, shown in figure 4.6c. In terms of the gases produced, the 150°C alginic acid HTC mass balance shows a relatively large 40% yield of gas, which would have the effect of reducing the amount of organics from the initial alginic acid compound available to remain within the solid and liquid phases. It is also interesting that the hydrochar is higher without any cation associated with the polymer. The general trend here is that alginic acid during HTC processing more readily degrades into gaseous products at lower HTC temperatures. This is due to simple decarboxylation at 150°C, but more complex reactions are possible at higher temperatures, which may in turn prevent gas formation. Carbon dioxide and methane are the main gases produced when hydrothermally carbonising biomass feedstocks, along with some carbon monoxide and hydrogen, depending on the reactions taking place. The aqueous phase and the hydrochar are the main phases analysed in this research, but further work could be done to analyse the gas fraction of these HTC reactions to further understand these findings.

Alginic acid is the only model compound from the aquatic type biomass feedstocks to consistently have a higher fraction of the feedstock remaining in the solid phase after HTC rather than the aqueous phase. This is reflected in figure 4.5, where the char yield as received is higher for alginic acid than the other samples. The alginic acid and its degradation products therefore seem to be more insoluble than the products from sodium and calcium alginate and mannitol. This higher formation of char indicates that the organics are polymerising more easily, which would agree with the understanding that the different amount of salts in the feedstock effects the degree of polymerisation. Hence when the

100% seaweed samples are analysed the proportion of the initial weight of the feedstock retained in the hydrochar may be due to the amount of alginic acid in the seaweeds. The biochemistry of seaweeds, as discussed in the literature review, can change depending on the time of year harvested, where it was cultivated or wild harvested, which species it is and its stage of growth [174], [175]. So, in order to optimise char yield, it is suggested that certain species with a large proportion of alginic acid, with the correct conditions, should be selected for HTC processing for a quality hydrochar to achieve the desired result.

For the mannitol model compound, this stable sugar predictably does not show much tendency to degrade when heated. The yields do not change noticeably and the fraction of the feedstock almost completely remains within the aqueous phase. The slight dip in the fraction of the initial mannitol weight remaining in the aqueous phase from 150°C to 200°C shown in figure 4.6d, coupled with the tiny increase in gas yield in figure 4.5 may demonstrate that some of the dissolved sugar may start to form carbon dioxide and methane at this temperature. However overall it stays mostly stable and does not seem to be the model compound causing certain break downs when seaweed undergoes HTC.

Mannitol is a stable sugar and even on evaporating the process waters in an oven for the yield calculation it recrystallizes back into its original solid phase. This further demonstrates that the compound does not break down during HTC and remains as a soluble sugar within the PW. For further use of the process water for anaerobic digestion, for example, this fraction of consistently dissolved sugar may be very useful as it can contribute to the production of biomethane. Hence the presence of mannitol within seaweed as a biomass feedstock for HTC may prove helpful in the downstream processing of the aqueous phase.

It would be interesting to analyse how the addition of mannitol to the *Miscanthus* feedstock might change the HTC yields as the mannitol may stabilise the *Miscanthus*, or it may become more unstable due to the presence of other organics in the *Miscanthus* and start to degrade more. The 100% pure biomass sample are first studied though, before the co-processed feedstocks are analysed, including this *Miscanthus*:mannitol mix and the *Miscanthus*:sodium alginate mix.

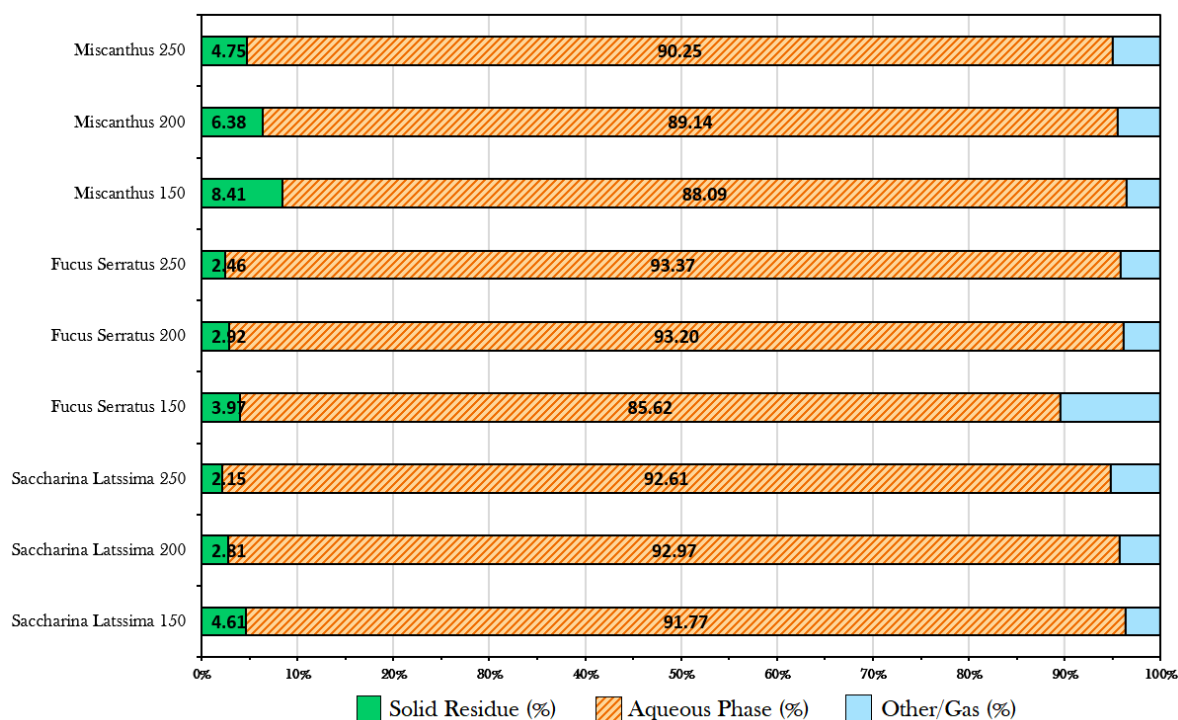


Fig. 4.7 Mass Balances as received for the 100% biomass feedstocks after hydrothermal carbonisation, for each of the three HTC temperatures, each held for one hour. This includes the 220ml of added water.

4.5 100% Biomass Feedstocks

Both of the seaweed feedstocks, as expected due to their affinity with an aquatic environment, had more proportion of the initial organics and nutrients remaining in the PW than the hydrochar phase for all three HTC temperatures, in contrast to the terrestrial biomass. This is shown in figures 4.8a, 4.8b and 4.8c for the Miscanthus with the reverse finding. Both of the seaweed feedstocks reduce in the fraction of initial feedstock remaining as hydrochar for each temperature increment for the HTC reactor. The reduction in the char yield would be due to the oxygen content becoming reduced as the temperature increases. The change in the proportion remaining in the PW phase does not alter quite so much overall, in fact it increases 10% from 200°C to 250°C for the sugar kelp, although the overall change is not much more than 5%. This may be caused by the polymerisation of some of the smaller degradation products at this higher temperature or those products may not be as hydrophilic as the larger compounds and hence there is a lower % remaining in the PW phase. The aqueous phase is further analysed in a

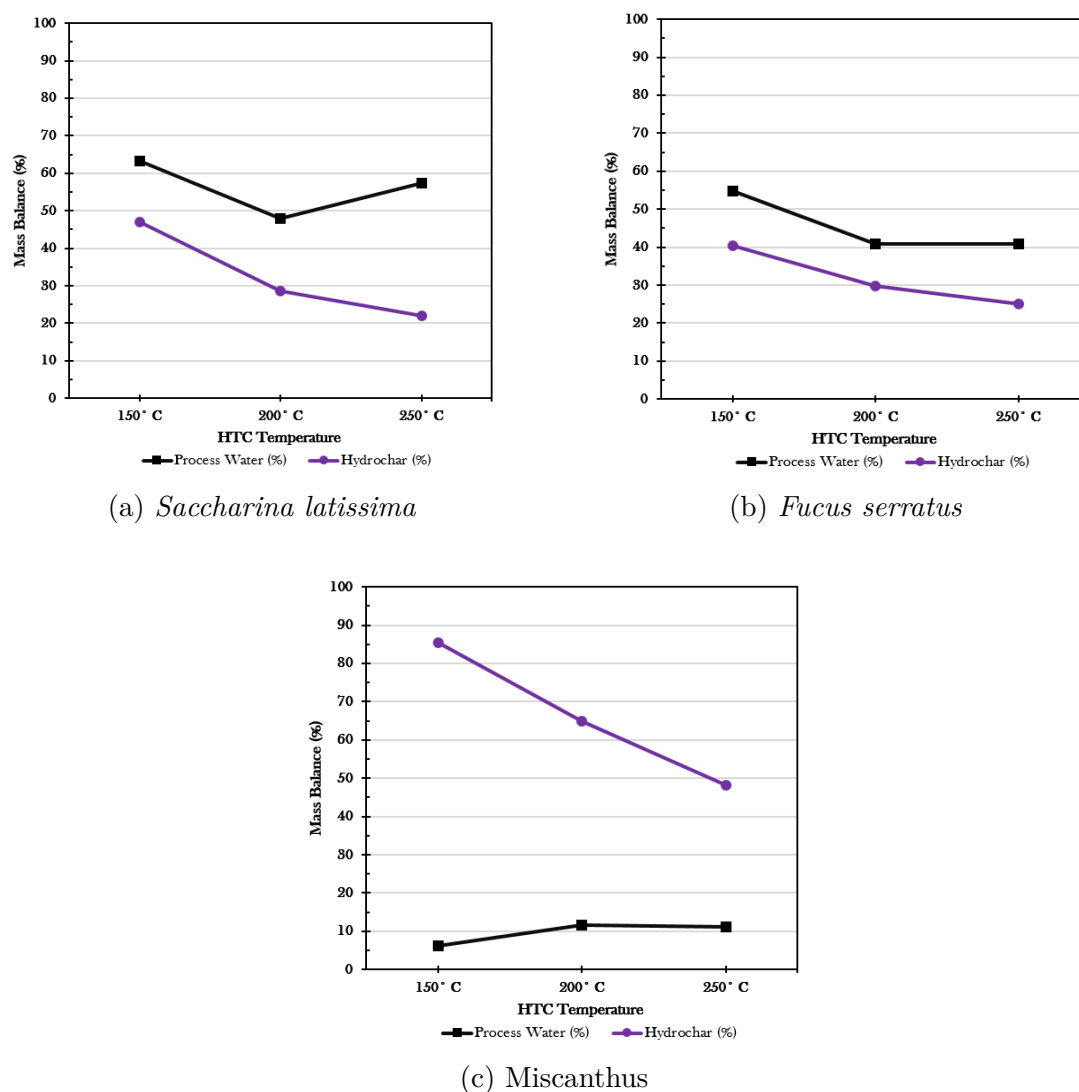


Fig. 4.8 Mass Balances of where the chemical compounds from the initial feedstock end up, for the process waters and the hydrochars, for the three different 100% biomass feedstocks. This is based on the fraction of feedstock processed.

separate chapter and the different chemical compounds found in these process waters will be identified, and the *Saccharina latissima* degradation mechanisms further understood.

The soluble fraction from the *Fucus serratus* shown in 4.8b reduces from 55% to 40% overall as T increased and therefore, its chemical compounds produced via degradation may not be as soluble as those produced from the degradation of *Saccharina latissima* under HTC. Instead, the favourable reactions taking place could be more extreme polymerisation at higher HTC temperatures, leading to an increased proportion of hydrochar (with more secondary char formed). This difference at the 250°C yields for the two seaweed feedstocks may be due to differing biochemical components in the species. Overall the *Fucus serratus* feedstock shows similar biomass qualities as the sugar kelp but with slightly lower solubility of the process waters.

The *Miscanthus* does indeed have a higher char mass balance yield, although it has process waters depleted of organics (11% or less for all three temperatures). The inverse correlation of the fraction of the initial feedstock weight resulting in hydrochar formation with HTC temperature (figure 4.8c) is not ideal on the surface for biofuel end usage for the higher HTC temperatures. However, the energy density of the char will be greater due to the increase in its HHV at the higher temperatures. Although the char should have most of the carbon from the feedstock remaining in it - rather than the PW - in order for it to be a suitable fossil fuel replacement. It remains true that the process water requires enough organic content and/or nutrients solubilised within it to provide another profit stream from biomethane production to further chemical extraction or sold as fertiliser. Hence, a balance between the *Miscanthus* and the seaweed yields should be met, with a ratio of 80:20 respectively seeming the appropriate value. This 80:20 co-processed mix is analysed in §4.5.

Some gas is produced by all three biomass samples, shown in figure 4.7, so perhaps the reduction in both the soluble and insoluble fractions may be explained by the rise in the organic gas yield after undergoing the HTC process. The organic acids produced during HTC may have degraded so much that they produce some gases, or some really short chain fatty acids may have escaped the reactor upon opening even at room or body temperature levels. The overall point to note is that the seaweeds have more feedstock remaining in the water than the hydrochar, which is not ideal if the main bioenergy is from the char. Nevertheless, the different pattern found for the *Miscanthus* is a better scenario for the biofuel industry, although the addition of some seaweed to the *Miscanthus* as a HTC feedstock may promote some organics and nutrients to find their way into the aqueous phase; thus creating a secondary product of enough quality able to undergo AD.

The following section 4.5 will investigate the co-processing mixes to see where this char and PW yield is as expected for an 80:20 *Miscanthus:Saccharina latissima* mix from the organics and what additive or inhibitory qualities the seaweed, sodium alginate and mannitol may have on the resultant yields and soluble/insoluble fractions. Perhaps the metals within the seaweeds catalyse some of the reactions occurring during the degradation of *Miscanthus*, resulting in an even higher % of organics solubilised in the process waters.

4.6 Co-Processed Feedstocks

It can be seen from figure 4.10a that adding the SL to the *Miscanthus* significantly changes the proportion of the organics remaining in the aqueous phase. This value jumps from a maximum of about 10% for the pure *Miscanthus*, to a maximum at 25% at 250°C for the co-processed MSL mix. Therefore the presence of the chemical compounds found within the SL have increased the solubility of the organics in the HTC slurry, so that 2.5 times more organics end up dissolved in the process water. The seaweed thus acts as an additive, as it results in a higher change than if there were no catalytic or additive properties of the seaweed; only 20% of this mix is seaweed, yet this solubility increased drastically. Perhaps the degradation products from the *Miscanthus* breakdown is because it becomes more soluble with the presence of some catalytic trace metals found in the seaweed, as it is known that the presence of salts effect polymerisation. Therefore these inorganics would affect the probability of some degradation reactions which may lead to more soluble products.

The slight dip in % PW yield from feedstock at 200°C is probably due to the same mechanism producing the dip for 100% SL at 200°C as well. This is not as severe a change, as clearly there is five times less seaweed, and only a 3% reduction rather than a 15% reduction as in the pure SL sample. The pure *Miscanthus* sample in figure 4.6(c) shows a slight increase in the organics solubilised in the PW between 150°C and 200°C, and these same degradation reaction may contribute to the steadier decline in solubility from 150°C to 200°C in the MSL mix. There is an increase in the solubility from 200°C to 250°C. *Miscanthus* on its own does not show this trait, however SL does, at a 10% increase in PW%. Therefore the same 10% increase in the MSL mix may be due to the SL presence in the feedstock, although with only 20% seaweed feedstock by weight, the molecules responsible for this extra solubility of the organics after HTC may be very plentiful in the SL.

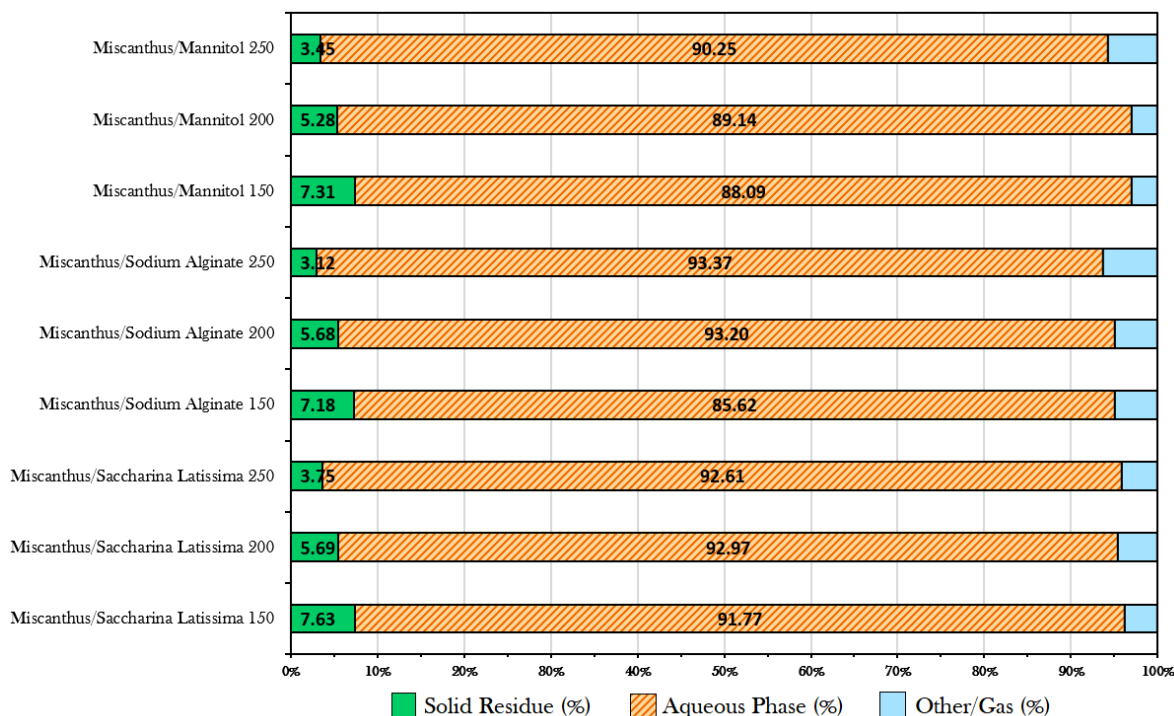


Fig. 4.9 Mass Balance as received for the mixed biomass feedstocks after hydrothermal carbonisation, for each of the three HTC temperatures, each held for one hour. This includes the 220ml of added water. The ratio of the *Miscanthus* and the mixed feedstock was 80:20 respectively.

The MSL mix in general shows similar yields to the 100% *Miscanthus* sample, although with slightly less hydrochar %weight, though with a nutrient and organic rich process water to make up for this. Overall this is a desirable ratio of %feedstock remaining in the hydrochar, and solubilised in the PW. This ratio seems to address sufficiently both the concerns with lack of useful properties of the PW for 100% *Miscanthus* and an organically depleted hydrochar in the SL due to the highly soluble contents. It will be addressed in chapter 5 whether this co-processed mix also satisfies the slagging and fouling propensity limits of the hydrochar, in order to be a viable biofuel option for industrial applications.

The *Miscanthus*:Sodium Alginate (MNA) results in figures 4.9 and 4.10b look generally rather similar to the MSL results. The presence of the sodium alginate as an inherent component of sugar kelp may therefore likely be helpful for increasing the solubility of the organics after HTC processing at the higher temperatures but not beneficial in the production of a particularly organic rich hydrochar. Future analysis of this process water will help determine which chemical compounds are responsible for these yield and mass

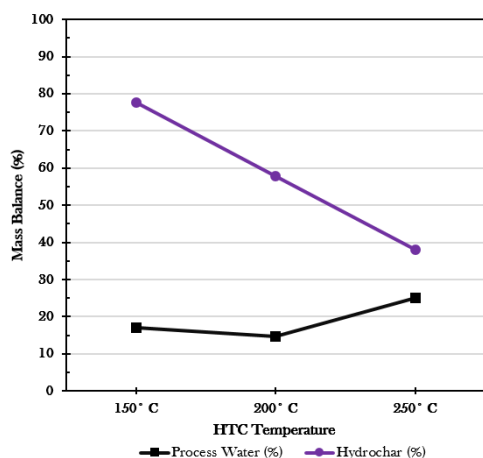
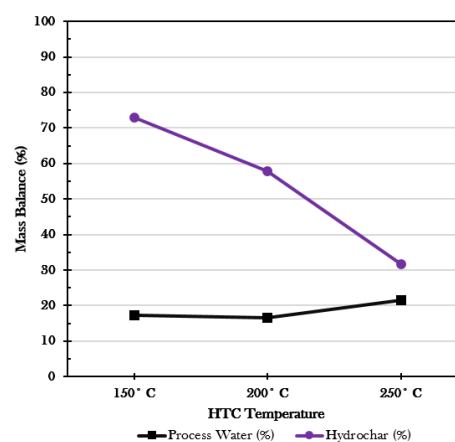
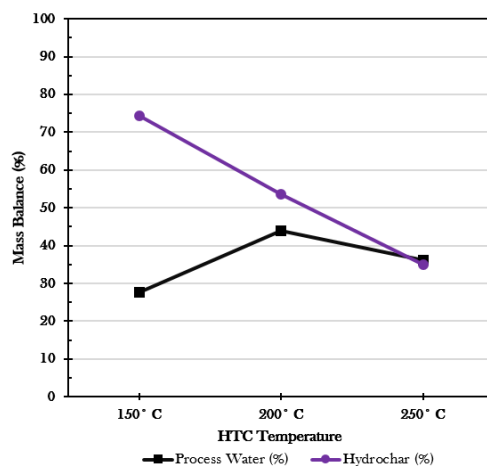
(a) *Miscanthus:Saccharina latissima*(b) *Miscanthus:Sodium Alginate*(c) *Miscanthus:Mannitol*

Fig. 4.10 Mass Balances of where the chemical compounds from the initial feedstock end up, for the process waters and the hydrochars, for the three different co-processed feedstocks. This is based on the fraction of feedstock processed.

balance patterns.

For the *Miscanthus:mannitol* mix (MMan), there is the same % of the feedstock that remains in the char and in the process water, at 34-36%, for the 250°C HTC temperature. As mannitol is so soluble in water, and so stable during HTC, this has the effect of making more of the HTC products in the MMan mix more soluble, creating a much higher organic fraction dissolved within the PW. Although it only makes up 20% of the initial feedstock weight, this mannitol causes an extra 34% more organics to be solu-

bilised in the PW at 200°C than the pure *Miscanthus* sample. There is a slight decrease from 200°C to 250°C in this pattern however, possibly caused by some of the mannitol breaking down into less soluble chemicals. This may be in part due to the presence of certain chemical compounds from the *Miscanthus* feedstock. The amount of insoluble feedstock remaining in the hydrochar is consistently 10% or thereabouts less than the % hydrochar from the feedstock in the 100% *Miscanthus* sample. Mannitol contained virtually no hydrochar after HTC at any temperature, so this follows that the lower yields of char for the MMan compared to the 100% *Miscanthus* is due to the mannitol not forming any hydrochar during HTC, with it accounting for a fifth of the initial weight.

The key here is to determine whether the co-processed samples lead to a simple summation of the relative seaweed and *Miscanthus* components of what would be expected from the 100% biomass feedstocks, or whether there appears to be some synergy from the co-processed mixtures. Therefore table 4.1 was produced to compare the SL, M, and MSL results, with values also calculated for the predicted M:SL values, if there were to be no promotive or inhibitive effects of the feedstock mix (and hence only a simple summation using the 80:20 ratios. The calculated MSL values were determined by multiplying the 100% *Miscanthus* values by 0.8 and adding this to 0.2 times the corresponding *Saccharina latissima* samples).

Table 4.1 A table comparing the 100% *Saccharina latissima* and 100% *Miscanthus* HTC samples post-HTC and the resultant calculated (calc.) M:SL mass balances and yields and the actual (act.) experimental results of the *Miscanthus:Saccharina latissima* HTC runs.

MSL = *Miscanthus:Saccharina latissima*, MB = Mass Balance, PW = Process Water.

Sample Name, HTC T (°C)	% Solids MB	% PW MB	Hydrochar yield (%)	PW yield (%)
<i>Saccharina latissima</i> 150	4.61	91.77	46.88	62.11
<i>Saccharina latissima</i> 200	2.81	92.97	28.61	46.46
<i>Saccharina latissima</i> 250	2.15	92.61	21.90	55.87
<i>Miscanthus</i> 150	8.41	88.09	85.50	6.41
<i>Miscanthus</i> 200	6.38	89.14	64.88	11.83
<i>Miscanthus</i> 250	4.75	90.25	48.25	11.19
MSL 150 calc.	7.65	88.83	77.78	17.55
MSL 200 calc.	5.67	89.91	57.63	18.76
MSL 250 calc.	4.23	90.72	42.98	20.13
MSL 150 act.	7.63	91.77	77.58	17.40
MSL 200 act.	5.69	92.97	57.88	14.86
MSL 250 act.	3.75	92.61	38.08	24.50

It can thus be determined via these comparative values that generally the mass balance and the fate of the feedstock (hydrochar and PW yields) is approximately predictable in

all cases. It appears however that the effect of adding the sugar kelp to the *Miscanthus* has a slightly additive effect on the PW yield at the 250°C temperature, and on the two higher temperature mass balances of the aqueous phase. This may be due to the increased solubility of the seaweed improving in turn the solubility of the chemical components within the *Miscanthus* organic compounds. Inhibitive effects of adding the seaweed to the *Miscanthus* before HTC processing was only found significantly for the PW yield at 200°C and the char yield at 250°C.

The addition of 20% seaweed does therefore slightly effect the MSL hydrochar and aqueous phase in other ways than a simple summation of the pure biomass feedstock results, with an higher increase on the solubility of the process water than predicted for the 250°C sample, with a resultant and corresponding greater decrease in char yield than predicted. It is speculated that this may be caused by the presence of the salts in the seaweed feedstock, which may reduce the probability of polymerisation to occur, which would in turn reduce the hydrochar yield. The effects of the inorganics in the hydrochar and different chemical compounds found in the HTC aqueous phase of the SL feedstock on the MSL product streams are further evaluated in chapters 5 and 6 respectively.

4.7 Conclusions

The main findings within the mass balance and yields evaluated here is that as the HTC temperature is raised, the chemicals within the biomass feedstock become more solubilised into the aqueous phase, and less of these organic compounds remains in the solid phase as char. It is expected that the hydrochar at the higher temperature will be more energy dense, however this HTC as a pre-treatment for feedstock before using as a biofuel must balance the energy efficiency of the hydrochar produced with the amount of char produced per kg of biomass feedstock. One of the key findings from this chapter is that the model biochemical components behave differently to the biomass samples. There is some clear differences to the way the terrestrial biomass model compounds behave compared to the seaweed based model compounds. The cellulose and lignin model compounds produced higher hydrochar yields than the protein feedstock. The sodium alginate sample appears to be affected by presence of cations, whereas the mannitol has proven to be a very stable compound under hydrothermal conditions.

In terms of the biomass feedstocks, the *Miscanthus* produces much higher hydrochar yields than the two seaweed samples, and blending of the sugar kelp with the *Miscanthus*

seems to exhibit non additive behaviour (in terms of hydrochar yield and HHV). This could be due to the influence of salts of polymerisation of hydrolysis products. More gas is produced at higher HTC temperatures, leading to lower hydrochar yields as well, as the organic components more readily react to form gases.

This reduction in hydrochar yield as HTC temperature increases is calculated in an energy balance table (table 7.3) in chapter 7, using the HHV of the hydrochar, analysed in chapter 5, and the samples' mass balances and yield results. The mass balances of the different feedstocks analysed in this chapter are therefore essential to consider when evaluating the overall best pre-treatment methods for biomass to improve the energy efficiency of the proposed biorefinery concept as a whole. Therefore although higher HTC temperatures may result in more organically rich and solubilised aqueous phase, and a higher HHV hydrochar, the lower yields and higher organics lost to the gases may override the advantages of an increased HTC temperature. This overall energy balance of each biomass feedstock will be explored once the potential for biochemical methane production of the HTC aqueous phase has been determined and the usability of the metal-rich hydrochars evaluated.

Chapter 5

Composition of Hydrochar following Hydrothermal Carbonisation

5.1 Introduction

In this chapter the solid phase, or hydrochar, from the HTC process is analysed, and evaluated for its suitability as a potential solid fuel. Each of the four different subgroups of feedstock are discussed in the four respective subsections within this chapter. The elemental, proximate and higher heating value (HHV) results are first compared, giving an overall picture of how well the hydrochars would behave as a solid fuel. The HHV values in particular will help quantify how efficient the hydrochar would be as a solid fuel, with the hope of achieving a high HHV with no detrimental effect on the respective aqueous phase's ability to be used as a by-product, or any slagging and fouling issues with the hydrochar. One of the key objectives is to determine what the impact blending macroalgae and seaweed has on these properties.

Figure 5.1 demonstrates which section of the biorefinery process this section covers. The hydrochar is separated from the HTC product via a vacuum, and is dried to reduce the moisture content. The resultant friable powder, black usually in colour, can then be further milled down to enable homogenisation. Accurate analysis of this product can then be achieved. On a large scale biorefinery such as the one proposed here, the powder would be collected and sent to boilers to be used as a fuel source. The fuel properties would hopefully be similar to the characteristic of coal powder. However, slagging and fouling of the boiler may be more likely to occur. The most suitable HTC feedstock should hence be chosen which would pass strict criteria for the hydrochar to be viable for use on an industrial scale. The characterisation of this hydrochar prod-

uct and their slagging and fouling propensity is thus evaluated within this chapter, in addition to the HHV of the hydrochar, which evaluates its energetic values as a fuel source.

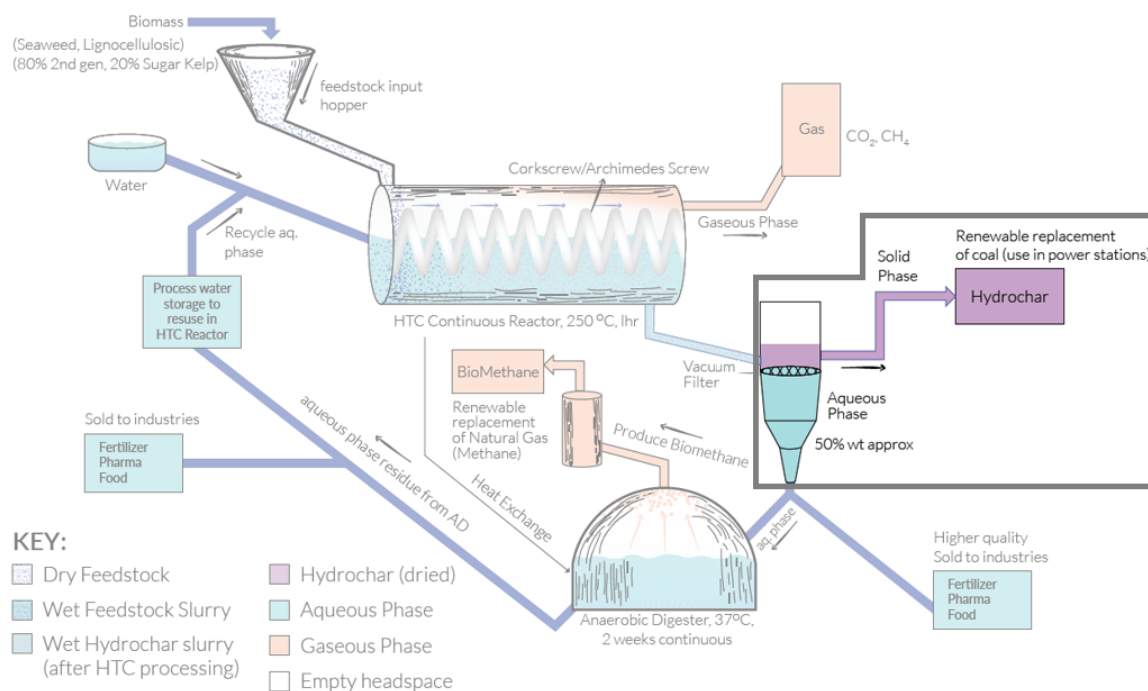


Fig. 5.1 A section of the biorefinery concept from figure 1.3, highlighted to demonstrate the aspect of the overall process focussed on in this chapter; the hydrochar production, analysis of the hydrochar qualities for use as a replacement fossil fuel.

To evaluate the slagging and fouling propensity of the biomass based hydrochars, XRF analysis of the chars, using pressed pellets, was undertaken for each sample. These results identify the feedstocks that meet the criteria for slagging and fouling using calculated indices (set out in table 3.1). It is predicted that the 100% seaweed feedstocks, due to their high metal content, would fail this criteria and hence would not be a suitable replacement solid fuel. However co-processing seaweed with *Miscanthus* (as an example terrestrial biomass) improves its combustion behaviour and passing the slagging and fouling limits. Hence, in the right proportions, seaweed in the form of *Saccharina latissima* or *Fucus serratus*, two very common seaweeds found in Europe, could be utilised as a solid fuel, if mixed with a lignocellulosic biomass with inorganic content. It is hoped that this would demonstrate real promise for industrial scale utilisation of seaweed in the biofuel industry, and alleviate the issues caused by the high inorganic/ash content found in seaweeds.

Micro and macro metal content in the hydrochar have been analysed, and any particular samples that may also have value as a fertiliser can be identified. This

application is another potential end use for the HTC products on a large scale.

The XRF of the aqueous phase is also analysed in §6, although this is not the phase of the HTC products that is proposed as the main biofuel product of hydrothermally processing seaweed. Nonetheless, it helps us to understand the fate of inorganics, and any effects this may have in the biomethane potential experiments of the aqueous phase.

Each of the four different subgroups of feedstocks are discussed in the four respective subsections within this chapter. The elemental, proximate and higher heating values are first studied and compared, giving an overall spectrum of how well the hydrochars would behave as a fuel. The HHV values in particular will help quantify how efficient the hydrochar would be as a fuel, with the hope of achieving a high HHV with no detrimental effect on the respective process waters ability to be used as a by-product, or any slagging and fouling issues with the hydrochar.

The following subsections will hence address the suitability of the different hydrochar samples generated by HTC under different conditions. The inorganic content of the hydrochars (micro and macro elements) are compared as bar charts. The level of metals in each of the hydrochars for every sample can be found in table A.2 in the Appendix for completeness.

Note that the slagging and fouling propensity analysis is performed on the 100% biomass samples and the co-processed samples, as this is where the focus needs to be, and the model compounds have impurity issues and can be analysed in enough detail via XRF analysis. The comparisons of the seaweed and *Miscanthus* samples and the effect of co-processing these feedstocks is the key research, and provides the only useful data (in terms of slagging and fouling propensity analysis). As such, these are compared and contrasted within one slagging and fouling section, §5.5.3.

It is hypothesised that the co-processed MSL mix would provide a suitably high HHV value in the range of 20-25 MJ kg⁻¹, (higher at the highest temperatures) but yet will have a significantly reduced propensity of slagging and fouling biomass boilers, falling well within the slagging and fouling indices limits compared to the pure seaweed samples. *Saccharina latissima* and *Fucus serratus* although expected to have a high HHV at the higher HTC temperatures, are expected to fail in the slagging and fouling tests due to a high metal content in the feedstocks. Hence they lack feasibility in the biofuel industry as a stand-alone feedstock, but this may be significantly improved upon in a 1:4 co-processing ratio with a less metal-rich feedstock such as *Miscanthus*.

5.2 Lignocellulosic Model Compounds

5.2.1 Ultimate and Proximate Analysis

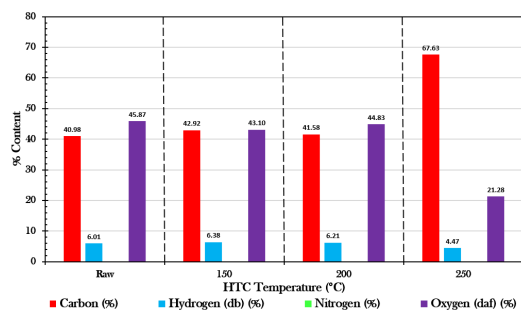
The elemental, proximate and higher heating value data for the hydrochars from the HTC of the lignocellulosic model compounds (LMC), are all shown for each sample in table 5.1 for the raw samples and the three different temperatures. In addition, bar charts of the C, H, N and O contents of these samples are shown in figure 5.2. The Van-Krevelen (V-K) diagram containing the H/C and the O/C ratios on an atomic basis is shown in figure 5.3. The position of the products on a Van-Krevelen diagram can be used to identify general trends on the types of reactions occurring (for example, protein losing oxygen via decarboxylation) as shown in the diagram on the bottom right of the VK diagram. The HHV values are shown for these LMC samples in the grouped bar chart in figure 5.4.

Table 5.1 CHNOS, TGA and HHV values for the lignocellulosic model compound HTC solid phase.

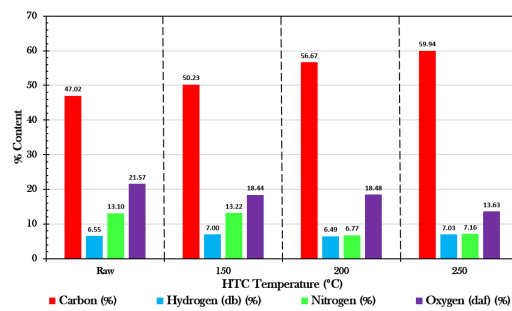
ACL = Sodium Alginate, Cellulose and Lignin blend, * = Calculated by difference.

Sample, HTC Temperature (°C)	CHNOS Data (%)						TGA Data (%)				HHV (db) (MJ/kg)
	N	C	H	S	H (db)	O (daf)*	M	VM	FC	Ash	
Cellulose Raw	0.00	40.98	6.27	0.05	6.01	45.87	2.39	87.83	5.08	4.71	16.26
Cellulose 150	0.00	42.92	6.70	0.00	6.38	43.10	2.85	87.27	5.13	4.76	16.97
Cellulose 200	0.04	41.58	6.53	0.00	6.21	44.83	2.89	86.42	6.24	4.45	16.47
Cellulose 250	0.00	67.63	4.71	0.00	4.47	21.28	2.16	51.56	41.82	4.46	26.65
Protein Raw	13.10	47.02	7.14	0.31	6.55	21.57	5.32	81.19	7.36	6.12	20.42
Protein 150	13.22	50.23	7.52	0.00	7.00	18.44	4.69	78.58	10.31	6.42	22.03
Protein 200	6.77	56.67	6.83	0.00	6.49	18.48	3.05	73.34	15.07	8.54	24.10
Protein 250	7.16	59.94	7.14	0.72	7.03	13.63	1.00	77.08	11.41	10.52	26.29
Lignin Raw	0.53	57.90	5.49	0.32	5.28	28.42	1.92	59.55	32.89	5.64	23.01
Lignin 150	0.27	66.19	6.28	0.53	6.03	19.73	2.29	61.75	30.98	4.97	27.81
Lignin 200	0.32	64.11	5.83	0.45	5.60	24.73	2.14	59.35	35.85	2.66	26.25
Lignin 250	0.41	66.59	5.76	0.41	5.53	22.49	2.00	55.52	39.92	2.57	27.48
ACL Raw	0.28	48.03	5.86	0.15	5.42	32.96	4.02	71.12	15.72	9.14	18.92
ACL 150	1.55	53.59	6.67	0.00	6.47	32.78	1.86	70.84	23.54	3.76	21.89
ACL 200	0.22	54.55	6.25	0.00	6.07	30.77	1.66	67.32	24.28	6.74	21.95
ACL 250	0.38	67.39	6.27	0.00	6.14	21.69	1.15	57.24	38.37	3.24	28.64

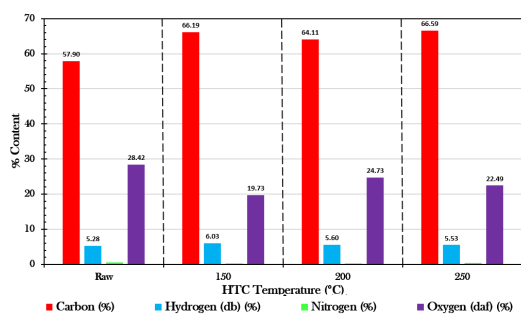
Cellulose has the largest reduction in Oxygen (O) with increasing temperature, from 46% down to 21%, with a significant reduction from 200°C to 250°C. The high oxygen levels contribute to the low fixed carbon (FC) levels for the cellulose samples, although the C 250°C sample performs the best in terms of energy efficiency of the hydrochar, due to the significant change in O and FC % levels, demonstrated graphically in figure 5.2a. This is likely due to the hydrolysis reaction of cellulose, breaking down to its constituent glucose molecules and further to humin. The higher FC at 250°C for cellulose may indicate that



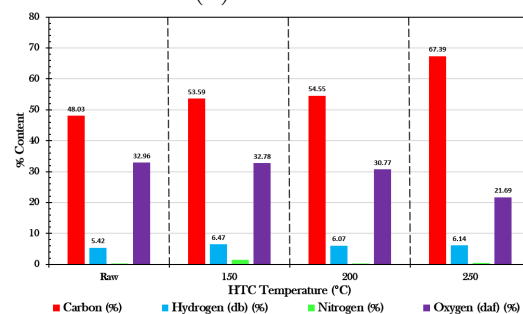
(a) Cellulose.



(b) Protein.



(c) Lignin.



(d) Sodium Alginate, Cellulose, Lignin blend (ACL).

Fig. 5.2 The CHNO values from the Hydrochar of the Lignocellulosic Model Compounds.

feedstocks with a high cellulose content would produce a higher energy-dense hydrochar at this temperature.

In contrast, the lignin samples' lack of significant change in FC content shows that apart from the removal of oxygen, there is little change in the structure of the lignin feedstock after hydrothermal carbonisation at the temperatures studied.

The Nitrogen content (N%) in the Protein hydrochar reduce with increasing HTC temperature. This is due to the nitrogen molecules being retained in the aqueous phase as part of the NH_4^+ ion, as part of the organic acid dissociation in the increasing 'superheated' water at the higher HTC temperatures. Feedstocks that are rich in protein produce high nitrogen containing hydrochar, which would produce fuel-bound NO_x molecules upon burning which is potentially a problem, as this is a GHG and causes acid rain. The much more gradual increase in carbon content of the protein hydrochars (shown in figure 5.2b) suggests the gradual decomposition of the complex protein compounds, with limited increase in FC as a result.

The ash levels shown in this table are not so indicative, as they were expected to be low, due to the model compound nature of these feedstocks. The high ash content found in the protein samples are likely due to 'filler' in the protein model compound used (Whey Protein purchased from an online store), possibly included in the protein to increase profit margins on the product. The type of lignin used for the model compound is similarly the cause of the presence of sulphur (S%) found in the Lignin ultimate analysis results, due to the sulphate ion (SO_4^{2-}) being present. The slagging and fouling analysis is performed on the actual biomass and co-processed biomass samples due to this issue, and the focus needs to remain on the biomass samples and how they compare, with the metal content via XRF from the model compounds taken into account.

Figure 5.3 shows that cellulose has the highest H/C and O/C ratios, until it is hydrothermally carbonised at the highest temperature, which results in cellulose 250°C having the lowest H/C ratio. The general trend is that the H/C and O/C ratios both reduce as the lignocellulosic model compounds undergo HTC, and the ratios reduce as the HTC temperatures increase, with the cellulose and ACL samples showing the most significant differences.

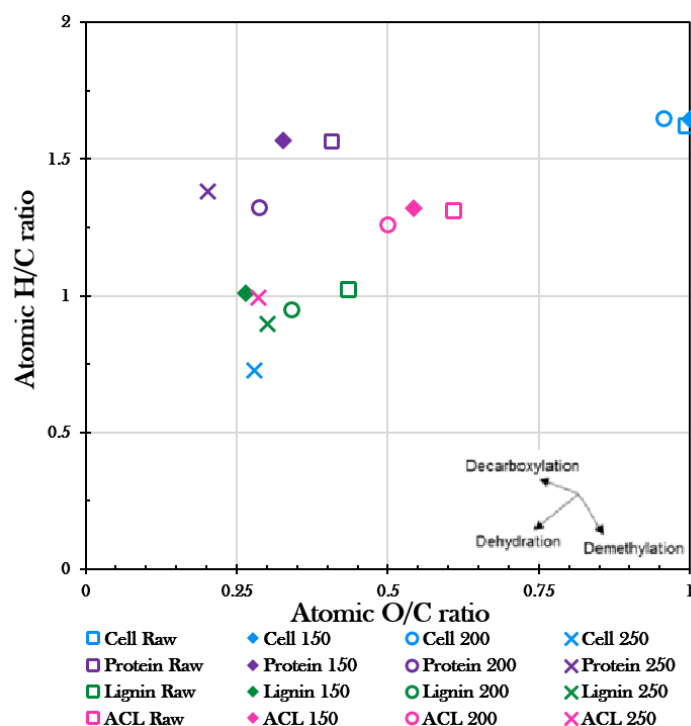


Fig. 5.3 Van-Krevelen diagram for the lignocellulosic model compounds solid phase. Cell = Cellulose, ACL = Sodium Alginate, Cellulose and Lignin blend.

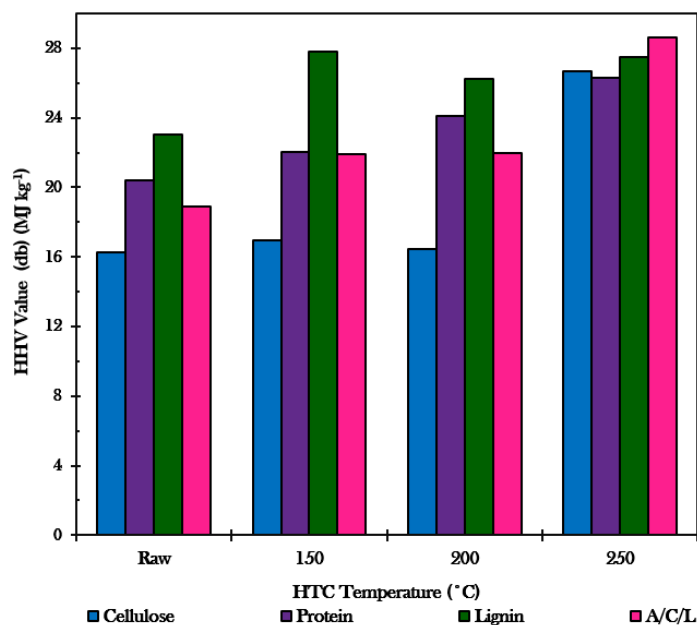


Fig. 5.4 The HHV values of the lignocellulosic model compound solid phase after HTC, presented as a function of the HTC temperature.

A/C/L = Sodium Alginate, Cellulose and Lignin blend.

Generally, the relationship between the Volatile Matter content (VM%) and the fixed carbon content is that VM would decrease with a corresponding increase in FC, at higher HTC temperatures, by roughly the same numerical values, which is indeed the case with the LMC results shown in table 5.1.

The FC content of all the LMC samples all tend to increase as HTC T increases, apart from P 200°C to P 250°C. This anomaly from the protein sample is probably because protein alone does not promote polymerisation. However, in the presence of carbohydrate Maillard reactions between the amino acids and reducing sugars takes place. The overall affect of HTC on these lignocellulosic model compounds is the energy densification of the hydrochar as the HTC temperature increases, as expected and in line with results in the literature, but confirmed in the case of individual model lignocellulosic based compounds.

The HHV values are shown in figure 5.4. It can be clearly seen that for each sample, the higher HTC temperature does indeed lead to a more energy dense hydrochar, as predicted. (Note that L 150°C is only slightly more than L 250°C). It is also very apparent from this that carbonisation only occurs after 200°C for cellulose. The HHV results of the 100% biomass and co-processed sub-groups of HTC feedstocks - rather than the model compounds seen here - will be compared and contrasted quantitatively

to the values found from similar HTC research in the literature.

The ash for the model compounds are not considered in too much detail, and more focus will be placed on the biomass feedstock results and the co-processing feedstocks, due to the higher importance of the results from the actual proposed feedstocks. These model compounds do, however, provide possible insights into which compounds are responsible for the biomass and co-processed ultimate and proximate results, and will therefore be referred to for comparison purposes in the analysis of those two subgroups of feedstocks.

5.2.2 Fate of Inorganics: Pressed Pellet X-Ray Florescence

The results from the XRF pressed pellets analysis of all the hydrochar samples after HTP processing (and subsequent milling) are shown in table A.2 in §10, in terms of % mass of the trace metals within the hydrochar sample. Using this data, the micro and macro elements are shown as a bar chart, for each of the samples. This will enable visual comparisons and trends to be seen for each subgroup more easily.

The scale of the metal content within the lignocellulosic model compounds are in trace amounts, with a y-axis range between 0.1 and 2%, with the exception of the Protein Macrometals. Comparing the overall amounts with the LMC aqueous phase XRF results, there are, on average, more % metal content in the hydrochar than the aqueous phase, by a factor of about 10 (see table 6.7). It is important to note that the model compounds would not be a feasible feedstock in the HTC concept, this analysis is to improve the understanding of the fate of the inorganics in the constituent components of the seaweed and terrestrial feedstock may reside after HTC, in the hydrochar or aqueous phase.

It is preferred that the metal content resides more within the aqueous phase than the hydrochar phase due to increased slagging and fouling propensity of the hydrochar with a high metal (hence ash) content, which may not pass strict limits. In terms of the aqueous phase, this product stream would become a more feasible fertiliser resource if it were to have a higher inorganic content, which would thus enable future profitable by-product options.

Figure 5.5 shows that the calcium levels increase as the cellulose sample is hydrothermally carbonised at higher temperatures. Also, increased levels of P and S are detected in the 200°C and 250°C cellulose hydrochar samples, respectively. These results are questionable due to the pure cellulose not containing any of these elements initially, and so, at such

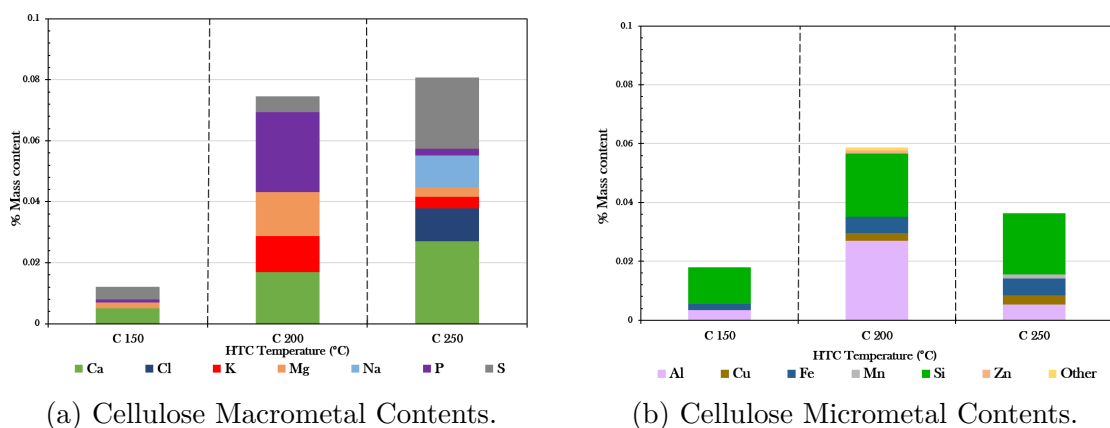


Fig. 5.5 The Inorganic Contents of the Cellulose hydrochar samples after HTC processing.

low levels detected, it is assumed that these trace amount of macro and micro-metals may be due to background noise or mis-readings from the metal sample container, or contamination during HTC processing.

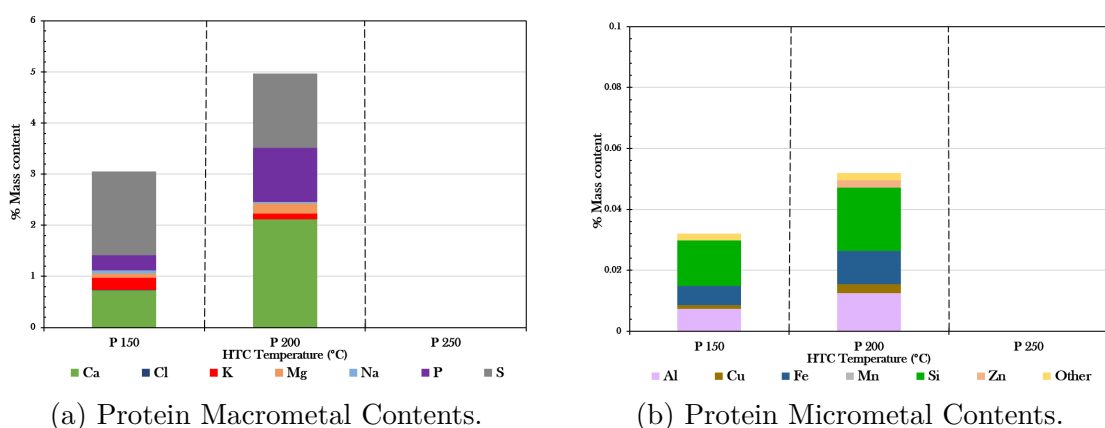


Fig. 5.6 The Inorganic Contents of the Protein hydrochar samples after HTC processing.

The total ash content from the Protein HTC hydrochars increases with HTC temperature from 6.4% at P 150°C to 8.5%, then 10.5% for P 250°C, which was significantly higher than other ash contents for the alternative lignocellulosic compound HTC feedstocks. This agrees well with the general trend of an increase of inorganics found via XRF in both the macrometals and the micrometals categories, shown in figure 5.6, as a higher metal content within the hydrochar would increase the amount of ash expected from the samples after burning. Most of the metals from the Protein were from the macrometals, just under 5% total mass content for P 200°C. The increase from P 150°C is largely due to the increase of calcium and phosphorus content. The sulphur content (roughly 1.5%) stayed fairly constant throughout the 150°C and 200°C temperatures. This may

be caused by the presence of methionine or cysteine amino acids. At this amount, this may contribute to a high level of sulphur dioxide emissions for a biomass feedstock high in protein.

For the protein aqueous phase samples, a low range of 1.3-1.5% of total phosphorus content was determined, with a decrease with HTC temperature increasing, shown in chapter 6. Therefore, the inorganics from the protein within a biomass sample is likely to remain in the hydrochar phase, rather than the aqueous phase. Note that this protein is sourced from a commercial protein whey powder, so results may differ depending on the source used.

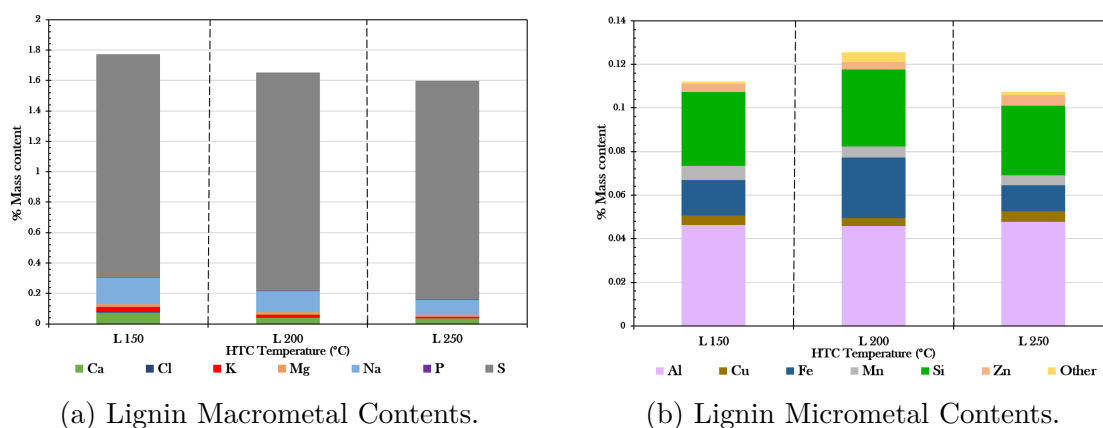


Fig. 5.7 The Inorganic Contents of the Lignin hydrochar samples after HTC processing.

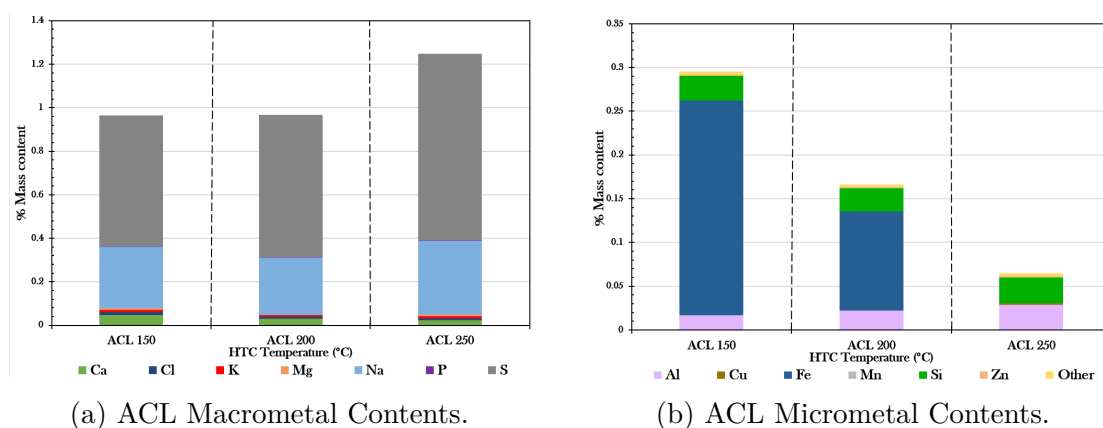


Fig. 5.8 The Inorganic Contents of the Sodium Alginate, Cellulose and Lignin (ACL) hydrochar samples after HTC processing.

The sulphur detected in the lignin hydrochars probably originate from sulphated groups or sulphonic groups. The high sulphur seen in figure 5.7a is caused by the method

used to extract the lignin from the source, and is the reason why lignin is so soluble in water. What is interesting here is that the high ratio of sulphur to the other metals, and the total amounts, remains the same over the three HTC temperatures. There is little change, indicating little happens during the higher temperature HTC process. There are also some sodium found within the lignin hydrochar samples, about 0.2%, and some trace aluminium, iron and silicon detected. Most of the sodium would be expected to be solubilised in the aqueous phase, however no sodium was detected in the liquid XRF, for any of the LMC samples.

The ACL mix is dominated by the sulphur from the lignin portion of the mix, and there is over 0.2% by mass of sodium for each ACL hydrochar samples. The sodium is higher in this ACL sample than from the pure lignin, cellulose and alginic acid (figure 5.14a) samples, so it is interesting that it is there in such amounts at all. This could be due to sodium alginate being lost via volatilisation in the pure AA samples, in contrast to the sodium alginate being retained in the ACL samples, due to interactions between cellulose and lignin, reducing the levels of volatilisation. In addition, the high iron content in the micrometals (figure 5.8b) suddenly appears at 150°C and at 200°C. This may originate from the stainless steel reactor walls, but if so, the ACL mixture must have allowed for some corrosion of the inner metal wall in these conditions.

Depending on the type of cellulose and lignin model compound sample used, the trace metals detected may vary. With such a low % mass range, the stainless steel Parr Reactor used for hydrothermal processing may also contribute to the amount of iron detected. Hence, the LMC XRF results may not be fully analysed in detail, although some samples are referred to in further discussions when examining the biomass feedstocks and co-processed XRF pressed pellet results and the liquid XRF results, to help understand where the metals within the feedstock end up.

The ash content from the proximate analysis of the model compounds are compared to the biomass feedstocks are also considered as part of this evaluation. Therefore some key trends and results are described here, whilst a more objective analysis of the fate of the inorganics originating from the model compounds can be found in §5.4.2 and §5.5.2 focussing on the hydrochar, and §6.4.7 and §6.5.7, focussing on the aqueous phase and overall fate of the metals within the samples after HTC.

5.3 Seaweed Model Compounds

5.3.1 Ultimate and Proximate Analysis

The CHNOS, TGA and HHV values of the seaweed model compounds, at the three different temperatures, are shown in table 5.2 for the raw samples and the three different temperatures. In addition, bar charts of the C, H, N and O contents of these samples are shown in figure 5.9. The Van-Krevelen (V-K) diagram containing the H/C and the O/C ratios on an atomic basis is shown in figure 5.10. The HHV values are shown for these LMC samples in the grouped bar chart in figure 5.11.

Table 5.2 CHNOS, TGA and HHV values for the seaweed model compound HTC solid phase. Note that there is no data for the HTC hydrochars of Mannitol, as there was a negligible amount of solid residue after hydrothermally processing mannitol, - it was all dissolved in the aqueous phase. Therefore the HHV of this char would in effect be zero, do to no char being produced. No Calcium Alginate was available for analysis for the raw sample.

NA = Sodium Alginate, CA = Calcium Alginate, AA, Alginic Acid, * = Calculated by difference.

Sample, HTC Temperature (°C)	CHNOS Data (%)						TGA Data (%)				HHV (db) (MJ/kg)
	N	C	H	S	H (db)	O (daf)*	M	VM	FC	Ash	
NA Raw	0.00	29.73	4.48	0.00	3.55	48.32	8.38	79.27	2.34	10.02	14.33
NA 200	0.44	57.89	5.75	0.00	5.39	17.90	3.28	52.96	28.65	15.10	23.08
NA 250	0.29	60.49	5.14	0.00	4.86	22.50	2.56	45.63	42.51	9.30	23.81
CA 150	0.12	30.56	4.98	0.00	3.55	36.44	12.85	59.00	11.66	16.49	14.48
CA 200	0.34	52.68	4.83	0.00	4.22	21.73	5.53	49.45	29.51	15.51	20.24
CA 250	0.26	47.64	4.50	0.00	4.00	20.14	4.49	50.70	21.34	23.47	18.48
AA Raw	0.00	37.34	5.23	0.00	4.34	47.14	8.03	70.36	18.46	3.16	15.51
AA 150	0.06	39.06	5.02	0.00	4.51	47.33	4.67	68.75	22.20	4.38	15.92
AA 200	0.17	62.16	4.50	0.00	4.02	25.42	4.32	49.18	42.59	3.91	23.75
AA 250	0.31	62.88	4.06	0.00	3.69	24.99	3.32	44.63	47.24	4.82	23.74
Mannitol Raw	0.00	38.03	7.53	0.00	7.49	53.40	0.35	98.92	0.00	0.73	14.80

Note here that due to the lack of hydrochar for the mannitol samples, as all the aqueous phase passed through the filter paper with minimal solid residue, there are no ultimate and proximate analysis of the mannitol hydrochars. For the same reason, the NA 150°C sample was unable to be analysed for CHNS and TGA also. These feedstocks were omitted from XRF pressed pellet analysis due to the lack of hydrochar sample and hence the slagging and fouling analysis, in addition.

Considering the fixed carbon trends in the seaweed model compound hydrochars, the sodium alginate promotes the carbonisation albeit with low yields, and is more similar to the alginic acid in this respect. Figure 5.11 demonstrates this HHV trend visually (although the hydrochar yields are not taken into account at this point). The calcium

alginate reduces in FC content at HTC temperature rises from 200°C to 250°C, whereas the other two hydrochar feedstocks rise in FC% progressively. This therefore demonstrates that the metals in the feedstock does indeed effect the reaction pathways during HTC. Unfortunately calcium alginate in its raw form was not analysed here as there was none available for use due to other research students using the chemical compound and the labs closing just before it was due to be provided. Calcium content would likely cause a reduction in FC% at higher HTC temperature, whereas sodium alginate and alginic acid content would have the opposite effect on the hydrochars, however there is a balance to be found, as the sodium alginate was found to have lower hydrochar yields.

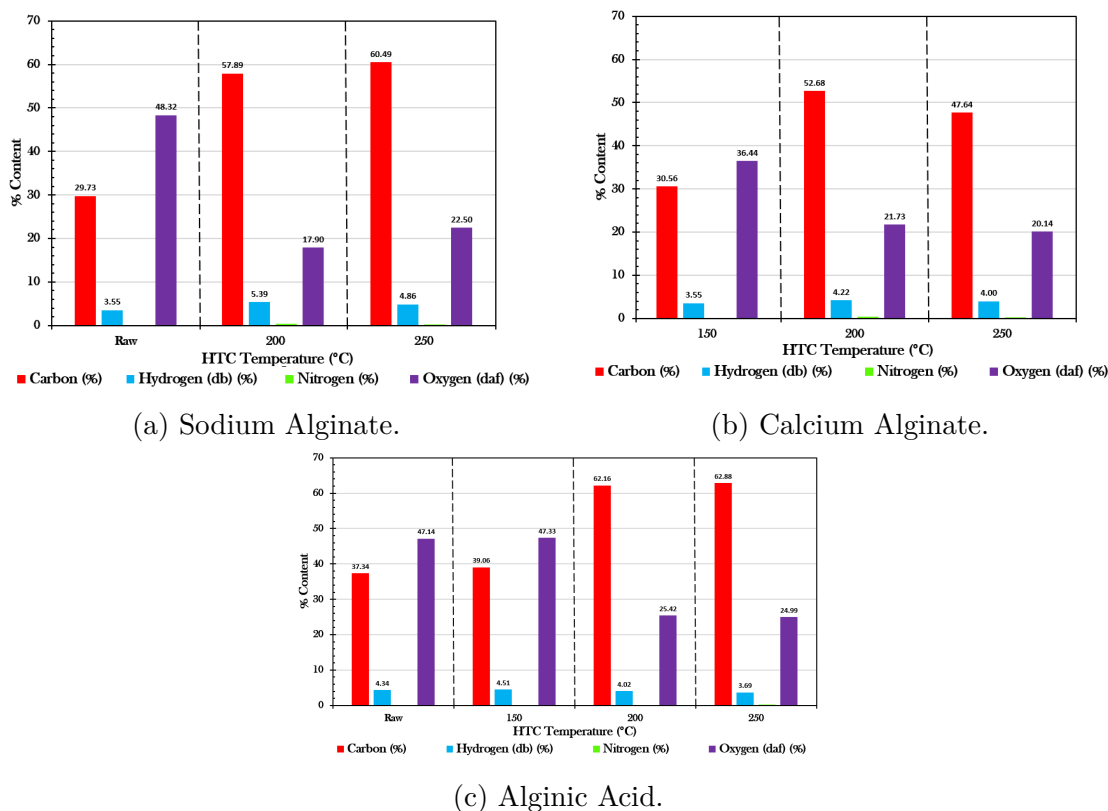


Fig. 5.9 The CHNO values from the Hydrochar of the Seaweed Model Compounds. Note that there is no Mannitol hydrochar data due to the lack of hydrochar produced after the HTC processing of the Mannitol Feedstock.

It is interesting that the NA samples that were tested, increases in terms of HHV more as T increases, which is more similar to the alginic acid samples than the calcium alginate samples with the HHV trends. This effect is possibly due to the solubility of the sodium alginate and the lower ash content at higher temperatures, as most of the sodium alginate

compounds remain absorbed into the aqueous phase after HTC. Alternatively, this could be due to contaminants present in the sodium alginate model compound feedstock, such as laminarin, which contains higher levels of glucose. This is also soluble and so may be present in the NA sample but not in the CA sample. Laminarin would behave more similarly to cellulose and would therefore cause this increase of HHV at the highest HTC temperature, if present.

Studying figure 5.9a it can be seen that there is significantly more carbon in the higher two HTC temperatures than the raw sample, despite the big differences in fixed carbon and ash contents of these two samples. The HHV is therefore similar due to the high C contents of the sodium alginate HTC hydrochars, although the slugging and fouling propensities may be different for these samples. The oxygen content trend shown in figure 5.9b shows an oxygen reducing effect of increasing HTC.

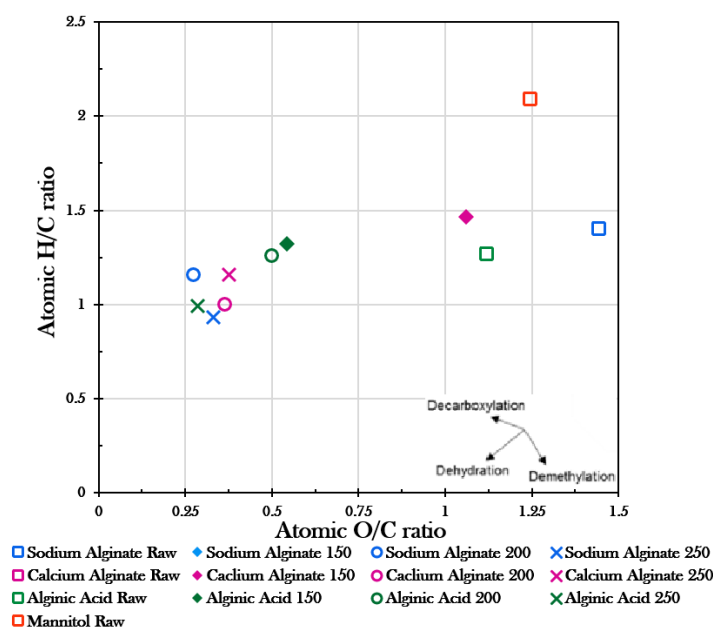


Fig. 5.10 Van-Krevelen diagram for the seaweed model compounds solid phase.

The main trend shown in figure 5.10 is that there's no more effects in the hydrochars with increasing HTC temperature other than deoxygenation. The highest two HTC temperatures results in the lowest O/C and H/C ratios for all the samples. The largest difference was found in the sodium alginate sample, which although the H/C ratio didn't reduce significantly, the O/C ratio reduced by over 1 between the raw samples and the 200°C and the 250°C hydrochar samples. Overall, the seaweed-based model compounds

become more coal-like in their H, C and O ratios after hydrothermal carbonisation, resulting in an increase in energy density. Indeed, figure 5.11 confirms an increase in HHV with increasing HTC temperature for the samples, with the highest two HTC temperatures reaching values of around 24 MJ/kg for the sodium alginate and alginic acid.

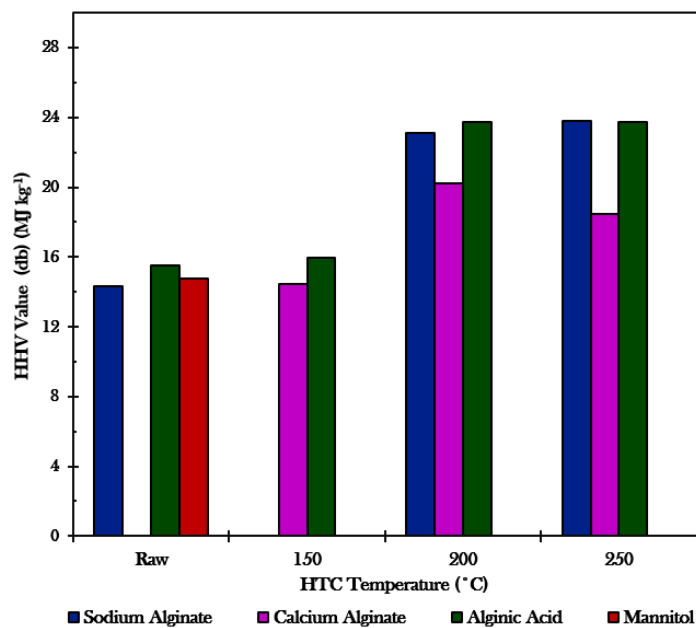


Fig. 5.11 The HHV values of the seaweed model compound solid phase after HTC, presented as a function of the HTC temperature.

5.3.2 Fate of Inorganics: Pressed Pellet X-Ray Florescence

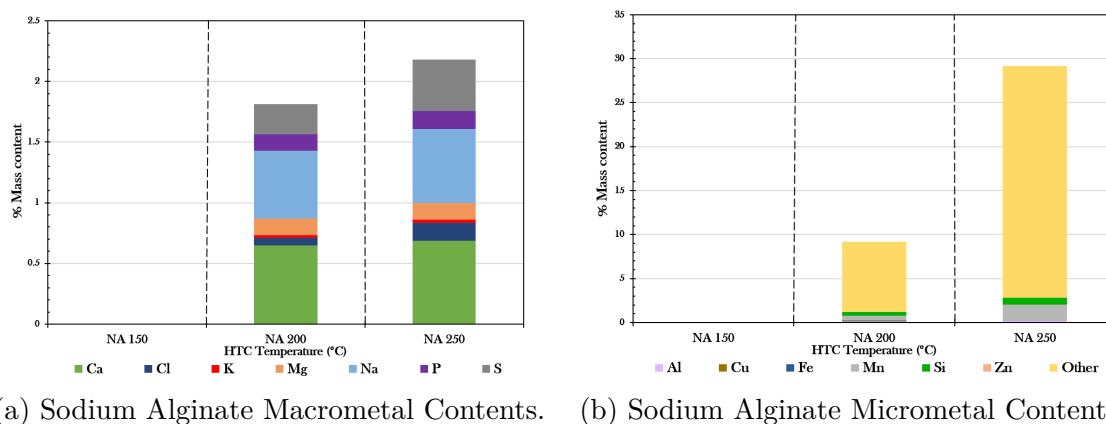


Fig. 5.12 The Inorganic Contents of the Sodium Alginate hydrochar samples after HTC processing.

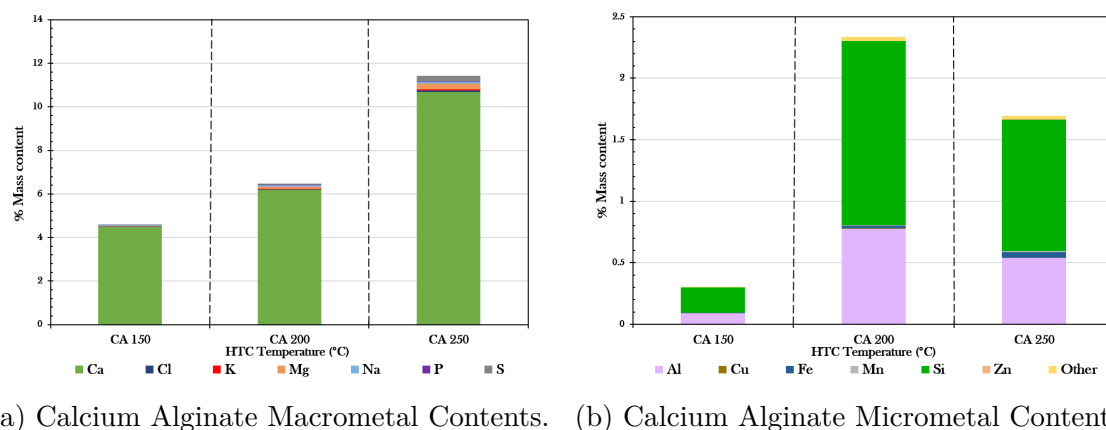


Fig. 5.13 The Inorganic Contents of the Calcium Alginate hydrochar samples after HTC processing.

Observing the micrometals bar chart for the sodium alginate, figure 5.12b, it is apparent that a large proportion of the inorganics is from the ‘other’, which from the raw data is due to high chromium levels. This is quite a significant amount, at 27% mass content, at NA 250°C, up from 7% chromium at 200°C. There was also some nickel in the % Other micrometals detected. The issue with the sodium alginate model compound being not the purest has arisen once again, as these results suggest that the NA is not just Na Alginate. This is shown by the large amount of calcium detected in the sample. Large amounts of S also are peculiar, and may indicate some fucoidan is present in the feedstock. These general XRF results for the sodium alginate may therefore only be taken as approximate.

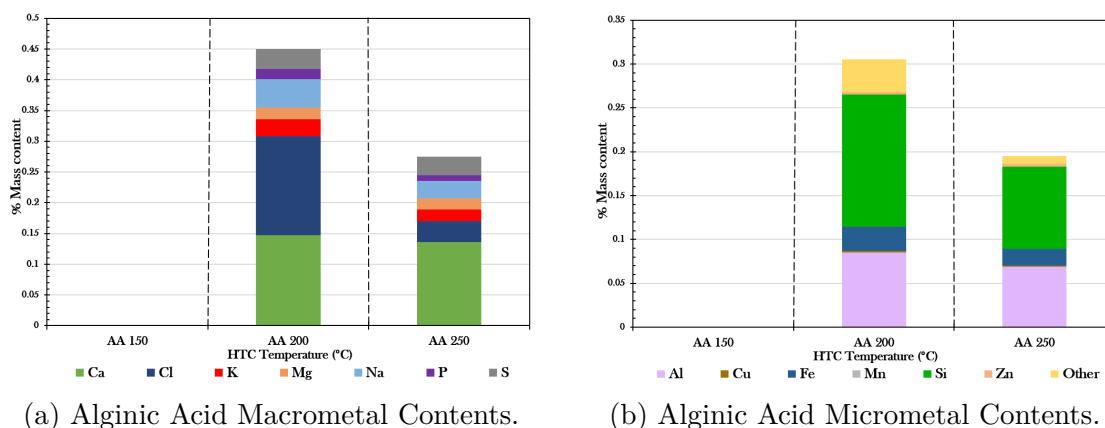


Fig. 5.14 The Inorganic Contents of the Alginic Acid hydrochar samples after HTC processing.

For the calcium alginate (figure 5.13), there is a clear trend that the amount of calcium remaining in the solid phase after HTC increases with HTC temperature increase, from 4% to 10%. This is expected somewhat due to the calcium alginate being the model compound feedstock, however it is interesting to learn this trend, coupled with the trend in the aqueous phase, shows that the solubility of the calcium decreases with increasing HTC temperatures. There was a lot of silicon and aluminium as well, although still less so than the macrometals in total (see the change in y-axis scale), more so at 200°C than 250°C. Generally, the calcium alginate certainly looks to be much more pure as a feedstock than some of the previous samples analysed.

For the alginic acid hydrochar (figure 5.14), the total inorganic content is much lower than the other samples, with small amounts of silicon and aluminium. However, seaweeds do not contain alginic acid on its own, rather it contains alginate associated with either mono or divalent cations, so extrapolating from the alginic acid model compound data to determine its effect on ash behaviour would be quite irrelevant here. Compared to the sodium and calcium alginate, there are much lower amounts of calcium and sodium, and more metals at the 200°C than the 250°C, unlike the trend with the other model compounds. There is also the presence of chlorine, mainly in the 200°C sample, which is not a significant component for the other results.

5.4 100% Biomass Feedstock

5.4.1 Ultimate and Proximate Analysis

The CHNOS, TGA and HHV values of the 100% biomass feedstocks, at the three different temperatures, are shown in table 5.3 for the raw samples and the three different temperatures. In addition, bar charts of the C, H, N and O contents of these samples are shown in figure 5.15. The Van-Krevelen (V-K) diagram containing the H/C and the O/C ratios on an atomic basis is shown in figure 5.16. The HHV values are shown for these LMC samples in the grouped bar chart in figure 5.17.

Table 5.3 CHNOS, TGA and HHV values for the 100% biomass feedstocks HTC solid phase.

SL = *Saccharina latissima*, FS = *Fucus serratus*, * = Calculated by difference.

Sample, HTC Temperature (°C)	CHNOS Data (%)						TGA Data (%)				HHV (db) (MJ/kg)
	N	C	H	S	H (db)	O (daf)*	M	VM	FC	Ash	
SL Raw	1.40	30.06	5.18	0.00	4.48	45.70	6.31	68.57	13.07	12.06	13.93
SL 150	2.56	36.78	5.20	0.05	4.56	38.08	5.73	67.84	14.18	12.24	15.62
SL 200	2.43	45.98	5.20	0.00	4.88	28.16	2.89	66.59	14.86	15.66	18.36
SL 250	2.29	52.54	5.51	0.00	5.26	20.90	2.25	62.63	18.37	16.76	20.93
FS Raw	1.97	36.79	5.58	0.00	4.49	40.30	9.82	66.26	16.80	6.62	15.57
FS 150	2.67	43.89	5.74	0.15	4.55	30.17	10.69	62.35	19.09	7.87	17.68
FS 200	2.65	47.85	4.84	0.00	4.38	24.98	4.12	57.20	22.66	16.03	18.94
FS 250	2.02	49.00	5.26	0.06	4.75	21.13	4.65	52.96	24.00	18.40	19.34
<i>Miscanthus</i> Raw	0.22	44.30	6.03	0.00	5.60	38.89	3.93	78.17	10.84	7.06	17.53
<i>Miscanthus</i> 150	0.31	46.94	6.25	0.00	5.85	37.91	3.54	79.30	11.72	5.44	18.59
<i>Miscanthus</i> 200	0.38	50.91	6.20	0.00	5.90	35.38	2.65	75.65	16.93	4.78	20.26
<i>Miscanthus</i> 250	0.57	65.46	5.02	0.00	4.79	22.58	2.01	53.03	40.38	4.57	26.08

As shown in figure 5.15, the amount of carbon in the 100% biomass hydrochars increases with HTC temperature rise, due to the formation of the carbon rich char due to the breakdown of the cellulose, hemicellulose and lignin in the samples, and the polysaccharides in the seaweeds. These large compounds under HTC conditions are known to breakdown into sugars and then short chain organic acids, with more carbon free to become polymerised and undergo solid-solid reactions, producing more solid products, which contains more carbon content at higher temperatures and hence higher proportion of material that has broken down in the more superheated water. See figure 2.11 for more detail on the breakdown mechanisms that form the solid products in the hydrochar.

The *Saccharina latissima* CHNO results shown in figure 5.15a shows a rather linear effect in the reduction of oxygen with increasing HTC temperature, directly corresponding with the linear increase in the carbon content. The hydrogen has a slight increase and small amounts of nitrogen are also present in the SL hydrochars, below 3%.

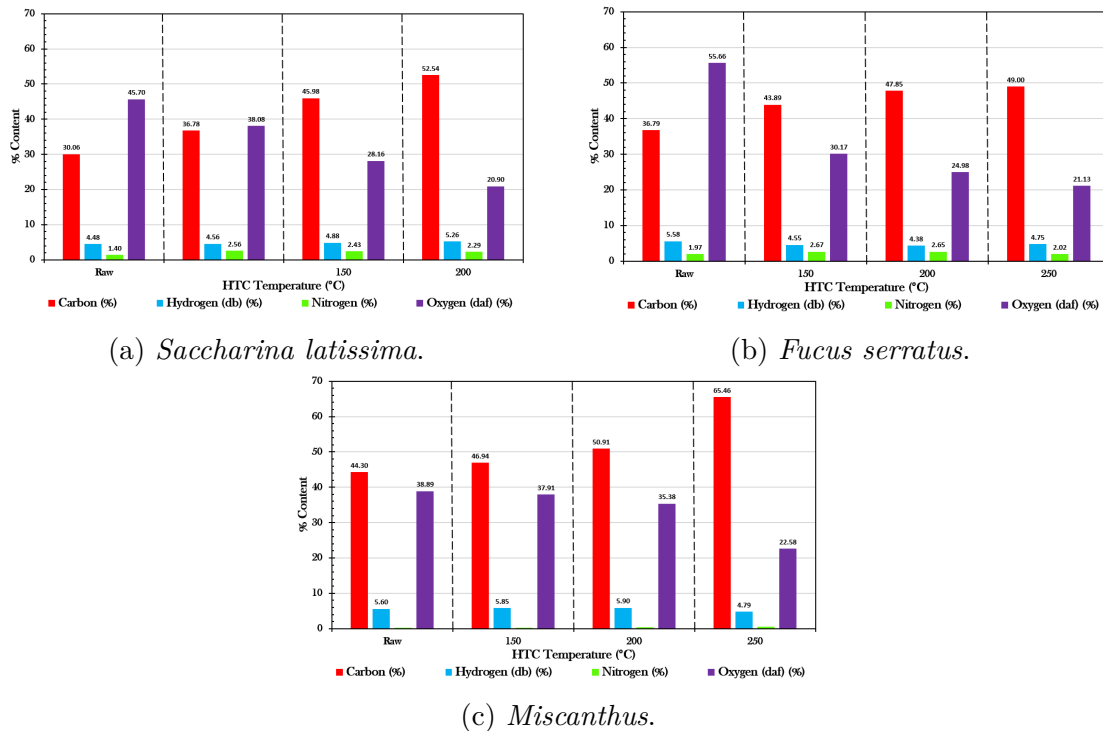


Fig. 5.15 The CHNO values from the Hydrochar of the 100% Biomass Feedstock.

The FS and M samples CHNO results, figures 5.15b and 5.15c respectively, show a similar trend in the O% reduction and C% increasing, although there's more of a jump from the raw sample to the HTC hydrochars at the lower HTC temperature for the *fucus* samples.

The *Miscanthus* feedstocks starts with the most similar O% and C% contents in the raw feedstock, yet results in the highest difference in the O and C contents in the 250°C hydrochar (over 40%). The linear O and C content trends in the M samples have a larger step from the 200 to 250 samples, indicating that more breakdown of the HTC feedstock occurs after the 200°C has been reached. Comparing this observation with the ultimate results from the cellulose model compound samples, this may be due to the cellulose breaking down more readily at these higher temperatures. Cellulose is a key component of the *Miscanthus* feedstock, but not in the seaweed samples. This would hence go some way to explaining this difference of the O% and C% trends in the ultimate analyses of the three biomass feedstocks after HTC at the highest two HTC temperatures. The *Miscanthus* samples also contain the least amount of nitrogen out of these biomass samples.

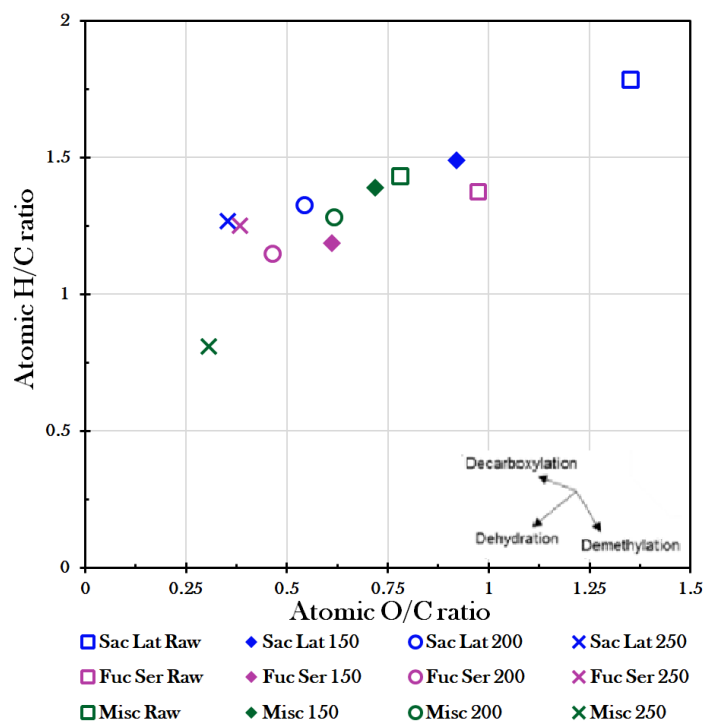


Fig. 5.16 Van-Krevelen diagram for the 100% biomass feedstocks solid phase.

The V-K diagram in figure 5.16 shows all the biomass samples undergoing progressive deoxygenation, as the data points shift to the bottom left corner of the diagram. This results in more 'coal-like' properties of the samples, in terms of their atomic O, C and H ratios. The M 250°C sample is hence the most 'coal-like'.

There is an overall trend of energy densification, looking at the HHV values in figure 5.17, of the three biomass feedstocks as the HTC temperature increases. This agrees with previous data and studies performed on the HTC of biomass, using these types of feedstocks.

The FC content also changes with corresponding opposite changes in the %VM content, as expected. The fixed carbon content increases with HTC temperature, and the *Miscanthus* sample has the most FC, due to highest C content for M 250°C, resulting in the largest HHV value of all the 100% biomass samples, of 26.08 MJ kg⁻¹. The gradual increase in HHV with increasing HTC temperature trend can be seen visually in figure 5.17. This figure shows that at the highest HTC temperature, the *Saccharina latissima* has a higher energy density than the *fucus*, but not as much as the *Miscanthus* 250°C sample.

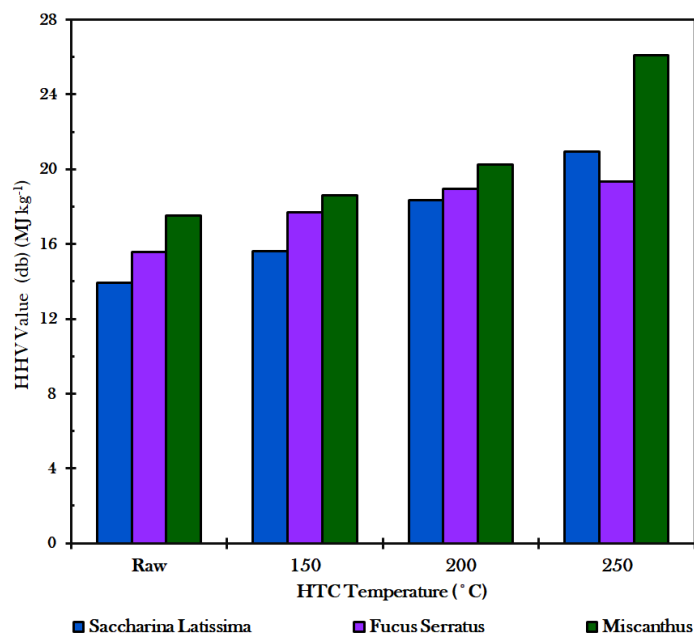
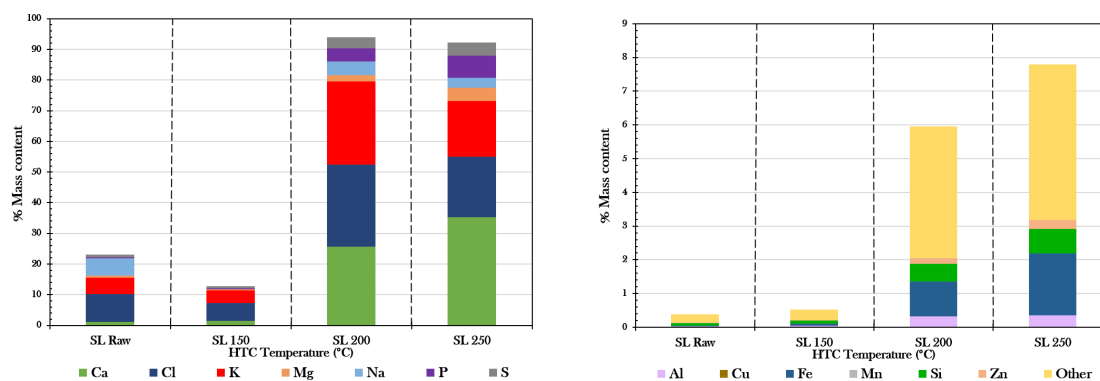


Fig. 5.17 The HHV values of the 100% biomass feedstocks solid phase after HTC, presented as a function of the HTC temperature.

5.4.2 Fate of Inorganics: Pressed Pellet X-Ray Florescence



(a) *Saccharina latissima* Macrometal Contents. (b) *Saccharina latissima* Micrometal Contents.

Fig. 5.18 The Inorganic Contents of the *Saccharina latissima* hydrochar samples after HTC processing.

As can be seen in figure 5.18a, SL 200°C still has a lot of calcium. There are plentiful amounts of potassium and chlorine as well, and a significant increase from 150°C, with a total of 11%, just less than the raw SL due to the lack of sodium from the seawater residue, to over 90% for both of the 200°C and 250°C samples. This is the highest mass content for metals compared to any of the samples studied in this research. This trend is

expected for the raw SL sample due to the known high metals content within seaweed and the salt from the seawater, although just how much this increases; over four fold, is an important observation. The extremely high total amounts of over 90% of macrometals for *Saccharina latissima* 200°C and 250°C samples may be a mistake caused by the XRF instrument picking up extra signals from the stainless steel pressed pellet holder, so caution must be taken when drawing conclusions from these results. For the seaweed to be a viable fuel option after hydrothermal carbonisation at temperatures above 200°C (high enough to allow a high density of energy in the hydrochar), the fuel needs to pass the slagging and fouling indice limits. The high value of total metals in both the macrometals analysis and the micrometals analysis, where a high level of strontium and iodine - the main components in the %Other category for the micrometals, up to 3% for Sr in SL 250°C - is expected in seaweeds.

These XRF results of the SL hydrochar demonstrate the main issue with using seaweed as a biomass feedstock on its own; co-processing the seaweed with biomass of a lower metal content is required to reduce the overall slagging and fouling propensity and ash content to acceptable levels. The high K, Cl and Ca values recorded here will contribute to increasing the alkali index (AI) of these samples, calculated in §5.4.3. These results demonstrate the chosen ratio of 80:20 *Miscanthus* to seaweed was a suitable proportion, because the relatively low amount of seaweed should limit the amount of metals in the sample, allowing for slagging and fouling indices to be passed by the co-processed mix. The results of the mixed feedstock will be evaluated later. In terms of the fate of the inorganics by comparison with the liquid XRF results, these will be analysed and compared to the pressed pellets XRF results in the following chapter.

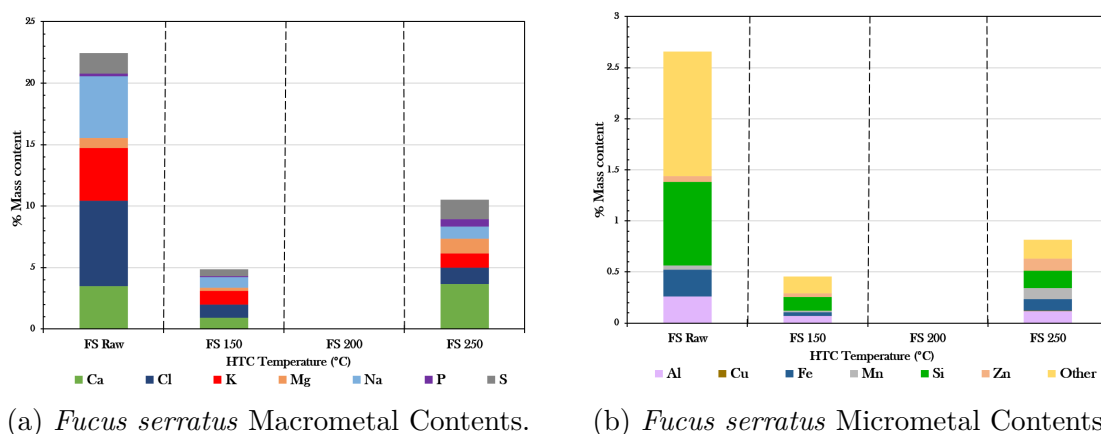


Fig. 5.19 The Inorganic Contents of the *Fucus serratus* hydrochar samples after HTC processing.

As shown in figure 5.19, unlike the *Saccharina latissima* XRF results the *Fucus serratus* total metal content reduces significantly after hydrothermal processing. This is true for both the micro and macro inorganics. There is a slight increase from 150°C to 250°C as the HTC temperature rises (mostly due to an increase in calcium levels), although the total metal mass content at 250°C remains less than half the original content from the raw *fucus*. The four main inorganics in the raw FS samples are; calcium, chlorine, potassium and sodium. Interestingly, however, the % ash of the *fucus* after hydrothermal processing is more than that of the *saccharina*, apart from the FS 150°C hydrochar sample (refer to table 5.3).

The fate of these organics will be studied in comparison to the liquid XRF results in the following chapter. It is thought that these metals would be detected at higher concentration after HTC than before processing in the aqueous phase of the *fucus* samples. This would improve the qualities of the process waters for use within the fertiliser industry, where high potassium and calcium contents are particularly beneficial. This drop in total metals compared to the sugar kelp feedstock may lead to improved slagging and fouling indices, which will be reviewed in the next section.

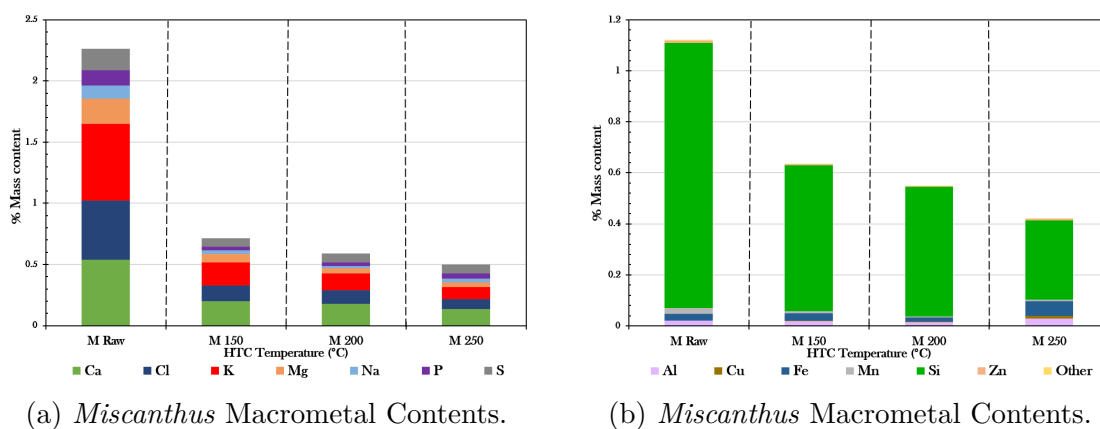


Fig. 5.20 The Inorganic Contents of the *Miscanthus* hydrochar samples after HTC processing.

Evaluating the *Miscanthus* inorganics in figure 5.20, it can be concluded that the overall ash content reduces compared to the initial feedstock after hydrothermal processing, with slightly lower ash at the higher temperatures. This is indeed verified in the %ash content results for *Miscanthus* in table 5.3. The ash content of the *Miscanthus* remains similar in proportion with regards to the different individual inorganic % mass content, throughout the four various samples. As with the *fucus*, the main inorganics are potassium, calcium and chlorine, with traces of magnesium and sulphur. Regarding the micrometals, this is

dominated for each sample by silicon. The silicon reduces after HTC processing, possibly due to being absorbed into the aqueous phase (although this actually only increases by 0.03%), and %Si was further reduced as the HTC temperature increased. A change in Si levels would positively effect the ABR, SI, FI and SVI indices (see equations 3.13 to 3.17).

Overall, there are significantly less macro and micrometals in the terrestrial feedstock than the algal feedstocks, both before and after HTC. This is as expected, and is reflected in the different to the ash contents of the three samples. Silicon is more prominent in the *Miscanthus* than the seaweeds, although this may also be due to changes in the temperature levels and precipitation levels where the *Miscanthus* was grown [176].

These XRF pressed pellet results verify that *Miscanthus* would bring down the ash content and subsequently the inorganics levels for a co-processed mix with seaweed. This hence would potentially allow for further combustion of the MSL hydrochar, due to a higher likelihood of passing the slagging and fouling indices. The level at which the 80:20 *Miscanthus:Saccharina latissima* will reduce the metals and ash in the feedstock will be quantified in the following section.

5.5 Co-Processed Feedstock

5.5.1 Ultimate and Proximate Analysis

The CHNOS, TGA and HHV values of the Co-processed biomass feedstocks after HTC processing are shown in table 5.4 for the raw samples and the three different temperatures. In addition, bar charts of the C, H, N and O contents of these samples are shown in figure 5.21. The Van-Krevelen (V-K) diagram containing the H/C and the O/C ratios on an atomic basis is shown in figure 5.22. The HHV values are shown for these LMC samples in the grouped bar chart in figure 5.23.

The co-processed SL 250°C mixed 1:4 with *Miscanthus* should still have high HHV due to M having a high amount of HHV. The predicted HHV of the M:SL 80:20 mix was calculated to be $(26.08 \times 0.8) + (20.93 \times 0.2) = 25.05$, which will be compared to the actual HHV determined via the MSL HTC experiments.

The main trends of the CHNOS contents shown in table 5.4 and displayed as bar charts in figure 5.21 shows that the carbon content increases with HTC T increasing, corresponding

Table 5.4 CHNOS, TGA and HHV values for the Co-processed biomass feedstock model compound HTC solid phase. *Calculated by difference.

Sample, HTC Temperature (°C)	CHNOS Data (%)						TGA Data (%)				HHV (db) (MJ/kg)
	N	C	H	S	H (db)	O (daf)*	M	VM	FC	Ash	
Misc/Sac Lat 150	0.40	44.71	6.44	0.00	6.09	38.96	3.11	75.69	14.46	6.74	17.73
Misc/Sac Lat 200	0.57	48.64	5.96	0.00	5.73	36.75	2.07	72.39	19.30	6.24	19.28
Misc/Sac Lat 250	0.91	60.71	5.45	0.00	5.12	23.95	2.89	51.84	38.86	6.42	24.22
Misc/NA 150	0.25	45.63	6.14	0.00	5.75	37.69	3.46	73.48	15.84	7.22	18.05
Misc/NA 200	0.28	47.76	5.95	0.00	5.51	41.41	3.92	68.54	25.09	1.13	18.84
Misc/NA 250	0.46	64.17	5.87	0.00	5.58	23.31	2.62	52.64	40.89	3.85	26.29
Misc/Man 150	0.24	44.27	6.28	0.00	6.01	41.50	2.45	82.13	9.89	5.53	17.54
Misc/Man 200	0.28	48.70	6.32	0.00	6.07	37.63	2.26	78.01	14.68	5.05	19.36
Misc/Man 250	0.38	64.38	5.73	0.00	5.43	18.77	2.73	52.79	36.17	8.30	26.22

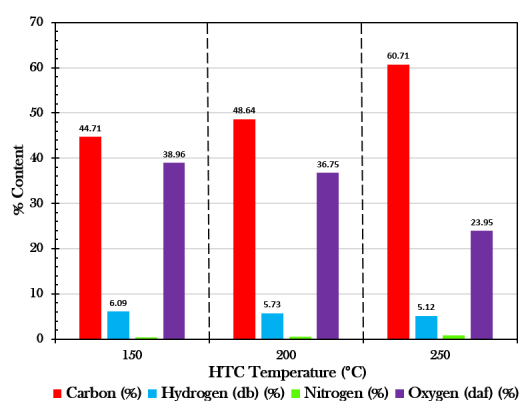
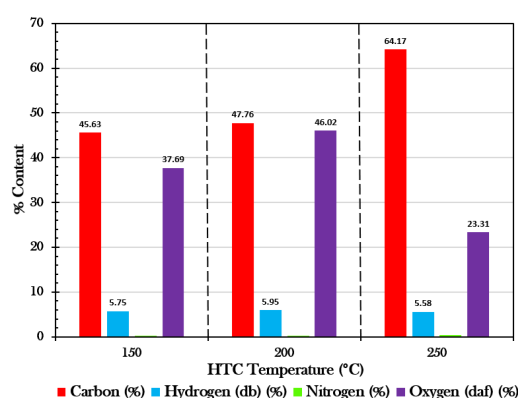
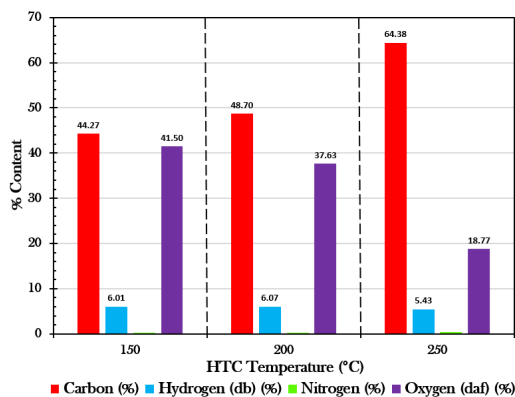
(a) *Miscanthus:Saccharina latissima*.(b) *Miscanthus:Sodium Alginate*.(c) *Miscanthus:Mannitol*.

Fig. 5.21 The CHNO values from the Hydrochar of the Co-Processed Feedstock.

with an anticipated reduction in the %O content. This corresponds with an increase in FC content and therefore the final HHV values.

Although the MSL and MMan HTC hydrochars both show this trend more linearly, the MNA sample interestingly has a spike in %O at the 200°C temperature, although the carbon content does still increase, albeit by only 2%. This may be due to more of

the oxygen containing organics caused by the degradation of the *Miscanthus* and the sodium alginate (which itself contains oxygen, $(C_6H_7NaO_6)_n$) solubilised in the water phase becoming more polymerised and fixing more oxygen atoms into the solid hydrochar phase.

The %ash content is rather low for the MNa 200°C sample compared to the other hydrochars, perhaps caused by the same mechanisms that cause the %O to increase at the 200°C temperature. The %ash for the MSL samples does not significantly change due to HTC temperature, and at around 6.5% is 10-12% less the ash contents of the SL 200 and 250°C hydrochars respectively, and half that of the SL 150°C hydrochar. This is a positive result in terms of improving the fuel suitability via mixing the feedstocks prior to HTC processing.

The three MSL %ash contents was found to be only 1-1.5% greater than the ash content of the 100% *Miscanthus* hydrochars and so although adding the seaweed to the *Miscanthus* at this ratio does increase the ash, the hydrochar produced may still be within the slagging and fouling limits. The act of co-processing the seaweed with the *Miscanthus* means that such a third generation feedstock actually has the potential to be used within a biorefinery in this way, due to a significant reduction in the %ash when mixed. The inorganic content of the hydrochars will be assessed in greater detail in the following section, and ultimately the slagging and fouling propensity changes due to co-processed evaluated.

The co-processing of the *Miscanthus* with the sugar kelp appears to effect the FC content by increasing it slightly (around 3%) for the lower two HTC temperatures, but reduces the total FC content by less than 2% at the 250°C HTC temperature. This is likely due to the much lower FC content of the 100% *Saccharina latissima* sample compared to the 100% *Miscanthus* sample at this temperature. The FC would be expected to be around $((18.37\% \times 0.2) + (40.38\% \times 0.8) =) 35.98\%$, if there were no interactions between the feedstocks. So, the fact that the MSL 250°C sample has a slightly higher FC than this theoretical value (38.9%) shows that the addition of the saccharina to the *Miscanthus* feedstock produces non-additive behaviour (it is not simply a dilution effect), in terms of producing an energy dense biofuel via HTC, due to the relatively high FC content in the MSL 250°C hydrochar.

The FC content changes with HTC temperature for the co-processed samples once again corresponds with a roughly equal in scale reduction of the %VM content. This is as expected and in agreement with the previous data analysed in this study.

The fact that the FC for the MSL 150°C and the 200°C samples are higher than

both the M and the SL 100% biomass feedstocks shows also that the addition of the seaweed, rich in metals, has a promotive effect of producing a more carbon-rich hydrochar (non-additive). It is possible that the metals within the seaweed could aid the breakdown mechanisms of the cellulose and hemicellulose from the *Miscanthus* feedstocks. The metal analysis of these samples and the fate of the inorganics will be analysed in the next section to determine the effects of the metal contents on the hydrochar formation.

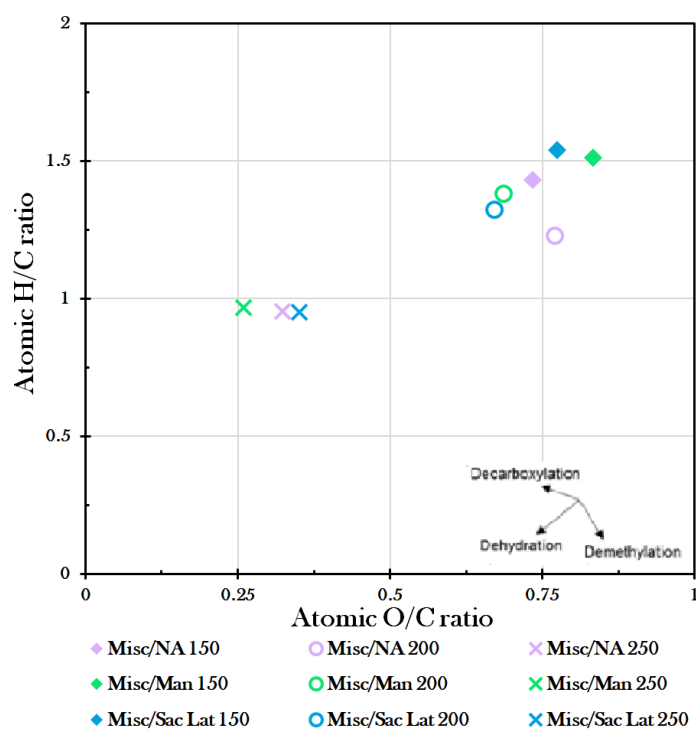


Fig. 5.22 Van-Krevelen diagram for the co-processed biomass feedstocks solid phase. NA = Sodium Alginate.

The effect of the FC having an increase with HTC temperature (particularly at the highest) results in higher HHV values for the higher HTC temperatures also. The significant increase of the HHV values for each co-processed feedstock between the 200°C and the 250°C hydrochar samples shows that this is the more preferred HTC temperature for biofuel production via hydrothermal carbonisation of *Miscanthus* whether co-processed or not (HHV of the 100% *Miscanthus* was higher at 250 by 6 MJ kg⁻¹ from 200°C).

The 50°C increase in HTC temperature results in a far higher HHV much more similar to that of coal, as also demonstrated in figure 5.22, and so is it encouraging for this research that this is still that case for all three of the co-processed samples. However, it should be noted that the HHV of the 100% *Miscanthus* was in fact slightly higher than

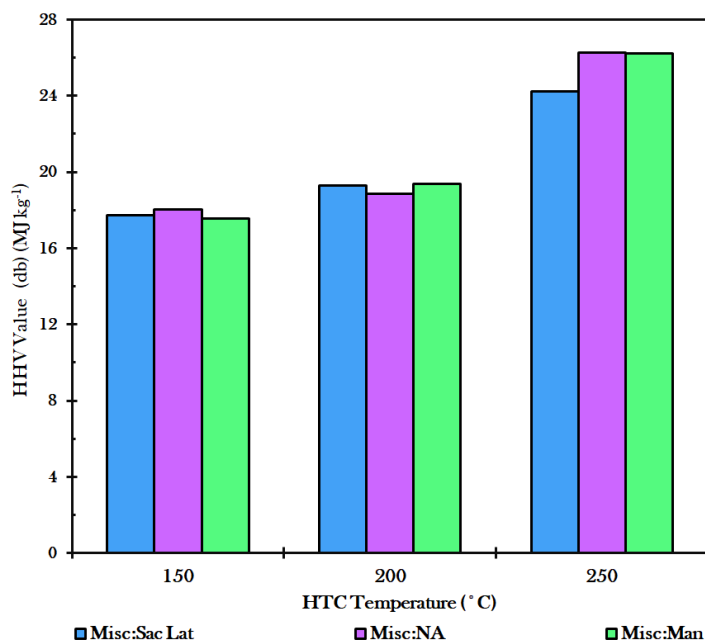


Fig. 5.23 The HHV values of the co-processed feedstocks solid phase after HTC, presented as a function of the HTC temperature.

NA = Sodium Alginate.

the HHV of the MSL mix, for each of the three HTC temperatures.

The overall trend of this higher HHV with higher HTC temperature also results in the hydrochar becoming more similar to that of coal in terms of its carbon/hydrogen and oxygen/hydrogen ratios, due to the oxygen reduction shown in figure 5.21 and the increase in carbon content. This can be seen in figure 5.22 as the higher temperature samples are closest to the $y = 0, x = 0$ point on the V-K diagram. Figure 5.23 shows the relatively higher HHV in the 250°C samples. In this figure it can also be seen that the HHV of the MSL co-processed sample is slightly lower than the *Miscanthus* and model compound co-processed hydrochars.

5.5.2 Fate of Inorganics: Pressed Pellet X-Ray Florescence

For the MSL mix hydrochars, the macrometal content shown in figure 5.24 shows a total inorganic content much lower than the 100% SL hydrochars, at just 2.7-3.3%, compared to 90% pure SL. Similarly to the M and the SL hydrochars, there are similar relative proportions of potassium, chlorine and calcium, with some sodium from the SL. There

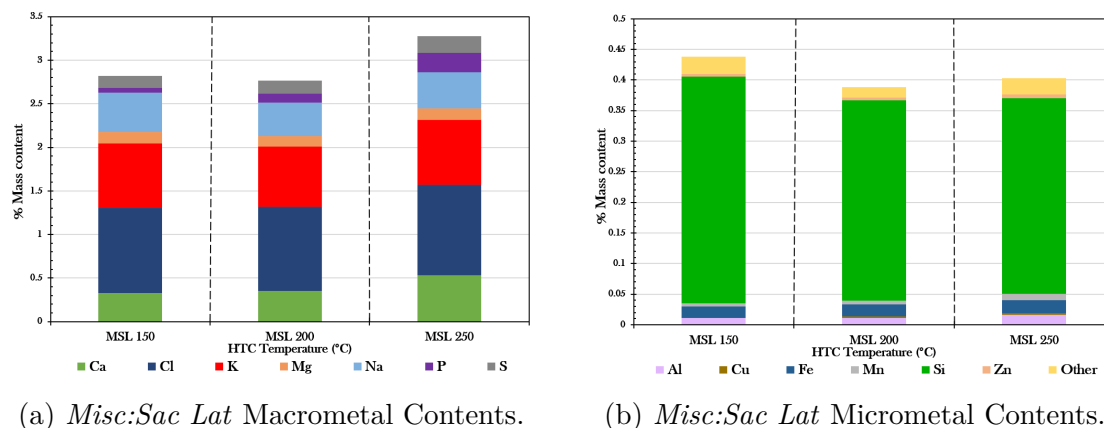


Fig. 5.24 The Inorganic Contents of the *Miscanthus:Saccharina latissima* hydrochar samples after HTC processing.

is also some silicon from the *Miscanthus*, of comparable values to the 100% *Miscanthus* results. The 250°C hydrochar has slightly more macrometals, due to a slight increase of calcium and phosphorus levels.

There are low overall values of the micrometals; less than 0.45%, despite the SL in the feedstock mix. Both the micro and macrometal total mass contents are at the same approximate percentage for all three hydrochar samples; between 3 and 4% in total. The lower total inorganics total for the MSL and the smaller values compared to the 100% SL demonstrate why the %ash values in table 5.4 are so similar for the MSL and are much lower than for 100% SL (6.2-6.2% compared to 12.1-15.7%). This should hence be reflected positively in the slagging and fouling calculations for the co-processed feedstocks, and therefore improve the feasibility of the hydrothermally carbonised MSL mix as a potential future biofuel option.

Comparing the micro and macrometal trends, the proportions of the inorganics remains broadly the same, so it appears that the HTC temperature does not significantly effect the different mass contents of the various inorganics individually. Therefore the slagging and fouling indices are expected to be similar throughout the three different HTC temperatures of the MSL co-processed hydrochars.

Observing the inorganic content found within the *Miscanthus*:sodium alginate hydrochars in figure 5.25, it is apparent that the lower HTC temperature results in the most macro and micrometals. This is most likely due to the metals becoming more absorbed into the process water at higher temperatures (see §6.5.7), which was indeed the case for almost every single metal identified in the liquid XRF, especially regarding the increase

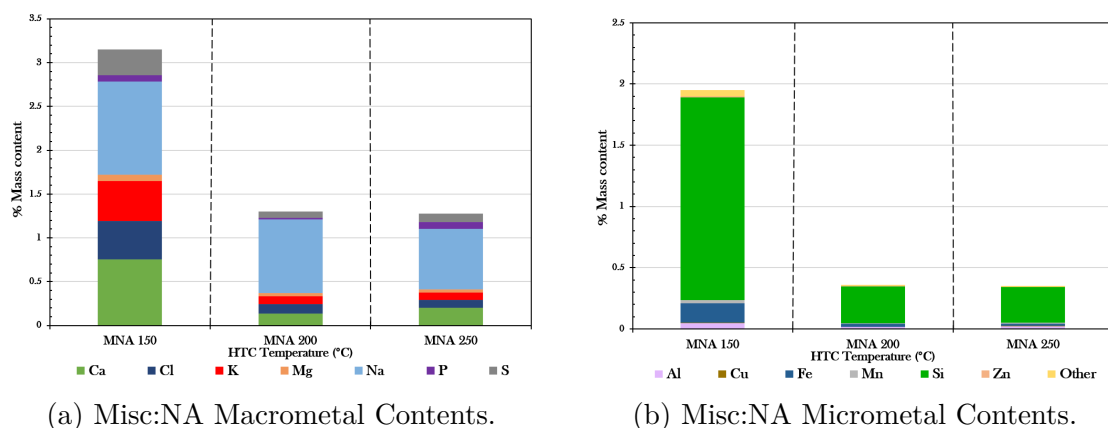


Fig. 5.25 The Inorganic Contents of the *Miscanthus*:Sodium Alginate hydrochar samples after HTC processing.

in the sodium levels in the aqueous phase. This total % inorganic content for 150°C, was roughly three times more than the 200°C and 250°C samples, which were almost identical.

Considering the distribution of different inorganic material, the main extra components of this 150°C sample contributing to the higher total was the potassium, chlorine, calcium and silicon contents. Interestingly, the silicon content reduced down to less than 0.5% in the hydrochar of the higher two HTC temperatures due to the presence of the sodium alginate, something that would be beneficial for a biofuel (as the slagging and fouling indices use silicon in the calculations often). These trends follow those found in the 100% *Miscanthus* samples, with similar % mass contents of the metals. However, as expected given the feedstock, there are higher amounts of sodium in these co-processed samples than the 100% *Miscanthus* samples. It is difficult to compare to the pure sodium alginate model compounds sample at the lowest temperature, as this HTC run did not produce enough hydrochar to create a pressed pellet for analysis. Nonetheless, comparison to the NA 200°C and NA 250 °C hydrochars, the micrometals in the M:NA hydrochars are more dominated by the silicon from the *Miscanthus* than the % Other from the sodium alginate, despite this high % other mass of over 25% for NA 250°C. The potassium in the M:NA hydrochars was caused by the *Miscanthus*, as none were present in the NA model compound hydrochars.

The overall inorganic content was much lower than the M:SL hydrochars, leading to the conclusion that the slagging and fouling indices for this feedstock would be better values. However in terms of a feasible feedstock, using a pure model compounds for a feedstock is not the aim here, - this gives an indication of how the sodium alginate within the

seaweed contributes to the slagging and fouling propensity levels of the M:SL potential co-processed HTC feedstock.

These inorganic content results demonstrate that seaweeds with a higher sodium alginate content would likely be beneficial to the feedstock if the hydrochar were to be used as a biofuel, due to reduced ash and a lower probability of slagging and fouling the biomass boilers, particularly if the HTC reactor is ran at 200°C or above. It is therefore likely that different chemical components of seaweed is responsible for the high inorganic content found in the 100% SL and M:SL hydrochars. The XRF results from the M:Man hydrochars will be analysed in the next paragraph, and the contribution from mannitol to the ash content and inorganics in the seaweed hydrochars evaluated.

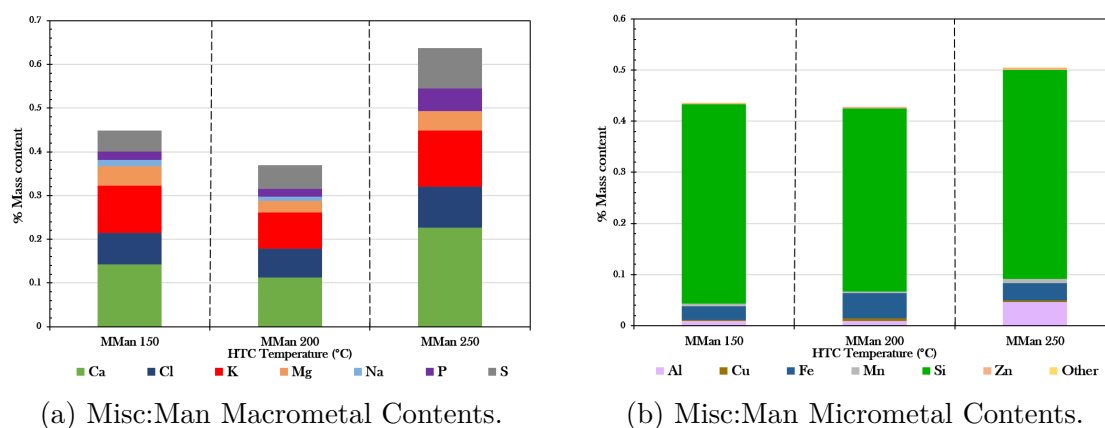


Fig. 5.26 The Inorganic Contents of the *Miscanthus*:Mannitol hydrochar samples after HTC processing.

For the *Miscanthus*:Mannitol hydrochars, figure 5.26, the total inorganic content actually increases with HTC temperature, albeit with a slight dip in total macrometals for the 200°C sample. The levels of silicon in the hydrochar are similar to the M 150°C and M 200°C samples, but the M:Man 250°C has a higher Si % than the corresponding M 250°C sample. The same trend is true for the levels of the different macrometals, again with an increase at 250°C for the mannitol co-processed mix due to slight increases in all the measured macrometals apart from sodium. However, with a total macrometal content just over 0.6%, the level of inorganics in the hydrochar is still very similar to the M 250°C sample and is much reduced compared to the untreated raw *Miscanthus* feedstock. This slight increase at 250°C is likely the cause of the increase in ash content at this temperature shown in table 5.4.

The trends and relative proportions of the different inorganics identified in the M:Man samples are more similar to the M:SL hydrochars than the M:SL is to the M:NA hy-

drochars, indicating that mannitol has a more important role to play in HTC conditions than the sodium alginate in the hydrochar slurry mix. The overall effect of the co-processing of the feedstock on the theoretical likelihood of the slagging and fouling of the boilers, using these inorganic results, will be evaluated in the next section.

5.5.3 Slagging and Fouling Indices

During the heating (for example in a biomass boiler) using biomass, the ash produced from the biomass feedstock becomes problematic. A high ash content is not desirable, and the contents of the ash, usually macro and micro metals are important to measure, as this effects the properties of the ash within the boiler [177]. The ability for a biofuel to pass these strict measures is essential for a future feedstock, as these are in place to ensure that the fuel does not stick to the inside of the boilers, requiring frequent cleaning, causing downtime and extra expenses, and more frequent infrastructure renewals if the boilers were to become corroded. The trace metals responsible for these types of slagging and fouling of the boilers are used to calculate certain characteristics of the fuel type; its' tendency to agglomerate and slag or foul. The BAI indice helps determine how likely the ash is to agglomerate in fluidized bed reactors [178], for example (more detail about each indice is in §3.5.3).

The main metals that are known to cause ash formation are Fe, Ca, Mg, K, Na, Al and Si [177], and these contents are used within the slagging and fouling indice calculations. These indices are calculated in their metal oxide % content form, which was determined via the pressed pellet XRF analysis, selecting 'metal oxides' in the software and recalculating the results measured to determine these figures. These metal oxide values are important to enable predictions of the melting and ash deposit behaviour of the hydrochar [177]. These limits are enforced in industry and any feedstock for biomass boilers would have to pass these criteria, although are only an indication of the ash properties.

More thorough ash behaviour of potential biofuels can be further studied by ash fusion tests. This is where a pellet of ash produced from the biomass is pressed and heated in a furnace. The shape of the pellet is observed by a camera as it deforms as the temperature is increased [88]. However, ash fusion experiments would require an abundance of each sample which was not available from these small-scale 600ml HTC batch reactor results. It is hence important to note that the slagging and fouling values are only an indication of their properties, and the characteristics may differ slightly in reality.

Tables 5.5 and 5.6 shows the slagging and fouling propensity of the 100% biomass feedstocks and the co-processed feedstock hydrochars respectively, via XRF analysis. These values are determined using the equations and methodology explained in §3.5.3, using equations 3.11-3.17. The indices are colour coded in this table so that green cells represent accepted values below (or above if appropriate) the respective thresholds and red cells are above (or below) the upper threshold. These thresholds are listed in table 3.1. A colour code of green, amber and red has been applied for the different values, with green for a pass value, amber for ‘medium’ values (where applicable, for the AI, and SI, FI and SVI values) and red for failed indice values. Unfortunately, the FS 200°C sample was lost due to the cyromill lid loosening during milling due to the resonance with the frequency of the instrument, which has been reported to sometime happen when using the cyromill.

Table 5.5 Slagging and Fouling Indices for the 100% Biomass Feedstock Hydrochars after HTC processing.

SL = *saccharina latissima*, FS = *fucus serratus*, Misc = *miscanthus*.

Sample Name, HTC Temperature (°C)	Alkali Index (AI)	Bed Agglomeration Index (BAI)	Acid Base Ration (ABR)	Slagging Index (SI)	Fouling Index (FI)	Slag Viscosity Index (SVI)
SL Raw	21.2772	0.0021	44.9377	0.0000	1331.9115	6.3993
SL 150	5.0440	0.0088	33.6274	1.6814	264.9435	7.1584
SL 200	16.0632	0.0341	39.1296	0.0000	1154.0105	3.1952
SL 250	9.0492	0.0860	32.1835	0.0000	609.5519	3.0661
FS Raw	9.1552	0.0317	8.2700	0.0000	115.0094	20.8793
FS 150	1.2748	0.0206	10.0387	1.5058	22.6261	14.4436
FS 250	1.3801	0.0587	17.2394	1.0344	46.0155	4.7291
Misc Raw	1.2199	0.3932	0.6288	0.0000	1.3448	63.2186
Misc 150	0.1420	0.1595	0.5546	0.0000	0.1464	73.8146
Misc 200	0.0910	0.1209	0.4719	0.0000	0.0870	76.0738
Misc 250	0.0691	0.5166	0.6856	0.0000	0.1235	66.6219

It is shown in table 5.5 that the 100% *Miscanthus* sample performs the best - after HTC almost all the *Miscanthus* samples pass all the slagging and fouling indices limits, with the exception of the M 200°C sample for BAI and ABR. This is expected, as the seaweeds are known to contain more heavy metals.

Both of the seaweed hydrochar feedstocks do indeed fail all the slagging/fouling limits, apart from the ABR and the SI indices, and the FI indice for the *fucus* 150°C. These findings are due to the high metal content determined using the XRF analysis prior, and the %ash content. Although the HTC process reduces the FS metals content, it increases

Table 5.6 Slagging and Fouling Indices for the Co-processed Feedstocks Hydrochars after HTC processing.

SL = *saccharina latissima*, NA = sodium alginate, Man = mannitol, Misc = *miscanthus*.

Sample Name, HTC Temperature (°C)	Alkali Index (AI)	Bed Agglomeration Index (BAI)	Acid Base Ratio (ABR)	Slagging Index (SI)	Fouling Index (FI)	Slag Viscosity Index (SVI)
Misc SL 150	0.8417	0.0184	2.7045	0.0000	4.0362	52.9964
Misc SL 200	0.6988	0.0209	2.8574	0.0000	3.8498	49.5187
Misc SL 250	0.5991	0.0217	3.4283	0.0000	4.9741	40.7425
Misc NA 150	1.1245	0.1116	0.9445	0.0000	1.9171	71.7679
Misc NA 200	0.6560	0.0274	2.2559	0.0000	2.8017	69.3706
Misc NA 250	0.3906	0.0268	2.0909	0.0000	2.1474	62.6150
Misc Man 150	0.0849	0.2512	0.5409	0.0000	0.0805	72.8333
Misc Man 200	0.0581	0.6246	0.4924	0.0000	0.0553	73.7513
Misc Man 250	0.0593	0.3087	0.6183	0.0000	0.0961	66.5954

the SL content. This is the reason behind the higher numbers for the AI and FI indices and lower SVI values for the SL samples, as compared to the FS.

Hence, the need to co-process the seaweed samples with feedstocks lower in inorganic contents such as *Miscanthus* is justified. Seaweed alone as a 100% feedstock not only would be difficult due to the amount required, but also the failure to meet stringent and necessary slagging and fouling limits enforced within the bioenergy industry. Although due to the wild origin of the seaweed samples, these may be higher in metal content than cultivated samples, due to bioaccumulation of the inorganics from the local ecosystem over time.

These results are as expected and qualify the need for co-processing of the seaweed with the *Miscanthus*. This will be analysed to determine the effects of the inorganics in the seaweed portion of the feedstock on the hydrochar characteristics and the aqueous phase after HTC, to ensure that this feedstock mix would indeed be appropriate for use within the bioeconomy. The next section will analyse the co-processed mixes and evaluate the performance of these feedstocks on the slagging and fouling indices. The 100% biomass feedstock hydrochars can thus be compared to these values and any differences analysed.

As can be seen in the results in table 5.6, The co-processed M:SL mix still does not meet the criteria for SVI, AI and BAI indice value, although it is much closer to passing the limit. Compared to the 100% SL hydrochars, the FI indice is now passed when SL was mixed with 80% *Miscanthus*, with improvement also seen in the ABR and SI indices,

which did pass already the criteria for the 100% SL samples. The 100% *Miscanthus* hydrochars did pass most of the criteria, although notably not the M 200°C for BAI and ABR indices. The MSL 200°C hydrochar feedstock succeeds in passing the ABR indice limits given in table 3.1.

The high potassium and sodium amounts, in addition to high calcium levels would negatively effect the AI, BAI and SVI indices, and the MSL and MNA hydrochar samples demonstrate these inorganics present in significant quantities in the XRF results (shown in figures 5.24 and 5.25).

The SVI indice upper limit of 63 is almost reached by the MSL hydrochars, and is actually met by the MNA 150°C and 200°C hydrochars plus the three MMan hydrochars. The presence of mannitol within the seaweed samples would not negatively impact the slagging and fouling propensity of the resultant hydrochar after hydrothermal processing, based on comparing these M:Man hydrochars with the 100% Misc hydrochar results. Therefore seaweed feedstocks containing a particularly low mannitol and/or high sodium alginate composition may have a reduction in their slagging/fouling potential, which can be taken into consideration due to seasonal changes in the proportions of these main components of seaweeds, or locational differences.

Using a 4:1 Misc:Sac Lat ratio as an initial mix for co-processing the feedstock does indeed result in a dramatic reduction in the chances of slagging and fouling compared to using seaweed alone, however to reach acceptable slagging and fouling indice levels within the criteria a smaller ratio of seaweed to *Miscanthus* may be proposed, to reduce the amount of inorganics remaining in the hydrochar after HTC. This would potentially pass the slagging and fouling ratios with a mix such as an 85:15 M:SL mix, although further study would have to be done to investigate this.

In addition, it is noted here that the calculated slagging and fouling indices here are only an indication of the propensity of the hydrochars to slag and foul during combustion, and further experiments on a large sample size would further establish the actual behaviour of the hydrochar ash under a combustion environment. Ash fusion, for example, would give a more accurate determination of the temperature at which the ash from the hydrochar would begin to deform from a pellet sample, and can be used to provide a better estimate of the true slagging and fouling indices of the material. However, ashing of the hydrochars would be required and not enough ash from the hydrochar samples would then be available to produce pellets of sufficient mass for ash fusion tests. It is hence recommended that potential feedstock mixes for industrial use be ran in a

larger scale HTC reactor and subsequently asked to analyse the behaviour of the hydrochar via ash fusion, in addition to XRF analysis and characterisation of the hydrochar.

5.6 Conclusions

Throughout the characterisation of the hydrochars analysed in this study, there has been a verified trend in overall energy densification of the main biomass-based feedstocks as the HTC temperature is increased, as expected. This is in agreement with similar research on the HTC of biomass stated in the literature. The carbon contents of the feedstocks generally increased, mostly on a linear trend, as the HTC temperature increased. This corresponds with a decreasing trend in the oxygen content in the hydrochars. The fixed carbon contents and volatile matter contents have opposite corresponding trends too, with the FC content increasing with HTC temperature. The hydrochars therefore become more coal-like in energy content as the HTC temperature increases and are therefore become a more suitable potential biomass feedstock after HTC processing for efficient energy production. The co-processing effect on the MSL sample results in a higher HHV value at 24.2 MJ kg^{-1} for the MSL 250°C hydrochar compared to the 100% *Saccharina latissima* hydrochar at the same temperature (20.9 MJ Kg^{-1}). However this MSL HHV value is a reduction of about 2 MJ Kg^{-1} compared to the 100% *Miscanthus* 250°C hydrochar.

The effect of adding the seaweed to the *Miscanthus* on the inorganic content of the hydrochars is important to consider due to its effect on the slagging and fouling propensities and ash behaviour of the hydrochars after HTC. It was found that the seaweed samples contain a significant total metals content, particularly at the higher two HTC temperatures. These over 90% metal content includes several problematic metals, namely calcium, potassium, chlorine and sodium. This solidifies the issue with using seaweed as a HTC feedstock as a stand-alone feedstock; it has to be mixed to reduce problems with slagging and fouling in the biomass boiler, which would cause significant financial and practical issues. Therefore the co-processing of seaweed with a higher proportion of a biomass such as *Miscanthus* is supported. Additionally, lower HTC temperatures were favourable for meeting the slagging and fouling indices, likely due to the much lower metal contents found in the 100% SL samples. It was found that although the M:SL hydrochars performed significantly better than the 100% SL hydrochars when calculating the slagging and fouling values, a slightly lower proportion of seaweed to *Miscanthus* in

the feedstock mix, or using seaweed with a slightly different biochemical content (due to differences in the seasonality, location or species) may improve the hydrochar such that it would pass these slagging and fouling limits. However, these are initial calculations predicting the behaviour, and perhaps ash fusion would give a better indication of the true slagging and fouling indices of the hydrochars.

The hydrochar is only part of the product stream post-HTC, and overall suitability of the feedstock will depend on the potential end usage options for the corresponding aqueous phase produced. The next chapter will characterise these aqueous phase samples and will improve understanding of the chemical reactions taking place within the hydrothermal carbonisation process, which effects the production of primary and secondary char formation. The overall energy balance and therefore suitability of the fuel will take into account both the hydrochar HHV content and the potential fuel output of the aqueous phase before a full analysis of the total energy output is performed in chapter 7.

Chapter 6

Composition of Aqueous Phase following Hydrothermal Carbonisation

6.1 Introduction

The portion of the biorefinery process evaluated in this chapter is the outlined section shown in figure 6.1. This section (adapted from figure 1.3) demonstrates the aspect of the overall process focussed on in this chapter, the analysis of the aqueous phase to determine potential future usage and suitable revenue streams as a by-product. This incorporates the analysis of the aqueous phase in order to determine its' potential end uses (objective 4). How the mixing of the seaweed feedstock and the *Miscanthus* feedstock effects the quality of the process water is also analysed in this chapter, linking in with the fifth objective.

By comparing the biomass results to the model compound results, and the effect of co-processing with seaweed on the process waters, this analysis will endeavour to conclude how useful this co-processing method is in enhancing the quality of the process water with its more soluble organic contents. This analysis will therefore aid future considerations into biomass feedstock selection for HTC, as the chemistry of the proposed feedstock could be used to predict the organic makeup of the process waters. The understanding of how macroalgae reacts in the wet slurry as they undergo the HTC process is still in its infancy, and so the results from this chapter will hope to improve the depth and scope of

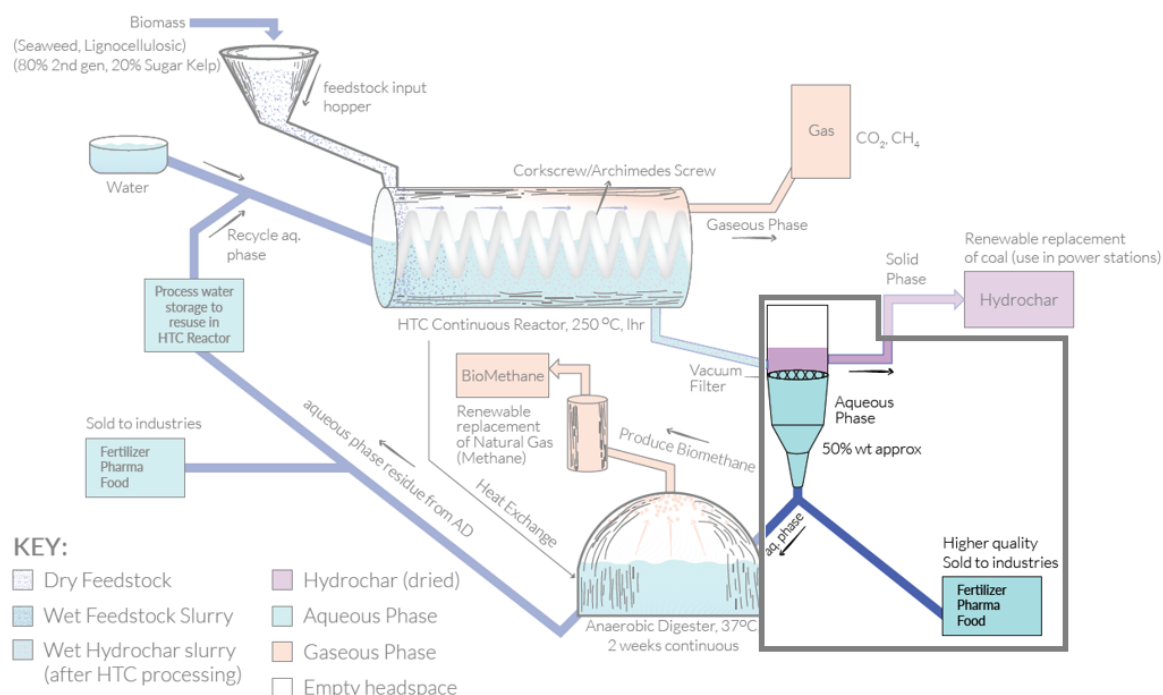


Fig. 6.1 A section of the biorefinery concept from figure 1.3, highlighted to demonstrate the aspect of the overall process focussed on in this chapter; the aqueous phase production and its' subsequent analysis.

this understanding.

The overarching aim of understanding the role macroalgae has to play in potential biorefinery set-ups is also approached here. As seaweed as a feedstock is inherently wet and so the advantage of using it for HTP is that it bypasses the energy intensive drying stage, it is important that the aqueous phase after hydrothermal processing is a useful product within this biorefinery concept. Potential end uses for this aqueous phase have therefore been considered and evaluated via detailed and varied analysis performed on the aqueous phase. Hence, objective six (from §1.3) is also one of the main points of discussion within this chapter.

The different techniques used for analysing the aqueous phase analysis are as follows;

- CHNOS and TGA analysis, HHV calculations and Van-Krevelen diagrams
- Total Organic Carbon Analysis (TOC)
- Nuclear Magnetic Resonance (NMR) (^1H)

- High Pressure Liquid Chromatography (HPLC) - for Sugars and VFAs
- Gas Chromatography with Flame Ionisation Detector (GC-FID)
- Liquid X-Ray Fluorescence (Liquid XRF)
- pH Analysis

These analytical techniques are discussed in the order listed above, for each of the different subgroups of feedstocks. Using these methods, it is possible to determine the suitability of the liquid phase from the HTC product to be utilised as either a further fuel source, via anaerobic digestion, it's qualities regarding use as a nutrient rich fertiliser, or it's potential for the further extraction of commodity or high value chemical compounds. Understanding the chemistry of the aqueous phase produced with these different feedstocks - especially the 100% biomass and co-processed feedstocks - is vital to ensure proper evaluation of the whole HTP concept and the use of the by-products. Any potential toxic chemicals, harmful acids for example, found in great quantities in the aqueous phase could have the effect of ruling out a certain type of feedstock for undergoing HTP. This would be due to further complications regarding the end use, or waste, of the aqueous phase after hydrothermal processing. This is why a lot of emphasis has been made on analysing this aqueous phase, as it is important to know which kind of chemicals are produced during HTC, and which chemical components they are likely to have originated from, to determine the best feedstock mix for HTP.

The different groupings of the feedstocks are as in §4. These are discussed in this order in the following subsections but are cross compared where relevant and any qualities of the biomass samples are compared and contrasted to their biochemical constituent model compounds HTC analysis where appropriate. The initial analysis focuses on the elemental analysis and the proximate analysis, with HHV calculations and Van-Krevelen (VK) diagrams produced. The discussion then introduces the NMR (^1H) technique for PW analysis. This then leads onto the HPLC analysis for the VFAs and Sugars. The GC-FID analysis of the volatile fatty acids (VFAs) then follows, to help identify more of the VFAs and their respective concentrations. These techniques study the different types of sugars and volatile fatty acids (short chain acids) identified in the PW samples.

The trace metals found in the liquid phase are analysed via liquid XRF, and the measurement of the pH will indicate the alkaline levels of the PW. With the NMR (^1H) analysis providing a good indication of any phenols present in the samples, in relation to the amount of sugars and VFAs, the overall picture of what makes up the liquid phase

samples will be created and discussed. Identification of the main trends can be initiated, and a more in depth analysis of any identified sugars and VFAs within the waters can then be done via HPLC and GC-FID. A wide range of chemical components of the liquid phase is analysed and discussed in this wide-ranging chapter; from heavy metals to formic acid.

The first model compounds to be discussed are the lignocellulosic model compounds: cellulose, lignin, protein and the ACL mix. Analysis of the PW samples of these model compounds will aid in the development of the understanding of how lignocellulosic based biomass such as *Miscanthus* break down and some organics become solubilised under HTC. The raw samples for the feedstock were not included in this analysis, as the raw feedstock is in solid form and hence was only shown in the analysis of the solid phase, in §5. The original water phase would have been pure water strictly speaking, however it is true that some of the organics would have solubilised in the water as it was mixed initially, before undergoing the HTC process.

6.2 Lignocellulosic Model Compounds

6.2.1 Ultimate and Proximate Analysis

The CHNS and TGA analysis is shown in table 6.1 below. The resultant CHNS bar charts for each feedstock is shown in figure 6.2. The VK diagrams and HHV values are shown in figures 6.3 and 6.4 respectively.

Upon drying in an oven, the CHNOS and TGA data for the resultant residues of the HTC aqueous phase from these feedstocks are tabulated below. Table 6.1 also includes the HHV values, determined using the CHNOS and TGA results. The CHNS results are further summarised in the bar charts in figure 6.3. Van-Krevelen (VK) diagrams were produced for these samples, from the O/C and H/C molecular ratios and is presented in figure 6.2. Finally, the HHV values were plotted in a scatter graph as a function of the HTC temperature, and each sample overlaid to aid with the comparative analysis and discussions. This can be seen in figure 6.4. There are limitations on this analysis however, as there was significant evaporative losses from the water samples due to the drying stage before CHNS and TGA analysis. Therefore these values are an underestimate as they do not include the organics from the VFAs that would evaporate at these temperatures; the TOC analysis that follows can aid interpretation of the organic content, as this was performed on the all of the samples in liquid form, with no drying required. This CHNS

and TGA analysis is not so important in terms of understanding the use of the aqueous phase as a fuel source, but is mainly performed to enable BMP theoretical calculations (see chapter 7).

Table 6.1 CHNOS, TGA and HHV values for the lignocellulosic model compound HTC aqueous phase after drying.

ACL = Sodium Alginate, Cellulose and Lignin blend, * = Calculated by difference.

Sample, HTC Temp (°C)	CHNOS Data (%)						TGA Data (%)				HHV (db) (MJ/kg)
	N	C	H	S	H (db)	O (daf)*	M	VM	FC	Ash	
Cellulose 150	1.02	38.44	5.60	0.07	5.43	46.27	1.55	82.01	9.22	7.23	15.64
Cellulose 200	0.27	38.10	5.74	0.00	5.50	52.59	2.18	71.21	25.25	1.36	15.41
Protein 150	2.14	64.61	6.60	0.00	5.95	15.91	5.89	84.96	3.65	5.51	27.12
Protein 200	2.76	25.42	3.26	0.00	2.74	57.03	4.65	84.39	3.56	7.39	14.81
Protein 250	2.45	28.76	3.77	0.00	3.28	63.77	4.44	93.21	5.05	-2.70	14.70
Lignin 150	10.68	38.65	5.79	0.00	5.57	31.61	1.98	71.57	14.94	11.52	16.93
Lignin 200	17.81	62.85	9.97	0.00	9.72	-11.33	2.22	72.14	6.92	18.73	31.98
Lignin 250	12.07	48.05	8.65	0.00	8.15	14.61	4.44	71.12	11.77	12.67	21.10
ACL 150	1.23	35.25	4.34	0.00	3.85	30.98	4.44	65.20	6.11	24.25	15.36
ACL 200	1.06	30.54	4.70	0.00	4.27	46.90	3.87	76.57	6.19	13.37	14.12
ACL 250	0.53	36.14	4.64	0.03	4.14	46.04	4.50	81.96	4.93	8.61	15.35

Due to the aqueous phase samples containing a range of materials such as soluble sugars, VFAs, phenols and humins, when the samples were evaporated, a lot of the volatile material was lost, leaving behind high molecular weight and non volatile material. Therefore this CHNS and TGA analysis, based upon the dried residues, does not represent the full story. Liquid CHNS methods would have been preferred if possible, however the alternative wet analysis methods used throughout this chapter helps explain these trends and identify VFAs present in the samples. Also to mention is the cellulose 250 sample after drying was not able to be scraped from the evaporating dish due to practical issues, and thus could not be analysed.

A brief analysis of the CHNS and TGA data for the lignocellulosic compounds highlights that HTC temperatures have very different effects on the model compounds. In terms of ash, Lignin has the second highest ash content, with ACL 150°C containing the highest ash. Lignin also has the highest N; with the most at 200°C. others have hardly any nitrogen content. This is possibly caused by some residual protein or nitrogen containing molecules due to the extraction process of the lignin. The carbon content was high in the P 150°C sample, getting lower as T increases. There are some anomalies in this data, particularly the negative O(daf) and ash contents, which were all calculated in accordance with the methodology, however these may be caused by some losses due to the drying and the flaky texture of the CHNS/TGA samples also containing some air or not being the appropriate powdered solid that the CHNS/TGA machines are used to

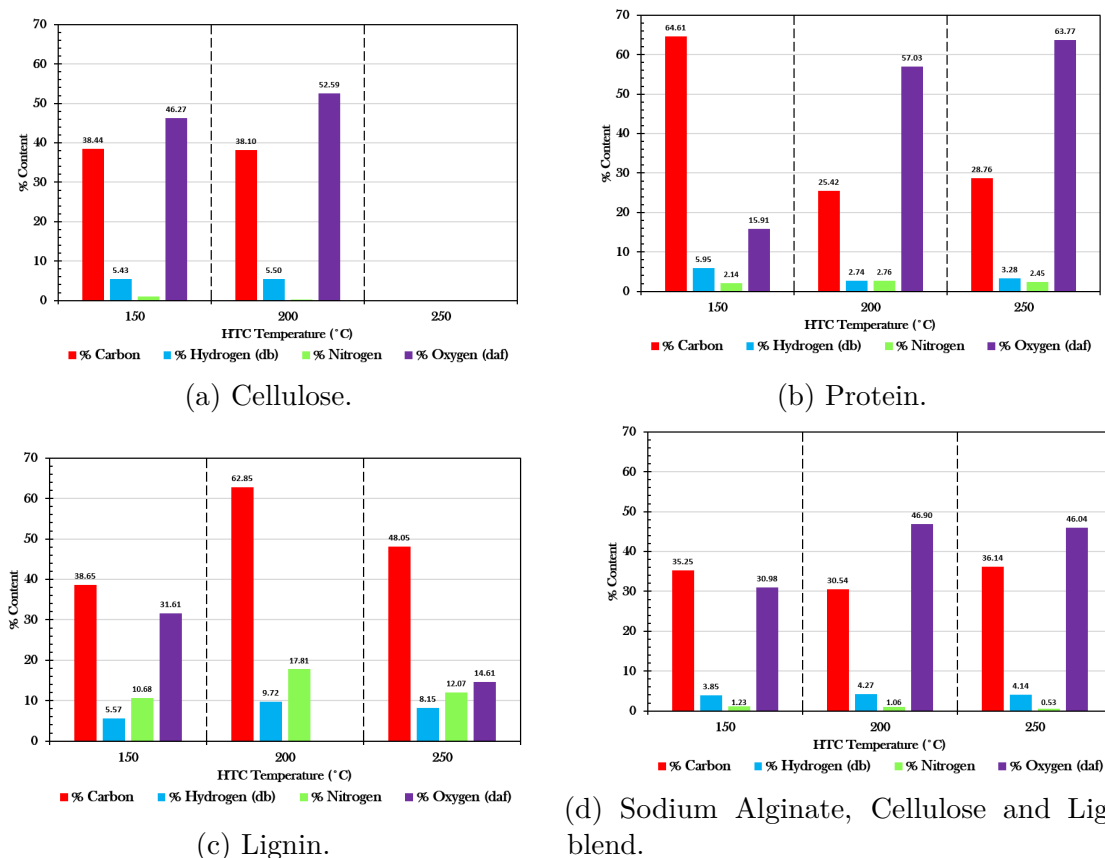


Fig. 6.2 The CHNO values from the process waters of the Lignocellulosic Model Compounds.

sampling. Further work would be to perform liquid CHNS on an adapted CHNS machine to get a more accurate result.

The Volatile matter (VM) content shown in 6.1 is quite high for the lignocellulosic group, with a range of 65-93%, likely due to some remaining lower chain fatty acids in the sample. This organic content may be further supplemented by the organic carbon found in the more volatile fatty acids in the liquid TOC analysis. The Fixed carbon (FC) was found to be highest for L 150°C and L 200°C. In terms of the HHV, it was the highest for L 200°C, although this result is dubious due to negative values and second highest (at 27.1MJ/kg) for the P 150°C, due to its high C content (>60%). Figure 6.4 shows the HHV values and trends.

The VK diagram in (figure 6.3), shows a large change in protein samples from 150°C to the higher temperatures. The cellulose VK ratios hardly changes, with higher O/C content slightly at 200°C and 250°C. The ACL mix has a similar HHV value for all temperature ranges, whereas the VK diagram shows a shift (higher ratio values for both

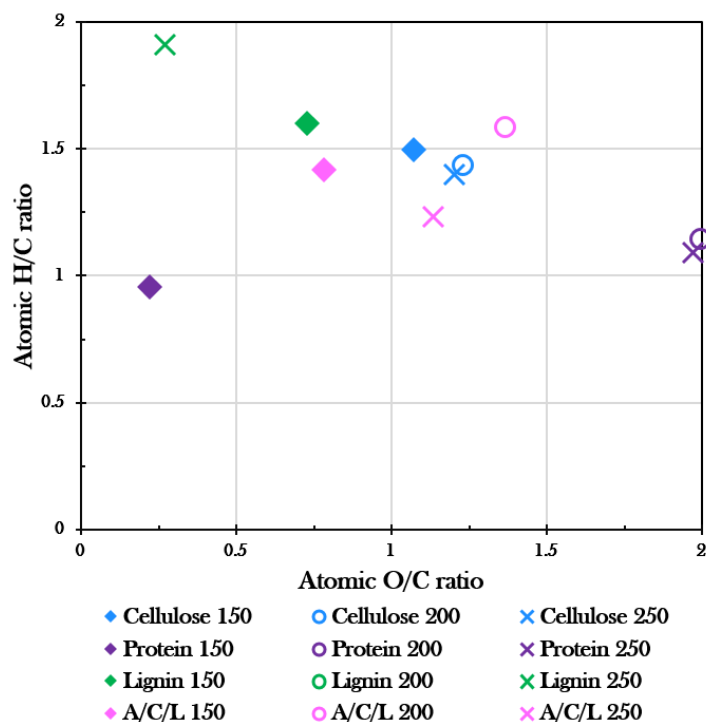


Fig. 6.3 Van-Krevelen diagram for the lignocellulosic model compounds aqueous phase. Note that the X axis scales up to 2, a larger O/C ratio than the following biomass feedstock O/C ratios.

O/C and H/C) at $T=200^{\circ}\text{C}$ and more so at $T=250^{\circ}\text{C}$.

These HHV and VK results are calculated from the CHNS values of the evaporated process waters, not the hydrochars, so it is not necessary to have desirable properties for fuel for this process water phase; these calculations helps us to evaluate by-product suitability and end product usage options via anaerobic digestion, by enabling BMP_{th} calculations. TOC analysis will account for the organic carbon not included in these calculations due to the evaporative losses during sample preparation.

6.2.2 Total Organic Content

The Total Organic Content (TOC) results for the Lignocellulosic Model Compounds are shown in figure 6.5.

The TOC results shown in figure 6.5 shows most obviously a large amount of organic carbon in the protein samples. The increase at the higher two HTC temperatures agrees with previous findings of an increase in process water yields and corresponding hydrochar

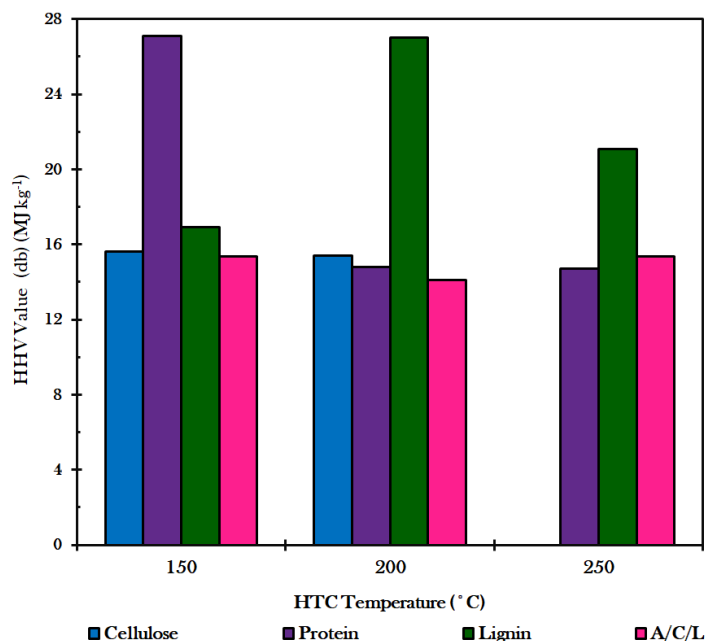


Fig. 6.4 The HHV values of the lignocellulosic model compound aqueous phase after HTC, presented as a function of the HTC temperature. The HHV y-axis range begins from a value of 12 in order to provide a clearer chart.

A/C/L = Sodium Alginate, Cellulose and Lignin blend.

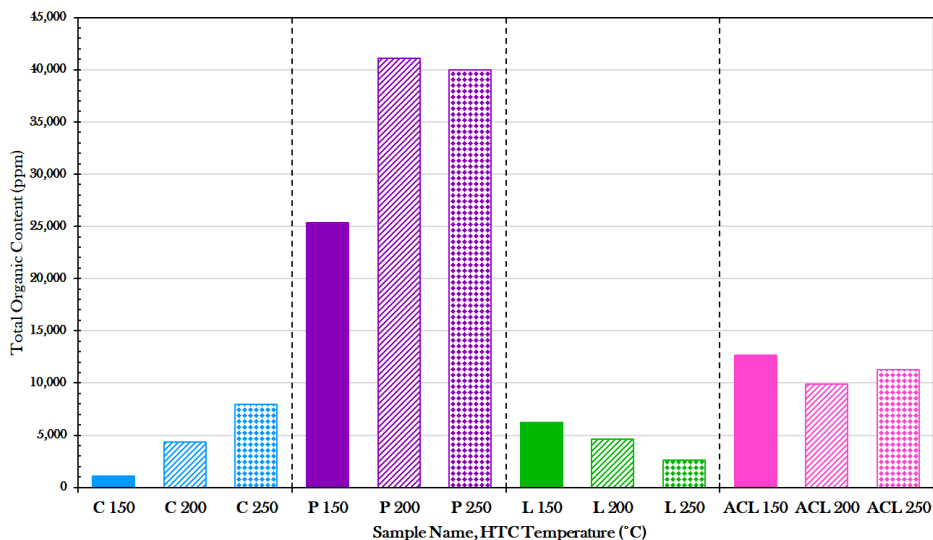


Fig. 6.5 A bar chart showing the TOC values for each HTC temperature for the Ligno-cellulosic Model Compound Aqueous Phase samples.

C = Cellulose, P = Protein, L = Lignin, ACL = Sodium Alginate, Cellulose and Lignin blend.

yield reduction at the higher two temperatures (figure 4.4b). The large protein structure

and the nature of its organics degradation products would account for a large number of covalent carbon bonds, resulting in very high TOC content across the HTC temperatures.

The increase in organic carbon shown in the cellulose feedstock is further evidence of a gradual degradation of the cellulose molecules as the HTC temperature increases, as it breaks up into its constituent monomers and possibly further into organic acids at the highest HTC temperature. Overall, the low TOC content for the cellulose compared to the other model compounds shows it is relatively stable under HTC conditions and it difficult to break down, as was predicted, although HTC certainly starts to enable the breakdown of cellulose at 200°C and 250°C. The opposite trend in organic carbon content is found for lignin, however. This corresponds with a reduction in process water yield shown in figure 4.4c.

6.2.3 Nuclear Magnetic Resonance

The NMR spectra for all the samples can be found in the Appendix, and the integrated values and their normalised percentiles are tabulated in each subsection. Table 6.2 shows the integrated values, and their normalised percentages, of the different lignocellulosic model compound HTC aqueous phase samples. The details of this calculation are found in §3.46, equation 3.15. Please note that the spectra in the Appendix sometimes show an intrinsic error due to phase error, causing some spectra to dip below the baseline. ¹H NMR spectra were acquired using an excitation sculpting (ES) pulse sequence that utilises a asymmetrical spin-echo that does not completely refocus all peaks. This has the tendency to manifest in dominant peaks as a small uncorrected phase error where the peak phase briefly dips below the baseline. This can be reduced by increasing the extent of exponential or Gaussian apodisation but this would reduce the observed resolution of each NMR dataset. It was decided to use process each dataset identically which is reflected in the variation of the observed phase error as this would be sample component dependent.

Table 6.2 is colour co-ordinated to aid evaluation of the different proportions of sugars, VFAs and phenolics for each sample. The more green the cell is, the higher the normalised relative proportion of that compound in the sample's integrated NMR peak area. The more yellow, the lower the value. Integer values are also given before the percentage proportion were calculated, for completeness.

From these values, any key trends can be identified, as can any similarities and anomalies. The spectra can be referred to for further understanding and are all shown in the appendix

Table 6.2 NMR (^1H 600MHz in D_2O) integrated values from the spectra of the lignocellulosic model compounds aqueous phase. Tabulated both as a given value and normalised to total 100%, and colour-coordinated to show the higher relative amount as green.

A/C/L = Sodium Alginate, Cellulose and Lignin blend.

Sample Name, HTC Temperature (°C)	Integrated Value Attributed			Normalised % Value		
	VFAs	Sugars	Phenolics	VFAs	Sugars	Phenolics
	0 -2.75	2.75-4.5	6-8	0 -2.75	2.75-4.5	6-8
Cellulose 200	1	3.68	0.41	19.65	72.30	8.06
Cellulose 250	1	0.38	0.06	69.44	26.39	4.17
Lignin 150	1	0.99	0.64	38.02	37.64	24.33
Lignin 200	1	0.72	0.56	43.86	31.58	24.56
Lignin 250	1	0.81	0.63	40.98	33.20	25.82
Protein 150	1	0.25	0.03	78.18	19.53	2.34
Protein 200	1	0.38	0.06	69.44	26.39	4.17
Protein 250	1	0.17	0.30	68.03	11.56	20.41
A/C/L 200	1	0.25	0.25	66.67	16.67	16.67
A/C/L 250	1	0.38	0.09	68.03	25.85	6.12

with stacked nmr spectra for each feedstock.

Note that whilst all VFA peaks would fall within this 0-2.75 range, not every peak found in this range is necessarily due to VFAs, so further analysis of the process waters via GC-FID and HPLC are required to confirm the presence of certain VFAs and their abundance. A similar caution to interpretation of the NMR analysis should be applied for the sugar range; HPLC will be performed to analyse the sugars in the process waters as a further clarification of these NMR sugar findings.

For the cellulose, relatively more sugars were found in the 200°C than 250°C. Note that the C 150°C sample foamed up during the nmr analysis on repeat instances and so could not be analysed via nmr for this temperature sample, although it is assumed to be mostly sugars, although may have traces of levulinic acid and HMF at lower HTC temperatures. A wider range of the spectra covers the VFAs phase in 250°C than the 200°C sample. Broadly, it can hence be deduced that as temperature increases, the sugars in the higher temperature HTC aqueous phase are more readily degraded into the shorter chain fatty acids, perhaps acetic acid or hydroxyacetic acid. Cellulose is a polymer made up from sugar molecules, so this was expected to show up in the NMR (^1H) spectra with a diminishing relative amount compared to the VFAs at higher T. Higher temperatures hence produce more hydrochar and lead to particular traits in the process waters. Cellulose is one of the main components of the feedstock *Miscanthus*, so it will be interesting to compare these model compound results to 100% *Miscanthus* feedstock NMR results.

Protein at 250°C has 20% of the spectra in the phenolic range. Note there are also other aromatic compounds that appear within this range on the NMR spectra, which are not 'phenolic compounds', e.g. phenylalanine. For the different cellulose aqueous phase samples, the highest amount of phenolics was found at the 200°C HTC temperature, albeit with a lower relative amount than the protein, at 8%. The protein and ACL samples have the most % in the VFA portion, so show the most degraded compounds, aside from C 250°C. The protein breaks down into amino acids, not sugars, so the acids are likely to have originated from any sugars added to the commercial whey protein used, as an adulterer to improve taste. This may also produce higher sugars before these degrade into organic acids at the higher HTC temperatures, and would be shown in the forthcoming HPLC results.

The NMR results for the lignin HTC aqueous phase seem fairly spread in terms of the VFAs, sugars and phenolics, at around the 40/35/25% respectively. There seems to be little change in these proportions with HTC temperature, - lignin is a complex structure so is relatively difficult to break down between 150°C and 250°C due to not being readily hydrolysed, although, some level of degradation occurs before 150°C, as lignin is insoluble in water when at room temperature and atmospheric pressure. However different lignins behave differently depending on how they are produced. (The exact source of this lignin is currently unknown due to the lab being closed). The sugars from the lignin aqueous phase samples detected via NMR here is unexpected, and likely caused by the presence of leftover cellulose from the extraction method used to produce the lignin model compound used in this study.

Lignin HTC samples contain a much higher proportion of phenolics compounds than the other samples. Lignin, as a complex organic polymer, has many aromatic subunits, and as there are so many aromatic rings in the structure, likely to be broken up during hydrothermal carbonisation, the presence of phenolics in the NMR (^1H) spectra is as expected. Phenolics, or phenols, are compounds which contain an aromatic hydrocarbon group, plus a hydroxyl group (-OH) bonded directly to it.

Phenols are generally high value chemicals if pure. If they could be extracted from the process water after HTC, this would result in an additional revenue stream. If the process water were high in phenol content, and the water is to be used for Anaerobic Digestion (AD) post-HTC, it becomes more necessary to extract these phenolic compounds, if the bacteria and microorganisms are unable to acclimatise, as these have been shown to inhibit the anaerobic digestion processes, and this will be investigated in chapter 7. There are indeed some polyphenols found in seaweed, although these are usually at low levels

and the level varies depending on the species. Extraction of phenols from natural sources, although practised already in the chemical industry [179], is not suited for extraction post-HTC. The addition of seaweed to a traditional woody type biomass would minimise the overall lignin content of the feedstock. Lignin is hard to break down, is quite fibrous and does not rot easily, so woody biomass is not as desirable as seaweeds in any case, mainly due to their physical properties caused by the lignin. The BMP productivity would therefore not be compromised if the HTC aqueous phase were to have a lower phenol content as a result of mixing seaweed to the *Miscanthus*.

When considering the theoretical BMP, the presence of phenols may cause a reduction in BMP produced in experiments. This effect is not taken into account in the calculations. Hence, these NMR results should be reviewed when analysing the BMP potential of the different process waters, as a reduction in experimental BMP compared to theoretical BMP may be in part due to any phenols present in the aqueous phase.

6.2.4 High Pressure Liquid Chromatography

The HPLC results for the Lignocellulosic Model Compounds are tabulated in table 6.3 for the sugars, and table 6.4 for the VFAs. The cells are coloured green where the presence of the numbered sugar or acid are identified and the amounts given where determined. The VFAs are further quantified in the GC-FID results. All of the HPLC Sugars and VFA chromatographs of the samples can be found in the Appendix, §10.3. The ‘Y’ means the sugar or VFA was identified as present, but was not quantified as the quantification was only performed for the samples which a standard was available for.

The LMC HPLC sugars results shown in table 6.3 shows an abundance of glucose and galactose/Mannose and ribose in the samples. From first glance the lack of glucose in the C 150°C and C 250°C samples would be confusing, however this is easily explained. The cellulose molecule is difficult to break down, and would stay mostly intact at the lower HTC temperature. It starts to degrade after this temperature is breached, and hence the C 200°C sample shows plentiful glucose amounts (over 20,000 μ RIU). At higher HTC temperatures, it is likely that the degradation products of the cellulose, including glucose, will be further liberated and form furfural and various other shorter chain organics, via dehydration. A lot of different reactions occur at these very high temperatures, and hence there is no clean glucose identified in the aqueous phase for the C 250°C samples. This is reflected in the increasing concentrations of formic acid and the detection of acetic acid at the second highest temperature shown in table 6.4, as the breakdown of glucose results in these shorter chain acids being produced, which are then most likely further

Table 6.3 HPLC Sugars peak identification and quantification data from the chromatographs of the lignocellulosic model compounds aqueous phase. The units are mg/L. C = Cellulose, P = Protein, L = Lignin, ACL = Sodium Alginate, Cellulose and Lignin blend.

Sample Name, HTC Temp (°C)		Sugars Present?					
		1 Sucrose	2 Lactose	3 Glucose	4 Galactose and Mannose	5 Arabinose	6 Ribose
C 150							
C 200		Y		23164.14	22698.94		
C 250							
P 150		Y	Y		672.37		
P 200			Y		187.62		
P 250					52748.59		
L 150			Y		51.98	60.65	787.81
L 200							1348.36
L 250				27.62			1083.72
ACL 150		Y		126.53	204.81	5.98	
ACL 200							
ACL 250							

Table 6.4 HPLC VFAs peak identification data from the chromatographs of the lignocellulosic model compounds aqueous phase. The units are mg/L. C = Cellulose, P = Protein, L = Lignin, ACL = Sodium Alginate, Cellulose and Lignin blend.

Sample Name, HTC Temp (°C)		VFAs Present?							
		1 Oxalic Acid	2 Maleic Acid	3 Citric Acid	4 Methyl-malonic Acid	5 Lactic Acid	6 Formic Acid	7 Acetic Acid	8 Levulinic Acid
C 150			Y		Y		0.0355		
C 200				Y	Y	Y	0.2600		Y
C 250			Y	Y	Y	Y	2.1708	2.6748	Y
P 150			Y	Y	Y		0.9940	3.0142	
P 200	Y		Y	Y	Y		15.4732	13.6575	
P 250			Y		Y		4.7826	3.2595	
L 150			Y		Y		0.3202	0.3915	
L 200				Y	Y	Y	0.0881	0.1111	
L 250					Y	Y		0.1471	
ACL 150			Y	Y			7.4841		
ACL 200	Y		Y	Y	Y	Y	0.9758	0.0714	Y
ACL 250		Y	Y	Y	Y	Y	0.7920	0.5692	Y

broken down into gaseous products at the highest temperature. Further organic acid analysis for the aqueous phase samples was achieved via GC-FID, which is discussed in the following section 6.2.5.

The origin of the detected sugars galactose and/or mannose in the cellulose aqueous phase samples is not as apparent. These are not molecules contained within the cellulose structure and are not known degradation products, and so this HPLC identification may have identified a very similar degradation product of glucose and misidentified it. Hemicellulose, for example, is made up of D-mannose and D-galactose units among others, so perhaps there was some hemicellulose present in the feedstock model compound

material. These are more likely to come from hemicellulose, but there is also a possibility that maybe under such extreme conditions, they can be produced from cellulose.

The sugars detected in the protein samples are similarly ambiguous. The protein molecules degrade into amino acids, and do not produce sugars as a further degradation product. It is therefore assumed that the sugars present in the protein HTC aqueous phase samples are caused by the presence of added sugars or potentially glycoproteins (amino acids with a sugar molecule attached) in the commercially available whey Protein used for this feedstock mix. Typical additions such as this would enhance the flavour of the protein, which is designed for mix with water or milk to be drunk with no further additions by the consumer, and hence some sugars may be added in the whey protein powder mix by the manufacturer. Therefore the sugars and resultant organic acids produced by the further breakdown of these sugars (shown in table 6.4) may be ignored as this is not a result of HTC processing on the actual protein molecule. Note that the decrease in the formic and acetic acids for these protein samples is due to the further breakdown of these C1 and C2 acids into gases during HTC processing at higher temperatures.

The lignin samples show less sugars present after HTC, with correspondingly less amounts of organic acids produced, particularly as the HTC temperature increases. Acetic acid can be formed as a by-product from the de-polymerisation and cracking reactions of lignin [180]. Lignin is difficult to break down and is the component of terrestrial biomass that leads to issues in using such biomass feedstocks for energy purposes, via milling and pretreatment methods.

The ACL 150°C sample has 7.5 μ RIU but yet less than 1 μ RIU at the two higher HTC temperatures. This indicates that the formic acid further degrades at these temperatures to form hydrogen and carbon dioxide, hence the reduction in formic acid concentration. This would reduce the overall acidity and result in a higher pH with increasing HTC temperature, which is as observed (see §6.2.6). Further concentrations of specified organic compounds in these aqueous phase samples including VFAs are determined in the GC-FID analysis that follows.

6.2.5 Gas Chromatography FID

The main VFAs detected in the lignocellulosic model compounds was ethanoic (or acetic) acid. This is most likely produced from the HMF compound, in turn from glucose. This

Table 6.5 GC-FID data for the lignocellulosic model compound aqueous phase after undergoing HTC. Units are given in ng/ μ l.

ACL = Sodium Alginate, Cellulose and Lignin blend.

Sample Name	Propanone	Methanol	Ethanol	Ethanoic acid	Propanoic acid	2-Methyl propanoic acid	Butanoic acid	3-Methyl butanoic acid	Pentanoic acid	4-Methyl pentanoic acid	Hexanoic acid	Heptanoic acid
Cellulose 150	16.30	0.00	2.53	21.35	3.73	0.00	0.00	30.75	0.00	7.76	5.50	39.04
Cellulose 200	8.36	18.20	0.00	46.79	2.49	2.75	0.00	0.00	0.00	0.00	1.35	1.07
Cellulose 250	129.78	118.60	12.87	696.27	67.90	1.71	5.19	1.34	1.62	1.35	1.91	3.78
Protein 150	9.22	13.26	0.00	229.20	7.86	0.00	4.50	48.88	1.59	2.13	0.94	3.17
Protein 200	54.79	0.00	0.00	491.88	40.49	11.13	4.64	18.18	2.91	2.99	28.82	4.04
Protein 250	105.34	0.00	0.00	738.09	119.68	15.31	11.87	5.47	9.47	70.90	16.01	16.34
Lignin 150	9.38	48.23	0.00	111.38	7.47	1.66	12.28	1.37	0.00	1.22	3.36	55.73
Lignin 200	25.99	135.94	0.00	195.74	9.96	1.77	11.27	1.45	1.17	1.40	2.70	1.68
Lignin 250	26.06	356.05	0.00	186.60	10.97	1.87	7.53	1.52	0.00	0.93	2.38	1.68
ACL 150	6.75	18.79	0.00	466.53	16.48	3.17	3.55	2.12	1.17	0.57	1.65	2.12
ACL 200	18.83	71.31	0.00	403.95	43.93	1.47	5.79	9.00	2.08	0.63	2.43	3.57
ACL 250	88.04	343.23	0.00	567.03	74.09	17.85	39.46	9.15	1.77	2.00	6.61	4.87

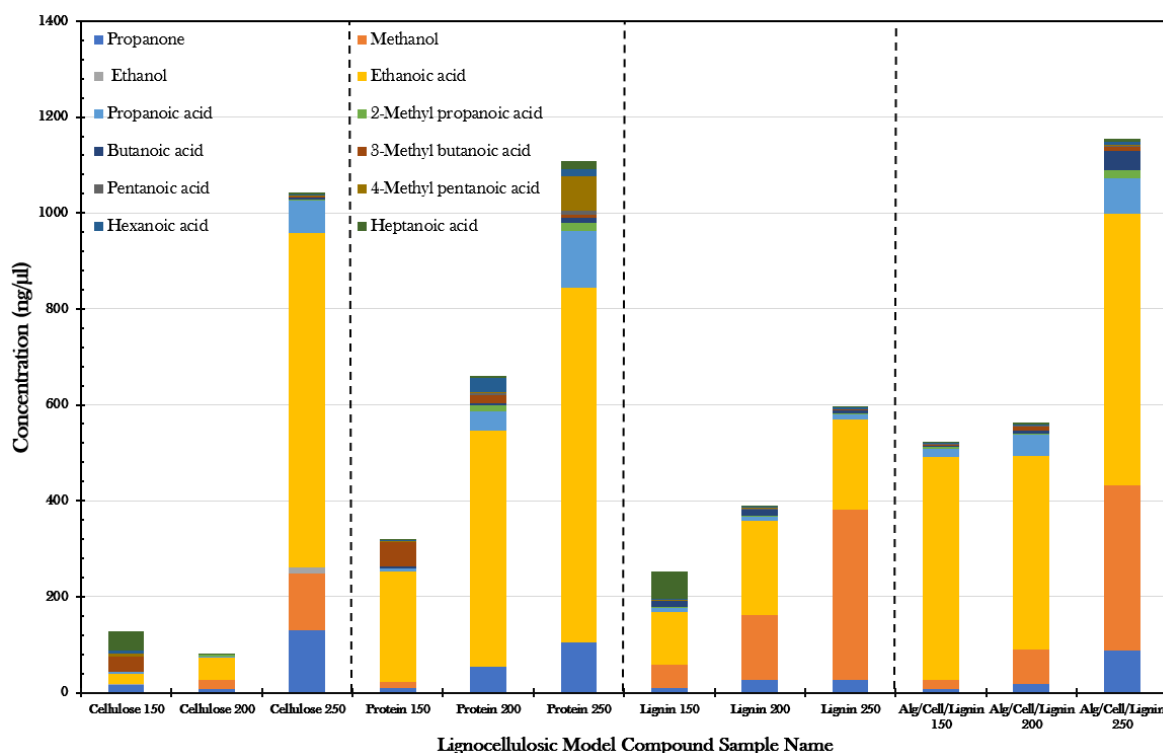


Fig. 6.6 Bar chart showing the results of the GC-FID analysis for the lignocellulosic model compound feedstocks aqueous phase samples after HTC.

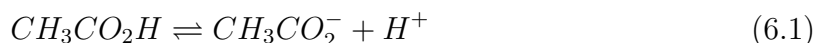
reaction is likely to be the cause of the high presence of acetic acid for these samples, especially at the levels found within the cellulose 250°C, protein 250°C and ACL mix 250°C, where perhaps the higher temperature water gives the ethanol a higher likelihood of oxidising due to the more excited oxygen molecules in the ionic, almost super-critical, water. This follows that the higher the temperature, the higher levels of smaller chain acids are detected compared to the larger ones, which appear later in the GC-FID

chromatograph. In order to compare the effects which the model compounds have on the biomass samples, and the effect of the co-processing.

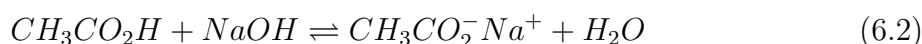
A more thorough discussion of these GC-FID results can be found later in this chapter, in §6.5.5, when all the GC-FID samples have been displayed within each respective subsection as bar charts and the GC-FID information can therefore be evaluated as a whole, focussing on the main acids produced.

6.2.6 Fate of Inorganics: Liquid X-Ray Florescence & pH

Determining the pH of the aqueous phase is of great importance for this research, as it dictates possible end uses and identifies any further issues the aqueous phase may cause. The pH of the process waters is altered by the amount of alkali metal salts contained within the liquid phase, and the amount of organic acids within the sample. The acids would release a H^+ ion, and exists in this equilibrium as detailed below, in equation 6.1:



This acetic acid would give a pH of 4 when dissolved in water. The pH may increase and become more alkaline due to the presence of Mg, Ca, K and Na, as these so called alkali metals are able to dissociate into salt ions [181]. For example, the chemical equilibrium that exists when calcium is dissolved in water is shown in equation 6.2:



For calcium, the equilibrium would produce a Ca^{2+} ion. Therefore the aqueous phase samples with a high alkaline metal content (as determined previously for the HTC aqueous phase samples via liquid XRF analysis) would likely have a more neutral pH [181]. Lacking these elements, the acids and H^+ ions produced via the degradation of the biomass during HTC would result in a low pH, as it is without enough OH^- ions to balance the pH.

Any end use of the process water via hydroponic systems (or for simialar fertiliser uses) may find that an extreme dilution of the product is required to lower the acidity. It is known that a pH levels should be ideally kept within the 6.5-9.5 range to limit corrosion of pipes (which would exasperate the issue by increasing the heavy metal content of the liquid) [181]. Likewise, a low pH (high acidity) lower than 2.5 would cause difficulties with handling and storing/transporting within a biorefinery, as this would cause skin damage and create major health and safety concerns [181]. Similarly, a pH of 11+ would

cause health and safety issues due to potential skin and eye irritations [181].

Therefore, any extreme in pH values determined via the pH analysis in this study will be evaluated and analysed, with considerations for the chemical compounds responsible for the pH values. The liquid XRF analysis will allow for deeper understanding of the affect of certain inorganics on the pH of the aqueous phase. This analysis also allows for metal content comparisons between the aqueous phase and the respective hydrochar metal contents from chapter §5.

The results for the pH of the Lignocellulosic Model Compounds HTP aqueous phase are shown in table 6.6. and results from the Liquid XRF analysis are shown in table 6.7.

Table 6.6 The pH results at each different HTC Temperature of the Lignocellulosic Model Compounds HTP aqueous phase samples.

ACL = Sodium Alginate, Cellulose and Lignin blend.

Sample Name	pH Value		
	150°C	200°C	250°C
Cellulose	4.58	3.16	2.51
Protein	5.63	7.36	7.98
Lignin	5.70	4.75	4.23
ACL	5.19	4.82	4.51

Table 6.7 Liquid XRF Results from the Lignocellulosic Model Compounds.

C = Cellulose, P = Protein, L = Lignin, ACL = Sodium Alginate, Cellulose and Lignin blend.

Sample Name	Metals												
	Al	As	Br	Ca	Cl	Fe	K	Mg	Na	P	S	Si	Sr
C 150	0.006			0.0329	0.0071			0.0387			0.1386	0.0015	0.0123
C 200	0.0088			0.0329		0.0017		0.046			0.1423		0.0127
C 250	0.0078			0.0368		0.0013		0.033			0.1357	0.0061	0.0122
L 150	0.0111			0.035			0.0119				0.1459	0.1139	0.0141
L 200				0.0357		0.0013	0.0077	0.0479			0.1445	0.0853	0.0145
L 250				0.0305			0.003	0.0424			0.1485	0.0473	0.0168
P 150				0.0503			0.0586	0.024			0.1522	0.046	0.0155
P 200				0.0336			0.0515	0.0352			0.1365	0.0778	0.0087
P 250				0.0367			0.0416				0.1375	0.0484	0.0109
ACL 150			0.0015	0.032			0.0025	0.0417			0.1454	0.0322	0.0103
ACL 200	0.0079		0.0013	0.0315		0.0021					0.1407	0.4	0.0133
ACL 250			0.0023	0.0376		0.0016	0.0035	0.0284			0.1417	0.0446	0.0112

All the samples here reduce their pH values as the HTC temperature is increased, except for the protein samples, which increases pH. This is due to the formation of organic acids during degradation of the cellulose and lignin, which is promoted with higher HTC temperatures. The protein samples contain the most potassium contents, shown in table

6.7, which would result in a more neutral pH, as explained above.

The liquid XRF results for the LMC samples generally shows a lower metal content compared to the corresponding hydrochars, as expected. Some metals do become dissolved within the aqueous phase however, with the highest contents being that of phosphorous at less than 0.15%. Trace amounts of calcium, magnesium and potassium were common in most of the samples, in addition to silicon and sulphur. It is unlikely these amounts would have come from the model compounds, as previously detailed in the hydrochar XRF analysis, due to the pure cellulose, lignin and protein compounds containing no metals. As these values are fairly consistent across these pure samples and also at very low levels, it is most likely these results are due to background noise from using the XRF liquid sample methodology. It is unlikely that the model compounds would contain high levels of metals, and the levels found here are indeed at low enough levels to disregard any effects of inorganics from the LMC feedstocks on the HTC products.

6.3 Seaweed Model Compounds

6.3.1 Ultimate and Proximate Analysis

The CHNS and TGA analysis is shown in table 6.8 below. The resultant CHNS bar charts for each feedstock is shown in figure 6.7. The VK diagrams and HHV values are shown in figures 6.8 and 6.9 respectively. Note that there is no data for the Man and AA samples for the 200°C temperature due to the aqueous phase samples going bad before analysis could take place, due to incorrect storage (not refrigerated) over a long period of time, when further aqueous phase analysis was not anticipated.

Table 6.8 CHNOS, TGA and HHV values for the seaweed model compound HTC aqueous phase after drying. *Calculated by difference.

Sample, HTC Temp (°C)	CHNOS Data (%)						TGA Data (%)				HHV (db) (MJ/kg)
	N	C	H	S	H (db)	O (daf)*	M	VM	FC	Ash	
Sodium Alginate 150	0.13	37.19	3.99	0.08	3.48	38.18	4.55	78.92	0.14	16.40	15.76
Sodium Alginate 200	0.14	37.12	3.67	0.07	3.46	42.26	1.91	82.48	0.57	15.04	15.76
Sodium Alginate 250	0.14	36.21	4.04	0.00	3.70	41.63	3.07	81.59	0.09	15.25	15.48
Calcium Alginate 150	0.14	34.09	3.82	0.02	3.26	39.27	5.08	67.94	8.83	18.16	15.25
Calcium Alginate 200	0.14	34.52	3.71	0.00	3.66	27.74	0.49	65.65	0.41	33.44	15.15
Calcium Alginate 250	0.22	34.78	4.10	0.00	3.65	31.13	4.04	69.76	0.02	26.18	15.21
Alginic Acid 150	0.23	41.55	4.62	0.00	4.03	42.45	5.29	76.24	12.03	6.45	16.71
Alginic Acid 250	0.57	49.91	4.63	0.00	4.36	33.49	2.42	64.18	24.15	9.24	19.36
Mannitol 150	0.12	39.41	7.61	0.00	7.60	52.24	0.08	99.32	0.06	0.54	15.37
Mannitol 250	0.03	40.73	7.54	0.00	7.52	50.64	0.14	98.87	0.06	0.93	15.96

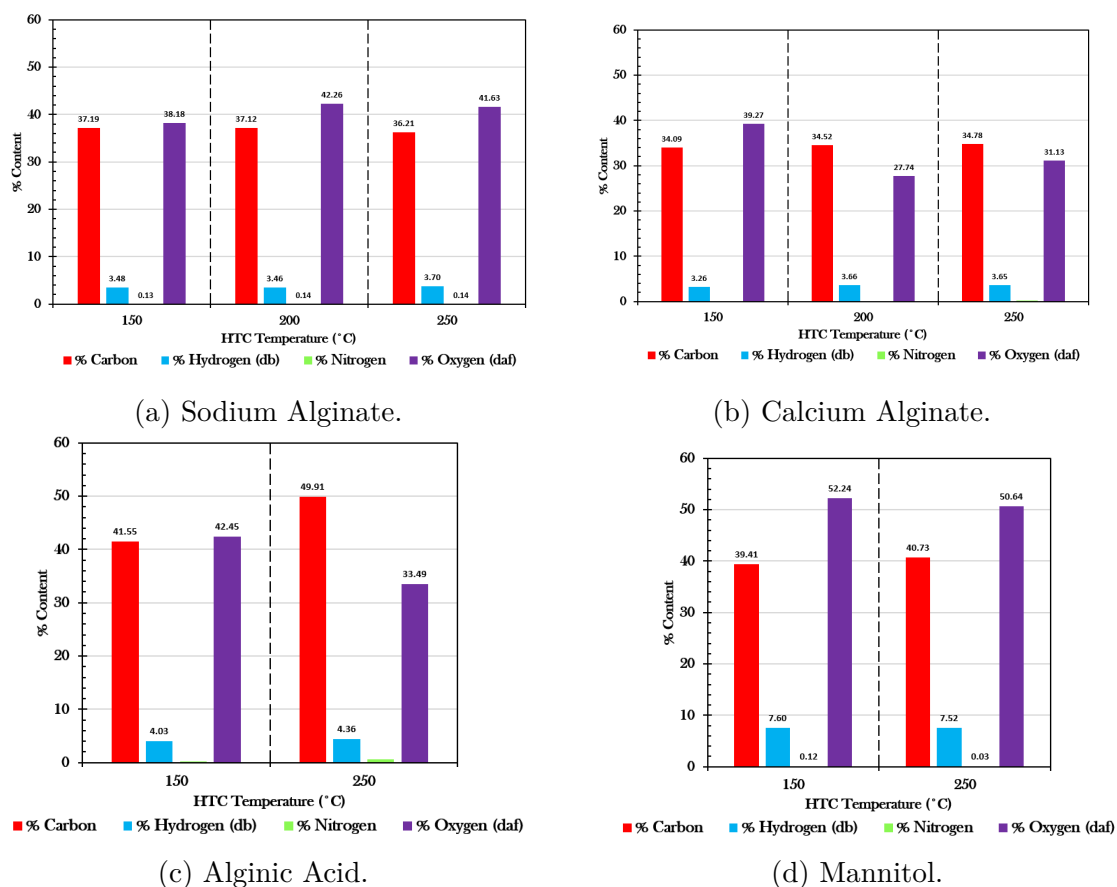


Fig. 6.7 The CHNO values from the process waters of the Seaweed Model Compounds.

The amount of C in the SMC samples ranges from 34% (for all three calcium alginate samples) to 50% for the AA 150°C sample. There was no sulphur detected in the samples. The low N in all samples is expected as these seaweed model compounds do not contain protein (seaweed contains protein, but alginate and mannitol do not). The highest ash content was found in CA 200°C (33%), with 26% in CA 250°C, up from 18% in the 150°C sample. The HHV is rather similar in all the seaweed model compounds; AA 250°C highest at 19.4 MJ/kg, and has the highest HHV throughout the T=150°C and T=250°C temperatures. Most of the SMC HHV values lie in the range of 15-16 MJ/kg. There is a smaller range in the HHV values for seaweed MC than for lignocellulosic MC groups, with more similar CHNOS results for the SMC group too. In terms of VM, there is a range of 64-99%, attributed to AA 250°C and Man 150°C respectively. The FC content for AA 250°C (lowest VM value) is the highest, leading to the highest HHV content.

No significant change was observed in the C/H/N/O/S contents with HTC temp for the SMC aqueous phase samples. The NA/CA/AA 150°C have all the same rough values

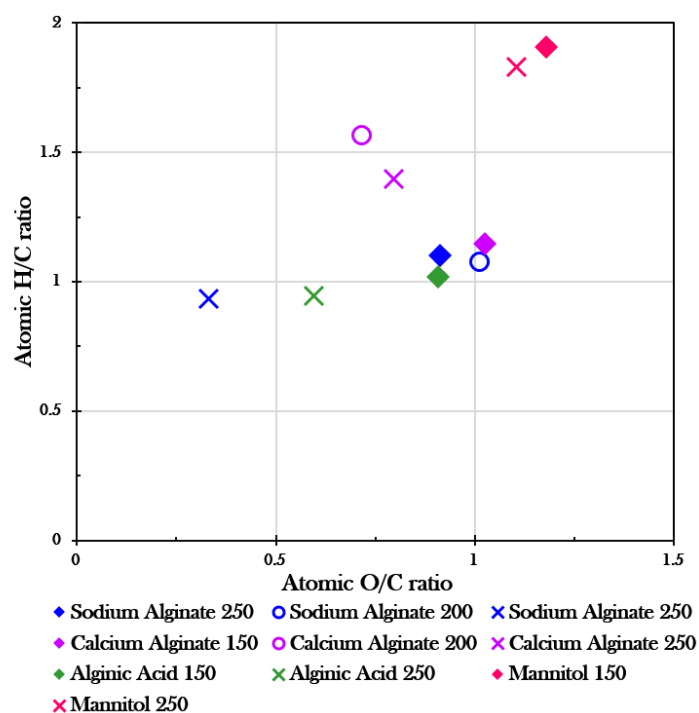


Fig. 6.8 Van-Krevelen diagram for the seaweed model compounds aqueous phase.

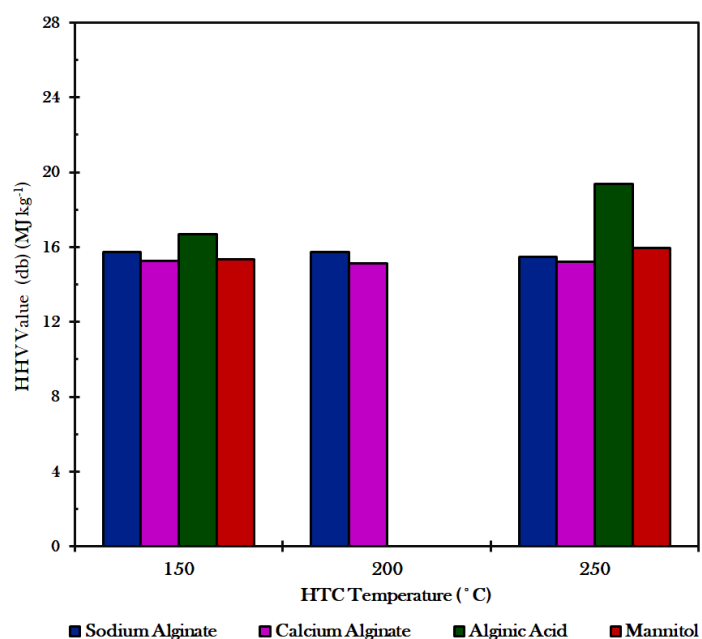


Fig. 6.9 The HHV values of the seaweed model compound aqueous phase after HTC, presented as a function of the HTC temperature. The HHV y-axis range begins from a value of 14 in order to provide a clearer chart.

for O/C and H/C ratios, with mannitol higher H/C at 150°C. Mannitol as expected does not change in terms of O/C and H/C ratio much as it is very stable under these conditions. Mannitol is very different, as it's not a polymer. Therefore is it not easily oxidised or hydrolysed and therefore over the range of HTC temperatures there is not much change in HHV or CHNS values. Mannitol is very different chemically to the other model compounds analysed in this subsection, so its' results should be evaluated individually, with limited comparisons made with the other model compounds analysed here.

6.3.2 Total Organic Content

The TOC results for the Seaweed Model Compounds are shown in figure 6.10.

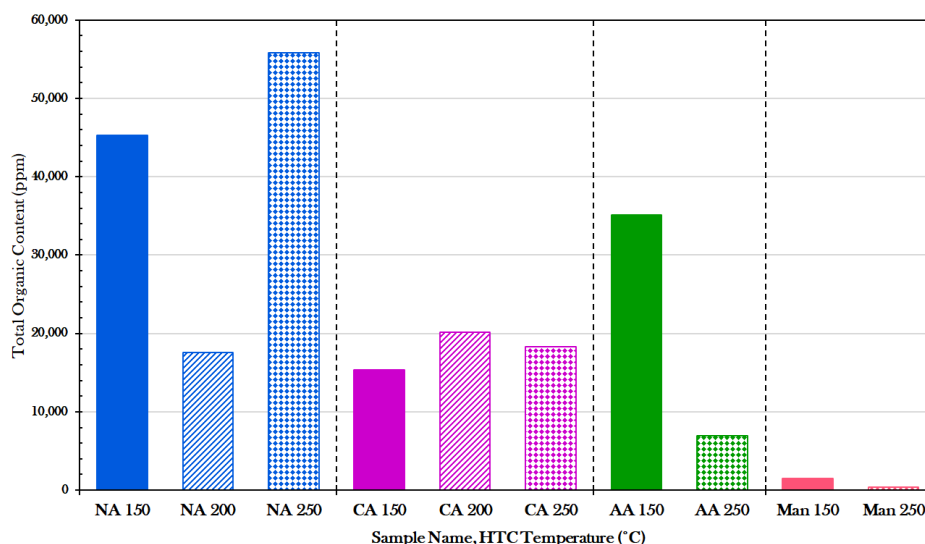


Fig. 6.10 A bar chart showing the TOC values for each HTC temperature for the Seaweed Model Compound Aqueous Phase samples.

NA = Sodium Alginate, CA = Calcium Alginate, AA, Alginic Acid, Man = Mannitol.

It can be seen from figure 6.10 that the sodium alginate 250°C contains the most organic carbon, at 55,800ppm. The dramatic reduction in organic carbon at the 200°C of the sodium alginate is interesting, and may be caused by other reactions within the feedstock slurry polymerising with the sodium alginate to produce organics in the solid phase, which may be further degraded at higher HTC temperatures to release the organic carbon again. The TOC results here also demonstrate just how stable the mannitol is even at high HTC conditions, and despite almost all the mannitol residing in the aqueous phase (see figure 4.6d), the organic carbon is still remaining within the dissolved sugar, as the

TOC detects the carbon atoms covalently bonded in organic molecules, and mannitol only has one covalently-bonded carbon unit [182], compared to two for sodium alginate [183], which partly accounts for the lower organic carbon content detected in mannitol via TOC analysis.

The calcium alginate does not show any significant trend with increasing HTC temperature, whereas the alginic acid significantly reduces its organic carbon content with higher HTC temperature. This is probably due to the further degradation of the alginic acid into smaller organic compounds and then reacting further, forming gases such as carbon dioxide and methane at the highest temperature. It appears the higher temperatures do not effect the calcium alginate molecule in the same way, as it is unlikely the CA would end up forming gaseous compounds at high HTC temperatures, and would instead remain dissolved in the aqueous phase, due to the highly absorbent nature of the calcium alginate compound.

6.3.3 Nuclear Magnetic Resonance

A table of the NMR (^1H) spectra for the seaweed model compound samples is shown in table 6.9 and is colour co-ordinated to aid evaluation of the different proportions of sugars, VFAs and phenolics for each sample. The more green the cell is, the higher the normalised relative proportion of that compound in the sample's integrated NMR peak area. The more yellow, the lower the value. Integer values are also given before the percentage proportion were , for completeness.

There were high proportions of VFAs (84-94%) relative to sugars and phenols identified for the NA samples. The VFA proportion peaks at 200°C, whereas the sugar proportion reduces from 9% to 0% after $T = 150^\circ\text{C}$. The NA compound during the HTC process is expected to degrade fully before $T=200^\circ\text{C}$, which would explain these results. The NA is essentially the sodium salt version of alginic acid, and would likely break down to their related compounds, which include; d-glucuronic acid, hexuronic acid, d-mannuronic acid and d-galacturonic acid, amongst others. The phenol proportions are relatively similar in all three temperatures, so perhaps these phenolic compounds found in the NA samples after HTC are very stable and would require higher temperatures to break down further.

Phenols in the AA 150°C samples degrade in the AA 250°C sample, so may break down during the temperature increase, being less stable phenolic compounds than those found in the NA samples, perhaps, or degrade more favourably in more acidic conditions. A higher acidity in the alginic acid sample compared to the Sodium Alginate sample is

Table 6.9 NMR (^1H 600MHz in D_2O) integrated values from the spectra of the seaweed model compounds aqueous phase. Tabulated both as a given value and normalised to total 100%, and colour-coordinated to show the higher relative amount as green. Note that the mannitol 200°C and alginic acid 200°C samples are not included in this analysis as these samples were not adequately refrigerated and thus had since degraded.

NA = Sodium Alginate, CA = Calcium Alginate, AA, Alginic Acid, Man = Mannitol.

Sample Name, HTC Temperature (°C)	Integrated Value Attributed			Normalised % Value		
	VFAs	Sugars	Phenolics	VFAs	Sugars	Phenolics
	0 -2.75	2.75-4.5	6-8	0 -2.75	2.75-4.5	6-8
NA 150	1	0.11	0.08	84.03	9.24	6.72
NA 200	1	0.00	0.06	94.34	0.00	5.66
NA 250	1	0.02	0.07	91.74	1.83	6.42
CA 200	1	0.00	0.00	100.00	0.00	0.00
CA 250	1	0.00	0.01	99.01	0.00	0.99
AA 150	1	0.38	0.06	69.44	26.39	4.17
AA 250	1	0.13	0.15	78.13	0.13	0.15
Man 150	1	4.51	0.55	16.50	74.42	9.08
Man 250	1	4.21	0.39	17.86	75.18	6.96

expected. The sugars vary from 26% relative amount to 0.13% at 150°C to 250°C for the alginic acid samples. The VFAs counter this, with an increase from 69% to 78% over the same temperature difference. The relative amount of phenolics in the AA samples reduce slightly with the HTC temperature increase, with the rest of the spectral peaks from the AA to make up to the 100% total peak are found outside of the ranges studied in detail here. It can be deduced therefore that the sugars and the phenols found in the AA process waters after HTC processing readily degrade at T lower than 250°C. As a main component of seaweed, it can be further induced that for seaweed based feedstocks, for HTC processing, 250°C would be a suitable HTC temperature, in regards to maximising the carbon content of the hydrochar, and minimising the phenol content of the process water if further used for AD.

Mannitol is known to be a stable sugar; a simple monomeric sugar, not susceptible to breakdown. It is also reduced, meaning there's no carbonyl functional group, which also has the effect of reducing its' reactivity. The spectra for the NMR of the mannitol samples aqueous phase samples show little if not no change with temperature (figure A.2d). These spectra results are reflected quantitatively in table 6.9, and demonstrate that the relative proportion of sugars compared to the other components in the water remain constant with changes in temperature, at 75%. As mannitol is such a stable sugar under HTC conditions, as a main component of seaweed, its presence in feedstock would

suit the biorefinery process if the process water is to be further used for biomethane production via AD, as there would be some sugar (mannitol) molecules potentially left after HTC for the bacteria to digest.

Mannitol is itself very soluble in water, resulting in not even enough milligrams of char after HTC to enable char analysis, so it is unlikely to be a helpful component in feedstock to improve the suitability of the hydrochar for biofuel usage. The solubility would however aid in the feedstock and water mix causing less blockages in the pipes and the final process water after HTC may be of higher economic value, as mannitol could still be extracted from this water and sold to the food industry. The effect mannitol has on the aqueous phase will be further discussed in the HPLC (sugars) section, §6.3.6, where concentrations and sugar identification allow for detailed analysis.

6.3.4 High Pressure Liquid Chromatography

The HPLC results for the Seaweed Model Compounds are tabulated in table 6.10 for the sugars, and table 6.11 for the VFAs.

Table 6.10 HPLC Sugars peak identification and quantification data from the chromatographs of the seaweed model compounds aqueous phase. The units are mg/L. NA = Sodium Alginate, CA = Calcium Alginate, AA, Alginic Acid, Man = Mannitol.

Sample Name, HTC Temp (°C)	Sugars Present?					
	1 Sucrose	2 Lactose	3 Glucose	4 Galactose and Mannose	5 Arabinose	6 Ribose
NA 150						
NA 200						
NA 250						
CA 150						
CA 200						
CA 250						
AA 150						
AA 250						
Man 150	Y				103.81	
Man 250						62782.52

As can be expected, there is a distinct lack of sugars present in the aqueous phase post-HTC of the calcium and sodium alginates, but some are present in the mannitol sample. There is no organic sugars present in the starting feedstock for those samples that do not show any sugars identified, and only appear for the sugar based seaweed model compound feedstock. However, for the acid analysis, a variety of acids are present in some of the samples.

For the formic acid, upon quantification of the samples using standards for formic and

Table 6.11 HPLC VFAs peak identification data from the chromatographs of the Seaweed model compounds aqueous phase. The units are mg/L.

NA = Sodium Alginate, CA = Calcium Alginate, AA, Alginic Acid, Man = Mannitol, n/n/ = not detected.

Sample Name, HTC Temp (°C)	VFAs Present?							
	1 Oxalic Acid	2 Maleic Acid	3 Citric Acid	4 Methyl-malonic Acid	5 Lactic Acid	6 Formic Acid	7 Acetic Acid	8 Levulinic Acid
NA 150		Y		Y				
NA 200		Y				n.d.		
NA 250								
CA 150								
CA 200								
CA 250								
AA 150		Y	Y	Y		n.d.		
AA 250		Y	Y	Y	Y	n.d.		
Man 150		Y		Y		n.d.		
Man 250			Y	Y	Y	0.0176	0.7525	

acetic acid, using the same sample results, this process did not output any nitrification of the formic acid for the NA 200°C, AA 150°C, AA 250°C and Man 150°C samples, despite the peaks being identified as formic acid previously. This is most likely due to the amount detected being below the required amount for the algorithm on the software to identify it as formic acid. Where this is the case, it is listed in the table as ‘not detected’ or n.d.. The presence of acids in the acetic acid HTC aqueous phase samples is not unexpected, due to the acidic nature of the feedstock. This acid has therefore degraded into different shorter chain acids, due to the high temperature environment in the HTC reactor.

The mannitol samples show that the sugar does indeed degrade more readily at higher temperatures, containing significant amounts of ribose, along with quantified amounts of formic and acetic acids amongst citric, methyl-malonic and lactic acids. This would decrease the pH as the Man HTC aqueous phase samples becomes more acidic at higher HTC temperatures, as is observed in table 6.13. As mannitol is a key component in the seaweed samples and is a stable sugar, these results indicate the HTC at high temperatures such as 250°C would indeed be enough to break this sugar down, and therefore enable greater fuel efficiency for downstream processing of seaweed based feedstocks and enhanced biomethane production via anaerobic digestion.

6.3.5 Gas Chromatography FID

Figure 6.11 demonstrates that yet again acetic (or ethanoic) acid is by far the most abundant of the several different VFAs detected in the HTC PW samples for these

Table 6.12 GC-FID data for the seaweed model compound aqueous phase after undergoing HTC. Units are given in ng/ μ l.

Sample Name, HTC Temp ($^{\circ}$ C)	Propanone	Methanol	Ethanol	Ethanoic acid	Propanoic acid	2-Methyl propanoic acid	Butanoic acid	3-Methyl butanoic acid	Pentanoic acid	4-Methyl pentanoic acid	Hexanoic acid	Heptanoic acid
Sodium Alginate 150	3.69	47.58	0.00	597.82	60.67	5.65	7.60	4.02	1.37	1.56	8.59	10.12
Sodium Alginate 200	10.14	17.55	0.00	541.20	193.15	5.39	7.06	7.26	18.99	22.17	4.13	14.74
Sodium Alginate 250	18.81	38.79	30.52	533.84	183.82	2.47	3.58	2.56	1.23	2.00	4.02	18.83
Calcium Alginate 150	0.00	0.00	0.00	277.77	23.77	2.71	3.04	7.03	1.66	11.45	6.21	5.67
Calcium Alginate 200	70.69	65.51	0.00	647.98	121.84	7.12	11.14	3.96	2.91	11.55	5.20	8.33
Calcium Alginate 250	97.70	89.86	76.18	880.12	12.94	11.74	6.97	4.04	3.50	6.56	20.09	19.23
Alginic Acid 150	3.16	0.00	0.00	37.18	2.91	0.00	0.00	0.00	1.09	0.00	4.40	10.04
Alginic Acid 250	22.30	11.74	4.48	399.53	18.98	2.66	5.78	1.58	0.86	2.05	1.16	9.99
Mannitol 150	0.00	0.00	0.00	64.55	20.65	0.00	5.35	0.00	0.00	9.21	6.66	11.79
Mannitol 250	0.00	0.00	0.00	72.16	10.10	11.51	2.85	3.34	5.28	3.43	8.45	4.51

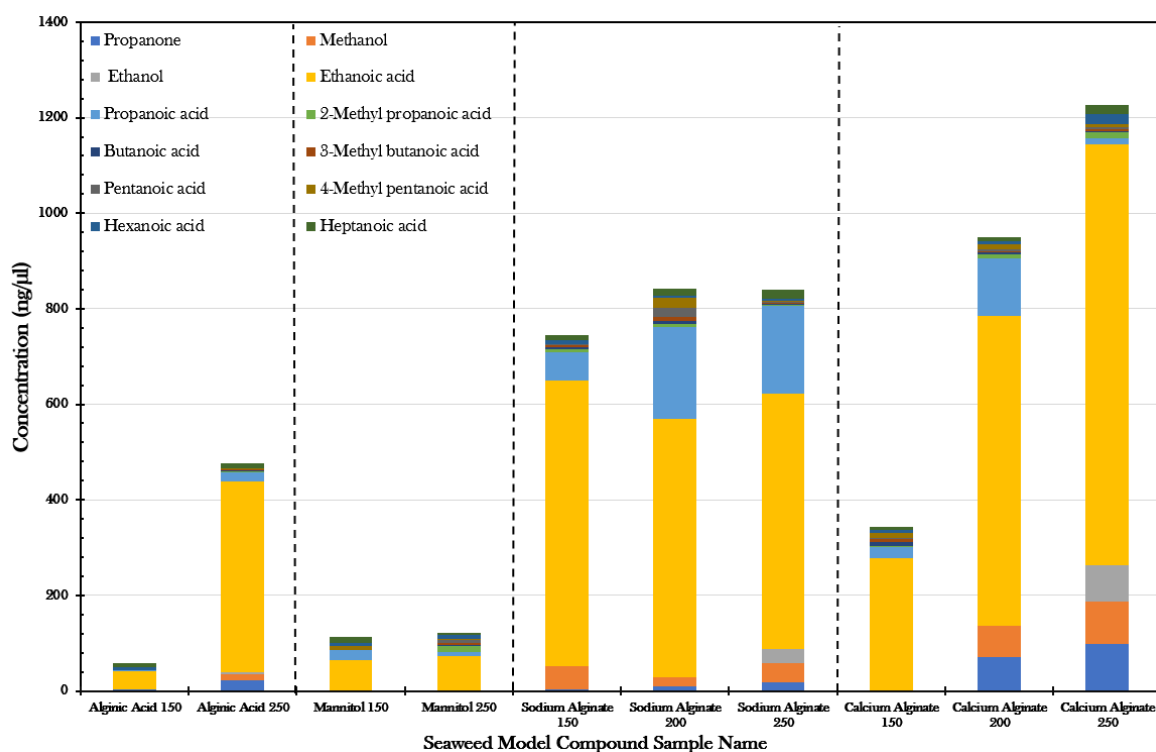


Fig. 6.11 Bar chart showing the results of the GC-FID analysis for the Seaweed model compound feedstocks aqueous phase samples after HTC.

model compounds. It is also plain to see that the alginic acid at 150 $^{\circ}$ C only produces a small amount of short chain acids, although when the HTC temperature reaches 250 $^{\circ}$ C this increases dramatically. This is likely due to the higher kinetic energy of the water molecules at this temperature, due to the super-heated water, meaning hydrolysis of the different molecules formed during HTC processing is far more probable to occur.

Mannitol does not produce much more VFAs at 250 $^{\circ}$ C than 150 $^{\circ}$ C, with a low overall amount for both temperatures. As a reduced sugar with no carbonyl compounds, mannitol is expected to be largely unreactive during hydrothermal processing. Therefore, the

liquid phase for the mannitol HTC runs contain very stable compounds, as predicted. This is also demonstrated in the mass balance yields for mannitol.

It seems that for calcium alginate, there is more ethanoic acid, in addition to more of the other types of VFAs detected, as the HTC temperature increases. This is unlike the results for the sodium alginate model compound, as for this sample, though the increase in propanoic acid increases from 150°C to 200°C, not much overall difference in abundance of VFAs is shown as a relation to HTC temperature. This difference in trends from the two alginate samples is interesting, although the ethanoic acid in seaweed feedstocks from the total amounts of various alginates (sodium, calcium, magnesium etc) found in the seaweed samples may result in any such increase in ethanoic acid levels with HTC temperature being less pronounced for the seaweed feedstock HTC aqueous phase samples.

This knowledge will aid in the process of determining which chemical reaction (likely some form of oxidation reaction) is key in the production of dissolved organics in the HTC aqueous phase. So, with the parent molecules known, the potential mechanisms responsible can be narrowed down for the seaweed biomass samples. The next GC-FID results discussed are the ones for the 100% biomass feedstock samples, including the two seaweed samples.

6.3.6 Fate of Inorganics: Liquid X-Ray Florescence & pH

The results for the pH of the Seaweed Model Compounds HTP aqueous phase are shown in table 6.13. Unfortunately the results from the Liquid XRF analysis of the seaweed model compounds, which were the last batch processed, were unable to be retrieved from the lab computer at the time of publication.

Table 6.13 The pH results at each different HTC Temperature of the Seaweed Model Compound HTP aqueous phase samples.

Sample Name	pH Value		
	150°C	200°C	250°C
Sodium Alginate	4.92	5.37	7.55
Calcium Alginate	3.81	4.33	5.61
Alginic Acid	2.19	2.27	3.25
Mannitol	3.92	3.41	3.30

As can be expected due to the nature of the initial model compound feedstock, the alginic acid HTC aqueous phase has a high acidity, with pH values ranging from 2.2-3.3. This

increase in pH as HTC T increases for acetic acid may be caused by the production of gas from the final breakdown stages of the organic acid under these conditions. This concurs with the comparatively high amount of gas produced during HTC (evident in figure 4.5) for the AA samples. The chemical equation for this reaction is as follows:



Therefore the pH of this short chain organic acid increases as the aqueous phase becomes more neutral due to the loss of acids upon the production of gases, during higher temperature HTC processing.

The sodium alginate has the highest pH of the samples, due to the inherent sodium present in the sample, and hence the OH^- ions present due to the elimination reaction with water. The higher pH value at 250°C is likely caused by increased solubility of the sodium alginate under these conditions and hence the higher sodium content dissolved in the water, releasing a higher proportion of OH^- ions. The same effect explains the same increase in pH for the calcium alginate aqueous phase samples.

Mannitol on the other hand remains fairly acidic throughout and becomes more so as HTC temperature increases. It is likely that this sugar, as shown in the HPLC results, degrades somewhat into smaller, simpler sugars and eventually into some organic acids (including formic and acetic acids), at the higher temperatures.

6.4 100% Biomass Feedstock

6.4.1 Ultimate and Proximate Analysis

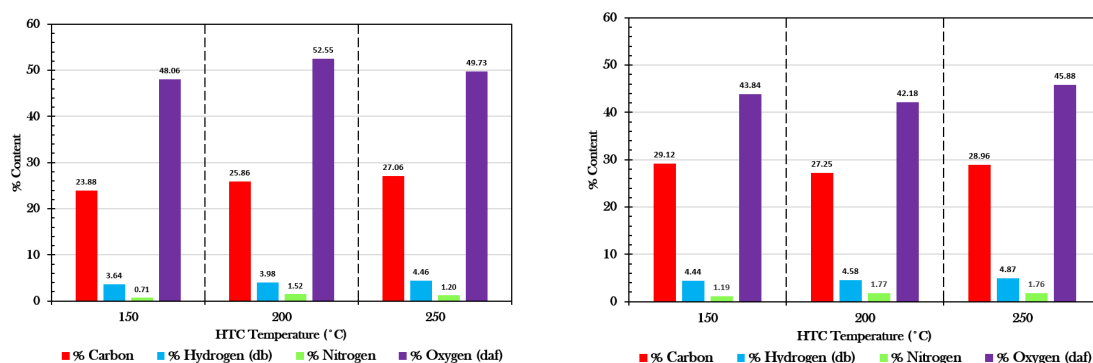
The CHNS and TGA analysis is shown in table 6.14 below. The resultant CHNS bar charts for each feedstock is shown in figure 6.12. The VK diagrams and HHV values are shown in figures 6.13 and 6.14 respectively.

Briefly analysing the CHNS and HHV from the 100% biomass samples gives one an indication of the potential for use in an AD reactor, although the usefulness of these values is limited by the loss of organic carbon from evaporated in sample preparation, (which is partly remedied using TOC analysis). It can be seen in the CHNS bar charts that the carbon content is highest in M 200°C and lowest for SL 150°C. From M 150°C to M 200°C there is a large reduction in O(daf) content, as it more than halves. The

Table 6.14 CHNOS, TGA and HHV values for the 100% biomass feedstock HTC aqueous phase after drying. Note that TGA was not performed on the *Miscanthus* 150°C sample as there was not enough sample remaining for this analysis initially, and the subsequent planned TGA analysis was cut short due to the sudden closure of all laboratories.

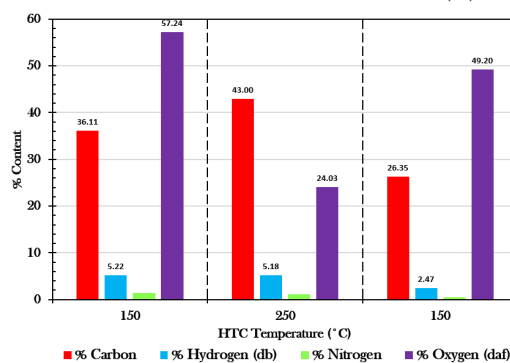
* = Calculated by difference.

Sample Name, HTC Temp (°C)	CHNS Data (%)						TGA Data (%)				HHV (db) (MJ/kg)
	N	C	H	S	H (db)	O (daf)*	M	VM	FC	Ash	
Saccharina latissima 150	0.71	23.88	4.26	0.04	3.64	48.06	5.54	60.60	15.74	18.12	13.51
Saccharina latissima 200	1.52	25.86	4.39	0.00	3.98	52.55	3.74	79.51	4.39	12.36	13.57
Saccharina latissima 250	1.20	27.06	4.83	0.00	4.46	49.73	3.27	78.30	4.14	14.28	13.31
Fucus serratus 150	1.19	29.12	4.99	0.00	4.44	43.84	4.99	71.35	7.24	16.43	13.73
Fucus serratus 200	1.77	27.25	5.10	0.00	4.58	42.18	4.65	75.26	0.53	19.56	13.32
Fucus serratus 250	1.76	28.96	5.20	0.00	4.87	45.88	3.00	81.17	0.30	15.53	13.45
Miscanthus 150	1.43	36.11	5.22	0.00	5.22	57.24					15.05
Miscanthus 200	1.18	43.00	5.69	0.00	5.18	24.03	4.57	54.72	18.67	22.03	17.19
Miscanthus 250	0.49	26.35	3.03	0.00	2.47	49.20	5.07	58.85	19.66	16.42	14.84



(a) *Saccharina latissima*.

(b) *Fucus serratus*.



(c) *Miscanthus*.

Fig. 6.12 The CHNO values from the process waters of the 100% Biomass Feedstock.

N content ranges from 0.5 to 2%, and is highest for the FS 250°C sample. With the lowest O content, the M 200°C aqueous phase sample also has the highest C content at 43.0% and the highest ash content (22.0%). The ash content might affect the pH, - it may represent a source of fertiliser, although it could also inhibit anaerobic digestion.

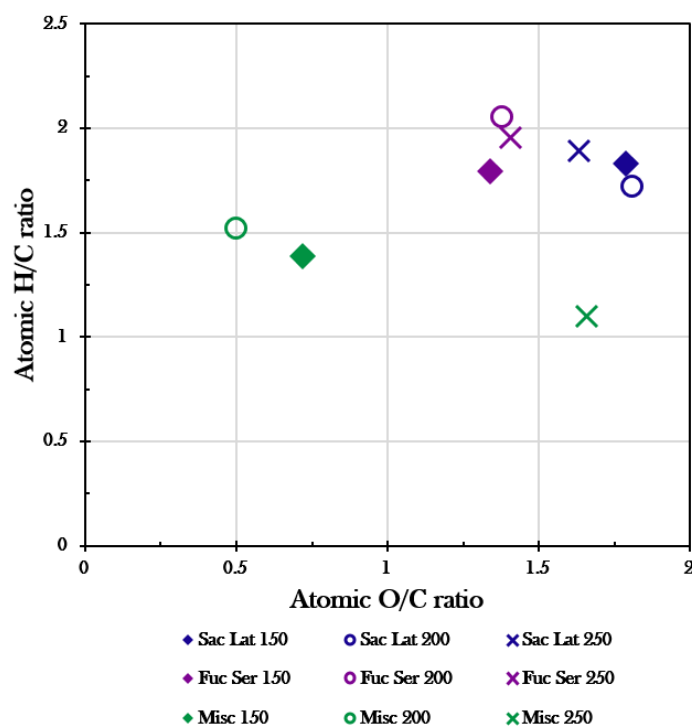


Fig. 6.13 Van-Krevelen diagram for the 100% biomass feedstocks aqueous phase.

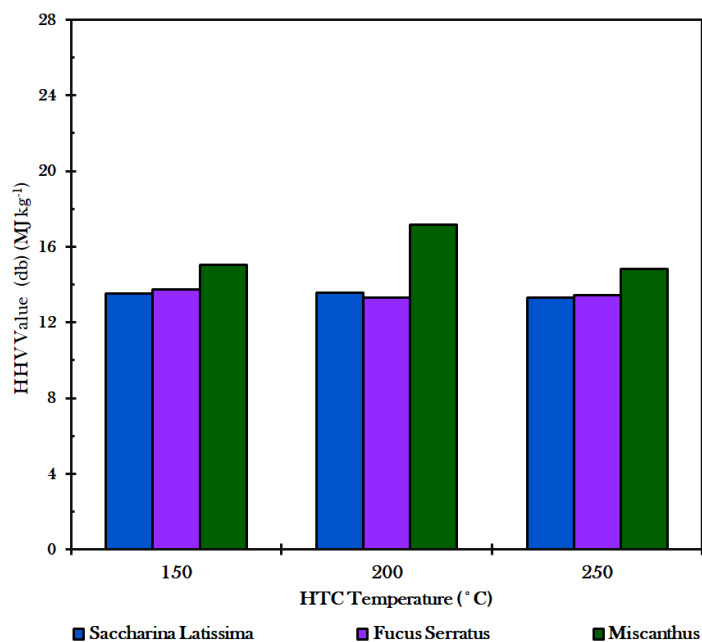


Fig. 6.14 The HHV values of the 100% biomass feedstocks aqueous phase after HTC, presented as a function of the HTC temperature.

The VM content ranges from 54% to 79.5%. The VM content represents how labile the hydrocarbon is, and may be linked to how easily it is broken down by micro-organisms. The FC content is the degree of polymerisation and may represent how much humin the sample contains. This humin may be more difficult to breakdown in AD. The FC is highest for the *Miscanthus* samples, followed by the SL 150°C sample, which then drops to 4% from 15.7% at T=200°C.

The SL samples has high O contents compared to C, both of which changes 4% over the HTC temperature range. For the FS samples, C% is around 28%, and O% at 45-42%, with not much change with change in HTC T. The Misc shows a carbon content peak at 200°C, where the O% also dips correspondingly.

There are limitations in this analysis as previously mentioned, as there is a loss of volatiles. It is noted here that the HHV ranges from 13.3 MJ/kg (FS 200°C) to 17.2 MJ/kg (M 200°C). However, the properties of the dried water phase as a fuel are not that relevant here, due to the material not being used in this way. Also, the C/N ratio is of importance in AD as the correct ratio for these two compounds is needed for efficient degradation via the micro-organisms (for the same reasons as getting the correct brown matter to green matter ratio in a compost heap). The forthcoming inorganic analysis will be important to link these results to the AD analysis in terms of the nutrients available and any inhibitive affects found.

6.4.2 Total Organic Content

The TOC results for the 100% Biomass Feedstock samples are shown in figure 6.15. The TOC content of the seaweeds is generally higher than the *Miscanthus* samples, particularly in the case of the *fucus*. The amount of organic carbon within the process waters reduces as the HTC temperature increases; this is thought to be due to increased polymerisation and further degradation of the volatiles, leading to increasing amounts of carbon residing in the hydrochar phase and more carbon molecules lost to the gaseous phase. These findings agree with the trend found by Erdogan et al. (2015) [184], which attributed the decreasing TOC levels to an increase in gas production. However, this trend is the opposite for the *Miscanthus*, so the organics in the *Miscanthus* samples appears to be less soluble, as expected, but also increasingly less so as HTC temperature increases.

The higher TOC content of the seaweed samples demonstrate that the macroalgae is easily degraded and solubilised in the aqueous phase compared to the less soluble *Miscant-*

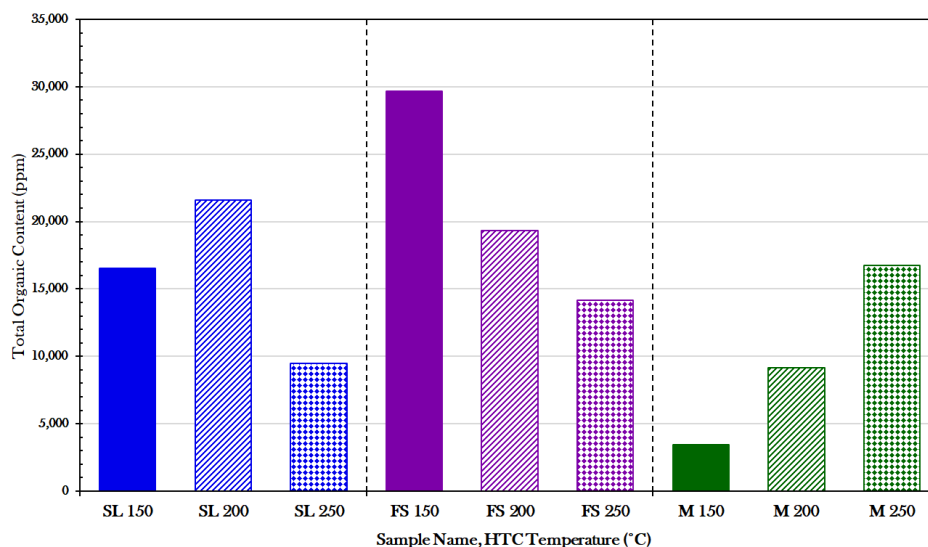


Fig. 6.15 A bar chart showing the TOC values for each HTC temperature for the 100% Biomass Feedstock Aqueous Phase samples.

SL = *Saccharina latissima*, FS = *Fucus serratus*, M = *Miscanthus*.

hus feedstock. The high amount of organic carbon in the aqueous phase shown in these results lends further impetus to ensure that this organically rich aqueous phase is used to its full potential; to extract organics and/or produce more renewable energy in the form of biomethane, to fully utilise as much of the organics as possible from the original feedstock.

6.4.3 Nuclear Magnetic Resonance

The numbers in table 6.15 as previously detailed, were produced via integration of the peaks in the NMR spectra at certain phase ranges. These sections are shown visually on an example of the NMR spectra for the three SL aqueous phase samples. These are outlined and labelled in figure 6.16. The spectra shown here demonstrate the different peaks in the VFA, sugar and phenol area (and other aromatic compounds). Note that the SL 250°C sample is zoomed in four times more compared to the SL 200°C and SL 150°C spectra. The NMR spectra for the *Miscanthus* samples are also shown in figure 6.17. The co-processed MSL NMR spectra can be found in §6.5.4, figure 6.25, without the different sections highlighted. These NMR spectra are of greater interest to this research than the other model compounds, of which the NMR spectra can be found in the Appendix.

Table 6.15 NMR (^1H 600MHz in D_2O) integrated values from the spectra of the 100% biomass feedstock aqueous phase. Tabulated both as a given value and normalised to total 100%, and colour-coordinated to show the higher relative amount as green.

Sample Name, HTC Temperature (°C)	Integrated Value Attributed			Normalised % Value		
	VFAs	Sugars	Phenolics	VFAs	Sugars	Phenolics
	0 -2.75	2.75-4.5	6-8	0 -2.75	2.75-4.5	6-8
Sac Lat 150	1	0.89	0.04	69.98	27.27	2.80
Sac Lat 200	1	0.45	0.00	68.97	31.03	0.00
Sac Lat 250	1	0.00	0.00	100.00	0.00	0.00
Fuc Ser 150	1	0.85	0.08	72.46	25.36	2.17
Fuc Ser 200	1	0.19	0.02	82.64	15.70	1.65
Fuc Ser 250	1	0.88	0.07	68.97	26.21	4.83
Misc 150	1	1.42	0.31	36.63	52.01	11.36
Misc 200	1	0.06	0.00	94.34	5.66	0.00
Misc 250	1	0.15	0.10	80.00	12.00	8.00

The percentage values of the proportions of sugars/VFAs/phenolics are colour co-ordinated to aid evaluation of the different proportions for each sample. The more green the cell is, the higher the normalised relative proportion of that compound in the sample's integrated NMR peak area. The more yellow, the lower the value. Integer values are also given before the percentage proportion were calculated, for completeness.

The *Saccharina latissima* samples, as shown in table 6.15, has about two thirds of the peak areas in the NMR spectra in the VFA range, with the remaining a third as sugars. SL 250°C spectra in figure 6.16 is zoomed in quite substantially, so the peak area under the sugars and phenols is actually negligible, and the integrated values in tab 6.15 show that there is a 100% relative amount of VFAs compared to sugars and phenols at this temperature. This suggests that for the mix of compounds in the seaweed feedstock, all the sugars and phenolics (with aromatic rings) have degraded in the aqueous phase to such an extent that the proportion of VFAs in the sample dwarfs them and is the main constituent group of compounds in the sample. The phenols and sugars do appear to be there, albeit in significantly lower concentrations than the VFAs. The HPLC sugars method would identify these. These results are as expected, due to the high HTC temperature breaking down the sugars at this temperature. Mannitol is a sugar found in seaweed, so some sugars were expected to remain, as mannitol has been shown to be stable under HTC at 250°C. Mannitol may be the main sugar left behind, shown in the spectra in figure 6.16.

There are only 3% phenols in SL 150°C, and at the higher temperatures <0.1%, so any phenolic compounds present at the lower temperature are unstable at temperatures

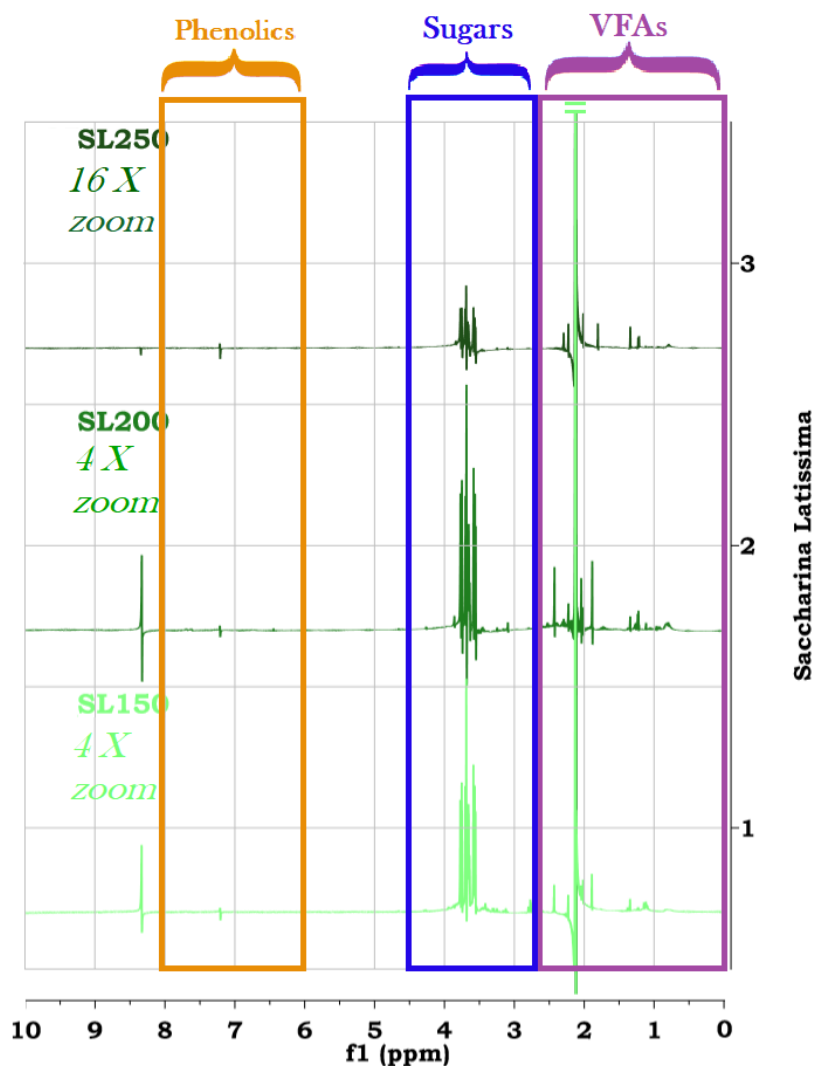


Fig. 6.16 NMR (^1H 600MHz in D_2O) Spectra for the three different aqueous phase samples from the *Saccharina latissima* feedstock.

between 150°C and 200°C. The higher amount of sugars degrading at the higher temperature should reflect in a higher HHV for the SL 250°C hydrochars, as more carbon molecules would be available and hence a higher %C content in these samples. This is indeed the case and hence 250°C is the preferred HTC temperature from those tested in order to improve the biofuel product. No inhibitory phenols for the AD process result from this temperature, yet some sugars (see the NMR spectra and HPLC results) remain in the process water, which would be digested by bacteria in the AD process to produce yet another biofuel; biomethane.

For the FS samples, there are broadly similar patterns to the SL samples, with some minor differences. FS 250°C has a lower proportion of VFAs than FS 200°C and FS 150°C, interestingly; 69% down from 83%. The spectra look similar (see Appendix, figure A.3) to one another, with sugars clearly present. There is a higher proportion of sugars in the FS 250°C sample compared to the VFAs, with respect to the SL 250°C sample. Therefore at this higher temperature, perhaps AD of the process water is more of a necessity if *Fucus serratus* is the seaweed feedstock, as some energy is still locked into the sugars even at this temperature.

However, there remains 5% phenols for FS 250°C, which could slow down the AD process or reduce the total biomethane produced from these samples. FS and SL process waters are both further used in AD bench scale experiments, so this can be investigated in §7.3. The increase in proportion of phenols from FS could be an advantage if the biorefinery process when applied on a large scale were to introduce a step extracting the phenols to sell as a by-product before anaerobic digestion. *Fucus serratus* could be considered a suitable feedstock, in this case, in order to generate more profits from this extraction step.

The *Miscanthus* results are quite interesting; half of the peak area in the M 150°C sample lie within the sugar range, which is a dominant feature in the spectra shown in the figure 6.17. There are also plenty of phenolic compounds in the M 150°C sample, at around 11%, with the rest in the VFA segment. This may be caused by the HMF formation, polymerising to produce humin, leaving behind many phenolic fragments. However in M 200°C, almost all the integrated peak area are found within the VFA phase (94%), which can be seen qualitatively in the NMR spectra for M 200°C. It seems that sugars and phenols which reside within the M 150°C aqueous phase mostly all degrade into acids between T=150°C and T=200°C. For the M 250°C sample, there are some sugars and 8% phenols detected. Perhaps some of the compounds from the solid phase have dissolved into the aqueous phase as they become more soluble in the more acidic water in the HTC reactor (which is approaching the critical point for water). HPLC and GC-FID results will be necessary to determine which degradation mechanisms are responsible for these results, and which sugars and acids are present in the aqueous phase.

There are lots of different peaks in the phenolic range in the spectra for *Miscanthus*, as expected. Phenols are widely known to be very prevalent in terrestrial biomass, which includes *Miscanthus*. The phenolic compounds in the *Miscanthus* after HTC are likely to become vaporised at high temperatures, and as the reactor is left to cool before the lid removed, some of these compounds would condense and therefore be retained within

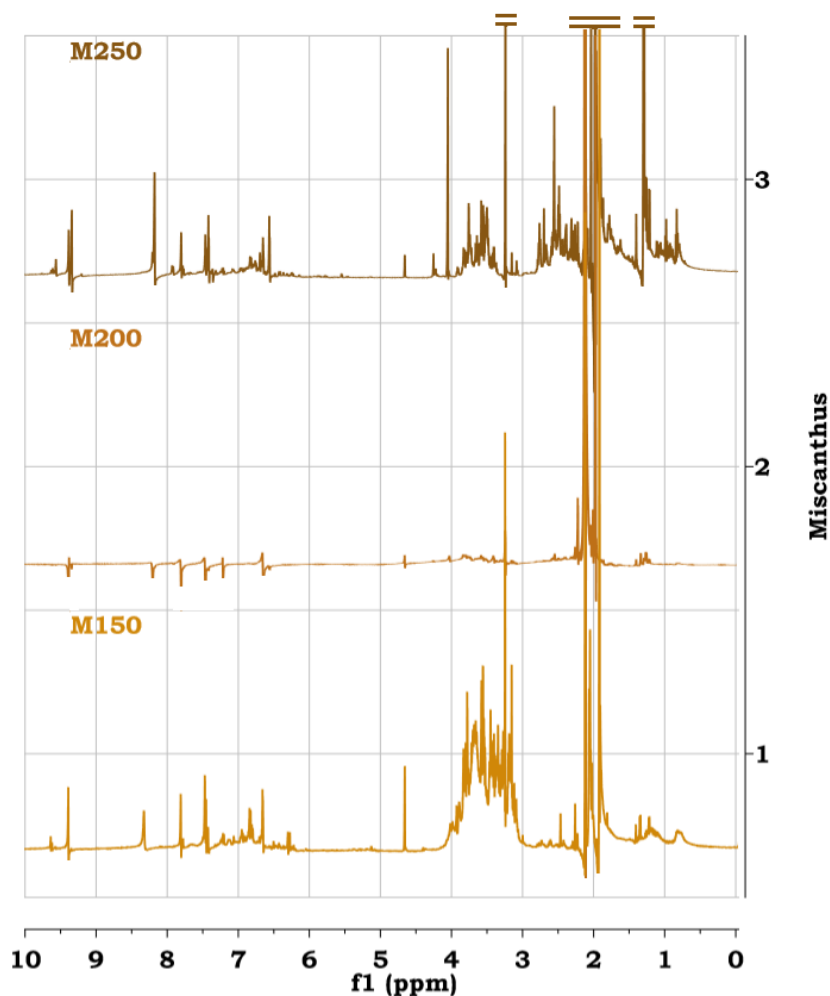


Fig. 6.17 NMR (¹H 600MHz in D₂O) Spectra for the three different aqueous phase samples from the *Miscanthus* feedstock.

the aqueous phase. This would explain the presence of the various phenolic peaks in the *Miscanthus* NMR results.

Co-processing the *Miscanthus* with the *Saccharina latissima* will have some interesting results, and how the mix of different lignocellulosic and seaweed compounds within these feedstocks interact during HTC and ultimately affect the VFA/sugar/phenol proportions can be initially evaluated with these NMR results.

6.4.4 High Pressure Liquid Chromatography

The HPLC results for the 100% Biomass Feedstock are tabulated in table 6.16 for the sugars and table 6.17 for the VFAs. The HPLC chromatographs for the *Saccharina latissima* and the *Miscanthus* samples are also shown for the HPLC sugars and HPLC VFAs in figures 6.18 and 6.19, respectively. The identified peaks in the HPLC chromatographs are numbered with the corresponding peak identifications labelled in the relevant subcaptions.

Table 6.16 HPLC Sugars peak identification and quantification data from the chromatographs of the 100% Biomass Feedstock aqueous phase. The units are mg/L.

SL = *Saccharina latissima*, FS = *Fucus serratus*, M = *Miscanthus*.

Sample Name, HTC Temp (°C)	Sugars Present?					
	1 Sucrose	2 Lactose	3 Glucose	4 Galactose and Mannose	5 Arabinose	6 Ribose
SL 150		Y	812.68	1698.65		
SL 200		Y		2056.68		
SL 250				2538.31		
FS 150		Y	505.6	2866.64		
FS 200		Y		4165.87		
FS 250				3100.52		
M 150	Y		94.08	317.04	20960.49	
M 200	Y		8889.22	9101.66	5.47	
M 250	Y		45.17	38.92		

Table 6.17 HPLC VFAs peak identification data from the chromatographs of the 100% Biomass Feedstock aqueous phase. The units are mg/L.

SL = *Saccharina latissima*, FS = *Fucus serratus*, M = *Miscanthus*.

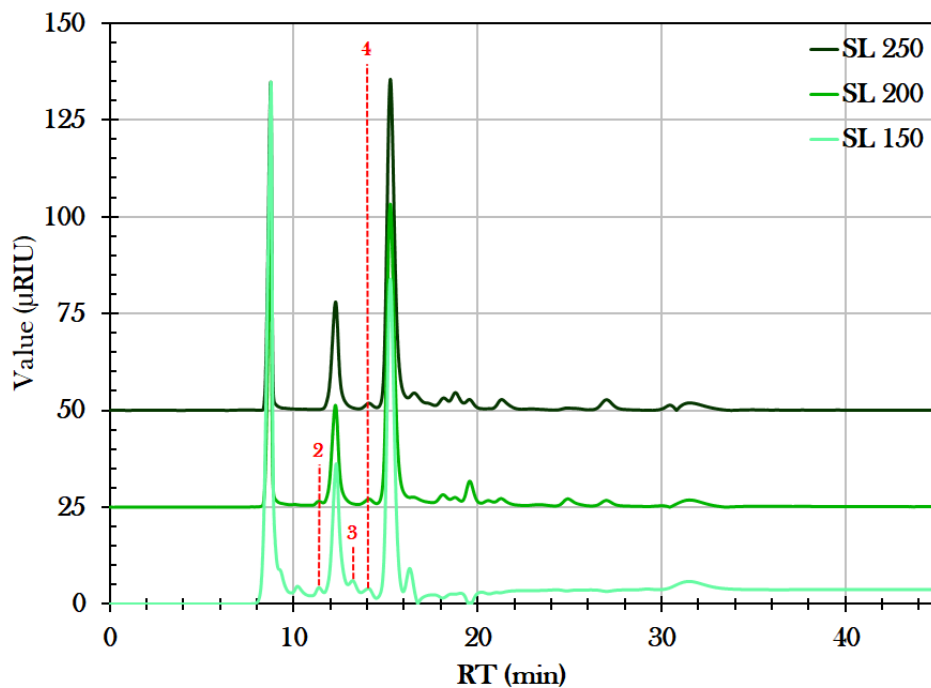
Sample Name, HTC Temp (°C)	VFAs Present?							
	1 Oxalic Acid	2 Maleic Acid	3 Citric Acid	4 Methyl-malonic Acid	5 Lactic Acid	6 Formic Acid	7 Acetic Acid	8 Levulinic Acid
SL 150	Y	Y	Y		Y	5.44	3.0607	Y
SL 200	Y		Y	Y	Y	4.6378	3.4578	Y
SL 250	Y	Y	Y	Y	Y	1.3876	1.9626	Y
FS 150	Y	Y	Y		Y	4.8908	3.2362	
FS 200	Y		Y	Y	Y	4.2047	4.1883	Y
FS 250	Y		Y	Y	Y	0.6626	1.8989	Y
M 150		Y	Y	Y		0.5500	1.0065	
M 200			Y	Y	Y	2.1376	6.2092	
M 250		Y	Y	Y	Y	0.6147	6.2886	Y

The variety of sugars identified in the two 100% seaweed samples (shown in table 6.16) is limited to lactose, a di-saccharide made up from galactose and glucose fragments, and glucose and galactose and mannose, from the range covered in the HPLC analysis. The

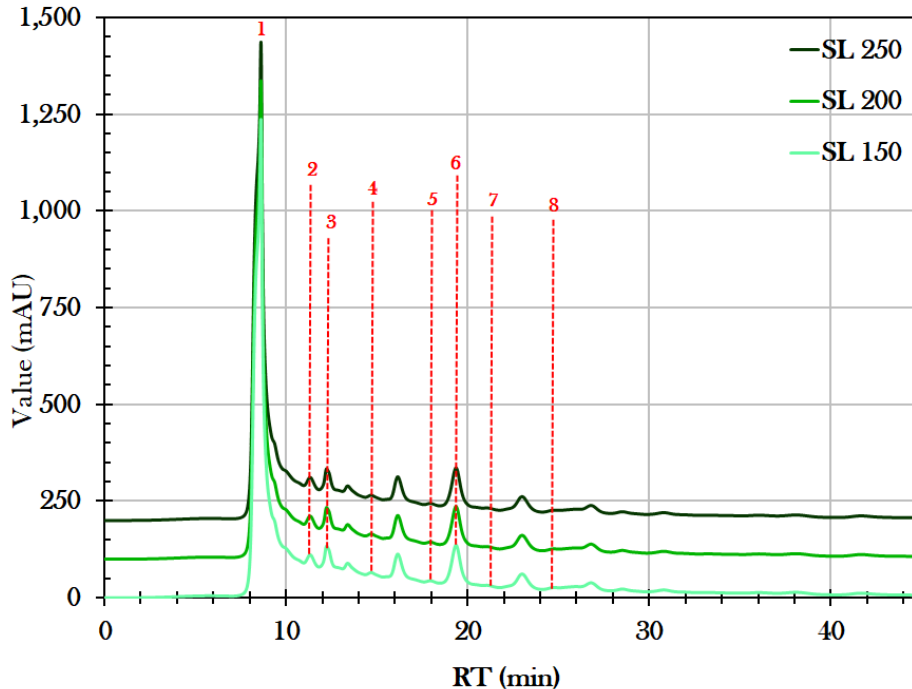
100% *Miscanthus* aqueous phase samples however also contains arabinose and sucrose, with no lactose detected. Sucrose having been only previously identified in the LMC samples and not in the SMC samples, is therefore only detected in the *Miscanthus* HTC aqueous phase samples due to its presence in the terrestrial biomass due to its protein and cellulose content. Sucrose, being a disaccharide, would degrade in HTC conditions via hydrolysis to form glucose and fructose, which is the first step in the caramelisation process [185].

The presence of glucose, particularly in the lower HTC temperature samples, is due to the breakdown of cellulose to form the glucose molecules under these 150°C HTC conditions. This agrees well with the trend shown in the NMR results (table 6.15) of the total sugar compounds reducing in relative amounts as the HTC temperature is increased. This glucose is more prevalent in the *Miscanthus* samples at the 200°C and therefore demonstrates that the cellulose breakdown within the terrestrial biomass breaks down at slightly higher temperatures, perhaps due to other inhibitory or competing mechanisms due to the presence of lignin. The polysaccharides in the seaweed samples hydrolyse, causing the breakdown of the constituent chemical compounds via splitting a bond by the water, producing glucose.

The lactose molecules are absent from the 250°C samples of the seaweeds likely due to the glycosidic link between the glucose and the galactose molecule breaking at such high temperatures and then further degrading under these HTC conditions [186].

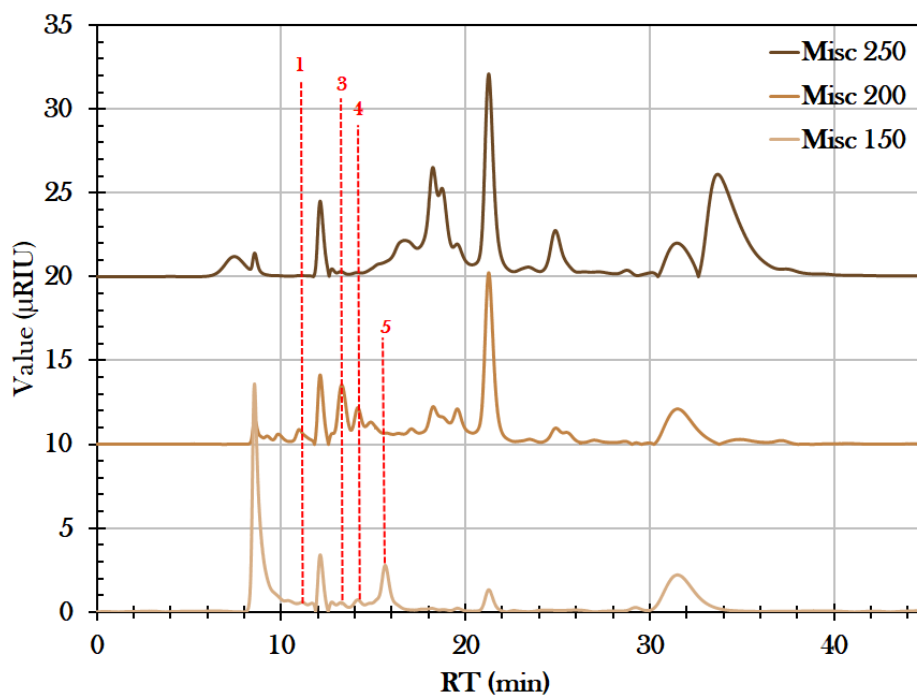


(a) *Saccharina latissima* Sugars. (2) - Lactose, (3) - Glucose, (4) - Galactose and Mannose.

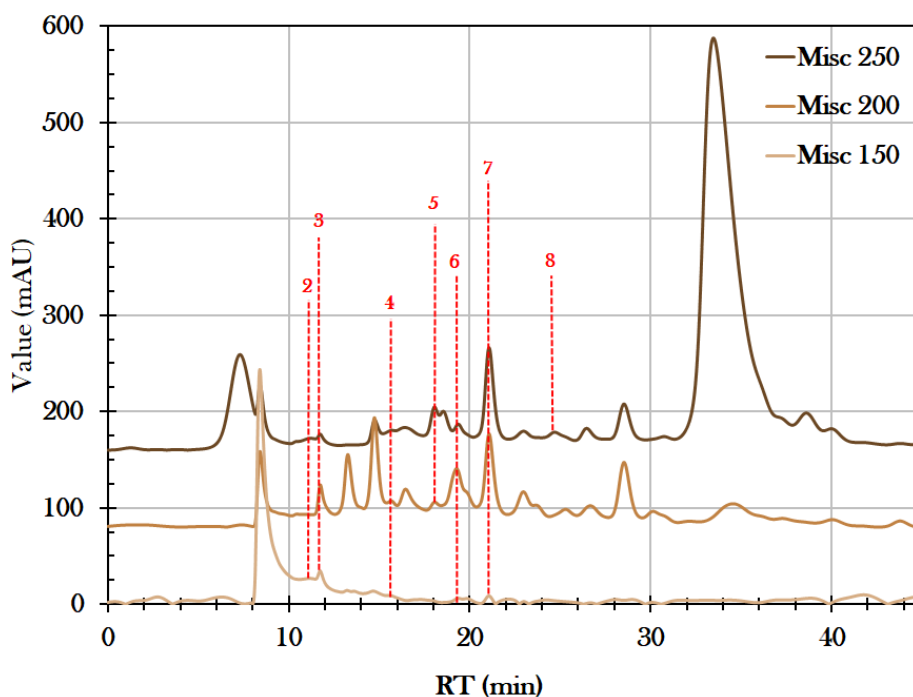


(b) *Saccharina latissima* VFAs. (1) - Oxalic Acid, (2)- Maleic Acid, (3) - Citric Acid, (4) - Methyl-malonic Acid, (5) - Lactic Acid, (6) - Formic Acid, (7), Acetic Acid, (8) - Levulinic Acid.

Fig. 6.18 Stacked HPLC Chromatographs of the *Saccharina latissima* aqueous phase samples after HTC for (a) Sugars and (b) VFAs.



(a) *Miscanthus* Sugars. (1) - Sucrose, (3) - Glucose, (4) - Galactose and Mannose, (5) - Arabinose.



(b) *Miscanthus* VFAs. (2) - Maleic Acid, (3) - Citric Acid, (4) - Methylmalonic Acid, (5) - Lactic Acid, (6) - Formic Acid, (7), Acetic Acid, (8) - Levulinic Acid.

Fig. 6.19 Stacked HPLC Chromatographs of the *Miscanthus* aqueous phase samples after HTC for (a) Sugars and (b) VFAs.

The arabinose present in the *Miscanthus* aqueous phase samples is due to the hydrolysis of hemicellulose, which is only present in the terrestrial biomass sample in this study. This pentose sugar is therefore identified in the lower HTC temperature HTC samples from *Miscanthus* and is further reduced at higher temperatures due to further dehydration of the pentose molecules into furfural, which in turn can result in the production of benzene or liquid fragmented compounds [187].

The reduction in glucose concentration in the seaweed aqueous phase samples as the HTC temperature increases is as predicted, and can be accounted for via the further breakdown via hydrolysis of this sugar into shorter chain organic acids (and also the 5-HMF compound). However, this increase in VFAs trend with HTC temperature increasing is not clear in the HPLC VFA analysis and so other mechanisms may be happening within the complex mix of chemical compounds in these samples, leading to an array of various organic compounds and gases produced at the higher temperatures, leading to less acids remaining in the aqueous phase. These other organic molecules in the process waters are identified and analysed using the forthcoming GC-FID results in §6.4.5.

Focussing more on the HPLC VFA results shown in table 6.17, the general finding is that lots of different volatile acids are produced via HTC. The concentrations of the acetic acid in the seaweed samples reduces significantly at the 250°C HTC temperature sample, due to the further degradation into gases, and the slight increase from 150°C to 200°C of the acetic acid amount can be attributed to the further degradation of the sugars into organics acids at the higher HTC temperature as it rises from 150°C to 200°C. The hydrolysis of cellulose to form hexoses and further degradation into organic acids is the likely mechanism for this, for the *Miscanthus*, and a similar route is likely for the polysaccharides in the seaweeds samples. These organic acids may further aromatise to form gases such as CO₂, H₂ and CH₄ or liquid fragments and products (see figure 2.11) and therefore contributes to the gases produced during HTC, which collectively causes the pressure to reach approximately 40 bar at 250°C using the 600ml Parr Reactor.

It was expected that as HTC temperature increases, the shorter chain acids become more abundant in the aqueous phase samples compared to the longer chain acids (citric C6, levulinic C5, maleic C4, methyl-malonic C4). Indeed, the formic acid (C1) is found in 100% of the pure biomass HTC aqueous phase samples, as well as the C2 acetic acid. However the ubiquitous presence of the citric acid is likely caused instead by the continued promotion of the degradation of the complex sugar molecules (such as mannose, glucose and arabinose) in the feedstocks into such acids as the HTC temperature increases, as

the sugars (mainly galactose and mannose) still remain as identified in all the 100% biomass samples [188]. The oxalic (C2) and maleic (C4) acids are less simple structures, being a di-carboxylic acids (albeit oxalic being the simplest one) and hence may not be as abundant in the aqueous phase samples due to the degradation mechanisms present, which favour simpler degradation products from the breakdown of larger molecules, via hydrolysis and fragmentation for example.

Overall it is observed that the cellulose and hemicellulose in the *Miscanthus* and the polysaccharides in the seaweed samples degrade into simple sugars and di-saccharides in the lower HTC temperatures. This is then followed by subsequent degradation via hydrolysis and fragmentation and some polymerisation to form shorter chain acids, simpler sugars and some aromatic gases and liquid fragments. At the highest HTC temperature the short chain acids further react to produce mainly carbon dioxide, hydrogen and some methane gases, in addition to much less sugar molecules remaining intact due to the superheated water conditions. Polymerisation of some of the organics also occurs to form secondary char during this process, reducing the abundance of certain organics in the higher HTC temperature samples.

The co-processing feedstock mix aqueous phase HPLC analysis will aid the determination of how the mix of the seaweed feedstock with the terrestrial *Miscanthus* may affect the production and degradation patterns of these sugars and acids. First, the range of organic molecules identified within the process water is further analysed and evaluated via GC-FID for the 100% pure biomass HTC aqueous phase samples.

6.4.5 Gas Chromatography FID

Table 6.18 GC-FID data for the 100% biomass feedstock aqueous phase after undergoing HTC. Units are given in ng/ μ l.

Sample Name, HTC Temp (°C)	Propanone	Methanol	Ethanol	Ethanoic acid	Propanoic acid	2-Methyl propanoic acid	Butanoic acid	3-Methyl butanoic acid	Pentanoic acid	4-Methyl pentanoic acid	Hexanoic acid	Heptanoic acid
Sac Lat 150	10.67	0.00	165.13	413.26	21.28	4.89	2.25	8.93	1.19	1.98	10.64	3.55
Sac Lat 200	30.35	26.21	0.00	57.33	31.68	1.47	3.18	5.55	0.00	6.53	8.58	23.50
Sac Lat 250	594.99	177.02	61.90	698.77	5.39	4.28	4.33	13.82	0.00	1.60	7.31	5.84
Fuc Ser 150	14.26	54.10	0.00	338.63	21.77	13.75	4.68	2.74	0.00	1.11	2.77	4.52
Fuc Ser 200	88.56	0.00	0.00	711.68	87.34	54.72	7.92	10.42	0.00	0.65	6.97	3.86
Fuc Ser 250	57.79	115.09	35.61	290.71	43.38	3.81	9.89	7.09	0.00	15.67	10.80	5.09
Misc 150	2.99	14.90	0.00	164.73	4.63	2.71	0.00	0.00	0.00	2.98	5.94	5.25
Misc 200	43.33	258.03	0.00	6887.32	25.68	23.06	5.72	2.20	1.85	2.26	3.27	4.41
Misc 250	92.15	199.22	0.00	1356.75	92.66	57.29	4.05	0.00	0.00	6.36	5.78	5.90

When interpreting figure 6.20 for the GC-FID results, it is worth noticing the difference in scale on the y-axis to the previous GC-FID bar charts. For example, the seaweed model compounds GC-FID bar chart reached just over 1200ng/ μ l total VFA content, in

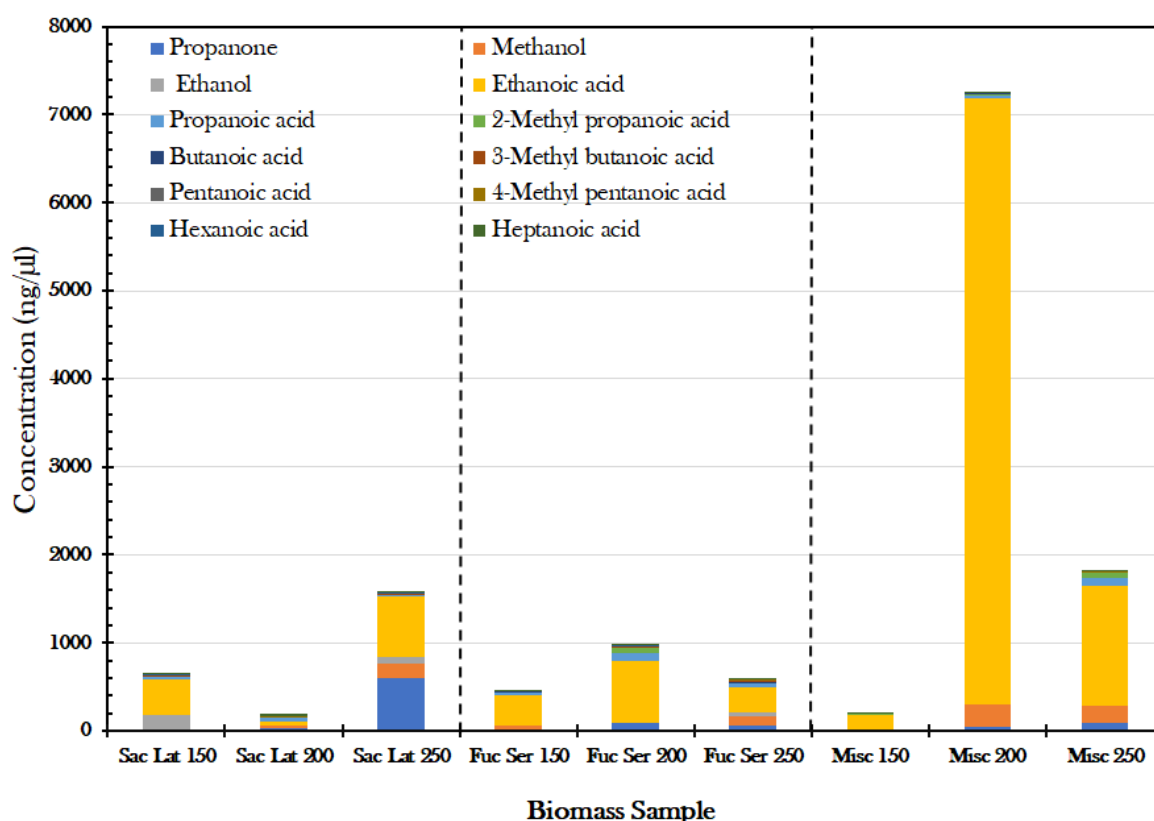


Fig. 6.20 Bar chart showing the results of the GC-FID analysis for the 100% biomass feedstocks aqueous phase samples after HTC.

comparison to over 7000ng/ μ l for the M 200°C HTC aqueous phase sample. All the other 100% biomass feedstock samples are around the scale of 100-2000ng/ μ l, with M 250°C and SL 250°C being the next highest in concentration respectively, each containing a higher concentration of VFAs in total than any of the seaweed model compound HTC samples. By far the change in VFA concentration is due to the increase in ethanoic acid; the most prevalent of the VFAs in any sample. SL 250°C contains a similar amount of propanoic acid as ethanoic acid, possibly due to presence of sodium alginate. The SL and *Miscanthus* mixed feedstock and the sodium alginate and *Miscanthus* mix will be analysed in the next section. Additionally, each of the different concentrations of the various VFAs identified (as displayed in the tables and also graphically in the bar charts) will be compared for all of the different HTC aqueous phase samples.

6.4.6 Fate of Inorganics: Liquid X-Ray Florescence & pH

The results for the pH of the 100% Biomass Feedstock HTP aqueous phase are shown in table 6.19 and results from the Liquid XRF analysis are shown in table 6.20.

Table 6.19 The pH results at each different HTC Temperature of the 100% Biomass Feedstock HTP aqueous phase samples.

Sample Name	pH Value		
	150°C	200°C	250°C
<i>Saccharina latissima</i>	4.55	4.64	7.34
<i>Fucus serratus</i>	4.73	4.60	6.90
<i>Miscanthus</i>	4.32	3.24	3.01

Table 6.20 Liquid XRF Results from the 100% Biomass Feedstock.

SL = *Saccharina latissima*, FS = *Fucus serratus*, M = *Miscanthus*.

Sample Name	Metals												
	Al	As	Br	Ca	Cl	Fe	K	Mg	Na	P	S	Si	Sr
SL 150		0.0011		0.1066	0.9666		0.6225	0.1836	1.9224	0.1846	0.0744	0.022	0.0017
SL 200	0.0083		0.0035	0.739	0.7409		0.5183	0.0758		0.1445	0.0543	0.0159	0.0055
SL 250		0.0008	0.0039	0.0805	0.8292		0.5848	0.1083	0.4628	0.1415	0.0444	0.0116	0.0062
FS 150	0.0127	0.0007		0.1098	0.368	0.002	0.3156	0.0878		0.1598	0.1461	0.0129	0.0028
FS 200			0.0028	0.0752	0.3476		0.3095	0.0901	0.3004	0.1517	0.0928	0.0143	0.0039
FS 250		0.0009	0.0028	0.0767	0.3006		0.2795			0.1429	0.0816	0.0138	0.0035
M 150				0.043	0.0181		0.025			0.1503	0.007	0.0124	
M 200	0.0074			0.0521	0.0179		0.0285	0.0339		0.1414	0.0059	0.0431	
M 250				0.0452			0.0248			0.1516	0.0071	0.0482	

The pH value of 7.3 for the of SL 250°C aqueous phase sample is the second most neutral overall, and 6.9 for FS 250°C is the most neutral, compared with all nine 100% biomass aqueous phase samples. This is therefore the most suitable pure biomass feedstock in terms of pH for certain end uses of the process water, for example involving any reintroduction to the aquatic ecosystem, e.g. as fertiliser for hydroponics or for recirculation within the seaweed cultivation site). This sample would also not cause as much corrosion to the pipework within such an industrial facility, as it within the range of 6.5-9.5. FS 250°C is the only other 100% biomass aqueous phase sample that sits within this desired range [181].

The M 200°C sample has the most acetic acid as shown in figure 6.20 (named ethanoic acid here), although the HPLC results shows similar amounts in the M 250°C sample. The two higher *Miscanthus* samples hence would have a lower pH due to the increased presence of this acid, in addition to the lower alkali metals shown from the XRF results.

The change in pH from 200°C to 250°C for both the SL and FS samples is significant, increasing by 2.7 and 2.3 respectively. Considering the pH is a logarithmic scale, this change in acidity must be extreme. This large difference in H⁺ ion concentration is likely caused by the shorter chain acids producing some more gas and therefore increasing the pH as the overall H⁺ ions decrease, increasing the pH. This is in addition to the increased solubility of the inorganics due to the water reaching supercritical levels.

As can be seen by the liquid XRF results in table 6.20 for the two seaweed samples, there is a higher proportion of calcium, potassium, sodium and magnesium contents compared to the *Miscanthus*, as can be predicted due to the seawater being the growing medium. Hence, the resultant pH of these seaweed samples is more neutral, and progressively more neutral as the HTC temperature is raised. The presence of the inorganics within the seaweed aqueous phase samples after HTC (especially at the higher temperatures) may have the effect of making the co-processed *Miscanthus* samples become more neutral, which considering the very high acidity of the *Miscanthus* samples, would be another benefit of co-processing.

6.5 Co-Processed Feedstock

6.5.1 Ultimate and Proximate Analysis

The CHNS and TGA analysis is shown in table 6.21 below. The resultant CHNS bar charts for each feedstock is shown in figure 6.21. The VK diagrams and HHV values are shown in figures 6.22 and 6.23 respectively.

Table 6.21 CHNOS, TGA and HHV values for the co-processed *Miscanthus* feedstock HTC aqueous phase after drying.

NA = Sodium Alginate, * = Calculated by difference.

Sample Name, HTC Temp (°C)	CHNS Data (%)						TGA Data (%)				HHV (db) (MJ/kg)
	N	C	H	S	H (db)	O (daf)*	M	VM	FC	Ash	
Misc/Sac Lat 150	1.10	28.97	4.51	0.00	3.86	46.54	5.82	65.13	15.34	13.72	14.12
Misc/Sac Lat 200	1.18	33.06	4.51	0.00	3.92	39.41	5.33	59.80	17.76	17.11	14.86
Misc/Sac Lat 250	0.74	37.18	5.16	0.00	4.66	41.31	4.52	67.67	16.20	11.60	15.46
Misc/NA 150	0.59	34.00	4.56	0.00	3.99	35.40	5.11	61.41	12.57	20.91	14.94
Misc/NA 200	0.41	30.48	4.42	0.00	3.75	35.68	6.09	63.10	7.23	23.58	14.37
Misc/NA 250	0.33	43.26	5.61	0.00	5.22	32.69	3.46	76.28	5.23	15.03	17.17
Misc/Man 150	0.45	40.38	7.30	0.00	7.17	45.04	1.22	88.87	4.18	5.73	15.92
Misc/Man 200	0.35	39.93	7.05	0.00	6.89	44.45	1.42	84.67	6.95	6.96	15.76
Misc/Man 250	0.31	40.26	6.64	0.00	6.43	43.78	1.87	80.05	10.74	7.35	15.97

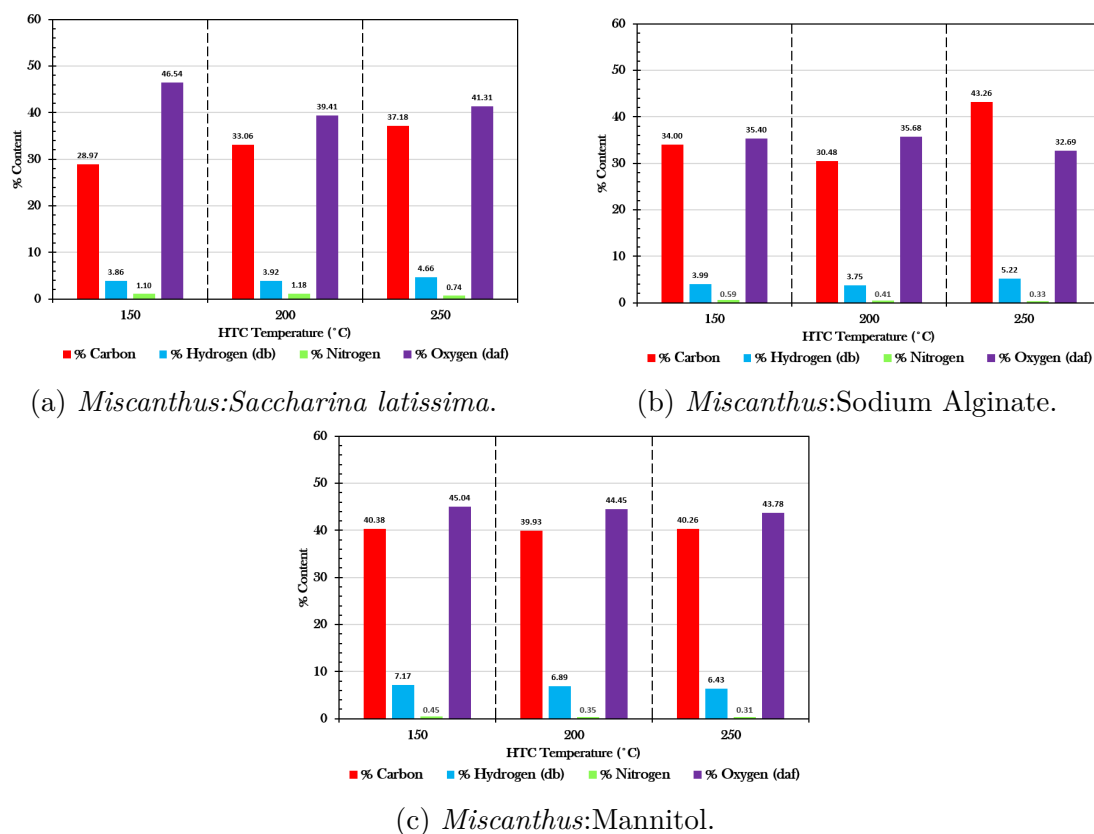


Fig. 6.21 The CHNO values from the process waters of the Co-Processed Feedstock.

Analysing the CHNS content, it can be seen that the highest C content is found in the MNA 250°C sample, with others at 250°C also similar percentages. The lowest carbon content was found in MSL 150°C, which also follows that this sample contains the highest % O (calculated by difference). The MSL co-processed mix was found to have a lower C% than the MNA and MMan mixes. The O% and C% contents were in general found to be fairly similar across the different feedstocks in this subgroup, with a range of 40-45%, with the largest relative difference in O and C for MSL 150°C, which evens out by T=250°C. The VK diagram shows this trend too, as the O/C and H/C ratios are similar in terms of sample type, and with changes in HTC temperature.

The HHV range was from 14.1 to 17.2 MJ/kg for this subgroup of feedstocks, and was found to be higher in the hydrochar than the process waters, which is the desired scenario. However, the most important properties of these process waters here are the VM, FC, ash contents.

The most ash was found in the MNA 200°C aqueous phase sample, whilst the lowest ash was found in MMan 150°C. The highest FC was detected in MSL 200°C, which has

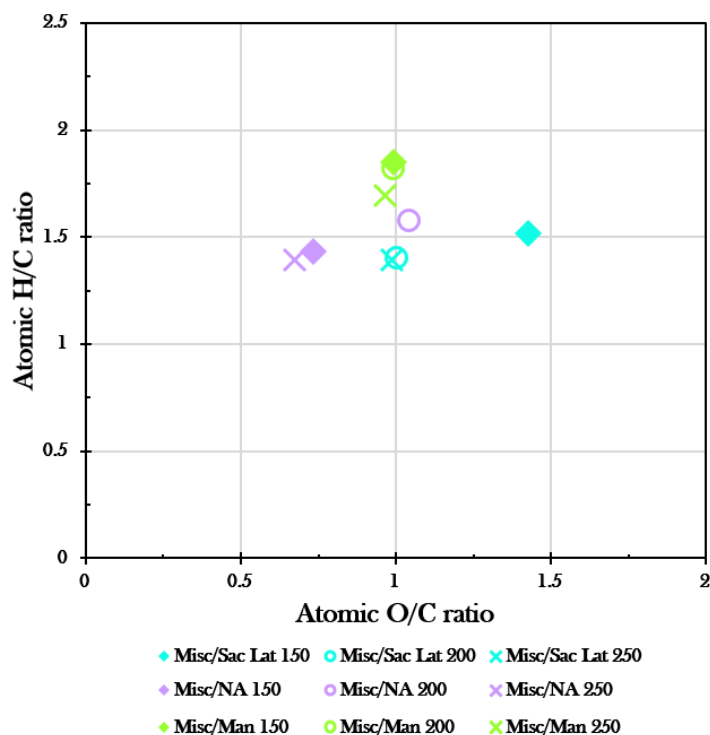


Fig. 6.22 Van-Krevelen diagram for the co-processed biomass feedstocks aqueous phase. NA = Sodium Alginate, * = Calculated by difference.

correspondingly the lowest VM% too. On the other hand, the lowest FC% was found in MMan 150°C, which also had the highest VM%.

6.5.2 Total Organic Content

The TOC results for the Co-processed Feedstock samples are shown in figure 6.24. With these co-processing results shown in figure 6.24, it can now be compared to the 100% biomass TOC results in figure 6.15 to see if the effects of co-processing is simply additive or not. With the TOC results showing significantly more organic carbon in the 100% seaweed aqueous phase samples compared to the 100% *Miscanthus* samples, it is interesting to note that the MSL 250°C sample has less TOC than the M 250°C sample, which may be caused by enhanced degree of polymerisation of the organics. Overall, there is less organic carbon in the respective MSL aqueous phase samples than the *Miscanthus* samples and SL samples, apart from the 150°C sample. The effect of the co-processing seaweed with the *Miscanthus* on the organic carbon in the aqueous phase after HTC has an adverse effect. This may reduce the total carbon in the aqueous phase available for further digestion to produce biomethane, however at the lower temperature,

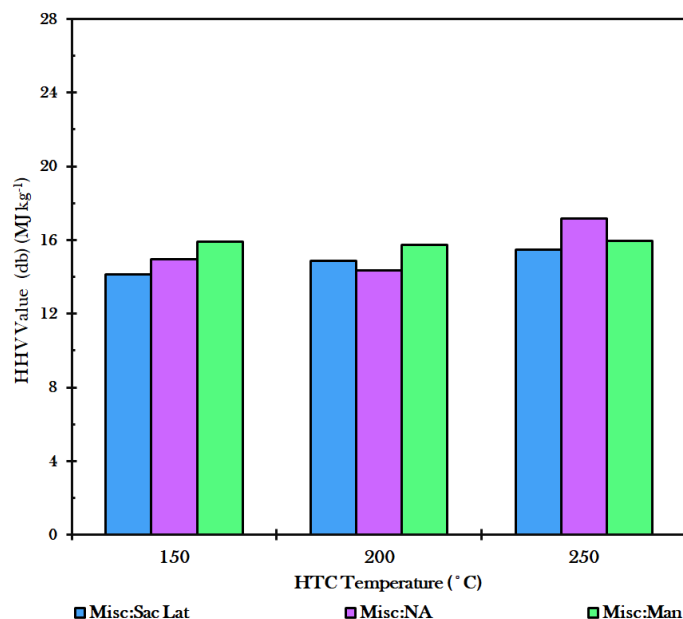


Fig. 6.23 The HHV values of the co-processed feedstocks aqueous phase after HTC, presented as a function of the HTC temperature.

NA = Sodium Alginate, * = Calculated by difference.

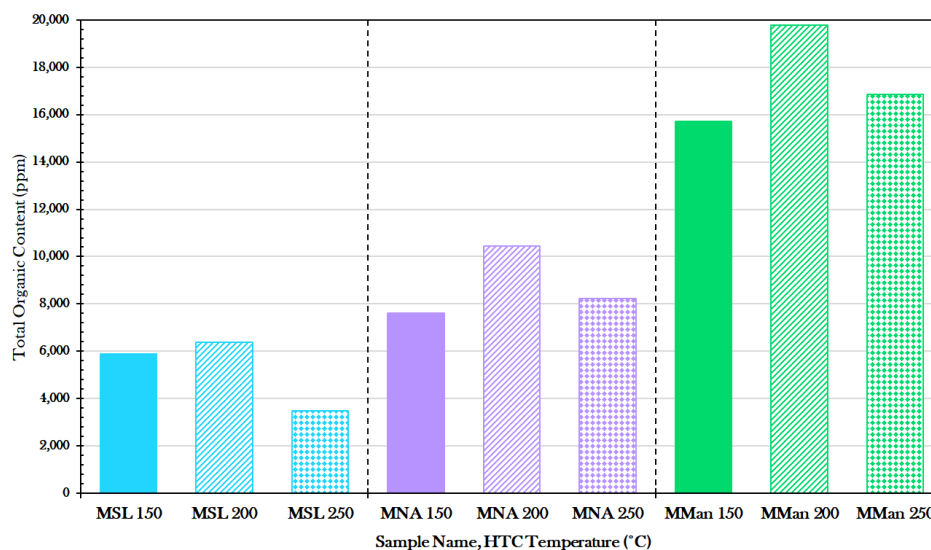


Fig. 6.24 A bar chart showing the TOC values for each HTC temperature for the Co-processed Feedstock Aqueous Phase samples.

MSL = *Miscanthus:Saccharina Latissima*, MNA = *Miscanthus:Sodium Alginate*, MMan = *Miscanthus:Mannitol*.

where there is expected to be more sugars, there is more organic carbon dissolved in the process water compared to the M 150 °C, so the overall BMP production may be based

on other factors, including the proportions of the sugars, VFAs and phenolic/aromatic molecules in which the organic carbon is contained within. The forthcoming NMR results of the co-processed biomass mixes will look into the relative amount of the three key types of molecules found within the aqueous phase.

6.5.3 Nuclear Magnetic Resonance

A table of the NMR (^1H) spectra for the co-processed feedstock is shown in table 6.22 and is colour co-ordinated to aid evaluation of the different proportions of sugars, VFAs and phenolics for each sample. The more green the cell is, the higher the normalised relative proportion of that compound in the sample's integrated NMR peak area. The more yellow, the lower the value. Integer values are also given before the percentage proportion were calculated, for completeness. The MSL spectra is shown in figure 6.25 for additional inspection. The other NMR (^1H) spectra discussed in the co-processed section can be found in §10.2, figure A.4.

Table 6.22 NMR (^1H 600MHz in D_2O) integrated values from the spectra of the co-processed feedstock aqueous phase. Tabulated both as a given value and normalised to total 100%, and colour-coordinated to show the higher relative amount as green. NA = Sodium Alginate.

Sample Name, HTC Temperature (°C)	Integrated Value Attributed			Normalised % Value		
	VFAs	Sugars	Phenolics	VFAs	Sugars	Phenolics
	0 -2.75	2.75-4.5	6-8	0 -2.75	2.75-4.5	6-8
Misc/Sac Lat 150	1	1.42	0.36	35.97	51.08	12.95
Misc/Sac Lat 200	1	0.30	0.14	69.44	20.83	9.72
Misc/Sac Lat 250	1	0.39	0.11	66.67	26.00	7.33
Misc/NA 150	1	0.34	0.11	68.97	23.45	7.59
Misc/NA 200	1	0.22	0.11	75.19	16.54	8.27
Misc/NA 250	1	0.24	0.11	74.07	17.78	8.15
Misc/Man 150	1	11.96	0.30	7.54	90.20	2.26
Misc/Man 200	1	2.47	0.25	26.88	66.40	6.72
Misc/Man 250	1	1.47	0.12	38.61	56.76	4.63

For the MSL co-processed samples, the sugars make up 50% of the NMR integrated peak areas in the 150°C sample. This is similar to the 100% *Miscanthus* sample at the same temperature (52%). However the MSL sample sugar content reduces relative to the VFAs and phenol content at HTC temperatures over 150°C; 21% and 20% are the sugar values for the 200°C and 250°C samples respectively. This finding does differ from

the values shown in the M 200°C samples. This may be due to the sugars found in the NMR spectra for the MSL samples at the 200°C temperature mark originating from the seaweed proportion of the MSL NMR samples, as this would agree with the 100% SL NMR findings, making up for the lower sugar proportion for the M 200°C sample. The type of sugars found within this spectra may be qualitatively analysed via the NMR spectra. The sugars will be more accurately identified using the HPLC sugars analysis in §6.5.6. From the spectra in figure 6.25, the shape and structure of the peaks within the sugar range look more similar to the peaks shown in figure 6.17 than those in figure 6.16.

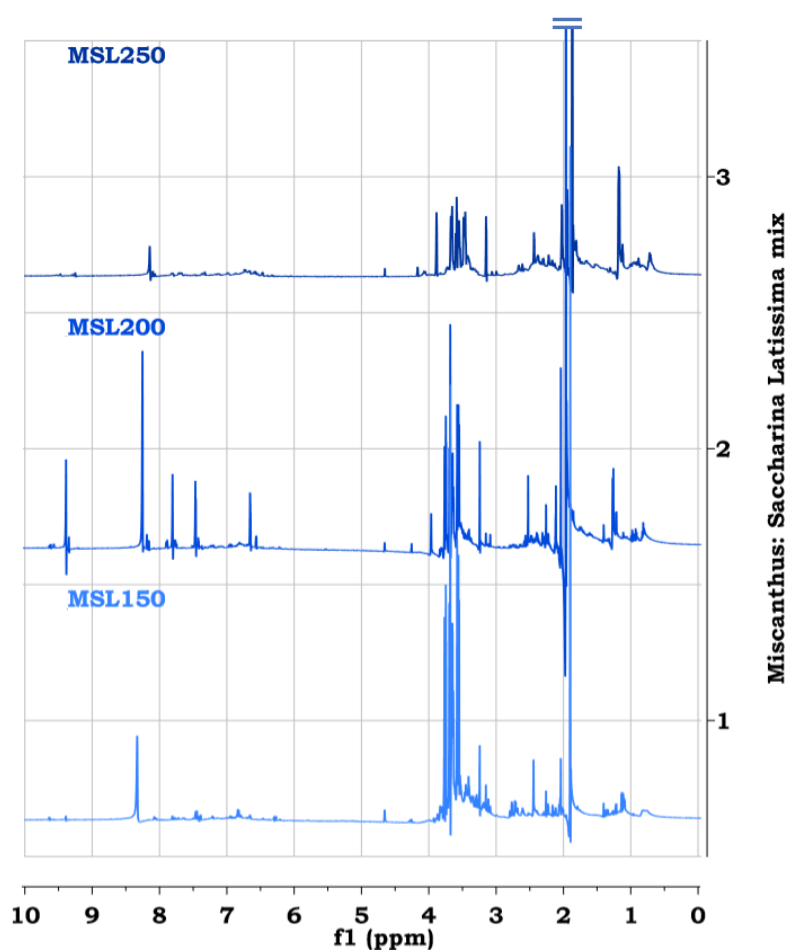


Fig. 6.25 NMR (^1H 600MHz in D_2O) Spectra for the three different aqueous phase samples from the *Miscanthus:Saccharina latissima* (MSL) feedstock.

The mannitol spectra (fig A.2d) looks dissimilar to the MSL spectra, as the peaks are more sharp and less broad for the pure mannitol. There is little deviations from the baseline of the spectra, with distinctive tall double peaks coupled with slightly shorter

sharp peaks either side at about the 3.7ppm mark. Therefore it appears that the sugars in the aqueous phase for the MSL are unlikely to be identified as mannitol. They are more likely to come from a terrestrial biomass origin, from the *Miscanthus* and not the seaweed. Likely compounds could be glucose, the monomer that forms cellulose. The HPLC analysis will further determine the quantities and identities of these sugar and VFA compounds found within the aqueous phase, although the NMR spectra does allow for proportionality of the sugars and the acids to be compared.

For the co-processed MNA samples, there were higher proportions of VFAs, less relative proportion of initial sugars (24%, half as much as MSL 150°C). The pH of the HTC process waters at this temperature is most likely the mechanism responsible for aiding the NA to break down the sugars, as the NA will render basic and hence reduces the hydrolysis of the compounds in the aqueous phase. The lowest relative proportion of sugars is found for MNA at 200°C, compared to all the tabulated co-processed feedstock samples. This is still at a similar level at 250°C. Therefore, this agrees with the known behaviour that at higher temperatures and pressures, the sugars degrade further still. Adding sodium alginate to the feedstock would hence potentially favour VFA production, which if desired for further chemical/economical end usages may be of interest. However, with some useful sugars remaining in the aqueous phase, a full biorefinery concept utilising anaerobic digestion of the process waters may be fulfilled with the MSL feedstock mix, at the lowest temperature. This would produce a higher proportion of sugars to VFAs than if the feedstock were to have sodium alginate added. However, exact amounts and trends cannot be fully evaluated just from the NMR spectra. The HPLC chromatographs for the sugars and VFAs in these samples can help with quantification. These can be found in the Appendix, figure A.14 and will be discussed alongside the MSL HPLC discussions.

MMan was found to have the highest proportion of sugars out of all the co-processed samples for the 150°C HTC temperature runs. Mannitol only consisted of 20% of the initial feedstock (by weight), yet seemingly has a large effect on the stability of other sugars in the misc feedstock. A proportion of 7.5% of VFAs were found in the MMan sample at 150°C, due to the high amount of sugars in the spectra that were included in the total peak area (to which the VFA amounts were normalised). The NMR spectra for MMan can be found in figure A.2d in §10.2. It is clear from these spectra that the mannitol NMR signature is the more dominant feature. However there are signs of VFAs in the spectra also and some compounds in the phenolic range (and above) to consider. Comparing the spectra to the mannitol model compound spectra in figure A.2d, the pure

mannitol although only accounting for 20% of the feedstock, shows a strong signature on the NMR spectra. HPLC data would be beneficial here to accurately quantify the sugar amounts and identify any other sugars and the VFAs present. The VFAs are likely formed via the degradation of sugars, which at 150°C is at the beginning stages of degradation; yet to occur for most of the sugar compounds in the aq phase. The VFA proportion rises to 27%, then up to 39% for the MMan samples, as the HTC temperature rises. This concurs with the aforementioned trend of sugars breaking down more readily at higher temperatures.

The stability of the sugars in the MMan samples would theoretically be an advantage if AD were to follow up the HTC process on a large scale implementation of the technology, as the sugars can be digested by the bacteria to produce biomethane. However, as an actual feasible large scale feedstock, mannitol, as an extracted, expensive and pure compound is not considered. The mannitol content in seaweeds, however, should hence be considered when deciding upon feedstocks for future industrial HTC processes. As long as its presence is not too high, the carbon content of the feedstock would mainly be formed into acids and hydrochar, leaving a small amount of sugars for further AD processing to produce biomethane, as verified in the MSL NMR results.

6.5.4 High Pressure Liquid Chromatography

The HPLC results for the Co-processed Feedstock are tabulated in table 6.23 for the sugars, and table 6.24 for the VFAs. The HPLC VFA and Sugars chromatographs are shown for the MSL sample in figure 6.26 in addition, with peaks labelled.

Table 6.23 HPLC Sugars peak identification and quantification data from the chromatographs of the Co-processed Feedstock aqueous phase. The units are mg/L.

MSL = *Miscanthus:Saccharina Latissima*, MNA = *Miscanthus:Sodium Alginate*, MMan = *Miscanthus:Mannitol*.

Sample Name, HTC Temp (°C)	Sugars Present?					
	1 Sucrose	2 Lactose	3 Glucose	4 Galactose and Mannose	5 Arabinose	6 Ribose
MSL 150		Y	815.78	404.04		
MSL 200	Y	Y	622.56	660.97		
MSL 250				76.10		
MNA 150	Y		162.55	182.29	826.05	
MNA 200	Y		10183.33	85.52	15.67	
MNA 250						
MMan 150	Y		53.14	7662.9		
MMan 200	Y		11257.16	10085.49		
MMan 250			84.17	813.92		15083.77

Table 6.24 HPLC VFAs peak identification data from the chromatographs of the Co-processed Feedstock aqueous phase. The units are mg/L.

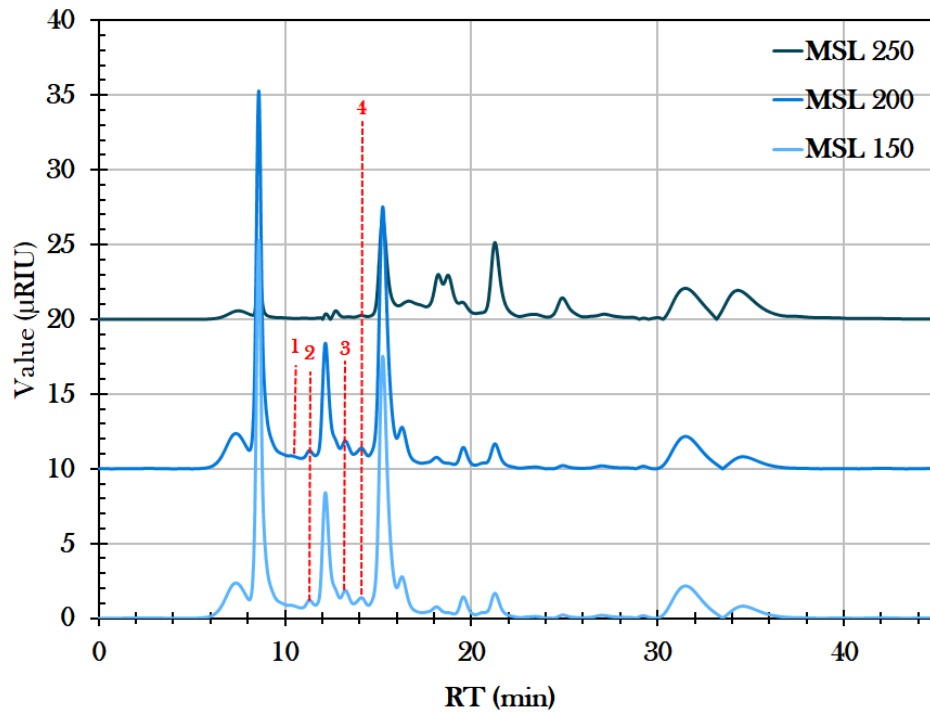
MSL = *Miscanthus:Saccharina Latissima*, MNA = *Miscanthus:Sodium Alginate*, MMan = *Miscanthus:Mannitol*.

Sample Name, HTC Temp (°C)	VFAs Present?							
	1	2	3	4	5	6	7	8
	Oxalic Acid	Maleic Acid	Citric Acid	Methyl-malonic Acid	Lactic Acid	Formic Acid	Acetic Acid	Levulinic Acid
MSL 150		Y	Y	Y		1.5074	1.8653	
MSL 200			Y	Y	Y	2.5302	4.2696	Y
MSL 250		Y	Y	Y	Y	0.6629	3.7023	Y
MNA 150		Y	Y	Y	Y	3.2679	3.6378	Y
MNA 200			Y	Y	Y	5.0324	7.1090	Y
MNA 250		Y	Y	Y	Y	2.2145	5.6396	Y
MMan 150		Y		Y		0.4445	1.1036	
MMan 200		Y	Y	Y	Y	1.6996	3.9128	
MMan 250		Y	Y	Y	Y	1.3832	5.5822	Y

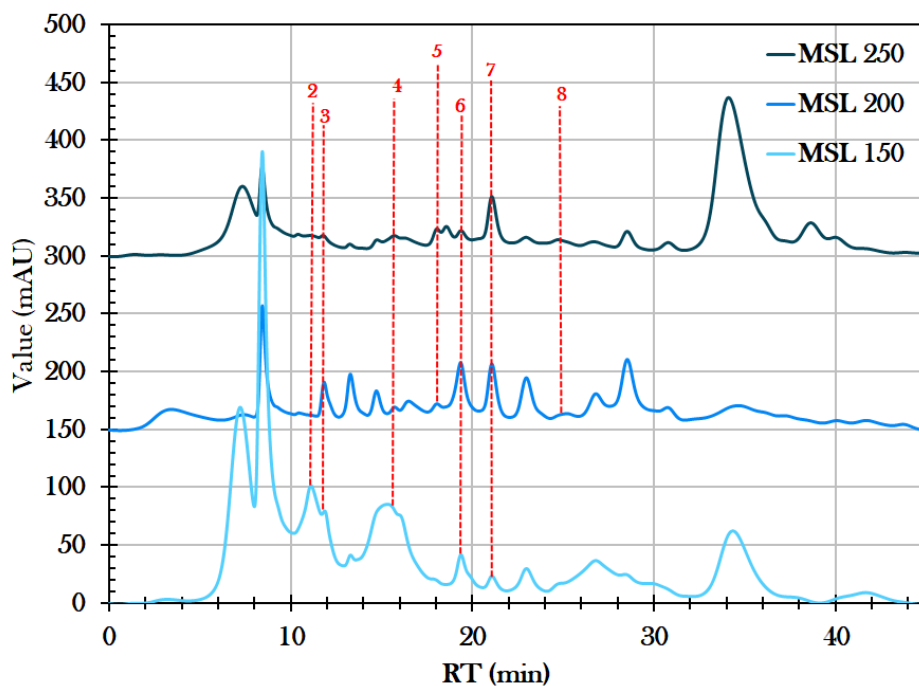
The general trend is that there are less sugar varieties identified at the highest HTC temperature - likely due to fully degrading into organic acids as environment becomes more superheated. Those varieties that are detected still in the 250°C samples are at a much lower concentration than the 200°C samples. For instance, the di-saccharide sugar sucrose appears in most of the feedstock aqueous phase samples in table 6.23, albeit a small peak as show in figure 6.26a, at the lower two HTC temperatures. As the HTC temperature breaches 200°C and is raised up to 250°C the environment inside the reactor is sufficient to fully breakdown and hydrolyse the sucrose molecule. From the pure biomass samples analysed in §6.4.4, the sucrose was only identified as present in the three *Miscanthus* HTC aqueous phase samples. Therefore is it thought that the addition of *Saccharina latissima* to the *Miscanthus* in this 80:20 feedstock mix promotes the degradation of this sugar molecule during HTC at 250°C. This is perhaps due to the presence of mannitol and sodium alginate in its chemical composition, as these Misc:NA and Misc:Man show the same trend.

This appears to be somewhat true for the glucose molecule as well, as glucose was identified in the 100% *Miscanthus* 250°C aqueous phase sample (see table 6.16), however is not detected in the 250°C aqueous phase samples of the MSL and the MNA co-processed samples. Glucose is present in MMan 250°C mix, suggesting that it is probably the presence of sodium alginate within the seaweed that promotes the degradation of the glucose molecule. Glucose doesn't appear in the two seaweed pure samples at 200°C even, and so appears to degrade at lower temperatures in the algal based HTC feedstocks, compared to the *Miscanthus*, which had much more glucose at 200°C than the other HTC temperatures. This explains the sharp rise in glucose concentration from the 150°C to the 200°C tem-

peratures, and then the lack of glucose at the highest temperature, due to full degradation.



(a) *Miscanthus:Saccharina latissima* Sugars. (1) - Sucrose, (2) - Lactose, (3) - Glucose, (4) - Galactose and Mannose



(b) *Miscanthus:Saccharina latissima* VFAs. (2) - Maleic Acid, (3) - Citric Acid, (4) - Methyl-malonic Acid, (5) - Lactic Acid, (6) - Formic Acid, (7), Acetic Acid, (8) - Levulinic Acid.

Fig. 6.26 Stacked HPLC Chromatographs of the *Miscanthus:Saccharina latissima* aqueous phase samples after HTC for (a) Sugars and (b) VFAs.

The only sugar to be detected within the aqueous phase samples which were hydrothermally carbonised at 250°C and not at the lower two temperatures was ribose, identified at over 15000 mg/l in the MMan aqueous phase sample. This does not appear in the 100% *Miscanthus* HPLC results but is present in large concentration for the 250°C mannitol aqueous phase sample, and therefore originates from the degradation of the mannitol molecule.

For the MNA aqueous phase sample at 250°C, no sugars within the range of the HPLC methodology were detected. Therefore it is assumed that this is caused by the full degradation of all the sugars into less complex chemical molecules (organic acids and gases, for example) due to the high temperatures and pressures in the HTC reactor.

The HPLC VFA data shown in table 6.24 shows this recurring trend of the organic acid concentrations in the aqueous phase samples peaking at 200°C, due to the increased likelihood of the sugars degrading under these conditions. Then the fall in abundance at the highest temperature is due to these short chain acids further reacting to form gases, and this trend is true for all three of the co-processed feedstocks. It appears that by adding the sugar kelp to the *Miscanthus*, there is a significant reduction in the acetic acid concentration of the aqueous phase at the higher two temperatures (4.3 and 3.7 down from 6.2 and 6.3 respectively) compared to the pure *Miscanthus* sample. This is perhaps due to further degradation and gaseous production, or inhibitory effects of the sugar degradation mechanisms, caused by the presence of the chemical compounds found within the seaweeds, such as mannitol which shows a reduction in acetic acid also, compared to 100% M. However, the scale of this difference is comparable to the fact that only 80% of the *Miscanthus* feedstock in the 100% *Miscanthus* sample is in these co-processed mixed samples, so any acids formed from the *Miscanthus* chemical components in these samples would theoretically be around 80% less abundant, if the degradation mechanisms were not adversely affected. Therefore this may play a large role in this acetic acid reduction as HTC temperature increases trend for the co-processed aqueous phase samples.

Quantities in this HPLC analysis are however only calculated for the formic and acetic acids here. Overall, seven out of eight of all the acids identified via this HPLC method are mostly present in the co-processed aqueous phase samples, in most of the various temperature samples. This is very similar to the pure biomass HPLC VFA analysis, with the notable lack of oxalic acid in the MSL, which was present in the 100% SL and FS samples. This general abundance of volatile fatty acids indicates a lot of different chemical compounds are broken down in a complex array of reactions inside the HTC reactor chamber, resulting in a mix of different short chain organic acids, liquid fragments

and gases to form, in agreement with the general accepted knowledge summarised in figure 2.11.

Several of these acids identified using HPLC here, along with other organic chemicals, are analysed more quantitatively in the GC-FID analysis of the HTC aqueous phase and are hence evaluated in greater detail in the following section 6.5.5.

6.5.5 Gas Chromatography FID

Table 6.25 GC-FID data for the co-processed feedstocks aqueous phase after undergoing HTC. Units are given in ng/ μ l.

NA = Sodium Alginate, Man = Mannitol.

Sample Name, HTC Temp (°C)	Propanone	Methanol	Ethanol	Ethanoic acid	Propanoic acid	2-Methyl propanoic acid	Butanoic acid	3-Methyl butanoic acid	Pentanoic acid	4-Methyl pentanoic acid	Hexanoic acid	Heptanoic acid
Misc/Sac Lat 150	9.29	23.75	0.00	155.30	8.30	4.55	0.00	1.74	0.00	18.50	4.50	4.36
Misc/Sac Lat 200	37.23	82.67	0.00	2149.47	31.18	26.53	5.08	1.58	2.01	1.58	6.91	2.29
Misc/Sac Lat 250	128.85	302.80	0.00	1746.17	52.81	15.41	6.14	3.54	1.25	0.92	3.06	3.18
Misc/NA 150	14.40	25.53	0.00	733.55	16.10	4.25	2.30	1.94	0.81	0.81	1.36	5.22
Misc/NA 200	39.95	247.52	0.00	1159.69	101.57	16.21	5.21	1.28	5.03	4.14	9.27	6.75
Misc/NA 250	73.53	361.20	0.00	2377.23	122.37	10.02	27.63	8.82	1.61	1.64	5.87	6.37
Misc/Man 150	6.62	0.00	27.55	637.23	21.73	1.70	11.83	13.47	1.01	1.65	6.42	1.86
Misc/Man 200	32.08	167.60	0.00	2359.99	17.70	11.81	7.10	1.63	1.90	1.54	1.38	4.22
Misc/Man 250	44.09	246.42	0.00	866.00	55.23	2.27	5.33	3.15	1.79	1.54	2.25	2.19

Once again it is observed that the ethanoic/acetic acid is the major component for the different co-processed feedstock, generally increasing in abundance with HTC temperature. The concentration of ethanoic acid decreases slightly from the MSL mix from 200°C to 250°C, possibly related to the same amount of increase in the methanol concentration at 250°C. On the other hand, the MNA sample increases in ethanoic acid concentration a similar amount for each temperature increment, with a rise in methanol production at each step as well. Although the methanol is still much less concentrated than the ethanoic acid. The MMan PW samples show a peak in ethanoic acid concentration at 200°C, with more methanol at the 200°C than at 150°C, and even more so at the 250°C temperature levels. In all three HTC feedstocks, the amount of propanone produced also increases as the HTC temperature increases. Propanoic acid also follows this pattern, apart from the MMan 200°C PW sample, which shows a dip in concentration from the 150°C sample (see table 6.25 for accurate values).

With all the GC-FID data from the different feedstock groups now shown, the cross-comparison between the different feedstocks and how the model compounds may affect production of certain acids during HTC of biomass types can be discussed more clearly. The discussion will now incorporate all of the GC-FID results from the four different subgroups of samples.

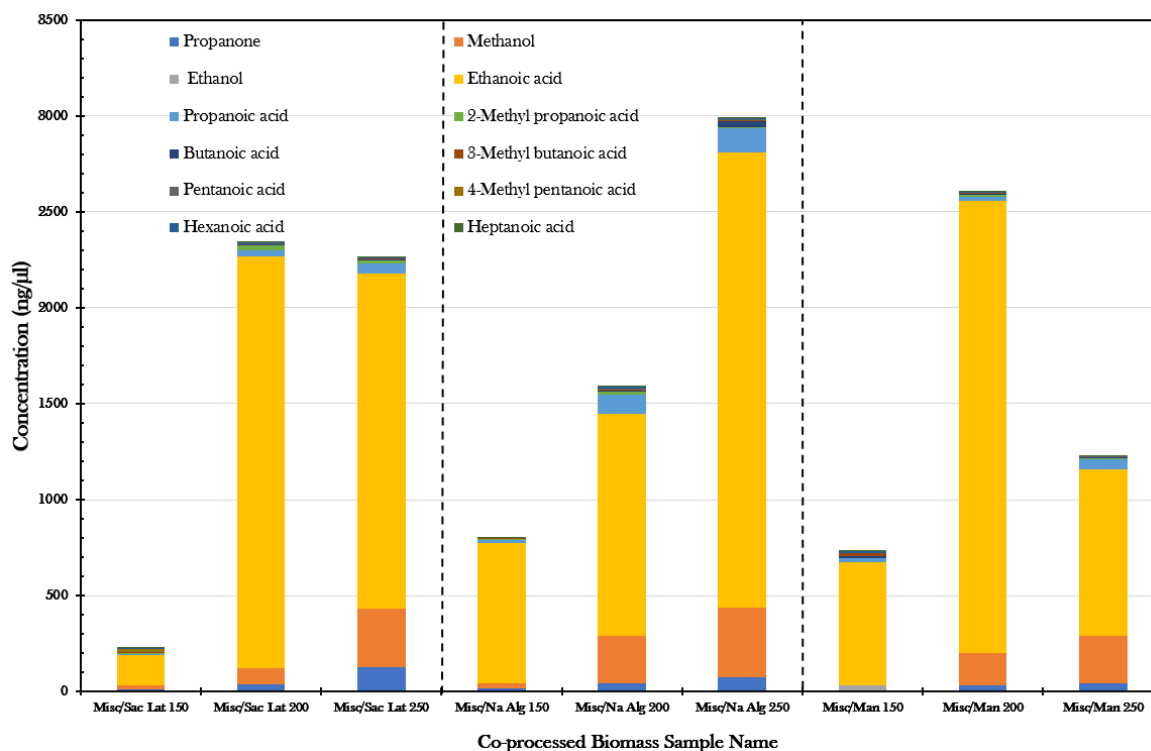


Fig. 6.27 Bar chart showing the results of the GC-FID analysis for the Co-processed biomass feedstocks aqueous phase samples after HTC.

GC-FID - Overall Discussion of Results

The different types of biomass feedstocks contain varied key components, such as the cellulose made up from monomers of glucose, the smaller mannitol monomer and the large, complex polysaccharides such as alginic acid in seaweeds. Different patterns in the eventual VFA mix in the aqueous phase after HTC are therefore indicative of the parent molecule from which they have originated. Different breakdown mechanisms within the hydrothermal reactor chamber, under high temperatures and pressures, cause degradation of these long chain compound into a complex mix of smaller, more reactive acids, alcohols and ketones. In order to ascertain the eventual suitability of the biomass feedstocks for hydrothermal carbonisation on a commercial scale, risks of the presence of certain acids in large quantities or concentrations in the downstream process waters must be assessed, along with any potential economic benefits of the production of certain desirable acids, to enhance the economic feasibilities of the process. Also, the potential for the aqueous phase to be anaerobically digested for biomethane production must be addressed; any acids or small organics that may hinder or help the anaerobic digestion

process may be identified using this analytical technique.

The production of these short chain fatty acids and small organics are generally known to be caused by the breakdown of larger structures down to the C1, C2 and C3 sized building blocks, dependant upon the exact chemical structure of the compounds. The GC-FID results for all the samples tested will be discussed within this section in ascending order of the number of carbons in the carbon chain, in groups of C1, C2, C3, C4 and C5+. Therefore the shorter acids will be discussed first, generally correlating to shorter retention times in the GC-FID results, i.e. from left to right of each of the GC-FID table column headings. The ketones and alcohols will also be discussed within their respective carbon length groupings with the acids.

C1 Organic Products

Large quantities of methanol were present in some of the samples; - between 25 and 350 ng μl^{-1} in feedstocks such as lignin 250°C and MNA 250°C. As the temperature increases, the concentration of methanol increases about fifteen times for the 250°C HTP samples. This, as a primary alcohol, is probably present due to the longer chain chemicals such as complex sugars and amino acids breaking down into the short alcohols under supercritical conditions. Feedstocks such as the *Miscanthus*, *Saccharina latissima*, lignin and cellulose have the highest concentrations; a few hundred methanol ng μl^{-1} , with higher concentrations as the HTP temperature increases. These feedstocks contain a large amount of sugar in their raw state, and hence the breakdown products of the sugars are far more concentrated in the HTP aqueous phase samples from these starting materials.

C2 Organic Products

Ethanol is only detected in a handful of samples. This is as expected as ethanol is unlikely to be present in the samples rather than it being converted into other chemicals during the HTC process. For some samples, not all ethanol was broken down (e.g. model compounds C 250°C, AA 250°C, NA 250°C, CA 250°C, and SL 250°C, FS 250°C), - perhaps due to a lack of other molecules present that are needed in the mechanism, or because much more ethanol was formed and therefore did not get the chance to fully break down. The production of acetic acid seems to start occurring at temperatures below

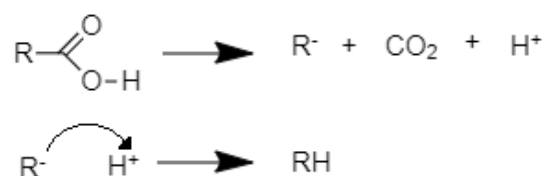
150°C, and is most probably produced from HMF, which is produced in turn from glucose.

Ethanoic acid, or acetic acid is the second most simple acid. It is worth noting here that methanoic acid, or formic acid, was not able to be detected with this GC-FID technique as the retention time would be too short to be detected using this methodology. The acetic acid was very highly concentrated in all the samples, reaching values of up to 6890 ng μl^{-1} for M 200°C. Therefore it is most important to properly evaluate the production of acetic acid via HTC processing.

Most of the aqueous phase samples had values in the 400 ng μl^{-1} region. MNA 250°C and MMan 200°C had the second and third highest concentrations of ethanoic acid, respectively, with a concentration of about a third that of Misc 200°C. It is possible then that the addition of NA and mannitol to the *Miscanthus* for the co-processing mixes has a slightly inhibitory effect on the breakdown mechanism responsible for ethanoic acid production, or favours a different mechanism which breaks down further, to methanoic acid for example. However, the large concentrations in all samples shows that whichever chemical pathways occur during hydrothermal treatment, a large amount of ethanoic acid is the main product of one of the main degradations, via HMF and glucose.

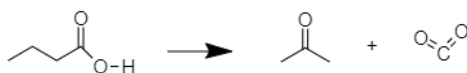
C3 Organic Products

Propanone, or acetone, appears the highest in SL 250°C, around six times the average amount, at 595 ng μl^{-1} . Only 30 and 10 ng μl^{-1} were detected in the SL 200°C and SL 150°C respectively. As a short (C3) chain ketone, this is likely caused by the further degradation of longer chain chemical compounds at temperatures between 200°C and 250°C, where the degradation mechanism takes greater effect. The reaction mechanism for most thermal decarboxylation reactions for carboxylic acids is given below [189].



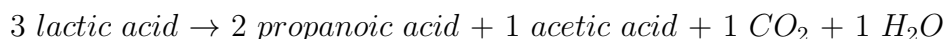
In this instance, as propanone represents R, butyric acid could be the responsible parent molecule for this reaction [189]. The production of carbon dioxide as a result of such reactions agrees with the observation of an increase in pressure at these temperatures during HTC. This reaction is shown for the propanone and butyric acid molecules

below [189].



Another example of high propanone content at the highest temperature sampled, is the cellulose, ACL and calcium alginate model compounds, and the MSL 250°C mix. This suggests that chemicals which, at 250°C > T > 200°C, break down to form propanone exist within the cellulose polymer, and the calcium alginate compound. These compounds are components of the *Saccharina latissima*, although also the cellulose is a large constituent of the *Miscanthus* feedstock. Therefore, it is suggested that components found within the seaweeds perhaps catalyse this breakdown. Perhaps this is a component within the calcium alginate compound, as propanone is produced at 200°C here.

Propanoic acid is a short chain acid, with three carbon atoms, and appears highest in concentration for the HTP seaweed feedstocks at 200°C, but for *Miscanthus* it peaks for the 250°C sample at 92.66 ng μl^{-1} . This follows the trend of the *Miscanthus* co-processing mixes, where the concentration of propanoic acid increases with HTP temperature, - rather dramatically for MNA 200°C and P 250°C. This follows that as temperature increases, formation of propanoic acid for the biomass feedstock increases, until it further breaks down into even shorter acid molecules for the third generation biomass feedstocks. Regarding the model compounds results for the propanoic acid concentrations, it can be deduced that its' presence is likely due to the presence of mannitol and sodium/calcium alginate, which are made up energy units, which degrade into sugars and then finally into propanoic acid, via the Fitz equation shown below, which yields over 50% propanoic acid [190].



Note that the lactic acid is a degradation product of glucose. This reaction also yields acetic acid, another common compound detected within the aqueous phase samples. [190] It is hence likely formed from the chemicals produced during HTP of the alginate compounds, and their subsequent degradation under supercritical water conditions.

The dip in concentration at 250°C for the calcium alginate model compounds HTP samples would maybe be due to the further breakdown into smaller chain acids. This

breakdown may be catalysed or favoured by the presence of some chemicals produced when calcium alginate is hydrothermally carbonised.

C4 Organic Products

2-Methyl propanoic acid, or isobutyric acid is highest in concentration for FS 200°C and M 250°C at values of 55 and 58 ng μl^{-1} respectively. Also notable is the 27 ng μl^{-1} for MSL 200°C and 18 ng μl^{-1} for ACL 250°C. This acid is not relatively highly concentrated for SL or MNA or MMan samples though. It appears that this acid is produced during the breakdown of protein molecules at $T > 150^\circ\text{C}$, from the reported increase in concentrations, with 0 ng μl^{-1} for P150°C. The protein in FS and Misc may therefore start to further breakdown at $T > 150^\circ\text{C}$ and begin producing isobutyric acid, although another chemical starting compound may also result in its' eventual formation, not just the protein. Due to its larger and fairly complex structure, it may breakdown into the smaller acids found at the smaller retention times, and hence its' concentration is relatively small compared to the more volatile fatty acids in the feedstocks. In fact, the only chemical with shorter retention times for the GC-FID analysis that was found to have a larger concentration was propanoic acid, for both the mannitol HTP samples.

ACL 250°C and MNA 250°C have the highest concentration of butanoic acid (or butyric acid), albeit still at very low concentrations. Therefore, this might be formed due to the breakdown of sodium alginate, in the presence of some other compounds, perhaps found in the *Miscanthus*, as the sodium alginate model compounds HTP samples only has concentrations of about a fifth of the aforementioned samples.

C5+ Organic Products

3-Methyl butanoic acid (isovaleric acid) is highest for P 150°C at 49 ng μl^{-1} , reducing for P 200°C and then again for P 250°C to 5.5 ng μl^{-1} . For C 150°C it has a concentration of 31 ng μl^{-1} , but 0 ng μl^{-1} for C 200°C and only 1.3 ng μl^{-1} for 250°C. For the SL HTP samples, it increases between $T=200^\circ\text{C}$ and $T=250^\circ\text{C}$. For the FS samples it peaks at 200°C. A general trend for the other samples is that it reduces in concentration from 150°C to 200°C, then increases at $T=250^\circ\text{C}$. It is likely that isovaleric acid is formed via degradation of the proteins found within the feedstock.

Pentanoic acid (valeric acid) in general has low concentrations for most of the samples. However, exceptions are the P 250°C (9.5 ng μl^{-1}), NA 200°C (19 ng μl^{-1}) and MNA

200°C (5 ng μl^{-1}). As Misc has around 2 ng μl^{-1} as a 100% feedstock, the 20ng μl^{-1} from the NA model compound to the 5 ng μl^{-1} for the co-processed MNA mix, must be due to the presence of sodium alginate, which is also directly relative to the 1:4 mix ratio of NA:Misc. Pentanoic acid appears to have formed in the protein samples, and forms most at 200°C for sodium alginate, but is further broken down in some chemical pathway it seems, at $T < 200^\circ\text{C}$ for sodium alginate.

Hexanoic acid (Caproic acid) is most concentrated at P 200°C (29 ng μl^{-1}) and CA 250°C (20ng μl^{-1}) and ranges from around 1 to 6 ng μl^{-1} for the other samples. This large acid would likely break down into the shorter chain acids, so its lack of presence and low concentrations relative to the shorted chain acids is to be expected after hydrothermal carbonisation.

Heptanoic acid is most highly concentrated for L 150°C, C 150°C, SL 200°C, NA 250°C and CA 250°C. It seems to break down into shorter chain acids at $T > 150^\circ\text{C}$ and not so much before this temperature has been reached, at least for pure lignin and cellulose feedstocks. It seems to form at 250°C for SL and the alginate samples, perhaps from the breakdown of even larger chemical structures that yield the long chain acid. At $T > 200^\circ\text{C}$, this acid may then further break down in the SL sample to shorter chain acids, such as the acetic acid, or formic acid (which is not measured in this analysis).

GC-FID Conclusions

It is apparent from the GC-FID results that there are very few aliphatic (non-aromatic) compounds, rather than the fatty acids described here. Other carboxylic acids are expected to also be present in the samples, namely: levulinic acid, succinic acid, glutaric acid and malonic acid. The HTC process is an oxidising environment, therefore the fatty acid chains detected in the GC-FID results would need to have previously existed within the HTC slurry. The products listed above are mostly oxidation and degradation products originating from the larger compounds within the feedstock, such as esters. For instance, trimethyl breaks up in supercritical water conditions (SCW) into fatty acid esters and triglycerides by effectively splitting in half. Therefore, the chain lengths of these shorter, daughter molecules and the respective locality of their functional group(s) depend on where along the chain the parent molecule has broken down. This in turn depends on various conditions such as the stability and structure of the compounds, temperature, pressure, pH and would vary depending on the presence of other, potentially more reactive or basic/acidic compounds within the HTC reactor.

Understanding the minute details of each reaction to occur within the HTC reactor

and the exact causes of each of the acids and sugars that reside in the aqueous phase is not the purpose of this evaluation due to it being beyond the scope of this work. The basic knowledge gained from these results is to understand whether the aqueous phase has the correct proponents in large enough quantities to enable further uses, and which uses might be the best fit, and which feedstock additives would improve the quality of the aqueous phase for the desired end use (objectives 4 and 6).

These GC-FID results allows for further understanding about the different type of acids formed within each sample and evaluate how certain trends may have come about. It seems that the most abundant acid formed (aside from potentially formic acid), is acetic acid. This is the shortest chain acid and so is the eventual daughter molecule of many varied breakdown pathways, hence expected. It is interesting just how much of this acid is produced with the M 200°C sample, compared to all of the other samples and acids, so perhaps this temperature most favours the eventual breakdown of the larger parent molecules, particularly those found within *Miscanthus* (cellulose, lignin, protein, carbohydrates).

With such a variety of acids produced, it may be an option to further profit from the aqueous phase by-product by selling the process water to chemical industries for extraction of commercially viable acids, however this would need to be of certain quantities to become a worthwhile enterprise. With the highest concentrations, only acetic acid would really be viable for this purpose, yet may not be as profitable as anaerobically digesting it to create biomethane to sell. Hence, due to the overall concept of the HTC reactor to enable renewable energy to be produced, the preferred option for further use of the aqueous phase is to anaerobically digest it, in order to create two streams of energy resources; hydrochar and biomethane. This would suit the idea of producing sustainable energy, which is the main aim that would be key to attracting investors and industry to the concept of creating a hydrothermal carbonisation reactor in the first place. The AD potential of the aqueous phase, both experimental and hypothetical, will be approached in §7.

The different metals found within the seaweed samples may affect certain degradation pathways via catalysis, as could the pH levels of the HTC contents. Therefore the comparison of these acids detected shall be cross compared with the different pH levels and trace metals content within the following subsection.

6.5.6 Fate of Inorganics: Liquid X-Ray Florescence & pH

The results for the pH of the Co-Processed Feedstock HTP aqueous phase are shown in table 6.26 and results from the Liquid XRF analysis are shown in table 6.27.

Table 6.26 The pH results at each different HTC Temperature of the Co-Processed Feedstock HTP aqueous phase samples.

Sample Name	pH Value		
	150°C	200°C	250°C
<i>Miscanthus:Saccharina latissima</i>	4.45	3.58	3.54
<i>Miscanthus:Sodium Alginate</i>	4.76	3.95	4.10
<i>Miscanthus:Mannitol</i>	4.27	3.24	2.95

Table 6.27 Liquid XRF Results from the Co-Processed Feedstock.

MSL = *Miscanthus:Saccharina Latissima*, MNA = *Miscanthus:Sodium Alginate*, MMan = *Miscanthus:Mannitol*.

Sample Name	Metals												
	Al	As	Br	Ca	Cl	Fe	K	Mg	Na	P	S	Si	Sr
MSL 150	0.0066		0.0018	0.0575	0.1996	0.0016	0.1877	0.0591		0.1558	0.0212	0.0140	
MSL 200				0.0499	0.1205		0.0964	0.0406		0.1484	0.0189	0.0475	0.0020
MSL 250	0.0111			0.0486	0.1070		0.0718	0.0891	1.2777	0.1481	0.0111	0.0488	0.0009
MNA 150			0.0015	0.0872	0.0198	0.0022	0.0176			0.1441	0.0115	0.0200	
MNA 200			0.0025	0.0460	0.0204	0.0018	0.0230	0.0473	0.8250	0.1457	0.0141	0.0557	
MNA 250	0.0103		0.0014	0.0416	0.0201	0.0013	0.0148	0.0997	2.1383	0.1504	0.0111	0.0401	
MMan 150	0.0102			0.0444	0.0276	0.0016	0.0269	0.0657	2.3534	0.1547	0.0106	0.0331	
MMan 200	0.0121			0.0508	0.0333	0.0014	0.0235	0.1240	3.7077	0.1536	0.0119	0.0643	
MMan 250	0.0071			0.0423			0.0150	0.0301		0.1442	0.0054	0.0364	

The MSL samples as shown in table 6.26 becomes less neutral as the HTC temperature increases, showing a similar trend as the 100% *Miscanthus* samples from table 6.19. The seaweed does not inflict a drastic enough effect on raising the pH, due to low seaweed to *Miscanthus* feedstock ratio. However it does increase the pH values for each HTC temperature compared to the 100% *Miscanthus* aqueous phase samples. This therefore does need to be taken into consideration when determining any potential end uses for the MSL aqueous phase within a biorefinery scenario.

Table 6.27 shows that the MSL samples have a significant increase in NA at the 250°C, which was probably kept within the solid hydrochar in the lower HTC temperatures. The Si and Mg levels increased, whereas the Cl, K, S and Ca all decreased in levels as the HTC temperature increased. For the MNA and MMan co-processed samples, the aqueous phase was found to contain more iron and sodium than the MSL samples, and similar levels of Ca, K, Mg, S, P and Si. Bromine was found to be present in all three MNA samples, yet was not detected in the MMan samples or two of the MSL

samples. The sodium was highest in the aqueous phase for the MMan 200°C. Perhaps the presence of different model compounds (sodium alginate or mannitol) co-processed with the *Miscanthus* has the effect of encouraging certain metallic elements to remain dissolved in the aqueous phase at certain HTC temperatures, which may further affect the pH levels.

The MSL is indeed less acidic than the pure *Miscanthus* biomass sample, increasing the pH from 3.01 to 3.54. The addition of the sugar kelp hence reduces the acidity and allows the aqueous phase to be less corrosive to pipeworks and after to handle and store, and increases slightly the variety of potential end uses for the aqueous phase. End uses are however still somewhat limited due to the acidic pH levels, and any reintroduction to the ecosystem of this aqueous phase on an industrial scale must require thorough dilution and potentially additives or alkali metals or buffers to reduce the acidity so as not to disrupt any aquatic life.

6.6 Conclusions

The overall findings from the analysis performed in this chapter results in a deeper understanding of how the different biochemical components break down under HTC conditions. The sugars, if present initially, in the form of cellulose for example, degrade first into more simpler monomers or disaccharides at the 150-200°C temperature range, and then further into organic acids and phenolic fragments at higher HTC temperatures. Depending on conditions, these acids can further react to form gases, resulting in a higher pressure at the higher temperatures and some organics lost to the gaseous phase. The HTC aqueous phase of the biomass based feedstock do indeed show some promise for further use as a substrate for anaerobic digestion, to produce biomethane. The CHNS, TOC and NMR results show a variety of sugars and organic carbon dissolved within the aqueous phase, which can be utilised fully via AD post-HTC. There were some phenolic and aromatic compounds found in some of the samples, and so this may account for low biodegradability from the BMP experimental results to follow.

The amount of VFAs found (via NMR, HPLC and GC-FID analysis), taking into account the underestimation of the CHNS and TGA results caused by loss of VFAs upon evaporation, and its increase in concentration as the HTC temperature increases, was a key trend identified. Smaller acids were more concentrated in general at the highest HTC temperature, with some losses to the gas phase for the shortest acids (acetic and

formic). This was expected due to the sub-critical water leading to numerous degradation reactions. The variety of acids (plus some others that likely are present yet not identified using the methodology here) from the biomass samples present an opportunity to produce commodity chemicals, in addition to the sugars in the process water, if this product stream were to be sold on to the food or pharmaceutical industry.

In addition, the different metals dissolved within the process water create possibilities that the aqueous phase may be used as a type of fertiliser. With a few potential possibilities of the end use of the chemically rich aqueous phase apparent, the potential to combine these uses with the AD of the aqueous phase (for example, extracting polyphenols before anaerobically digesting) could therefore be considered in further development of the biorefinery concept. The polyphenols therefore would be extracted and not inhibit the AD process, otherwise acclimatisation of the bacteria may be required, in this example. The extensive work performed in this chapter to highlight the different degradation mechanisms of the biochemical components and the effect of co-processing is of great use in the fast-developing HTC research area, and further work will no doubt be performed in future to increasingly identify key reactions happening within the HTC reactor chamber in different conditions. The thorough analysis on the aqueous phase samples in this chapter will be a helpful insight into how the different model compounds and feedstock mixes react under hydrothermal conditions, including detail on which sugars and acids are produced and degrade within the HTC over the three temperatures studied.

The novel use of the NMR peak areas to identify relative proportions of the VFAs, sugars and phenolic/aromatic compounds from HTC processing has proven to be a useful method and may be incorporated into future research techniques in this field. This chapter has thoroughly analysed the aqueous phase and from the results included here, BMP predictions can be made according to the chemical compositions of the aqueous phase, and quantitative BMP_{th} values for the relevant feedstocks can be determined, meeting objectives 4 and 5 of the PhD. Further analysis of the aqueous phase via its potential use as an AD feedstock post-HTC is addressed and evaluated in chapter 7.

Chapter 7

Potential Biochemical Methane Production from Macroalgae following HTC

7.1 Introduction

In order to make full use of the nutrients and chemical compounds left within the aqueous phase after hydrothermal carbonisation, anaerobic digestion is considered for post-treatment, to produce another product stream of renewable energy; biochemical methane (sometimes referred to as biomethane). In the HTC concept schematic, shown in figure 7.1, the anaerobic digestion stage follows on from the filtering of the HTC aqueous phase. The water may still be warm at this point, and any excess heat from the HTC reactor may be used to warm the digester to the required 37°C for AD to take place, via heat exchange pipes on a large scale facility to minimise costs.

Due to the high sugar content and other carbon rich compounds remaining within the HTC aqueous phase, coupled with the fact that the time-consuming initial hydrolysis step in figure 2.13 has already begun during HTC processing, it was expected that a sufficient amount of biomethane would be produced during anaerobic digestion of the aqueous phase from the two seaweed feedstocks. During HTC, it has been shown via NMR and GC-FID that the polysaccharides found in the seaweed feedstocks break down into disaccharides (lactose and sucrose) and simpler sugars such as glucose and mannose. The degradation products of the simpler monomeric sugar compounds residing in the organically rich aqueous phase should be an ideal source for the *inoculum* bacteria to

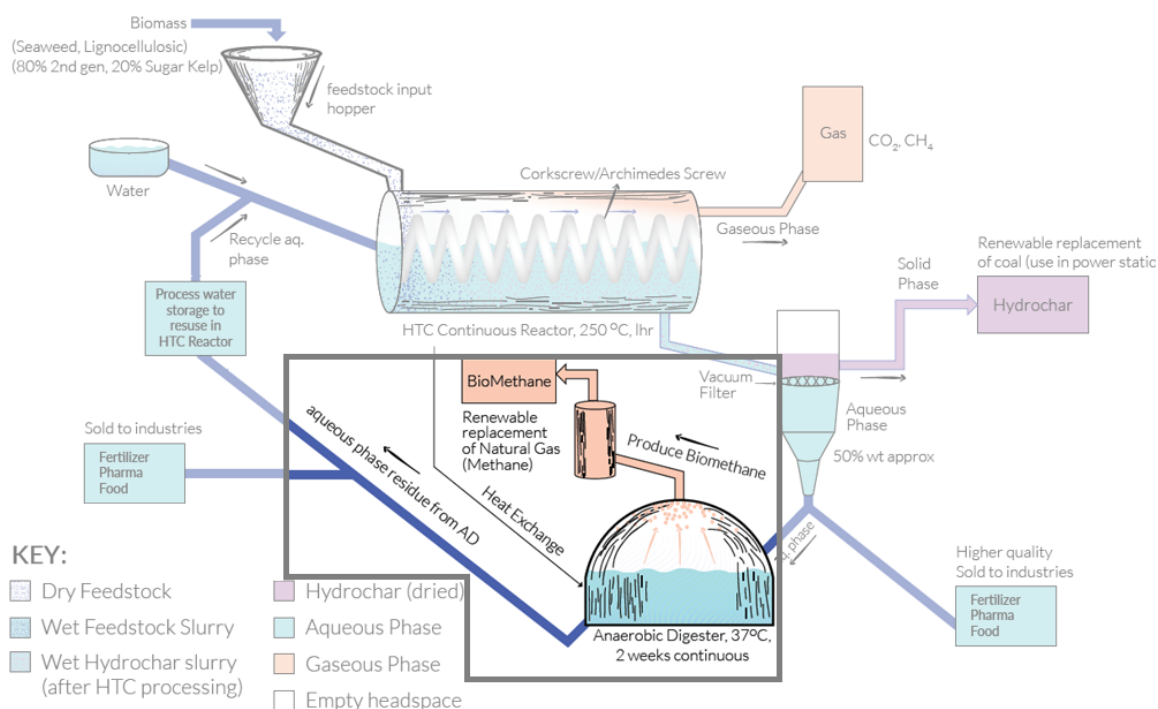


Fig. 7.1 A section of the biorefinery concept from figure 1.3, highlighted to demonstrate the aspect of the overall process focussed on in this chapter; the potential for Anaerobic Digestion of the aqueous phase to produce biomethane.

produce CH_4 from the anaerobic digestion process, via equation 7.1;



There may, however, be some barriers to the degradability of the aqueous phase samples, due to phenolic compounds dissolved in the aqueous phase which are known to be inhibitory to the AD process. These phenolics are found more in the *Fucus serratus* sample, with the NMR results in table 6.15 showing a relative proportion of nearly 5% for the FS 250°C sample, compared to 0% for the SL 200°C and SL 250°C samples. This is likely due to fucoids containing a higher polyphenol content [191]. This table also shows the *Saccharina latissima* also has a higher proportion of sugars in the aqueous phase for the 250°C sample, which would indicate a higher BMP yield in theory. Therefore, it is expected that the experimental biomethane yields for the *Fucus serratus* is lower than the amounts produced from the *Saccharina latissima*, due to a lower biodegradability index. It is also expected that the best performing sample would be the SL 250°C sample due to the high sugar content and the likelihood that these sugars are more thoroughly

broken down into monomeric sugars, which are simpler for the bacteria to digest.

However, the theoretical values of the biomethane production (BMP) may differ for these feedstocks due to their differing ultimate and proximate analysis results. Overall, it will be interesting to determine the more suitable seaweed sample to produce biomethane from both theoretically using the CHNS results, and comparing to the experimental findings after BMP tests, due to some key variations in the relative proportions of the phenolic and sugar contents.

As previously outlined, the bacteria used for this analysis was *inoculum* (from Esholt, UK), used at a 1:1 inoculum:feedstock ratio with the samples, in terms of their COD per gl^{-1} values. Different bacteria to feedstock ratios may produce more biomethane, or different types of bacteria used etc, due to higher bacterial activity for example. However, this research will look at the simplest ratio to reliably compare the different aqueous phase feedstocks and use the results as a proof of concept. Defining the ideal parameters for anaerobic digestion of a specific feedstock requires a lot of time-consuming AD experiments and is beyond the scope of this research, and this further research is currently being carried out by a research colleague. Unfortunately there was not enough aqueous phase of the MSL samples at this stage to enable BMP tests to be ran, but the overall effect of HTC temperature on the BMP yields can still be identified in terms of the seaweed proportion of the feedstock. The main focus of the PhD is the analysis of the hydrochar and the aqueous phase samples, and therefore these AD experiments are simply used as a tool for a proof of concept for use within the biorefinery concept. Further work may be performed to refine the AD methodology as required, and is ongoing within the research group. The SL and FS aqueous phase samples at the three different HTC temperatures were each run in duplicate, with a blank and a cellulose standard for comparison. The errors associated with the experimental BMP production were determined via standard deviation using the two duplicate experimental results, as per the methodology detailed in §3.6.10.

The *Fucus serratus* and *Saccharina latissima* aqueous phase feedstocks were ran in separate batches and were each ran for two weeks. The SL experiment ran for 15 days, and the FS for 17, due to the FS BMP experiment running over an extra weekend. The quicker the biomethane is produced, the more can be made in any given time-frame, hence the more profit can be made per month and less gas used from unsustainable sources as a result. Hence, if the feedstock were to produce most of the biomethane *after* the two week limit, this would not be especially useful in an economic and practical

sense, due to AD systems mostly being a continual process.

It is also noted that the quicker the final cumulative amount of biomethane is produced from the feedstocks after HTC processing, the more suitable the feedstock is for use within a large scale biorefinery. The hydrolysis step in the four-step AD process is generally the longest step, and so pre-treatment of these aqueous phase samples via HTC would reduce the time taken in this step, as most of the sugars within the samples would be hydrolysed within the HTC reactor. It is thus hoped and predicted that the rate of biomethane production would plateau within a shorter time-frame than if the same feedstocks were anaerobically digested without HTC pre-treatment. This would, if shown to be the case, be another advantage of using HTC within a biorefinery process involving further AD of the aqueous phase. The overall energy balance of the hydrochars and the corresponding BMP yields of the HTC aqueous phase samples will also be addressed and compared for each sample.

The theoretical biomethane production of the six macroalgae feedstocks are determined using the Buswell and Boyle equations, as explained in detail in §3.6.10. These results are calculated to predict performance on a bench scale reactor, and any that show a low BMP_{th} may not be further analysed via BMP_{ex} due to a low maximum theoretical value. However, it is likely that due to the pre-determined CHNS values of the *Saccharina latissima* and the *Fucus serratus*, it is expected that the calculated BMP_{th} yield should be sufficiently high. Due to the Boyle equation (equation 3.22) taking into account nitrogen, unlike the Buswell equation, it is expected that the calculations using this method would give a slightly more accurate total biomethane production value when compared to the BMP_{ex} , due to the presence of nitrogen (0.7-1.8%) in the aqueous phase samples, as determined via CHNS analysis (table 6.14). However the biodegradability of the different samples will play a bigger part in determining the total amount of biomethane produced than the slight differences between Boyle and Buswell equations, it is thought. Both equations are used for completeness, and subsequent BI are calculated for each BMP_{th} value from both equations also.

The biodegradability index plays a big part in the analysis here as well. For instance, if sample A were to have a much higher BMP_{th} value than sample B, but yet only 30% of the actual organics in sample A degraded into biomethane (BI= 30%), then sample B may have more actual biomethane produced via the experimental AD, if it has a significantly higher BI. Likewise, a higher BI value does not translate to a feedstock producing more biomethane, if the BMP_{th} values are small to begin with. Therefore, although the BMP_{th} values are important calculations to determine how suitable a feedstock may be for

anaerobically digesting, reliable conclusions can only be drawn upon after subsequent experimental BMP analysis due to biodegradability differences within the samples. A lower BI may be caused by inhibitory compounds in the aqueous phase, such as phenolics in the case of *Fucus serratus*.

To effectively evaluate the overall suitability of the six various seaweed samples, their BMP_{th} values must be evaluated alongside the BMP_{ex} values, and their subsequently calculated biodegradability index values. A high BMP_{th} value coupled with a high BI indicates a suitable feedstock for anaerobic digestion, with only limited undigested resources left in the aqueous phase after the chosen two week time-scale. In addition, the feedstock would be even more suitable for this HTC concept (figure 7.1) if the BMP production reached capacity within a few days, as opposed to a few weeks.

Initially, the BMP_{th} values calculated via Boyle's and Buswell's equations, and converted to grams of COD per l were analysed. Then the BMP_{ex} results for the *Saccharina latissima*, followed by the *Fucus serratus* aqueous phase samples were analysed following bench scale anaerobic digestion with *inoculum*. This leads onto a comparison between the SL and the FS BMP_{ex} values in §7.3.3, followed by a brief consideration of their respective biodegradability indices. Finally, there are some overall concluding remarks on the biomethane potential of the aqueous phase samples from these two different macroalgae species after prior HTC processing, including an evaluation of these preliminary AD results based on the context of an industrial scale HTC Biorefinery concept.

7.2 Theoretical BMP Analysis

Table 7.1 shows the resultant BMP values using the Boyle and Buswell equations, converted from VS gl^{-1} to units of COD gl^{-1} and corrected for any loss of volatiles on evaporation, using TOC loss results from the *Fucus serratus* samples at the three HTC temperatures. These were also used for the *Saccharina latissima* BMP_{th} calculations.

The *Fucus serratus* aqueous phase samples each have a higher potential BMP production for each HTC temperature than the corresponding *Saccharina latissima* samples in theory, as determined by the Boyle and Buswell equations. The corrected BMP_{th} difference between the two feedstocks, measured via the Boyle equation in units of ml CH_4 per g COD, is substantial; 178 for 150°C, 199 for 200°C and 109 for 250°C. With total BMP_{th} values between 350 and 400 ml $CH_4/gCOD$, this difference represents a large

Table 7.1 A table showing the values calculated for the determination of the BMP Theoretical values, using both Boyle's equation and Buswell's equation. The Correction factor (Corr.) was calculated from the TOC_{loss} upon drying the *fucus* aqueous phase samples, equations 3.19-3.20.

SL = *Saccharina latissima*, FS = *Fucus serratus*.

Sample Name, HTC (°C)	COD (g/l)	VS (g/l)	COD:VS	BMP (Boyle) (mL CH ₄ /g VS)	BMP (Boyle) (mL CH ₄ /g COD)	Corr. (Boyle)	BMP (Buswell) (mL CH ₄ /g VS)	BMP (Buswell) (mL CH ₄ /g COD)	Corr. (Buswell)
SL 150	47.18	68.96	0.68	199.75	136.67	177.20	207.31	141.84	183.91
SL 200	38.37	51.98	0.74	190.29	140.47	189.66	204.88	151.24	204.20
SL 250	47.25	53.20	0.89	237.99	211.38	242.45	250.37	222.37	255.06
FS 150	53.96	58.91	0.92	299.48	274.32	355.68	313.32	287.01	372.12
FS 200	41.75	42.91	0.97	296.07	288.09	388.98	317.56	309.00	417.22
FS 250	40.15	37.83	1.06	289.03	306.76	351.85	308.67	327.61	375.77

proportion of the BMP_{th} values. From this calculation, it is expected that the *Fucus serratus* samples would produce a higher amount of BMP during the experimental runs (BMP_{ex}), although the difference may not be as large between the *fucus* and *saccharina*, due to the phenolics present in the *Fucus serratus* samples.

As expected, the difference between the Boyle and Buswell equations are minimal; ranging from 28.2 ml CH₄/gCOD for the FS 200°C sample and 6.7 ml CH₄/gCOD for the SL 150°C sample. The difference between the two equations after correction is larger for each of the three *Fucus serratus* than for the three *Saccharina latissima* aqueous phase samples, possibly due to the higher N content for the FS samples. The Boyle equation is therefore regarded as more accurate due to its inclusion of nitrogen in the formula. In addition, this is of greater importance for the BMP_{th} predicted values of the *Fucus serratus* samples and hence would be the best equation to be used for future BMP_{th} calculations for feedstocks of similar chemical components to these species of macroalgae, regarding the nitrogen content in particular.

The proportion of these organics that theoretically could degrade to produce methane, if 100% degraded would be a very high figure compared to previous studies. However the actual amount that produces biomethane after anaerobic digestion will be less than this optimistic theoretical maximum figure. The experimental results for the BMP_{th} will therefore be a lower figure than the BMP_{ex} figures tabulated here, given the assumption that the correction from the TOC_{loss} from the *Fucus serratus* samples are reliable. The BMP_{ex} results are hence analysed in the next section, and the BI index determined using these BMP_{th} and the BMP_{ex} values. The effect of the inhibitory compounds within the samples will be evident in the forthcoming BMP_{ex} results, as there may be significantly less overall biomethane produced than the theoretical BMP_{th} values determined in table

7.1. The biomethane may also be produced after a longer period of time for the samples containing higher phenolic:sugar ratios.

7.3 Experimental BMP Analysis

The BioMethane Experimental study was performed in the AMPTS (II) bench scale reactor for both the SL samples and the FS samples, for all three temperatures, in duplicate. These results are discussed in terms of ml biomethane produced per gram of COD of feedstock. The *Saccharina latissima* results in terms of the cumulative total biomethane produced, and the rate of production will be analysed first, with the *Fucus serratus* results discussed after. This is then followed by a comparison between the two macroalgal species' cumulative BMP results.

7.3.1 *Saccharina latissima* BMP_{ex}

The anaerobic digestion of the *Saccharina latissima* was performed using a 1:1 *Saccharina latissima:inoculum* ratio. These results are shown cumulatively in figure 7.2. The samples' respective flow rates of BMP production per day are shown in figure 7.3. The cellulose sample that was ran alongside the samples, which helped to verify that the experiment was working as it should be, is also included in this figure as the dashed line for comparison.

The SL 150°C and the SL 200°C samples initially performed the best, with a higher flow rate of over 75 ml CH₄/gCOD for the lower temperature HTC sample. However these flow rates peaked early, shown in figure 7.3 at just one day (two days for SL 200°C). Ultimately, the SL 250°C sample outperformed the two lower temperature SL samples in terms of total accumulated BMP, from the third day of the experiment onwards.

The SL 200°C sample interestingly began increasing at 11 days until 15 days, despite plateauing at day two. The SL 150°C and SL 200°C have a similar cumulative total amount of biomethane production, after just two days, indicating a similar total amount of sugars were present after being hydrolysed from the complex organic structures during HTC. Increased HTC temperatures would improve the rate of hydrolysis of the feedstock, therefore freeing up the simpler, smaller sugars and acids for further digestion from the fermentative bacteria. This is expected to cause a higher BMP_{ex} results for the SL 250°C sample.

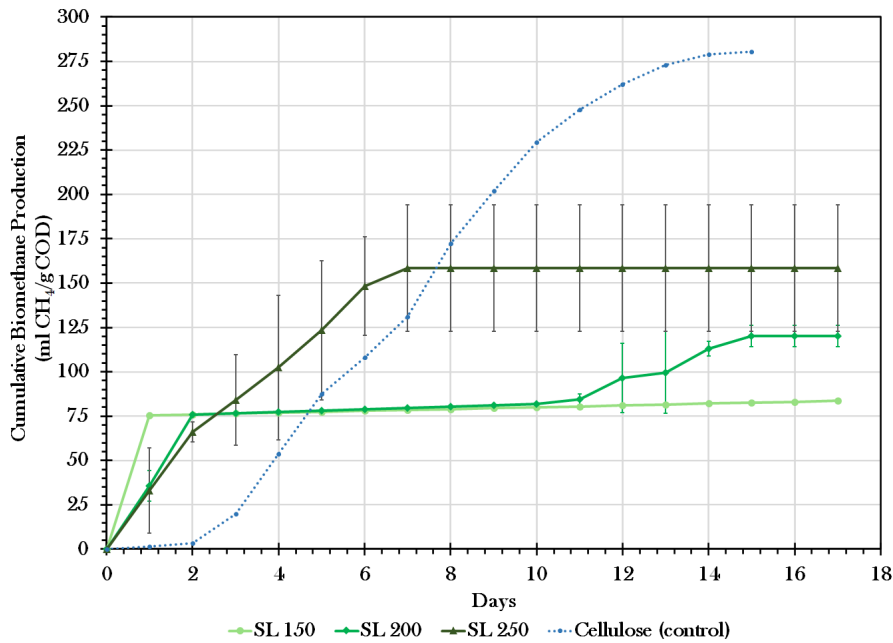


Fig. 7.2 *Saccharina latissima* Cumulative BioMethane Production, with the cellulose control added for comparison.

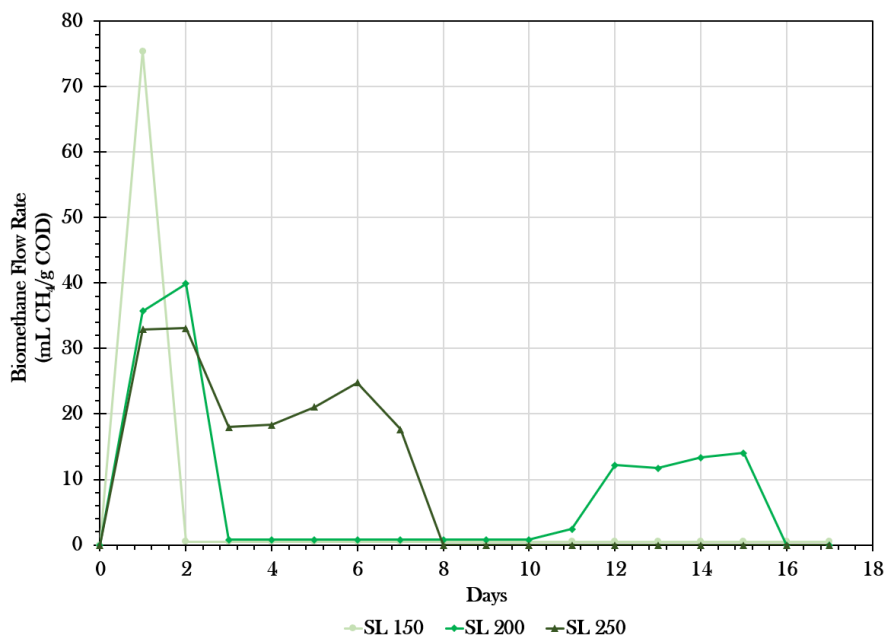


Fig. 7.3 *Saccharina latissima* BMP Experimental flow rate of BMP production.

The total biomethane production for the higher HTC temperature SL sample increased at an almost linear rate, until it plateaus starting from seven days into the experiment. The total accumulated biomethane production from this SL 250°C sample

was 158.5 ml CH₄/gCOD, albeit with a rather large error margin due to difference in the duplicate samples. However, even at the lower end of the error margin, the total BMP is higher than the other two samples. The experiment was concluded after 15 days, at which point the rate of BMP production of the 150°C and 250°C samples had already dropped to a rate of 0 ml CH₄/gCOD per day. These samples had been at (or very close to) this rate of BMP production since day two and eight respectively.

Initial HTC processing has the effect of reducing the need for the first, time-consuming, step of AD; hydrolysis (see figure 2.13). Therefore, with the water being even more super-heated and closer to its' critical point for the SL 250°C sample, hydrolysis will be more likely to occur and more quickly. Thus, the already exposed simple sugars available for further digestion are more numerous within the 250°C aqueous phase. This agrees with the experimental results shown in figure 7.2 of the increased cumulative methane production for the SL 250°C sample compared to the lower temperatures SL samples.

These samples produced most of the biomethane in the first two days, but ultimately produced just over 80 ml CH₄/gCOD for the SL 150°C and 120 ml CH₄/gCOD for SL 200°C. The bacteria seemed to have had no inhibitory issues to digest the sugars and produce the biomethane. The bacteria digested these organic compounds that were readily available to digest within a matter of days. However, for the SL 250°C sample, the bacteria started digesting the sugars from day one, although at a slower initial rate. This continued until an apparent lack of food for the bacteria after seven days, although there was almost twice as much activity from the *inoculum* for the SL 250°C sample.

In terms of improving the BMP yield, there is scope to improve the biomethane amount produced by altering the BMP conditions such as changing the inoculum:substrate ratio. Brown et al 2020 [192] found that *Saccharina latissima* and *Fucus serratus* had an improved BMP yield with a 2:1 feedstock:substrate ratio compared to the results here, with an otherwise identical BMP set up and feedstocks. They found that actually the trend differed, with the lowest HTC temperature aqueous phase samples (150°C producing the most biomethane; 214 ml CH₄/g COD. With further BMP tests there is therefore potential to improve upon these biomethane yields, and find a reliable preferred HTC temperature for the aqueous phase sample to produce the most BMP. Note that with the 150°C HTC temperature producing the most BMP as in the case for Brown et al 2020[192], this would further increase the overall energy balance of this temperature compared to the values calculated from these results.

7.3.2 *Fucus serratus* BMP_{ex}

The anaerobic digestion of the *Fucus serratus* was likewise performed using a 1:1 *Fucus serratus:inoculum* ratio. These results are shown cumulatively in figure 7.4. The samples' respective flow rates of BMP production per day are shown in figure 7.5.

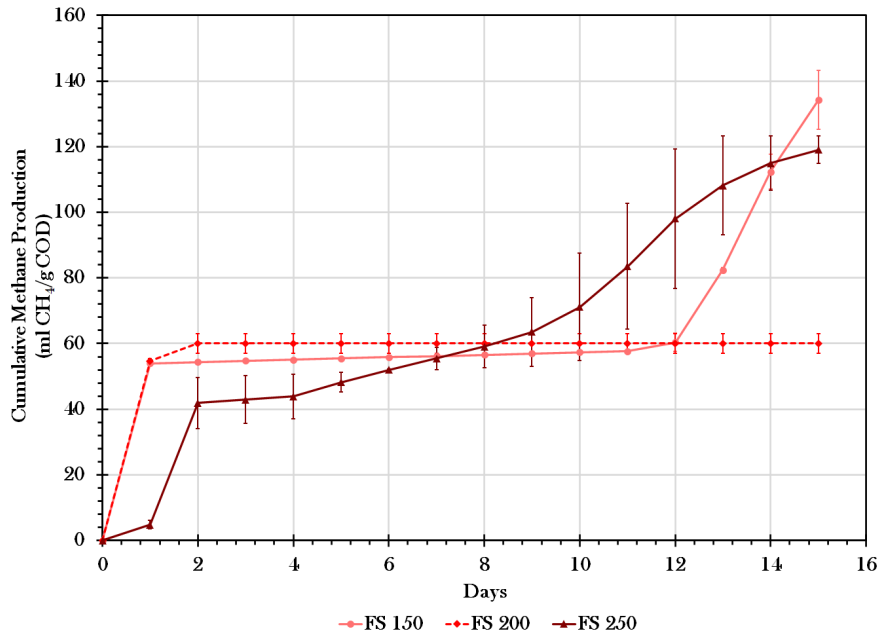


Fig. 7.4 *Fucus serratus* Cumulative BioMethane Production.

Broadly speaking, the three *Fucus serratus* samples averaged the same cumulative BMP production, within a 20 ml CH₄/gCOD between days two and eight. Figure 7.4 shows that after only two days, the FS 200°C sample had ceased methane production, at a level of 60 ml CH₄/gCOD. Similarly, the FS 150°C sample after only the first day plateaus at around 55 ml CH₄/gCOD, slightly increasing over time to 60 ml CH₄/gCOD until day 11 when the biomethane production rate increases, peaking at a rate of 30 ml CH₄/gCOD produced per day on the two week mark (see figure 7.5). This results in a cumulative BMP_{ex} total of 134.2 ml CH₄/gCOD on the last day of the experiment, overtaking the FS 250°C total BMP production.

The FS 250°C sample initially started out producing biomethane at a lower rate, producing a total of just over 40 ml CH₄/gCOD. This then increases due to a fairly linear increase in BMP production at a rate of approximately 4 ml CH₄/gCOD per day. Therefore by day eight, the FS 250°C sample leads the other two HTC temperature samples in total

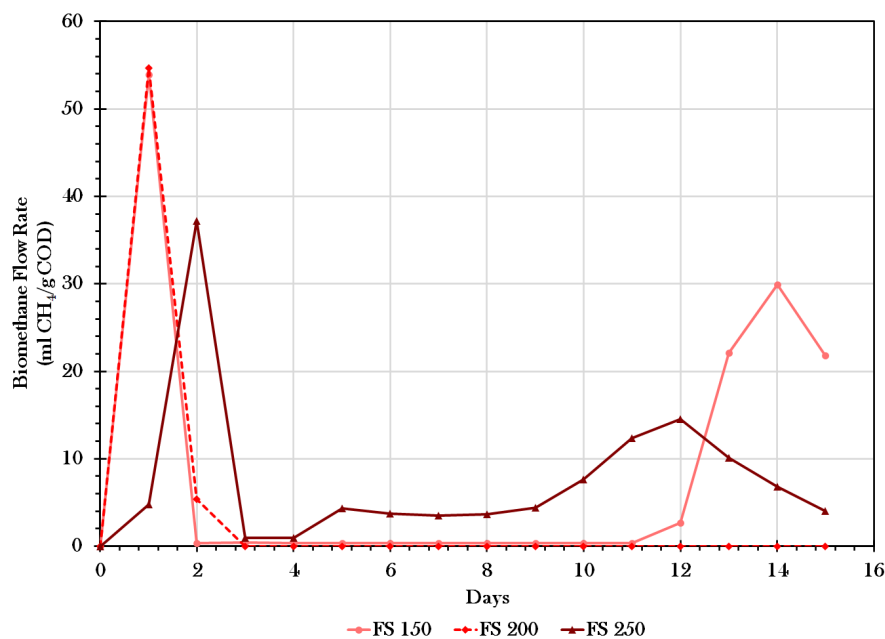


Fig. 7.5 *Fucus serratus* BMP Experimental flow rate of BMP production.

cumulative BMP production. By the end of the 15 days, the total BMP_{ex} produced by the FS 250°C was 119 ml $CH_4/gCOD$, due to a late increase in BMP flow rate, reaching a rate of 14.6 ml $CH_4/gCOD$ per day at day 12, shown in figure 7.5.

The FS 200°C samples therefore remains as the lowest producer of biomethane via anaerobic digestion of the HTC aqueous phase. This may be due to the 1.65% relative proportion of phenolic compounds to sugars and VFA compounds in the sample, as found via NMR analysis. The FS 250°C and 150°C samples had 2.17% and 4.83% relative phenolics respectively, so it was expected that the phenolics would inhibit the FS 150°C and the FS 250°C even more so than the FS 200°C sample. Perhaps the sugars are also less degraded at the 200°C temperature, and there is less simple sugars for the bacteria to digest, in comparison to the FS 250°C sample, where the biomethane production rate picks up again. It is hence concluded that the inhibition of the bacteria to digest the sugars due to the presence of the phenolics is a key factor in total BMP production. Comparing these results to the BMP_{th} results, it can be deduced that the biodegradability index for *Fucus serratus* is poor. These BI values will be quantified in §7.4.

Overall, the FS 250°C is the best sample to use if the AD time-frame is between nine and eleven days. Any timescale over this range, the FS 150°C would produce the most CH_4 . It is also concluded that the *Fucus serratus* HTC aqueous phase samples do not lend themselves to anaerobic digestion on a large scale continuous biorefinery scenario,

due to the length of time (eight days plus) it takes to produce a significant amount of biomethane. This is likely caused by the phenolics in the samples. These *Fucus serratus* samples will be compared to the *Saccharina latissima* samples in terms of the total BMP produced after 15 days in the following section.

7.3.3 Comparison of Seaweed BMP_{ex} Results

Figure 7.6 shows how the total accumulated biomethane production varies for each seaweed sample as a function of HTC temperature.

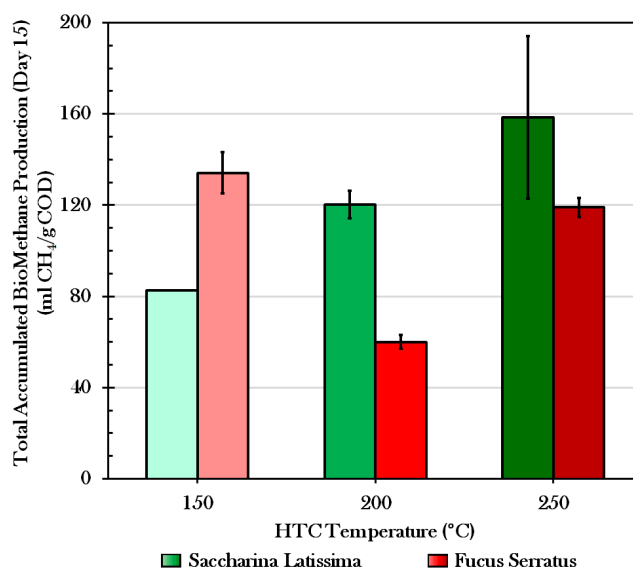


Fig. 7.6 A bar chart showing the total BMP_{ex} results after 15 days for both the *Saccharina latissima* samples and the *Fucus serratus* samples, for each of the three HTC temperatures.

Comparing the different total BMP values after 15 days for the two seaweed samples, it is clear that overall the highest biomethane producer is the SL 250°C sample. The trend for the SL samples show a linear increase in total biomethane production after the 15 day timescale as the HTC temperature increases. This demonstrates the lack of inhibitory compounds appearing at certain HTC temperatures, as it is caused by the increased amount and availability of simple sugars for the bacteria to digest, as the water becomes more superheated with HTC temperature.

The amount of biomethane that would be produced via anaerobic digestion, using a 1:1 *inoculum:Saccharina latissima* ratio, after 15 days can therefore be predicted reliably if the chosen HTC reaction temperature is known. However, the same cannot be said for

the *fucus* HTC aqueous phase samples, as these AD feedstocks had a distinctly non-linear relationship of biomethane production as a function of HTC temperature. This may not be representative of the *fucus* feedstock as a whole, but certainly for the research conducted here this has been the case.

The *Fucus serratus* samples, as previously discussed, show a dip in biomethane productivity for the FS 200°C sample, possibly due to the presence of phenolics. Therefore, as compared to the *saccharina* sample, the amount biomethane produced using *fucus* HTC aqueous phase as a feedstock is more complicated, and varies due to other indirect factors, rather than just a linear relationship with the HTC temperature. The *Saccharina latissima* samples outperform the *Fucus serratus* samples for total BMP_{ex} produced, despite the initial BMP_{th} calculations showing a much higher biomethane theoretical amount for the *fucus*. This effect is evaluated in the following section, comparing the biodegradability indices for the six samples.

Based on these results, the time-frame was compared for each of the samples to reach their maximum biomethane yield. The *Saccharina latissima* samples were the best seaweed for a large scale continuous HTC concept, due to their greater efficiency of biomethane production. This feedstock would therefore be a better choice for both practical and economic reasons. For context, if figure 7.6 were based on results after just a week, the BMP_{ex} range from the *fucus* samples would be 56.2 to 57.7 ml CH₄/gCOD, but is 78.5 to 158.5 ml CH₄/gCOD for the *Saccharina latissima* BMP_{ex} results. Even when considering the larger errors for the SL 250°C sample, it still produces more biomethane than the FS. After surpassing the two day mark, the *saccharina* samples produce more biomethane than the *Fucus serratus*.

Overall, it is hence the case that the *Saccharina latissima* HTC aqueous phase samples provide more access to the simple sugars within, to enable increasing biomethane production levels with HTC temperature during anaerobic digestion than the *fucus*. Also, the sugar kelp samples are more predictable in BMP production and are faster producers of biomethane, despite the lower theoretical BMP values. To produce more biomethane, other inoculum to substrate ratios could be explored, but this is a proof of concept and a comparison of the two seaweed feedstocks, so the total biomethane produced could still be improved upon with tweaking the AD parameters.

7.4 Biodegradability Index

The Biodegradability Index (BI) of the *Saccharina latissima* and *Fucus serratus* samples were determined by comparing the BMP_{th} to the BMP_{ex} values using equation 3.17. The results are shown in table 7.2. The higher the BI value, the higher the total theoretical proportion of the sample has degraded via anaerobic digestion during the experimental runs, with a maximum of 100%.

Table 7.2 A table showing the calculated Biodegradability Indices of *Saccharina latissima* and *Fucus serratus* using both Boyle's equation and Buswell's equation, after correction for losses.

SL = *Saccharina latissima*, FS = *Fucus serratus*.

Sample Name, HTC (°C)	BMP _{ex} (ml CH ₄ /g COD)	Biodegradability Index (BI) (%)	
		Boyle	Buswell
SL 150	83.60	47.18	45.46
SL 200	120.20	63.38	58.86
SL 250	158.50	63.31	62.14
FS 150	134.18	37.72	36.06
FS 200	60.00	15.42	14.38
FS 250	119.03	33.83	31.68

The BI results demonstrate numerically that the effect of the phenolics in the *Fucus serratus* samples are considerable. The difference between the BMP_{th} and the actual BMP_{ex} of the *fucus* samples demonstrates the need to do bench scale AD tests to ensure the feedstocks that are theoretically high biomethane producers are actually able to match up to expectations. Due to prior NMR analysis, it was expected that the *fucus*, due to the small amount of phenolics present, would produce less biomethane than the theoretical BMP values show. However it was not known to what extent the phenolics would have an effect. Both a high enough BMP_{th} and a high BI is essential for a suitable total biomethane production for certain feedstocks to be effective in future biorefineries, such as the one proposed.

It appears to be the case that, in order for the biorefinery concept shown in figure 7.1 to be feasible using an anaerobic digester to process wastewater streams, feedstocks showing a low amount of phenolics would need to be thoroughly tested via small scale AD before incorporating the species as a HTC feedstock, and that sugar kelps and seaweeds lower in phenolics after hydrothermal processing would be preferred. Total phenolic tests may be performed on potential HTC feedstocks (after testing via HTC) for a large scale

biorefinery in order to determine suitability for AD, in addition to using Boyle's equation for BMP_{th} determination.

7.5 Energy Balance Analysis

The different energy outputs (EO_{char} , EO_{BMP}) of the two product streams from HTC processing of the 100% *Saccharina latissima* and the 100% *Fucus serratus* feedstocks are tabulated alongside the corresponding energy input required (EI) to heat the reactor and their calculated overall net energy balance for each feedstock (EB). For more detail on these calculations please see §3.7.

Table 7.3 Energy Balance table including the energy input of heating the HTC reactor, and the two different energy outputs, calculated for 1kg dried biomass with a 10% solid loading ratio. All energetic values are given in units of MJ kg⁻¹.

Sample Name, HTC T (°C)	EO_{char}	EO_{BMP}	EO_{tot}	EI	EB
<i>Saccharina latissima</i> 150	7.32	1.58	8.90	5.44	+3.46
<i>Saccharina latissima</i> 200	5.25	1.89	7.14	7.61	-0.47
<i>Saccharina latissima</i> 250	4.58	3.06	7.64	9.79	-2.15
<i>Fucus serratus</i> 150	7.13	2.74	9.87	5.44	+4.43
<i>Fucus serratus</i> 200	5.62	1.03	6.65	7.61	-0.96
<i>Fucus serratus</i> 250	4.82	1.97	6.79	9.79	-2.99

As shown in table 7.3, the overall energy balance is negative for the two higher HTC temperatures, and positive only for the 150°C HTC runs. This is due to increased energy input from heating the reactor, using the 10% biomass to water loading ratio. This can be reduced by using an insulated continuous reactor so that the energy required to heat the reactor up in the first place is only required at the start, and therefore over time the energy input per hour is greatly reduced. Also the use of any residual heat to warm the anaerobic digester will further reduce the energy input required for this part of the process, although the energy input for the AD was not taken into account for these calculations. Therefore there is potential to improve upon these values with better process efficiencies in place, but the trend would remain similar regardless; lower HTC temperatures produce the highest overall net energy output. This is caused by the higher hydrochar yield, and is despite the higher HHV of the hydrochar and the higher BMP values at the higher HTC temperatures.

The 10% solid loading ratios (SLR) may also affect the EB. As it requires less energy to heat up 1kg of biomass than it does for 1 L of water (specific heat capacities of 1.5 MJ/kg/K instead of 4.2 MJ/kg/K), the energy input can be significantly reduced just by

changing the SLR to 20%. This would result in lower energy input values of 2.81, 3.93 and 5.06 MJ/kg for the 150, 200 and 250°C HTC temperatures respectively, resulting in a positive energy balance for all three temperatures for each seaweed feedstock, assuming that the EO_{tot} is not significantly reduced. The energy outputs may be further improved by further BMP tests using different inoculum to substrate ratios, which have been found to improve the BMP of SL HTC process waters, particularly for the 150celsius HTC temperature compared to the results from the 150°C SL sample used in this study.

7.6 Conclusions

The overall finding from the BMP experimental and theoretical results is that SL performed better than FS, due to lower biodegradability of the FS, despite its initial higher BMP theoretical predictions, highlighting the importance of analysing the process waters for any inhibitory compounds present. The higher HTC temperatures performed better in terms of total biomethane production, although this was not sufficiently higher than the lower temperature samples to overcome the larger energy input and lower hydrochar yield of the 250°C HTC sample, resulting in a net overall negative energy balance.

It is recommended that the phenolics in HTC aqueous phase samples are quantified in future when performed AD on such samples in the future in order to reliably predict BMP suitability, as the presence of phenolics in the FS samples reduced the total biomethane produced, as phenolics are a known inhibitory compounds in AD. In addition, in future studies in which HTC is proposed in conjunction with biomethane production of the feedstocks, seaweed species to be used as HTC feedstock should be carefully selected so as to reduce the phenolic content such that the aqueous phase remains suitable for anaerobic digestion.

The overall energy balance is calculated here to be only positive for the lower HTC temperature. It follows that the most suitable HTC parameter for further development within a HTC biorefinery concept is the 150°C temperature. This is combined with a view to slightly increase the solid loading ratio, and further refine the AD parameters and seaweed:*Miscanthus* feedstock mixing ratio to result in better performing hydrochar for inorganic analysis, reducing slugging and fouling propensity, and potentially different AD SLRs for improved yields of biomethane.

Chapter 8

Conclusions

This study has looked at different HTC product streams and utilisation of the aqueous phase to produce a secondary renewable energy source in addition to the use of hydrochar as a biofuel. An overall continuous HTC biorefinery concept was proposed and the seaweed model compounds were analysed as well as co-processing seaweed and *Miscanthus*, a novel experiment. Analytical methods were used to characterise the products and further understand the complex chemical reaction pathways that take place inside the reactor, with particular attention paid to the effects of adding the seaweed to the *Miscanthus* feedstock.

The mass balance analysis of the HTC product streams samples are as expected, with higher solubility of the organic compounds found within the aqueous phase of the seaweed samples. This leads to an increased solubility of the MSL process waters compared to the 100% *Miscanthus* aqueous phase samples. This added seaweed acted to promote the yield of aqueous phase and inhibit hydrochar production, as 4.9% less hydrochar and 4.4% more aqueous phase respectively were found compared to a simple summation of the 80:20 100% M:100% SL results at the 250°C HTC temperature. As expected, the hydrochar yield generally reduced as the HTC temperature increased, which has a significant effect on the eventual energy balance. This is due to the higher chance of reactivity of the organic compounds, which are in a more superheated environment. At these extreme temperatures and pressures, degradation via hydrolysis of cellulose and other relatively stable sugars is more likely to occur. The fate of the organic material from the biomass feedstock is more likely to be within the aqueous phase, resulting in increased potential for further uses within the food, cosmetic and chemical industry, and this study considers further utilisation of this organically rich aqueous phase via

anaerobic digestion to produce a secondary renewable energy product: biomethane.

The characterisation of the hydrochar analysed in chapter 5 has shown that at higher HTC temperatures, the HHV of the biomass feedstocks increase, as expected. A higher heating value of 24.2 MJ kg^{-1} was achieved for the hydrochar from the MSL co-processed mix, a slight reduction compared to the 100% *Miscanthus*, but overall a large improvements compared to the corresponding raw feedstocks (which range from 13.9 to 17.5 MJ kg^{-1}) and the 100% SL hydrochar. However, due to the lower yields of hydrochar from the higher temperature HTC runs, the overall total energy output from the hydrochar reduces as the HTC temperature increases.

The reduction in percentage proportion of seaweed from 100% to 20% in the MSL mix had the advantage of significantly reducing the overall ash content from 12-17% for 100% SL to 6-7% for MSL. The lower inorganic content also caused more of the slagging and fouling indices to be met for the MSL hydrochar than the 100% SL hydrochar. This was verified as a potential problem that may delay and inhibit the utilisation of seaweed as a biomass, so co-processing was shown to be a suitable solution to this. HTC temperatures of 150°C was also determined to be the preferred temperature to improve the chances of the hydrochar meeting the slagging and fouling limits.

Characterisation of the aqueous phase was also performed, using a variety of analytical techniques. NMR was utilised to determine the relative proportions of sugars, phenolics/aromatics and VFAs in the process waters, to then indicate best methodologies for further analysis via HPLC methods and GC-FID. It was found that at the lower HTC temperatures, the large organics within the biomass feedstocks such as polysaccharides and cellulose begin to degrade into simpler sugars, including some di-saccharides (such as sucrose and lactose). At HTC temperatures reaching 200°C these sugars further react to produce a mix of short chain volatile fatty acids. The concentration of the simplest two, formic and acetic acid were quantified and the trend was a peak in production at 200°C followed by a drop in concentration. This was due to further degradation of the organic compounds as the water inside the HTC reactor reaches super-critical levels, resulting in the VFAs degrading to produce gaseous products such as methane, carbon dioxide, hydrogen and carbon monoxide via known mechanisms.

In addition, the more acidic *Miscanthus*-based process waters at the higher HTC temperatures also may cause extra health and safety issues in a large scale facility and cause corrosion to the pipework. The addition of seaweed in the feedstock mix reduces the acidity of the higher temperature process waters, and the aqueous phase from the

seaweed samples have increased alkalinity at higher temperatures, conversely to the *Miscanthus* trend.

It is hence suggested that although the solubility of the aqueous phase increases with HTC temperature, in order to avoid much of the organic content being lost to the gaseous products and being retained instead within the aqueous phase, 150°C or 200°C HTC temperatures should be considered for large scale implementation, dependent upon performance of biomethane production. Biomethane production requires sufficient sugars contained within the aqueous phase for suitable quantities of methane to be produced by the bacteria. Therefore it follows that the aqueous phase samples with the most sugars dissolved within it would produce more biomethane, although inhibitory compounds may reduce the overall biomethane produced.

There was a greater amount of total biomethane produced using the SL HTC aqueous phase feedstock compared to the FS, due to its higher biodegradability. SL was found to produce more biomethane as the HTC temperature increased. As these BMP experiments are an initial experiment and not extensive in its evaluation of the most suitable AD parameters, changes in inoculum:substrate ratio may further improve the amount of biomethane produced, as indicated in Brown et al's recent study [192]. The *Fucus serratus* was found to have low BI due to a large relative proportion of inhibitory phenolic compounds in the aqueous phase compared to *saccharina*. Further work would include doing AD experiments on the M:SL co-processed mix, which was not produced in enough quantity to run on the AMPTS(II) instrument.

The overall energy balance includes the energy output from the BMP experiments, calculated in terms of MJ kg⁻¹. Although the BMP results shows that the higher the temperature, the more BMP is produced for the sugar kelp, the additional energy produced is not sufficient to overcome the higher energy input of the higher HTC temperatures, coupled with the lower yields of hydrochar for higher temperatures. Therefore, from the results found in this study it can be concluded that the best HTC temperature out of the three evaluated here, for overall energy production from any of the biomass feedstocks is 150°C.

Hydrothermal carbonisation certainly has its place in the constantly evolving renewable energy sector. Naturally abundant *Saccharina latissima* and intertidal wracks such as *Fucus serratus* are prime candidates for use as a HTC feedstock. HTC remains the most viable option for using seaweed as source of bioenergy in the near future, as well as good opportunities for anaerobic digestion, due to these processes being water-based. The

lack of the energy intensive drying step is essential to keep the overall energy balance at suitable levels. Mixing seaweed feedstocks with terrestrial biomass as proposed in this study would vastly improve the fuel quality of the hydrochar, by reducing its likelihood of slagging and fouling the biomass reactors, with the addition of improved energy density compared to the raw feedstocks. The UK is well-placed to investigate this and the establishment of new seaweed farms on the UK coast will no doubt increase interest in this abundant, chemically rich and as yet underutilised natural resource.

8.0.1 Further Work

If more time was available for this research, additional seaweed samples would have been run, in addition to using another commonly used terrestrial feedstock derived from waste (e.g. crop residues such as wheat straw) as part of the feedstock blend with seaweed. Different seaweed to *Miscanthus* ratio would have also been trialled, had more *Miscanthus* been available. More HTC temperatures around 150 to 200 would have been ran as well, and a larger 2l reactor used for scaling up experiments, and to generate more sample for additional analysis of the solid phase, ash fusion tests for example. More time would have also allowed for scanning electron microscope analysis to be done on the solid phase, to aid the interpretation of the hydrochar structure.

If more money was available, certain expensive model compounds such as fucoidan and laminarin could have been included in the seaweed model compound feedstock samples ran in the HTC, which would have provided an even greater insight into the different chemical reactions taking place during HTC for the seaweed feedstocks.

There is plenty of scope for further work within this fast developing area. To further refine potential biorefinery concepts utilising seaweed as a feedstock, different solid-loading ratios and different blending ratios could be trialled and compared. Slightly lower *Saccharina latissima* to *Miscanthus* feedstock ratios (e.g. 15:85 or 10:90) is recommended for future HTC co-processing experiments, as three of the slagging and fouling indices were not quite met in this study, although significant improvements were identified for the AI, BAI and SVI indices. It is hoped that lowering slightly the amount of seaweed will reduce the slagging and fouling propensity. Additionally, using cultivated seaweed that has had a shorter lifespan than the wild collected samples may be advantageous, as there is likely to be less bio-accumulated metals contained in the feedstock. Cultivated seaweed would be the large-scale biorefinery feedstock so using seaweeds already cultivated for further

analysis and scale-up is also recommended as a HTC feedstock for further work in any case.

Also, it is suggested that further experiments using ash fusion techniques for analysing the slagging and fouling propensity on future work is performed, to provide more accurate slagging and fouling data, rather than predictions based on predictive equations, which themselves were developed using mineral-derived fuel properties (and so may not be accurate for these samples). The ash fusion tests of the ash in a pellet form was not able to be conducted here due to the lack of sample, however runs in larger reactors, or multiple runs to gather enough sample are encouraged. Using larger reactors for a more likely mass balance is also beneficial as an industrial scale HTC reactor would undoubtedly have some differences in parameters compared to a bench-scale Parr Reactor used in this study. The surplus sample resulting from such a scaled-up reactor (using a 2l Parr reactor at first) can provide more accurate values, as duplicate XRF pressed pellet analysis could be run, in addition to duplicate TGA analysis and ash fusion tests. HTC runs using a similar but larger HTC reactor is thus recommended, to provide a more detailed and reliable prediction of ash behaviour.

Further work would also include doing more anaerobic digestion experiments on the M:SL co-processed mixes, which was not produced in enough quantity to run on the AMPTS(II) instrument. The co-processed blends ran in future recommended HTC runs should be ran in duplicate, or in a larger reactor to enable further AD experiments via the bench-scale AMPTS(II) reactor, to study how easily digestible to co-processed blend is compared to similar AD feedstocks, and further refine the AD parameters to maximise biomethane production, such as the substrate:feedstock ratio. Analysis on the resultant digestate should also be performed in a more in-depth study to ensure there are indeed suitable post-AD uses for the digestate by-product. (fertiliser for example).

Steps can also be taken to improve the energy balance of the proposed biorefinery system. The energy input required for such a biorefinery may be reduced by taking steps to mitigate the energy loss upon re-heating the HTC reactor, by utilising a fully continuous, heavily insulated HTC reactor as described in figure 1.3. Heat recovery may be implemented to enable efficient heating of the proposed anaerobic digester for the post-treatment of the HTC aqueous phase. This would in turn further improve the overall true energy balance, however the calculations made here do not take into account the energy required to heat the AD reactor. Additionally, the solid loading ratio (SLR), currently 10%, of the feedstock to the added water into the HTC reactor may be doubled, which would have the effect of reducing the energy input, as it takes less

energy to heat seaweed than it does water. Utilising the gases produced, particularly if the higher HTC temperatures were further researched, could further improve the energy balance, if a suitable amount of biomethane is produced. Potentially, the data on energy inputs required for such a continuous reactor could be provided by similar continuous pilot scale HTC reactors already in use in Europe to enable thorough calculations to take this change in energy input and any efficiency affects into account to determine the overall energy balance for a HTC-based biorefinery at scale.

Further work is needed to completely determine the most suitable HTC and AD parameters of the proposed biorefinery concept. However, this study has helped improve the current understanding of how the organic chemicals and inorganics alike within the seaweed sample effects the *Miscanthus* HTC aqueous phase, the different hydrochars and their respective slagging and fouling propensities, and subsequent biomethane production of the aqueous phase from the seaweed feedstocks. These results pave the way for further in depth research that can focus on defining the most desirable feedstock mixes and HTC and AD parameters for a future HTC biorefinery.

References

- [1] M. Parry, O. Canziani, J. Palutikof, P. van der Linden, and C. Hanson, “Climate Change 2007: Impacts, Adaptation and Vulnerability. Contribution of Working Group II to the Fourth Assessment Report of the Intergovernmental Panel on Climate Change, Eds., , , 976pp.,” tech. rep., IPCC, Cambridge University Press, Cambridge, UK, 2007.
- [2] S. Twidale, “Britain has first coal-free week in over a century,” 2019.
- [3] D. Beillo, “CO2 Levels for February Eclipsed Prehistoric Highs,” 2015.
- [4] K. Loria, “CO2 levels are at their highest in 800,000 years,” 2018.
- [5] J. Blunden, D. S. Arndt, and Eds, “State of the Climate in 2018,” *Bull. Amer. Meteor. Soc.*, vol. 100, no. 9, 2019.
- [6] Q. Wang and M. Su, “A preliminary assessment of the impact of COVID-19 on environment – A case study of China,” *Sci. Total Environ.*, p. 138915, apr 2020.
- [7] The Guardian, “The Guardian view on Covid-19 and transport: walk to the future,” 2020.
- [8] L. Hobson, “Covid-19 might lead to long-term action on climate change,” 2020.
- [9] M. Weaver, “UK firms fined for breaking EU carbon rules,” 2006.
- [10] UK Government, “The Climate Change Act 2008,” 2008.
- [11] Official Journal of the European Union, “Directive (EU) 2018/2001 of the European Parliament and of the Council of 11 December 2018 on the promotion of the use of energy from renewable sources,” tech. rep., European Union, Brussels, Belgium, 2018.
- [12] A. Vaughan, “EU raises renewable energy targets to 32% by 2030,” 2018.

-
- [13] G. Vince, “The heat is on over the climate crisis. Only radical measures will work,” 2019.
- [14] UN, “Paris Agreement,” tech. rep., United Nations, Paris, 2015.
- [15] IPCC, “Climate Change 2014 Synthesis Report Summary for Policymakers,” tech. rep., IPCC, 2014.
- [16] A. Guterres, “Secretary-General’s remarks at opening ceremony of UN Climate Change Conference COP25 [as delivered],” 2019.
- [17] A. Guterres, “Secretary-General’s statement on the results of the UN Climate Change Conference COP25,” 2019.
- [18] UN Environment Programme, “Emissions Gap Report 2019,” tech. rep., UNEP, Nairobi, 2019.
- [19] Drax, “Drax to stop using coal well ahead of UK’s deadline,” 2020.
- [20] BEIS, “Digest of United Kingdom Energy Statistics 2019,” tech. rep., Department for Business, Energy & Industrial Strategy, London, 2019.
- [21] I. Staffell, “The 100 years from coal to clean power,” 2019.
- [22] Drax, “Carbon dioxide now being captured in first of its kind BECCS pilot,” 2019.
- [23] Drax, “Drax sets world-first ambition to become carbon negative by 2030,” 2019.
- [24] DEFRA, “Crops Grown For Bioenergy in the UK: 2018,” tech. rep., DEFRA, London, UK, 2019.
- [25] European Commission, “NNFCC - National Non-Food Crops Centre.”
- [26] NNFCC, “Anaerobic Digestion Deployment in the United Kingdom: Sixth Annual Report,” tech. rep., NNFCC, York, 2019.
- [27] DECC, “The UK renewable energy strategy,” tech. rep., DECC, London, UK, 2009.
- [28] J. Van Hal, W. Huijgen, and A. López-Contreras, “Opportunities and challenges for seaweed in the biobased economy,” *Trends Biotechnol.*, vol. 32, pp. 231–233, 2014.

- [29] E. Kostas, “Development of a bio-refinery process for the production of speciality chemical, biofuel and bioactive compounds from *Laminaria digitata*,” *Algal Res.*, vol. 28, pp. 211–219, 2017.
- [30] A. Ross, “Opportunities for Energy and Nutrient cycling using Hydrothermal Carbonisation,” in *1st Int. Symp. Hydrothermal Carbonis.*, (London), Queen Mary University of London, 2017.
- [31] HTCycle, “Hydrothermal carbonisation for a clean-running world,” 2020.
- [32] European Commission DG ENV, “Biofuels - the way forward?,” *DG Environ. News Alert Serv.*, pp. 1–8, feb 2008.
- [33] OECD Green Growth Studies, “Energy,” tech. rep., OECD, 2011.
- [34] A. Ajanovic, “Biofuels versus food production: Does biofuels production increase food prices?,” *Energy*, vol. 36, pp. 2070–2076, apr 2011.
- [35] Biofuel, “First Generation Biofuels,” 2010.
- [36] R. Lee and J.-M. Lavoie, “From First- to Third-Generation Biofuels: Challenges of Producing a Commodity from a Biomass of Increasing Complexity,” *Anim. Front.*, vol. 3, pp. 6–11, 2013.
- [37] K. Stone, P. Hunt, K. Cantrell, and K. Ro, “The potential impacts of biomass feedstock production on water resource availability,” *Bioresour. Technol.*, vol. 101, pp. 2014–2025, mar 2010.
- [38] Biofuel, “Second Generation Biofuels,” 2010.
- [39] L. Brennan and P. Owende, “Biofuels from microalgae—A review of technologies for production, processing, and extractions of biofuels and co-products,” *Renew. Sustain. Energy Rev.*, vol. 14, pp. 557–577, feb 2010.
- [40] C. Posten and G. Schaub, “Microalgae and terrestrial biomass as source for fuels—A process view,” *J. Biotechnol.*, vol. 142, pp. 64–69, jun 2009.
- [41] Euronews, “Seaweed: sea fuel? - futuris,” 2013.
- [42] MarLIN, “*Saccharina latissima* with red and brown seaweeds on lower infralittoral muddy mixed sediment,” 2018.
- [43] The Seaweed site, “Kelps: *Laminaria* and *Saccharina*,” 2020.

- [44] M. Bhattacharjee and E. Siemann, “Low algal diversity systems are a promising method for biodiesel production in wastewater fed open reactors,” *ALGAE*, vol. 30, pp. 67–79, mar 2015.
- [45] D. A. Roberts, N. A. Paul, A. J. Cole, and R. de Nys, “From waste water treatment to land management: Conversion of aquatic biomass to biochar for soil amelioration and the fortification of crops with essential trace elements,” *J. Environ. Manage.*, vol. 157, pp. 60–68, jul 2015.
- [46] J. Hansen, L. Nazarenko, and E. al, “Earth’s Energy Imbalance: Confirmation and Implications,” *Science (80-.)*, vol. 308, pp. 1431–1435, 2005.
- [47] A. J. Cole, R. de Nys, and N. A. Paul, “Biorecovery of nutrient waste as protein in freshwater macroalgae,” *Algal Res.*, vol. 7, pp. 58–65, jan 2015.
- [48] H. Hickey, “UW will investigate seaweed as a tool to fight ocean acidification in Puget Sound,” 2015.
- [49] M. Guiry, “Sweet Kelp (*Saccharina latisima*),” 2020.
- [50] N. White and C. Marshall, “Sugar kelp (*Saccharina latissima*),” tech. rep., Marine Biological Association of the United Kingdom, Plymouth, 2007.
- [51] E. Paterson, “Interest in seaweed cultivation is growing,” 2020.
- [52] “Scarborough Council agrees to SeaGrown seaweed farm grant,” 2019.
- [53] Canadian Museum of Nature, “Types of Seaweeds,” 2004.
- [54] Integrated Multi-Tropic Aquaculture, “Seaweeds - A part of everyday life,” 2012.
- [55] K. Anastasakis, *The potential of the production of fuels and chemicals from marine biomass*. PhD thesis, The University of Leeds, 2011.
- [56] E. Borgese, *Seafarm: the story of aquaculture*. New York, USA: Harry N. Abrams, Incorporated, 1980.
- [57] M. Guiry, “What are seaweeds?,” 2014.
- [58] M. Guiry, “Rhodophyta: Red Algae,” 2011.
- [59] M. Guiry, “Phaeophyceae: Brown Algae,” 2014.
- [60] M. Guiry, “Chlorophyta: Green Algae,” 2014.

- [61] NNFCC, “Miscanthus: Crop Fact Sheet,” 2011.
- [62] S. Arnoult and M. Brancourt-Hulmel, “A Review on Miscanthus Biomass Production and Composition for Bioenergy Use: Genotypic and Environmental Variability and Implications for Breeding,” *BioEnergy Res.*, vol. 8, no. 2, pp. 502–526, 2015.
- [63] E. Jensen, P. Robson, K. Farrar, S. Thomas Jones, J. Clifton-Brown, R. Payne, and I. Donnison, “Towards Miscanthus combustion quality improvement: the role of flowering and senescence,” *Glob. Change Biol. Bioenergy*, vol. 9, pp. 891–908, may 2017.
- [64] A. M. Smith, C. Whittaker, I. Shield, and A. B. Ross, “The potential for production of high quality bio-coal from early harvested Miscanthus by hydrothermal carbonisation,” *Fuel*, vol. 220, pp. 546–557, may 2018.
- [65] J. Adams, “An overview on seaweed uses in the UK : Past, present and future,” *Seaweed Resour.*, vol. 36, pp. 16–21, jun 2016.
- [66] R. Araujo, J. Assis, R. Aguillar, L. Airoidi, I. Criado, I. Bartsch, T. Bekkby, H. Christie, D. Davoult, S. Derrien-Courtel, C. Fernandez, S. Fredriksen, F. Gevaert, H. Gundersen, A. Gal, L. Lévêque, N. Mieszkowska, K. Norderhaug, P. Oliveira, and I. Sousa Pinto, “Status, trends and drivers of kelp forests in Europe: an expert assessment,” *Biodivers. Conserv.*, vol. 25, 2016.
- [67] A. Handå, S. Forbord, W. Xinxin, O. Broch, S. Dahle, T. Størseth, K. Reitan, Y. Olsen, and J. Skjermo, “Seasonal- and depth-dependent growth of cultivated kelp (*Saccharina latissima*) in close proximity to salmon (*Salmo salar*) aquaculture in Norway,” *Aquaculture*, vol. 414-415, pp. 191–201, 2013.
- [68] SAMS, “Farming the sea research at SAMS,” 2020.
- [69] O. Broch, I. Ellingsen, S. Forbord, X. Wang, Z. Volent, M. Alver, A. Handå, K. Andresen, D. Slagstad, K. Olsen, and J. Skjermo, “Modelling the cultivation and bioremediation potential of the kelp *Saccharina latissima* in close proximity to an exposed salmon farm in Norway,” *Aquac. Environ. Interact.*, vol. 4, pp. 187–206, 2013.
- [70] G. S. Grebe, C. J. Byron, A. S. Gelais, D. M. Kotowicz, and T. K. Olson, “An ecosystem approach to kelp aquaculture in the Americas and Europe,” *Aquac. Reports*, vol. 15, p. 100215, nov 2019.

- [71] J. C. Sanderson, M. J. Dring, K. Davidson, and M. S. Kelly, "Culture, yield and bioremediation potential of *Palmaria palmata* (Linnaeus) Weber & Mohr and *Saccharina latissima* (Linnaeus) C.E. Lane, C. Mayes, Druehl & G.W. Saunders adjacent to fish farm cages in northwest Scotland," *Aquaculture*, vol. 354-355, pp. 128–135, 2012.
- [72] D. Carrington, "Seaweed biofuels: a green alternative that might just save the planet," 2013.
- [73] W. Crookes and L. Robinson, "SeaGrown," 2019.
- [74] Ofgem, "Non-Domestic Renewable Heat Incentive: Guidance Volume 1," tech. rep., Ofgem, 2018.
- [75] K. Anastasakis, A. Ross, and J. Jones, "Pyrolysis behaviour of the main carbohydrates of brown macro-algae," *Fuel*, vol. 90, pp. 598–607, feb 2011.
- [76] M. Aresta, A. Dibenedetto, and G. Barberio, "Utilization of macro-algae for enhanced CO₂ fixation and biofuels production: Development of a computing software for an LCA study," *Fuel Process. Technol.*, vol. 86, pp. 1679–1693, oct 2005.
- [77] P. Kumar, D. Barrett, M. Delwiche, and P. Stroeve, "Methods for Pretreatment of Lignocellulosic Biomass for Efficient Hydrolysis and Biofuel Production," *Ind. Eng. Chem. Res.*, vol. 48, pp. 3713–3729, 2009.
- [78] A. Yousuf, "Biodiesel from lignocellulosic biomass - Prospects and challenges," *Waste Manag.*, vol. 32, pp. 2061–2067, 2012.
- [79] S. Petersen, "What Are the Functions of Starch in Plant Cells?," 2018.
- [80] T. A. Davis, B. Volesky, and A. Mucci, "A review of the biochemistry of heavy metal biosorption by brown algae," 2003.
- [81] D. H. LEWIS and D. C. SMITH, "SUGAR ALCOHOLS (POLYOLS) IN FUNGI AND GREEN PLANTS. I. DISTRIBUTION, PHYSIOLOGY AND METABOLISM," *New Phytol.*, vol. 66, pp. 143–184, apr 1967.
- [82] E. Percival, "The polysaccharides of green, red and brown seaweeds: Their basic structure, biosynthesis and function," *Br. Phycol. J.*, vol. 14, pp. 103–117, jun 1979.

- [83] A. Tarantola, "From Ice Cream to Toothpaste: Seaweed's Hidden Uses," 2014.
- [84] C. Gallery, "3 Vegetarian Substitutes for Gelatin (Because Vegans Love Jello Too!)," 2014.
- [85] J. Temple, "Seaweed could make cows burp less methane and cut their carbon hoofprint," 2018.
- [86] M. Warwicker and A.-L. Taylor, "Seaweed: Should people eat more of it?," *BBC News*, 2012.
- [87] A. Grant, "Using Seaweed For Compost: Learn How To Compost Seaweed," 2020.
- [88] A. M. Smith and A. B. Ross, "Production of bio-coal, bio-methane and fertilizer from seaweed via hydrothermal carbonisation," *Algal Res.*, vol. 16, pp. 1–11, jun 2016.
- [89] J. Milledge and S. Heaven, "Methods of energy extraction from microalgal biomass: A review," *Rev. Environ. Sci. Bio/Technology*, vol. 13, 2014.
- [90] A. Demirbaş, "Biomass Resource Facilities and Biomass Conversion Processing For Fuels And Chemicals," *Energy Convers. Manag.*, vol. 42, pp. 1357–1378, 2001.
- [91] L. Yu, S. Wang, X.-M. Jiang, N. Wang, and C. Zhang, "Thermal analysis studies on combustion characteristics of seaweed," *J. Therm. Anal. Calorim.*, vol. 93, pp. 611–617, 2008.
- [92] S. Wang, X. Jiang, Q. Wang, X. Han, and H. Ji, "Experiment and grey relational analysis of seaweed particle combustion in a fluidized bed," *Energy Convers. Manag.*, vol. 66, pp. 115–120, feb 2013.
- [93] A. B. Ross, J. M. Jones, M. L. Kubacki, and T. Bridgeman, "Classification of macroalgae as fuel and its thermochemical behaviour," *Bioresour. Technol.*, 2008.
- [94] J. Yang, M. Xu, X. Zhang, Q. Hu, M. Sommerfeld, and Y. Chen, "Life-cycle analysis on biodiesel production from microalgae: Water footprint and nutrients balance," *Bioresour. Technol.*, vol. 102, pp. 159–165, jan 2011.
- [95] U.S. Department of Energy (DOE), "National Algal Biofuels Technology Roadmap," tech. rep., U.S. Department of Energy, Office of Energy Efficiency and Renewable Energy, Biomass Program, Washington, DC, USA, 2010.

- [96] M. Balat, H. Balat, and C. Öz, “Progress in bioethanol processing,” *Prog. Energy Combust. Sci.*, vol. 34, pp. 551–573, oct 2008.
- [97] D. Puri, S. Heaven, and C. Banks, “Improving the performance of enzymes in hydrolysis of high solids paper pulp derived from MSW,” *Biotechnol. Biofuels*, vol. 6, 2013.
- [98] J. Gressel, “Transgenics are imperative for biofuel crops,” *Plant Sci.*, vol. 174, pp. 246–263, 2008.
- [99] M. Yanagisawa, S. Kawai, and K. Murata, “Strategies for the production of high concentrations of bioethanol from seaweeds: Production of high concentrations of bioethanol from seaweeds,” *Bioengineered*, vol. 4, 2013.
- [100] A. Golberg, E. Vitkin, G. Linshiz, S. Khan, N. Hillson, Z. Yakhini, and M. Yarmush, “Proposed design of distributed macroalgal biorefineries: Thermodynamics, bio-conversion technology, and sustainability implications for developing economies,” *Biofuels, Bioprod. Biorefining*, vol. 8, 2014.
- [101] M. Borines, R. de Leon, and J. Cuello, “Bioethanol Production from the Macroalgae *Sargassum* spp.,” *Bioresour. Technol.*, vol. 138C, pp. 22–29, 2013.
- [102] M. Huesemann, L.-J. Kuo, L. Urquhart, G. Gill, and G. Roesijadi, “Acetone-butanol fermentation of marine macroalgae,” *Bioresour. Technol.*, vol. 108, pp. 305–309, 2012.
- [103] M. Meinita, Y.-K. Hong, and G.-T. Jeong, “Detoxification of acidic catalyzed hydrolysate of *Kappaphycus alvarezii* (cottonii),” *Bioprocess Biosyst. Eng.*, vol. 35, pp. 93–98, 2011.
- [104] G. Roesijadi, A. Copping, M. Huesemann, J. Foster, and J. Benemann, “Techno-Economic Feasibility Analysis of Offshore Seaweed Farming for Bioenergy and Biobased Products,” tech. rep., PNNL-19944; U.S. Department of Energy, Washington, DC, USA, 2010.
- [105] T. Potts, J. Du, M. Paul, P. May, R. Beitle, and J. Hestekin, “The Production of Butanol from Jamaica Bay Macro Algae,” *Environ. Prog. Sustain. Energy*, vol. 31, 2012.
- [106] M. Huesemann, G. Roesijadi, J. Benemann, and F. Metting, *Biomass to Biofuels: Strategies for Global Industries*, pp. 165–184. John Wiley & Sons, Ltd, 2010.

- [107] P. McKendry, "Energy production from biomass (part 2): conversion technologies," *Bioresour. Technol.*, vol. 83, pp. 47–54, may 2002.
- [108] R. Saidur, E. Abdelaziz, A. Demirbas, M. Hossain, and S. Mekhilef, "A review on biomass as a fuel for boilers," *Renew. Sustain. Energy Rev.*, vol. 15, pp. 2262–2289, jun 2011.
- [109] L. Li, J. Rowbotham, C. Greenwell, and P. Dyer, "An introduction to pyrolysis and catalytic pyrolysis: Versatile techniques for biomass conversion," *New Futur. Dev. Catal. Catal. Biomass Convers.*, pp. pp.173–208, 2013.
- [110] A. Marcilla, L. Catalá, J. García-Quesada, F. Valdés, and M. Hernández, "A review of thermochemical conversion of microalgae," *Renew. Sustain. Energy Rev.*, vol. 27, pp. 11–19, nov 2013.
- [111] J. H. Choi, D. J. Suh, and H. C. Woo, "Pyrolysis of Seaweeds for Bio-oil and Bio-char Production," *Chem. Eng. Trans.*, vol. 37, 2014.
- [112] J. Yanik, R. Stahl, N. Troeger, and A. Sinag, "Pyrolysis of algal biomass," *J. Anal. Appl. Pyrolysis*, vol. 103, pp. 134–141, sep 2013.
- [113] P. McKendry, "Energy production from biomass (part 3): gasification technologies," *Bioresour. Technol.*, vol. 83, pp. 55–63, may 2002.
- [114] I. Ahmed and A. Gupta, "Pyrolysis and gasification of food waste: Syngas characteristics and char gasification kinetics," *Appl. Energy*, vol. 87, pp. 101–108, jan 2010.
- [115] Q. Guan, P. E. Savage, and C. Wei, "Gasification of alga *Nannochloropsis* sp. in supercritical water," *J. Supercrit. Fluids*, vol. 61, pp. 139–145, jan 2012.
- [116] L. Nikolaisson, J. Dahl, K. Bech, A. Bruhn, M. Rasmussen, A. Bjerre, H. Nielsen, P. Ambus, K. Rost, and Z. Kadar, "Energy production fom macroalgae," in *Proc. 20th Eur. Biomass Conf.*, (Milan, Italy), pp. 18–22, 2012.
- [117] R. Cherad, J. A. Onwudili, U. Ekpo, P. T. Williams, A. R. Lea-Langton, M. Carmargo-Valero, A. B. Ross, M. Camargo-Valero, and A. B. Ross, "Macroalgae supercritical water gasification combined with nutrient recycling for microalgae cultivation," *Environ. Prog. Sustain. Energy*, vol. 32, 2013.

- [118] J. A. Onwudili, A. R. Lea-Langton, A. B. Ross, and P. T. Williams, "Catalytic hydrothermal gasification of algae for hydrogen production: Composition of reaction products and potential for nutrient recycling," *Bioresour. Technol.*, vol. 127, pp. 72–80, jan 2013.
- [119] J. Rowbotham, P. Dyer, C. Greenwell, D. Selby, and M. Theodorou, "Copper(II)-mediated thermolysis of alginates: A model kinetic study on the influence of metal ions in the thermochemical processing of macroalgae," *Interface Focus*, vol. 3, p. 20120046, 2013.
- [120] N. Neveux, A. Yuen, C. Jazrawi, M. Magnusson, B. Haynes, A. Masters, A. Montoya, N. Paul, T. Maschmeyer, and R. de Nys, "Biocrude yield and productivity from the hydrothermal liquefaction of marine and freshwater green macroalgae," *Bioresour. Technol.*, vol. 155C, pp. 334–341, 2013.
- [121] D. Vardon, B. Sharma, G. Blazina, K. Rajagopalan, and T. Strathmann, "Thermochemical conversion of raw and defatted algal biomass via hydrothermal liquefaction and slow pyrolysis," *Bioresour. Technol.*, vol. 109, pp. 178–187, 2012.
- [122] A. B. Ross, "Potential integration of heat and pressure based systems with anaerobic digestion," in *Waste Biorefinery Platf.*, (Birmingham, UK), AquaEnviro, 2015.
- [123] U. Jena, "Comparative Evaluation of Thermochemical Liquefaction and Pyrolysis for Bio-Oil Production from Microalgae," *Energy & Fuels*, vol. 25, pp. 5472–5482, 2011.
- [124] T. Minowa, S. Yokoyama, M. Kishimoto, and T. Okakura, "Oil production from algal cells of *dunaliella-tertiolecta* by direct thermochemical liquefaction," *Fuel*, vol. 74, pp. 1735–1738, 1995.
- [125] M. Streefland, "Report on Biofuel Production Processes from Micro, Macroalgae and Other Aquatic Biomass," *AquaFUELS*, 2010.
- [126] K. Anastasakis and A. B. Ross, "Hydrothermal liquefaction of the brown macro-alga *Laminaria Saccharina*: Effect of reaction conditions on product distribution and composition," *Bioresour. Technol.*, 2011.
- [127] D. Zhou, L. Zhang, S. Zhang, H. Fu, and J.-M. Chen, "Hydrothermal Liquefaction of Macroalgae *Enteromorpha prolifera* to Bio-oil," *Energy Fuels - ENERGFUEL*, vol. 24, 2010.

- [128] P. Biller and A. B. Ross, *17. Production of biofuels via hydrothermal conversion*, ch. 17. Elsevier, 2016.
- [129] Q.-V. Bach, M. V. Sillero, K.-Q. Tran, and J. Skjermo, “Fast hydrothermal liquefaction of a Norwegian macro-alga: Screening tests,” *Algal Res.*, vol. 6, pp. 271–276, oct 2014.
- [130] M. T. Reza, J. Andert, B. Wirth, D. Busch, J. Pielert, J. Lynam, and J. Mumme, “Review Article: Hydrothermal Carbonization of Biomass for Energy and Crop Production,” *Appl. Bioenergy*, vol. 1, 2014.
- [131] M. Lucian, M. Volpe, and L. Fiori, “Hydrothermal Carbonization Kinetics of Lignocellulosic Agro-Wastes: Experimental Data and Modeling,” *Energies*, vol. 12, no. 516, 2019.
- [132] A. Funke and F. Ziegler, “Hydrothermal carbonization of biomass: A summary and discussion of chemical mechanisms for process engineering,” *Biofuels, Bioprod. Biorefining*, vol. 4, no. 2, pp. 160–177, 2010.
- [133] A. Kruse, A. Funke, and M.-M. Titirici, “Hydrothermal conversion of biomass to fuels and energetic materials,” *Curr. Opin. Chem. Biol.*, vol. 17, no. 3, pp. 515–521, 2013.
- [134] M. Sevilla and A. B. Fuertes, “The production of carbon materials by hydrothermal carbonization of cellulose,” *Carbon N. Y.*, vol. 47, no. 9, pp. 2281–2289, 2009.
- [135] A. Kruse, D. Jung, and P. Körner, “Hydrothermal Carbonisation: Elimination Reaction of water in water as a solvent,” in *2nd Int. Symp. Hydrothermal Carbonization*, (Berlin, Germany), 2019.
- [136] Y. Shen, S. Yu, S. Ge, X. Chen, X. Ge, and M. Chen, “Hydrothermal carbonization of medical wastes and lignocellulosic biomass for solid fuel production from lab-scale to pilot-scale,” *Energy*, vol. 118, pp. 312–323, jan 2017.
- [137] L. Higgins, Brown, Andrew, Ross, Andrew, and Mishra Bhoopesh, “Studying the fundamental properties of hydrochars using synchrotron radiation,” in *2nd Int. Symp. Hydrothermal Carbonization*, (Berlin, Germany), 2019.
- [138] T. Klausli, “5- HMF as Key Enabler in Bio-Based Chemistry by Thomas Kläusli,” in *10th Int. Conf. Bio-bases Materials*, (Köln, Germany), 2017.

- [139] Selleckchem.com, “5-Hydroxymethylfurfural,” 2013.
- [140] J. Goldfarb, L. Fiori, M. Volpe, L. Gao, M. Lucian, G. Ischia, and G. Severini, “Looking beyond routine characterizations to understand opportunities and limitations of HTC for carbon-based products and applications,” in *2nd Int. Symp. Hydrothermal Carbonization*, (Berlin, Germany), 2019.
- [141] J. Kern and J. Libra, “Post-treatments of HTC chars for use in agriculture,” in *2nd Int. Symp. Hydrothermal Carbonization*, (Berlin, Germany), 2019.
- [142] P. Arauzo, M. Olszewski, X. Wang, J. Pfersich, V. Sebastian, J. Manyà, N. Hedin, and A. Kruse, “Assessment of the effects of process water recirculation on the surface chemistry and morphology of hydrochar,” *Renew. Energy*, 2020.
- [143] M. Lucian, M. Volpe, L. Gao, G. Piro, J. L. Goldfarb, and L. Fiori, “Impact of hydrothermal carbonization conditions on the formation of hydrochars and secondary chars from the organic fraction of municipal solid waste,” *Fuel*, vol. 233, pp. 257–268, dec 2018.
- [144] I. Zabaleta, P. Marchetti, C. R. Lohri, and C. Zurbrügg, “Influence of solid content and maximum temperature on the performance of a hydrothermal carbonization reactor,” *Environ. Technol.*, vol. 38, no. 22, pp. 2856–2865, 2017.
- [145] C. I. Aragón-Briceño, O. Grasham, A. B. Ross, V. Dupont, and M. A. Camargo-Valero, “Hydrothermal carbonization of sewage digestate at wastewater treatment works: Influence of solid loading on characteristics of hydrochar, process water and plant energetics,” *Renew. Energy*, vol. 157, pp. 959–973, 2020.
- [146] American Biogas Council, “What is Anaerobic Digestion?.”
- [147] A. et al. Anukam and A. et al. Anukam, “A Review of the Chemistry of Anaerobic Digestion: Methods of Accelerating and Optimizing Process Efficiency,” *PROCCE*, vol. 7, p. 504, 2019.
- [148] The Editors of Encyclopædia Britannica, “Hydrolysis,” 2016.
- [149] M. Bibra, J. Wang, P. Squillace, R. Pinkelman, S. Papendick, S. Schneiderman, V. Wood Braband, V. Amar, S. Kumar, D. Salem, and R. Sani, *Biofuels and Value-added Products from Extremophiles*, pp. 17–51. I.K. International Publishing House New Delhi, 2015.

- [150] G. Roesijadi, S. Jones, L. Snowden-Swan, and Y. Zhu, "Macroalgae As A Biomass Feedstock: A Preliminary Analysis," *Analysis*, 2010.
- [151] F. Murphy, G. Devlin, R. Deverell, and K. McDonnell, "Biofuel production in Ireland – an APPROACH to 2020 targets with a focus on algal biomass," *Energies*, vol. 63390, pp. 6391–6412, 2013.
- [152] A. M. Buswell and H. F. Mueller, "Mechanism of Methane Fermentation," *Ind. Eng. Chem.*, vol. 44, no. 3, pp. 550–552, 1952.
- [153] G. E. Symons and A. M. Buswell, "The Methane Fermentation of Carbohydrates^{1,2}," *J. Am. Chem. Soc.*, vol. 55, no. 5, pp. 2028–2036, 1933.
- [154] M. Alvarado-Morales, A. Boldrin, D. Karakashev, S. Holdt, I. Angelidaki, and T. Astrup, "Life Cycle Assessment of Biofuel Production from Brown Seaweed in Nordic Conditions," *Bioresour. Technol.*, vol. 129C, pp. 92–99, 2012.
- [155] A. Sutherland and J. Varela, "Comparison of various Microbial Inocula for the Efficient Anaerobic Digestion of *Laminaria hyperborea*," *BMC Biotechnol.*, vol. 14, p. 7, 2014.
- [156] Corrosionpedia, "Volatile Solids," 2019.
- [157] O. Lefebvre and R. Moletta, "Treatment of Organic Pollution in Industrial Saline Wastewater: A Literature Review," *Water Res.*, vol. 40, pp. 3671–3682, 2007.
- [158] Y. Chen, J. Cheng, and K. Creamer, "Inhibition of anaerobic process: a review. Bioresour Technol," *Bioresour. Technol.*, vol. 99, pp. 4044–4064, 2008.
- [159] Parliamentary Office of Science and Technology, *Biofuels from Algae; Postnote*. London, UK: UK Parliament, 2011.
- [160] T. Atkins and M. Escudier, "Dulong's formula," 2013.
- [161] Parr Instrument Company, "4540 High Pressure Reactors: Operating Instruction Manual."
- [162] B. Jenkins, L. Baxter, T. Miles, and T. Miles, "Combustion properties of biomass," *Fuel Process. Technol.*, vol. 54, pp. 17–46, mar 1998.
- [163] D. W. Bapat, S. V. Kulkarni, and V. P. Bhandarkar, "Design and operating experience on fluidized bed boiler burning biomass fuels with high alkali ash," in *14. Int. Conf. Fluid. bed Combust. Vancouver*, (Vancouver, Canada), 1997.

- [164] P. P. PŁAZA, N. Syred, and A. J. Griffiths, *The Development of a Slagging and Fouling Predictive Methodology for Large Scale Pulverised Boilers Fired with Coal/Biomass Blends*. PhD thesis, Cardiff University, 2013.
- [165] V. Benavente, “Additives for ash related problems prevention in HTC fuels,” in *2nd Int. Symp. Hydrothermal Carbonization*, (Berlin, Germany), 2019.
- [166] N. Amin and T. Claridge, “Quantitative NMR Spectroscopy,” tech. rep., The University of Oxford, Oxford, UK, 2017.
- [167] Magritek Ltd, “Analytical NMR – Identification, Quantification (qNMR) and Mixture Analysis,” 2013.
- [168] E. Danso-Boateng, G. Shama, A. Wheatley, S. Martin, and R. Holdich, “Hydrothermal carbonisation of sewage sludge: Effect of process conditions on product characteristics and methane production,” *Bioresour. Technol.*, vol. 177, pp. 318–327, feb 2015.
- [169] R. Lin, C. Deng, L. Ding, A. Bose, and J. D. Murphy, “Improving gaseous biofuel production from seaweed *Saccharina latissima*: The effect of hydrothermal pretreatment on energy efficiency,” *Energy Convers. Manag.*, vol. 196, pp. 1385–1394, sep 2019.
- [170] Engineering Toolbox, “Fuels - Higher and Lower Calorific Values,” 2003.
- [171] L. Konermann, *Protein Unfolding and Denaturants*. Chichester, UK: John Wiley & Sons, Ltd, 2012.
- [172] D. G. Barkalow and R. L. Whistler, “Cellulose,” *AccessScience, McGraw-Hill Educ.*, 2019.
- [173] O. Therasme, T. A. Volk, A. M. Cabrera, M. H. Eisenbies, and T. E. Amidon, “Hot Water Extraction Improves the Characteristics of Willow and Sugar Maple Biomass With Different Amount of Bark,” *Front. Energy Res.*, vol. 6, p. 93, 2018.
- [174] S. Marsham, G. W. Scott, and M. L. Tobin, “Comparison of nutritive chemistry of a range of temperate seaweeds,” *Food Chem*, vol. 100, no. 4, pp. 1331–1336, 2007.
- [175] H. R. Fletcher, *Microwave Assisted Hydrothermal Extraction of Carbohydrates from Macroalgae and the Impact of Seasonal Variation*. PhD thesis, The University of Leeds, 2017.

- [176] K. P. Woli, M. B. David, J. Tsai, T. B. Voigt, R. G. Darmody, and C. A. Mitchell, "Evaluating silicon concentrations in biofuel feedstock crops *Miscanthus* and switchgrass," *Biomass and Bioenergy*, vol. 35, pp. 2807–2813, jul 2011.
- [177] P. Pintana and N. Tippayawong, "Predicting Ash Deposit Tendency in Thermal Utilization of Biomass," *Eng. J.*, vol. 20, pp. 15–24, 2016.
- [178] S. Capareda, "Biomass Combustion," in *Introd. to Biomass Energy Conversions*, p. 493, CRC Press, illustrate ed., 2013.
- [179] J. Dai and R. Mumper, "Plant phenolics: extraction, analysis and their antioxidant and anticancer properties.," *Molecules*, vol. 15, no. 10, pp. 7313–7352, 2010.
- [180] J.-S. Kim and G.-G. Choi, "Pyrolysis of Lignocellulosic Biomass for Biochemical Production," *Waste Biorefinery*, pp. 323–348, jan 2018.
- [181] Fondriest Environmental Inc, "pH of Water: Fundamentals of Environmental Measurements.," 2013.
- [182] National Center for Biotechnology Information., "Mannitol (Compound): Chemical and Physical Properties."
- [183] National Center for Biotechnology Information, "Sodium;(2R,3R,4R,5R,6S)-3,4,5,6-tetrahydroxyoxane-2-carboxylate."
- [184] E. Erdogan, B. Atila, J. Mumme, M. Reza, A. Toptas, M. Elibol, and J. Yanik, "Characterization of products from hydrothermal carbonization of orange pomace including anaerobic digestibility of process liquor," *Bioresour. Technol.*, vol. 196, pp. 35–42, 2015.
- [185] K. S. Woo, Hyun Young Kim, I. G. Hwang, Sang Hoon Lee, and Heon Sang Jeong, "Characteristics of the Thermal Degradation of Glucose and Maltose Solutions," *Prev Nutr Food Sci*, vol. 20, no. 2, pp. 102–109, 2015.
- [186] B. JM, T. JL, L. Stryer, J. L. T. JM Berg, and L. Stryer, "Biochemistry," in *Sect. 11.2, Complex Carbohydrates Are Form. by Link. Monosaccharides.*, New York: W H Freeman, 5th editio ed., 2002.
- [187] National Center for Biotechnology Information, "L-Arabinose."

-
- [188] J. et al Maddox, I.S., Spencer, K., Greenwood, “Production of citric acid from sugars present in wood hemicellulose using *Aspergillus niger* and *Saccharomycopsis lipolytica*,” *Biotechnol Lett*, vol. 7, pp. 815–818, 1985.
- [189] B. R. Brown, “The mechanism of thermal decarboxylation,” *Q. Rev. Chem. Soc.*, vol. 5, no. 2, pp. 131–146, 1951.
- [190] Z. Xu, Z. Shi, and L. Jiang, “3.18 - Acetic and Propionic Acids,” in *Compr. Biotechnol. (Second Ed.* (M. Moo-Young, ed.), pp. 189–199, Burlington: Academic Press, second edi ed., 2011.
- [191] T. Wang, R. Jónsdóttir, and G. Ólafsdóttir, “Total phenolic compounds, radical scavenging and metal chelation of extracts from Icelandic seaweeds,” *Food Chem.*, vol. 116, pp. 240–248, sep 2009.
- [192] A. Brown, G. Finnerty, A. C.-V. Miller, and A. Ross, “Valorisation of Macroalgae via the Integration of Hydrothermal Carbonisation and Anaerobic Digestion. (Submitted).,” *Bioresour. Technol.*, 2020.

Appendix A

Appendix

A.1 Sample Size Reduction

The table specifying which milling technique was used for each of the HTC samples and raw feedstocks prior to characterisation analysis is shown in table [A.1](#).

A.2 XRF Raw Data

The results from the XRF pressed pellets analysis of the hydrochar after HTP processing (and subsequent milling) are shown in table [A.2](#), in terms of % mass of the trace metals within the hydrochar sample. The software also allowed for the results to be portrayed in terms of metal oxides, which was used to calculate the slagging and fouling propensities of the hydrochars. The trace metals in terms of the metal alone are listed here. For conciseness and ease of comparison, all the XRF results from the four different subgroups of samples are tabulated in table [A.2](#), both the micro and macro elements.

The slagging and fouling indices along with the metal oxides values, as calculated on the software, are tabulated in table [A.3](#). The calculations are stated in §3.5.3 which were used to deduce these values. The slagging and fouling indices are displayed with the sample names in the relevant results chapter, but here the metal oxides accompany the figures. All the samples are listed within the sample table for comparison and reference purposes.

Table A.1 The various milling techniques used for sample size reduction. A 'Y' indicates that the technique in the associated column heading was used for the reduce the particle size of that specific sample. Note that there was no hydrochar residue from the mannitol feedstocks, so these samples are not present in the list of samples in this table.

Cell = Cellulose, ACL = Sodium Alginate, Cellulose and Lignin blend, AA = Alginic Acid, SL = *Saccharina latissima*, FS = *Fucus serratus*, Misc = *Miscanthus*, Man = Mannitol.

Sample Name, HTC Temperature (°C)	Disc Mill	Cyro Mill (with N ₂)	Cyro Mill (no N ₂)	Pestle and Mortar
Saccharina Latissima Raw	Y			
Fucus Serratus Raw	Y			
Miscanthus Raw		Y		
Cell 150 60	Y			
Cell 200 60	Y			
Cell 250 60	Y			
Protein 150 60	Y			
Protein 200 60	Y			
Protein 250 60	Y			
Lignin 150 60	Y			
Lignin 200 60	Y			
Lignin 250 60	Y			
ACL 150			Y	
ACL 200			Y	
ACL 250			Y	
Na Alg 150				Y
Na Alg 200				Y
Na Alg 250				Y
Ca Alg 150				Y
Ca Alg 200				Y
Ca Alg 250				Y
AA 150				Y
AA 200				Y
AA 250				Y
SL 150	Y			
SL 200	Y			
SL 250	Y			
FS 150	Y			
FS 200	Y			
FS 250	Y			
Misc 150		Y		
Misc 200		Y		
Misc 250			Y	
Misc:SL 150		Y		
Misc:SL 200		Y		
Misc:SL 250			Y	
Misc:NA 150		Y		
Misc:NA 200		Y		
Misc:NA 250			Y	
Misc:Man 150		Y		
Misc:Man 200		Y		
Misc:Man 250			Y	

Table A.2 The trace metal content in the hydrochars in terms of % mass. Note that any trace metals detected in only one or two samples were omitted in this table. ACL = Sodium Alginate, Cellulose and Lignin blend, Misc = *Miscanthus*, Man = Mannitol.

Sample Name, T(°C)	Metals																
	Al	As	Br	Ca	Cl	Cu	Fe	K	Mg	Mn	Na	Ni	P	S	Si	Sr	Zn
Cellulose 150	0.0034			0.0050		0.0026	0.0021	0.0117	0.0019				0.0011	0.0041	0.0125		
Cellulose 200	0.0269			0.0170		0.0031	0.0056	0.0145	0.0145			0.0009	0.0263	0.0050	0.0215		0.0011
Cellulose 250	0.0053			0.0271	0.0107	0.0012	0.0058	0.0038	0.0032	0.0014	0.0103		0.0023	0.0234	0.0207		
Protein 150	0.0074	0.0009		0.7278	0.0041	0.0012	0.0064	0.2452	0.0752		0.0639		0.2981	1.6358	0.0148	0.0013	
Protein 200	0.0125			2.1162	0.0053	0.0029	0.0110	0.1135	0.1859		0.0389		1.058	1.4489	0.0208	0.0025	0.0023
Protein 250	0.1342			63.4627		0.0042	0.8309	0.4516	1.7635	0.0064	0.1750		13.2873	19.5939	0.3507	0.1252	
Lignin 150	0.0464			0.0740	0.0089	0.0036	0.0165	0.0275	0.0174				0.0040	1.4656	0.0339	0.0009	0.0037
Lignin 200	0.0458	0.0009		0.0405	0.0043	0.0036	0.0278	0.0158	0.0176	0.0052	0.1379		0.0011	1.4350	0.0353		0.0032
Lignin 250	0.0477			0.0359		0.0048	0.0122	0.0118	0.0134	0.0045	0.0965	0.0013	0.0010	1.4405	0.0318		0.0049
ACL 150	0.0169		0.003	0.0466	0.0143		0.0100	0.0090	0.0074		0.2848		0.0027	0.6008	0.0283	0.0006	0.0008
ACL 200	0.0220		0.0025	0.0302	0.0094		0.0090	0.0084			0.2625		0.0029	0.6547	0.0264		0.0013
ACL 250	0.0288		0.0030	0.0239	0.0097	0.0017	0.0147	0.0088	0.0070		0.3390	0.0009	0.0033	0.8574	0.0294		0.0013
Sac Lat 150	0.0537	0.006		1.4902	5.7725		0.0491	4.1282	0.4195		2.2076		0.2490	0.7442	0.1027	0.1917	0.0082
Sac Lat 200	0.3183	0.0766		25.6194	26.848		1.0405	27.0191	2.1595		4.4533		4.2259	3.7143	0.5257	2.9869	0.1746
Sac Lat 250	0.3504			35.2416	19.8182		1.8431	18.1111	4.3468		3.1938		7.1761	4.3207	0.7212	4.2938	0.2655
Fuc Ser 150	0.0680		0.0148	0.8956	1.1060	0.0011	0.0358	1.1172	0.2567	0.015	0.8482		0.0535	0.5817	0.1364	0.0840	0.0349
Fuc Ser 250	0.1154	0.0035	0.0106	3.6608	1.3422	0.0070	0.1111	1.1264	1.2198	0.1108	1	0.0028	0.5690	1.6044	0.1694	0.1670	0.1183
Misc 150	0.0189		0.0008	0.1986	0.1316	0.0014	0.0295	0.1863	0.0689	0.0077	0.0298	0.0014	0.0296	0.0694	0.5724		0.0030
Misc 200	0.0155			0.1770	0.1130	0.0014	0.0156	0.1380	0.0434	0.0055	0.0139	0.0012	0.0313	0.0753	0.5082		0.0022
Misc 250	0.0296			0.1338	0.0838	0.0102	0.0579	0.0985	0.0374	0.0048	0.0312		0.0435	0.0703	0.3114	0.0014	0.0053
Misc Sac Lat 150	0.0108		0.0045	0.3254	0.9829		0.0193	0.7395	0.1324	0.0055	0.4480		0.0563	0.1355	0.3701	0.0234	0.0044
Misc Sac Lat 200	0.0114		0.0038	0.3511	0.9691	0.0021	0.0198	0.6909	0.1179	0.0060	0.3846		0.1018	0.1491	0.3278	0.01300	0.0043
Misc Sac Lat 250	0.0160	0.0022	0.0041	0.5301	1.0398	0.0025	0.0221	0.7439	0.1342	0.0099	0.4148		0.2237	0.1926	0.3200	0.0201	0.0058
Misc Man 150	0.0093			0.1421	0.0720	0.0024	0.0263	0.1080	0.0450	0.0052	0.0144		0.0195	0.0480	0.3895	0.0010	0.0025
Misc Man 200	0.0089			0.1127	0.0661	0.0058	0.0492	0.0825	0.0266	0.0034	0.0097		0.0183	0.0532	0.3573		0.0033
Misc Man 250	0.0461		0.0010	0.2265	0.0933	0.0038	0.0336	0.1292	0.0440	0.0085			0.0515	0.0930	0.4082		0.0042
Misc NA 150	0.0469		0.0359	0.7534	0.4381	0.0047	0.1591	0.4588	0.0702	0.0249	1.0609		0.0733	0.2953	1.6555	0.0038	0.0087
Misc NA 200	0.0169		0.0084	0.1385	0.1079	0.0018	0.0238	0.0901	0.0344	0.0039	0.8416		0.0175	0.0725	0.3017		0.0016
Misc NA 250	0.0233		0.0064	0.2016	0.0914	0.0013	0.0193	0.0825	0.0392	0.0057	0.6898		0.0742	0.0984	0.2932		0.0021

Table A.3 Metal Oxide Values and Slagging and Fouling Indices Values for all the different feedstock hydrochars after HTC processing. C = Cellulose, P = Protein, L = Lignin, ACL = Sodium Alginate, Cellulose and Lignin blend, AA = Alginic Acid, NA = Sodium Alginate, CA = Calcium Alginate, SL = *Saccharina latissima*, FS = *Fucus serratus*, Misc = *Miscanthus*, Man = Mannitol.

Sample Name, T(°C)	K ₂ O	Na ₂ O	Fe ₂ O ₃	CaO	MgO	SiO ₂	TiO ₂	Al ₂ O ₃	%S	AI	BAI	ABR	SI	FI	SVI
C 150	0.0000	0.0000	0.0030	0.0069	0.0031	0.0268	0.0000	0.0064	0.0000			0.3916	0.0000	0.0000	67.3367
C 200	0.0142	0.0000	0.0080	0.0238	0.0240	0.0461	0.0000	0.0508	0.0000		0.5634	0.7224	0.0000	0.0103	45.2404
C 250	0.0047	0.0142	0.0086	0.0390	0.0055	0.0455	0.0000	0.0103	0.0000		0.4550	1.2903	0.0000	0.0244	46.1460
P 150	0.2932	0.0856	0.0091	1.0108	0.1239	0.0315	0.0000	0.0138	0.0000		0.0240	33.6115	0.0000	12.7320	2.6802
P 200	0.1355	0.0518	0.0155	2.9335	0.3049	0.0440	0.0000	0.0233	0.0000		0.0828	51.1322	0.0000	9.5771	1.3342
P 250	0.0000	0.0000	0.0000	0.0000	0.0000	0.0000	0.0000	0.0000	0.7200						
L 150	0.0329	0.2346	0.0234	0.1029	0.0286	0.0722	0.0000	0.0871	0.5300		0.0875	2.6516	1.4053	0.7093	31.7922
L 200	0.0189	0.1849	0.0394	0.0564	0.0291	0.0751	0.0000	0.0861	0.4500		0.1933	2.0391	0.9176	0.4156	37.5500
L 250	0.0142	0.1298	0.0174	0.0501	0.0221	0.0679	0.0000	0.0899	0.4100		0.1208	1.4804	0.6069	0.2132	43.1111
ACL 150	0.0105	0.3974	0.0156	0.0663	0.0166	0.0606	0.0000	0.0353	0.0000		0.0382	5.2805	0.0000	2.1539	38.0893
ACL 200	0.0101	0.3530	0.0128	0.0421	0.0000	0.0564	0.0000	0.0415	0.0000		0.0353	4.2697	0.0000	1.5503	50.6739
ACL 250	0.0106	0.4557	0.0209	0.0333	0.0116	0.0627	0.0000	0.0542	0.0000		0.0448	4.5518	0.0000	2.1225	48.7938
AA200	0.0331	0.0616	0.1509	0.2057	0.0317	0.3224	0.0140	0.161	0.0000		1.5935	0.9710	0.0000	0.0920	45.3637
AA250	0.0235	0.0385	0.0927	0.1904	0.0292	0.2001	0.1300	0.0000	0.0000		1.4952	1.1339	0.0000	0.0703	39.0515
NA250	0.0254	0.6556	67.167	0.7292	0.1771	1.2435	0.0308	0.2329	0.0000		98.6300	45.6172	0.0000	31.0653	1.7939
CA 150	0.0086	0.0596	0.0382	6.0522	0.0383	0.4197	0.1614	0.0000	0.0000		0.5601	10.6641	0.0000	0.7273	6.4092
CA 1200	0.0233	0.0969	0.3127	8.5586	0.1659	3.1657	0.0492	1.4531	0.0000		2.6015	1.9617	0.0000	0.2358	25.9422
CA 250	0.0549	0.1198	0.293	14.9702	0.4425	2.2827	0.0351	1.0152	0.0000		1.6772	4.7646	0.0000	0.8324	12.6898
SL 150	4.9262	2.9526	0.0695	2.0654	0.6899	0.2178	0.0000	0.1005	0.0500		0.0088	33.6274	1.6814	264.9435	7.1584
SL 200	24.0116	5.4804	1.0051	25.1750	3.1984	0.9697	0.0000	0.5348	0.0000		0.0341	39.1296	0.0000	1154.0105	3.1952
SL 250	15.1169	3.8230	1.6283	32.4109	6.2385	1.2740	0.0000	0.5660	0.0000		0.0860	32.1835	0.0000	609.5519	3.0661
FS 150	1.2150	1.0389	0.0465	1.1313	0.3860	0.2640	0.0000	0.1163	0.1500		0.0206	10.0387	1.5058	22.6261	14.4436
FS 250	1.3374	1.3318	0.1566	5.0484	1.9971	0.3575	0.0000	0.2151	0.0600		0.0587	17.2394	1.0344	46.0155	4.7291
Misc 150	0.2239	0.0401	0.0421	0.2773	0.1141	1.2220	0.0000	0.0356	0.0000		0.1595	0.5546	0.0000	0.1464	73.8146
Misc 200	0.1657	0.0187	0.0223	0.2469	0.0717	1.0839	0.0000	0.0292	0.0000		0.1209	0.4719	0.0000	0.0870	76.0738
Misc 250	0.1336	0.0466	0.0931	0.2109	0.0690	0.7445	0.0000	0.0624	0.0000		0.5166	0.6856	0.0000	0.1235	66.6219
Misc SL 150	0.8893	0.6031	0.0275	0.4545	0.2192	0.7906	0.0000	0.0205	0.0000		0.0184	2.7045	0.0000	4.0362	52.9964
Misc SL 200	0.8300	0.5173	0.0282	0.4899	0.1951	0.6996	0.0000	0.0215	0.0000		0.0209	2.8574	0.0000	3.8498	49.5187
Misc SL 250	0.8932	0.5577	0.0315	0.7394	0.2219	0.6826	0.0000	0.0302	0.0000		0.0217	3.4283	0.0000	4.9741	40.7425
Misc Man 150	0.1295	0.0194	0.0374	0.1980	0.0743	0.8303	0.0000	0.0175	0.0000		0.2512	0.5409	0.0000	0.0805	72.8333
Misc Man 200	0.0993	0.0131	0.0702	0.1574	0.0441	0.7634	0.0000	0.0167	0.0000		0.6246	0.4924	0.0000	0.0553	73.7513
Misc Man 250	0.1555	0.0000	0.0480	0.3165	0.0729	0.8720	0.0000	0.0869	0.0000		0.3087	0.6183	0.0000	0.0961	66.5954
Misc NA 150	0.5515	1.4783	0.2266	1.0518	0.1109	3.5317	0.0000	0.0884	0.0000		0.1116	0.9445	0.0000	1.9171	71.7679
Misc NA 200	0.1084	1.1335	0.0340	0.1937	0.0570	0.6448	0.0000	0.0319	0.0000		0.0274	2.2559	0.0000	2.8017	69.3706
Misc NA 250	0.0991	0.9279	0.0275	0.2813	0.0649	0.6259	0.0000	0.0440	0.0000		0.0268	2.0909	0.0000	2.1474	62.6150

Table A.4 The results from the Liquid XRF analysis of the HTP aqueous phase. ACL = Sodium Alginate, Cellulose and Lignin blend, NA = Sodium Alginate, Misc = *Miscanthus*, Man = Mannitol.

Sample Name, T(°C)	Column Labels												
	Al	As	Br	Ca	Cl	Fe	K	Mg	Na	P	S	Si	Sr
Cellulose 150	0.0060			0.0329	0.0071			0.0387		0.1386	0.0015	0.0123	
Cellulose 200	0.0088			0.0326		0.0017		0.0460		0.1423		0.0127	
Cellulose 250	0.0078			0.0368		0.0013		0.033		0.1357	0.0061	0.0122	
Protein 150				0.0503			0.0586	0.0240		0.1522	0.0460	0.0155	
Protein 200				0.0336			0.0515	0.0352		0.1365	0.0778	0.0087	
Protein 250				0.0367			0.0416			0.1375	0.0484	0.0109	
Lignin 150	0.0111			0.0350			0.0119			0.1459	0.1139	0.0141	
Lignin 200				0.0357		0.0013	0.0077	0.0479		0.1445	0.0853	0.0145	
Lignin 250				0.0305			0.0030	0.0424		0.1485	0.0473	0.0168	
ACL 150				0.0015	0.0320		0.0025	0.0417		0.1454	0.0322	0.0103	
ACL 200	0.0079			0.0013	0.0315	0.0021				0.1407	0.0400	0.0133	
ACL 250				0.0023	0.0376	0.0016	0.0035	0.0284		0.1417	0.0446	0.0112	
Sac Lat 150		0.0011		0.1066	0.9666		0.6225	0.1836	1.9224	0.1846	0.0744	0.0220	0.0017
Sac Lat 200	0.0083			0.0739	0.7409		0.5183	0.0758		0.1445	0.0543	0.0159	0.0055
Sac Lat 250		0.0008		0.0805	0.8292		0.5848	0.1083	0.4628	0.1415	0.0444	0.0116	0.0062
Fuc Ser 150	0.0127			0.1098	0.3680	0.0020	0.3156	0.0878		0.1598	0.1461	0.0129	0.0028
Fuc Ser 200				0.0028	0.3476		0.3095	0.0901	0.8004	0.1517	0.0928	0.0143	0.0039
Fuc Ser 250		0.0009		0.0767	0.3006		0.2795			0.1429	0.0816	0.0138	0.0035
Misc 150				0.0430	0.0181		0.0250			0.1503	0.0070	0.0124	
Misc 200	0.0074			0.0521	0.0179		0.0285	0.0339		0.1414	0.0059	0.0431	
Misc 250				0.0452			0.0248			0.1516	0.0071	0.0482	
Misc Sac Lat 150	0.0066			0.0575	0.1996	0.0016	0.1377	0.0591		0.1558	0.0212	0.0140	
Misc Sac Lat 200				0.0499	0.1205		0.0964	0.0406		0.1484	0.0189	0.0475	0.0020
Misc Sac Lat 250	0.0111			0.0486	0.1070		0.0713	0.0891	1.2777	0.1481	0.0111	0.0438	0.0009
Misc Man 150	0.0102			0.0444	0.0276	0.0016	0.0269	0.0657	2.3534	0.1547	0.0106	0.0331	
Misc Man 200	0.0121			0.0508	0.0333	0.0014	0.0285	0.1240	3.7077	0.1536	0.0119	0.0643	
Misc Man 250	0.0071			0.0423			0.0150	0.0301		0.1442	0.0054	0.0364	
Misc NA 150				0.0015	0.0372	0.0018	0.0176			0.1441	0.0115	0.0200	
Misc NA 200				0.0025	0.046	0.0018	0.0230	0.0473	0.8250	0.1457	0.0141	0.0557	
Misc NA 250	0.0103			0.0014	0.0416	0.0013	0.0148	0.0997	2.1383	0.1504	0.0111	0.0401	

A.3 NMR Spectra

The NMR spectra from the aqueous phase of the four respective subgroups of samples are shown in the four respective figures; [A.1](#), [A.2](#), [A.3](#) and [A.4](#). Each figure contains four sub-figures, of which the NMR spectra is stacked by increasing HTC temperature for each sample. However, as the 100% SL, 100% Misc and the MSL co-processed aqueous phase samples were included in chapter 6, these are omitted in this Appendix. Note that all the NMR spectra shown here were zoomed to equal magnification levels so they are all comparable, unless stated otherwise.

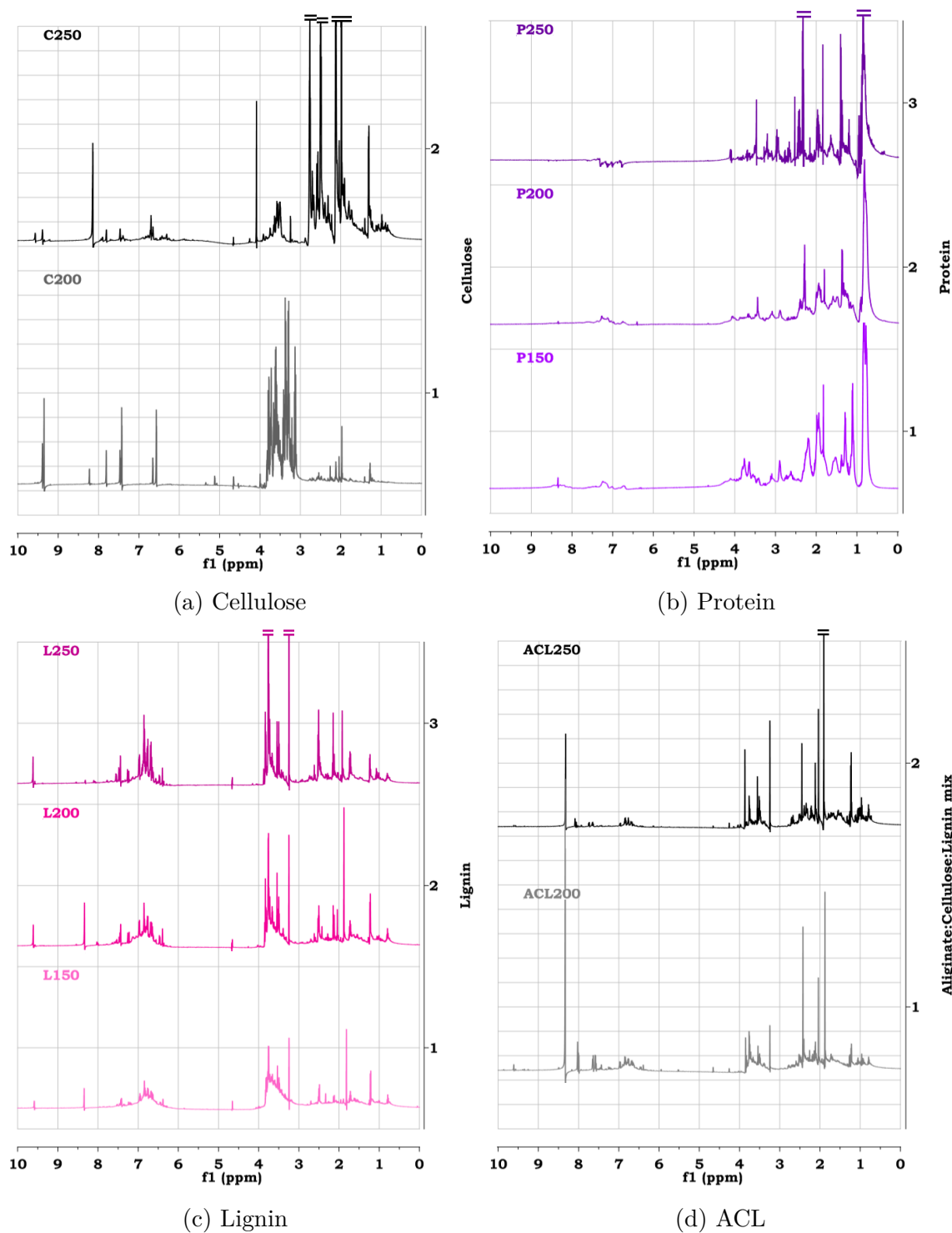


Fig. A.1 Stacked NMR (^1H 600 MHz in D_2O) Spectra from the Lignocellulosic Model Compounds aqueous phase after HTC. ACL = Sodium Alginate, Cellulose and Lignin blend.

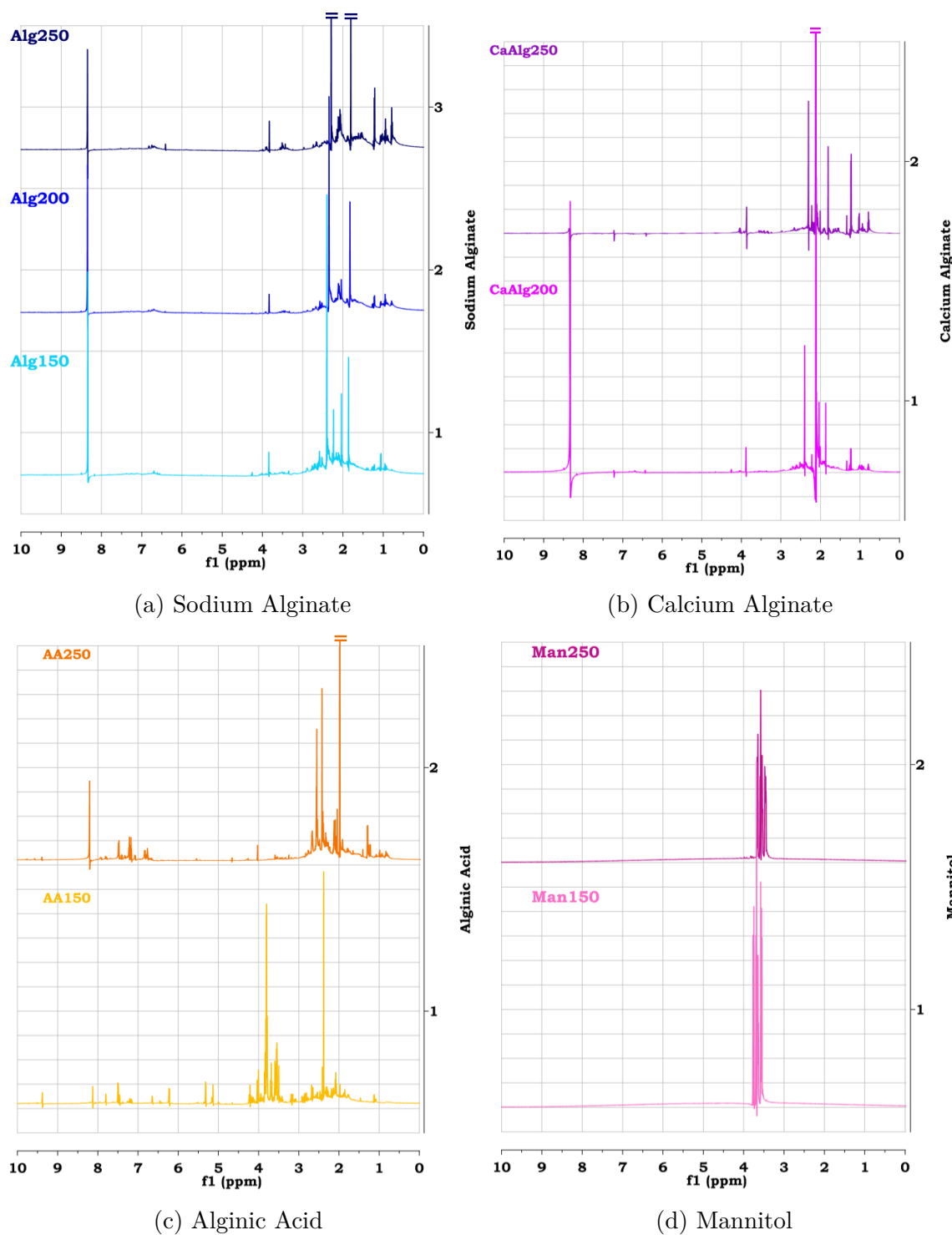


Fig. A.2 Stacked NMR (^1H 600 MHz in D_2O) Spectra from the Seaweed Model Compounds aqueous phase after HTC.

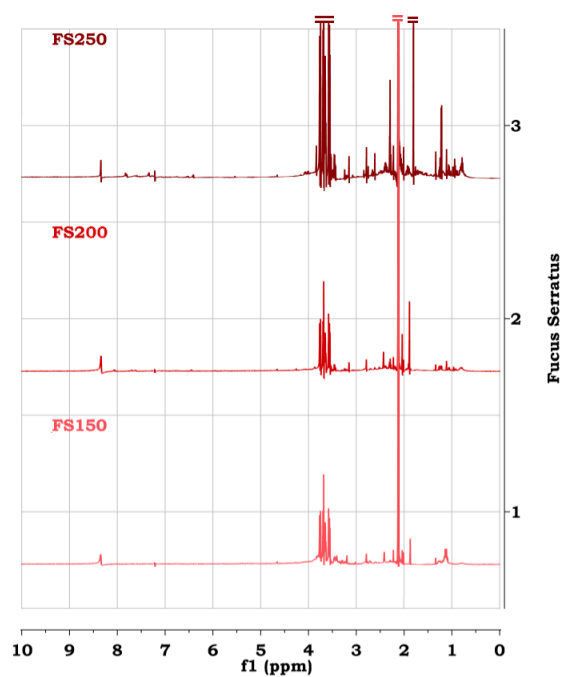


Fig. A.3 Stacked NMR (^1H 600 MHz in D_2O) Spectra from the 100% *Fucus serratus* Biomass Feedstock aqueous phase after HTC.

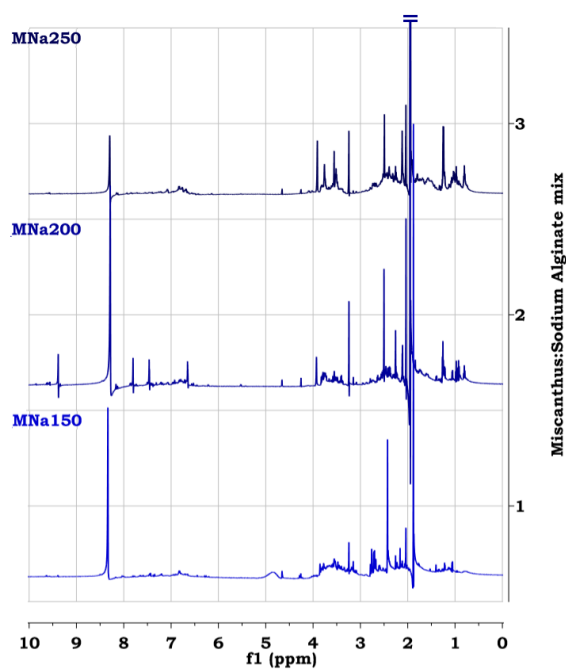
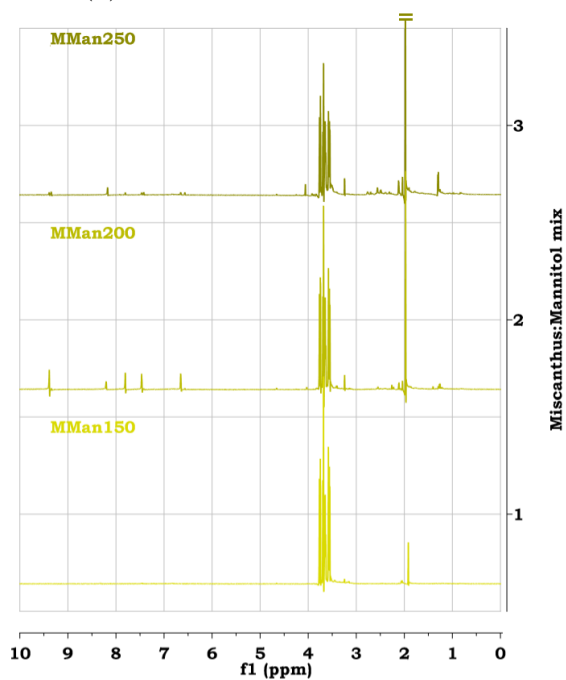
(a) *Miscanthus*:Sodium Alginate(b) *Miscanthus*:Mannitol

Fig. A.4 Stacked (^1H 600 MHz in D_2O) NMR Spectra from the Co-processed Feedstock aqueous phase after HTC.

A.4 HPLC Chromatographs

The HPLC chromatographs, using the sugar method, are shown for each sample, with the HPLC Chromatograph for the VFA method shown below. Note that some HPLC chromatographs are not included in this Appendix as they were previously shown in the results chapter for in-depth discussion.

The peaks that were identified in the chromatographs are labelled on the figures and numbered in order of retention time. For each chromatograph the numbers refer to the same molecules. For example, if there was no lactose detected in a sample, the numbering will jump from 1 to 3. These molecules are listed in the column headings for the HPLC peak identification tables and in the figure captions in §6. They are also listed below for ease of reference.

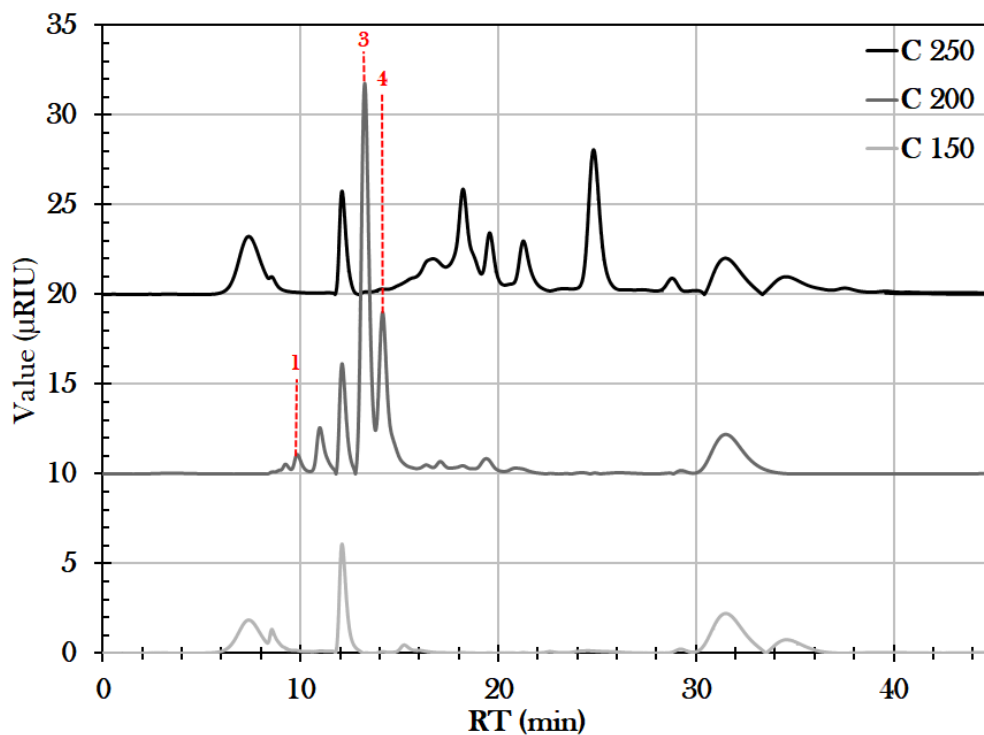
Sugars;

- (1) - Sucrose
- (2) - Lactose
- (3) - Glucose
- (4) - Galactose and Mannose
- (5) - Arabinose
- (6) - Ribose

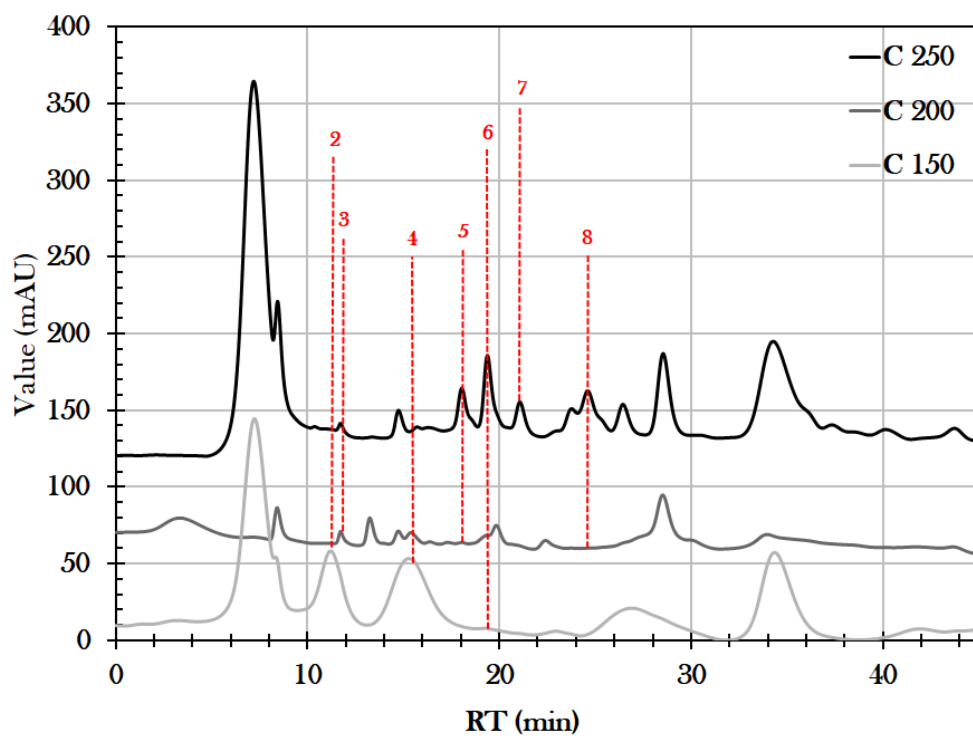
These sugars, except for the sucrose and lactose, could also be quantified. These quantities are indicated where applicable in the HPLC Sugar peak identification tables in chapter 6. The acids that were detected and identified via the HPLC analysis using the VFA method are listed below.

VFAs;

- (1) - Oxalic Acid
- (2) - Maleic Acid
- (3) - Citric Acid
- (4) - Methyl-malonic Acid
- (5) - Lactic Acid
- (6) - Formic Acid
- (7) - Acetic Acid
- (8) - Levulinic Acid

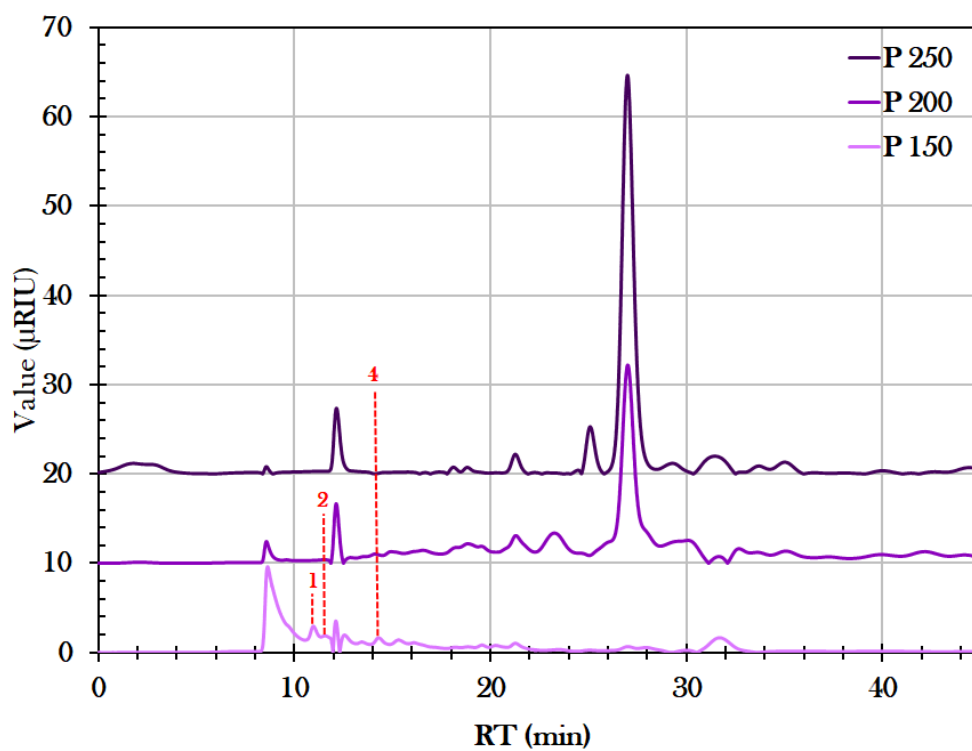


(a) Cellulose Sugars

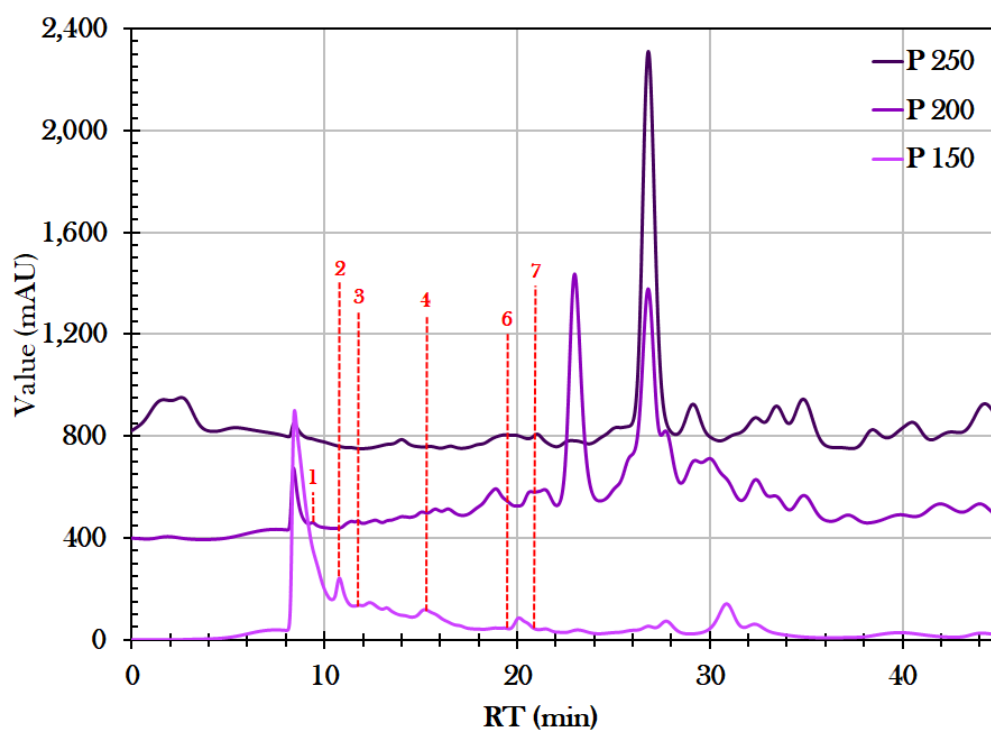


(b) Cellulose VFAs

Fig. A.5 Stacked HPLC Chromatographs of the Cellulose aqueous phase samples after HTC for Sugars (a) and VFAs (b).

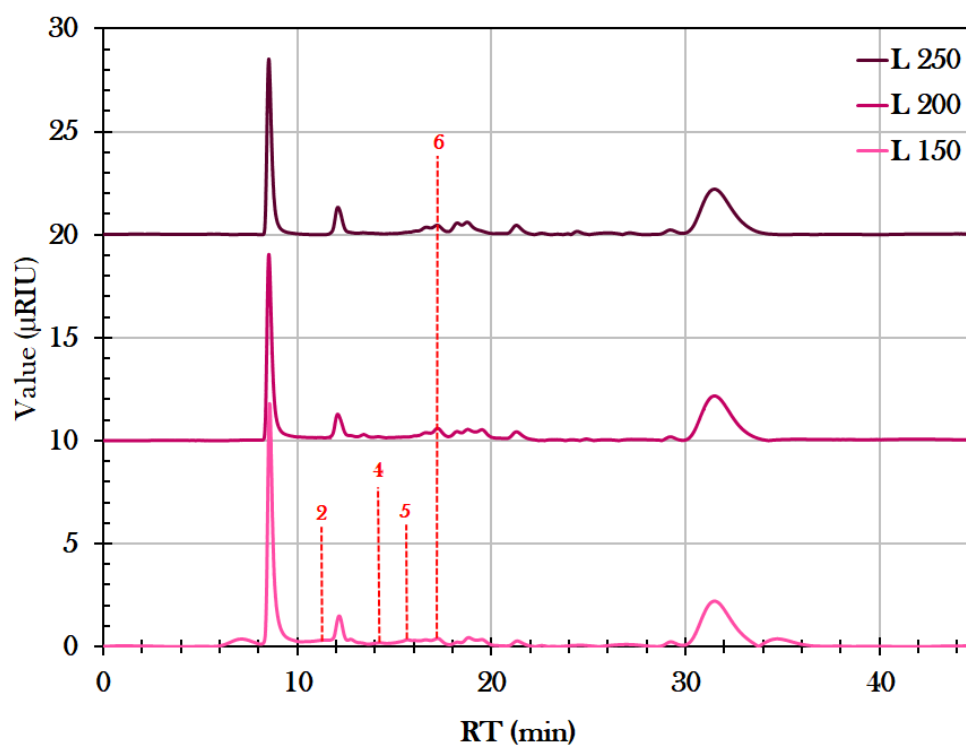


(a) Protein Sugars

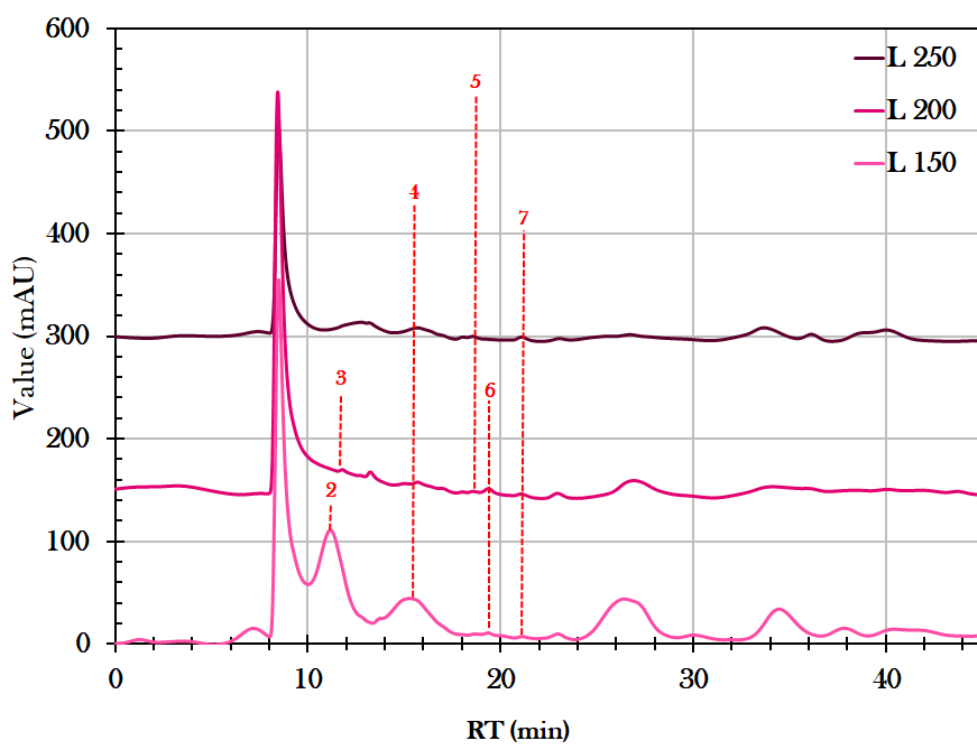


(b) Protein VFAs

Fig. A.6 Stacked HPLC Chromatographs of the Protein aqueous phase samples after HTC for Sugars (a) and VFAs (b).

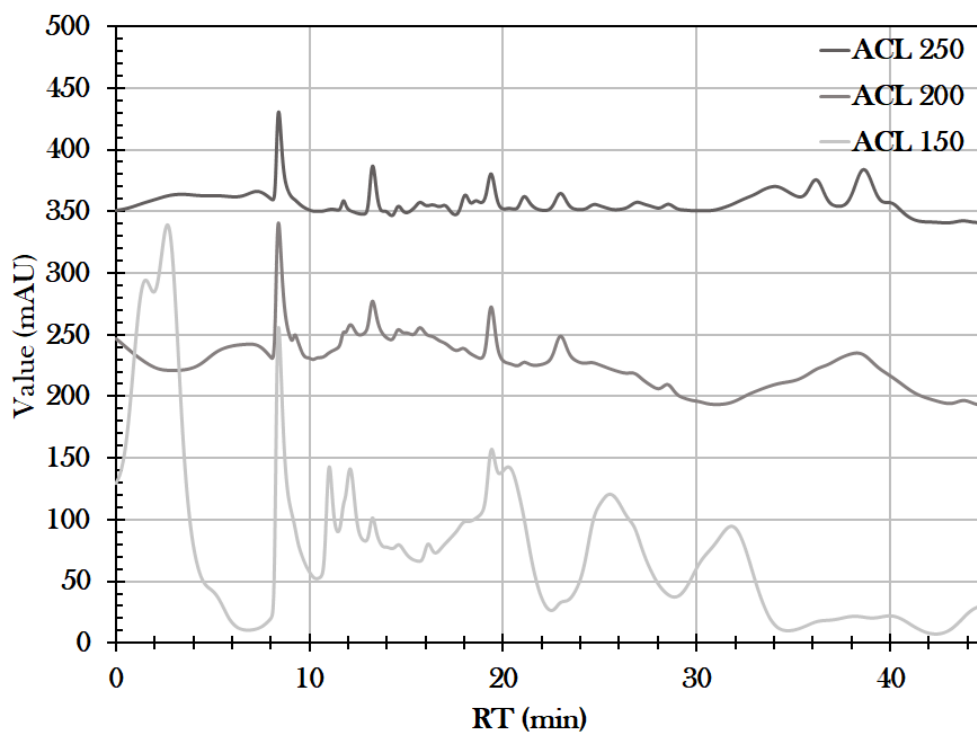


(a) Lignin Sugars

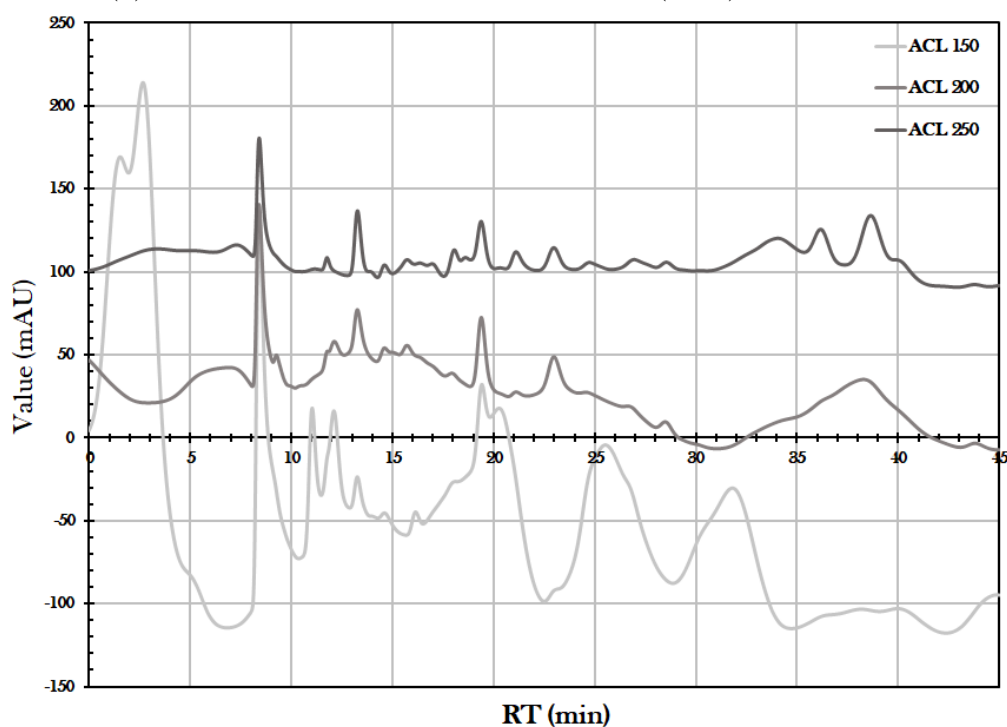


(b) Lignin VFAs

Fig. A.7 Stacked HPLC Chromatographs of the Lignin aqueous phase samples after HTC for Sugars (a) and VFAs (b).

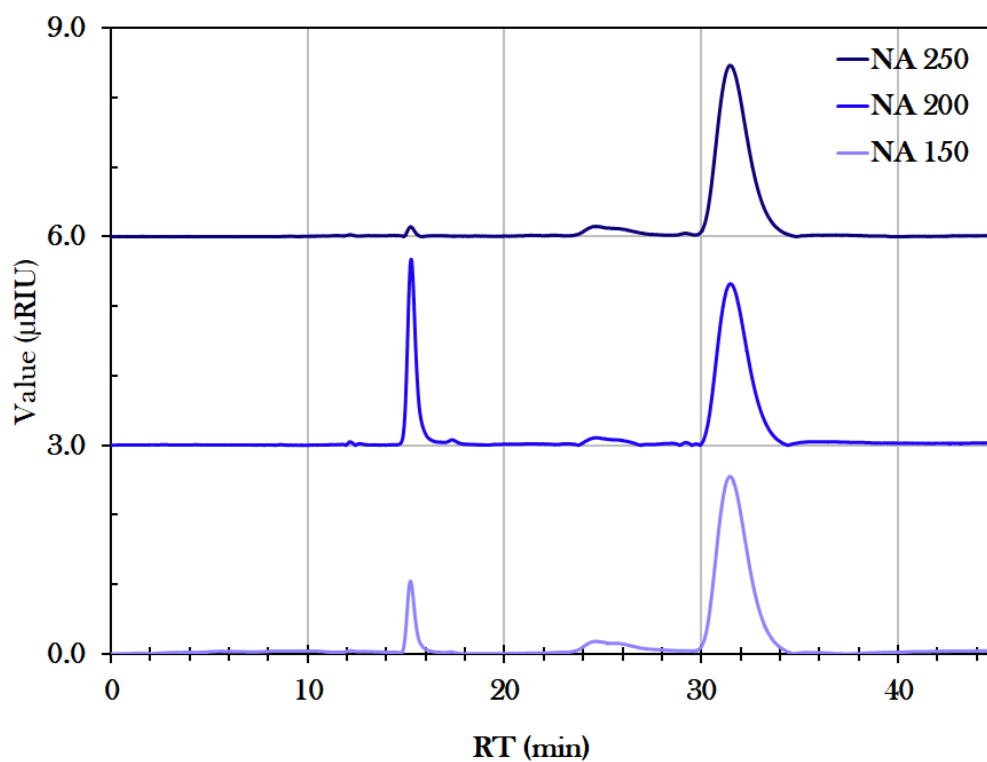


(a) Sodium Alginate, Cellulose and Lignin (ACL) blend Sugars

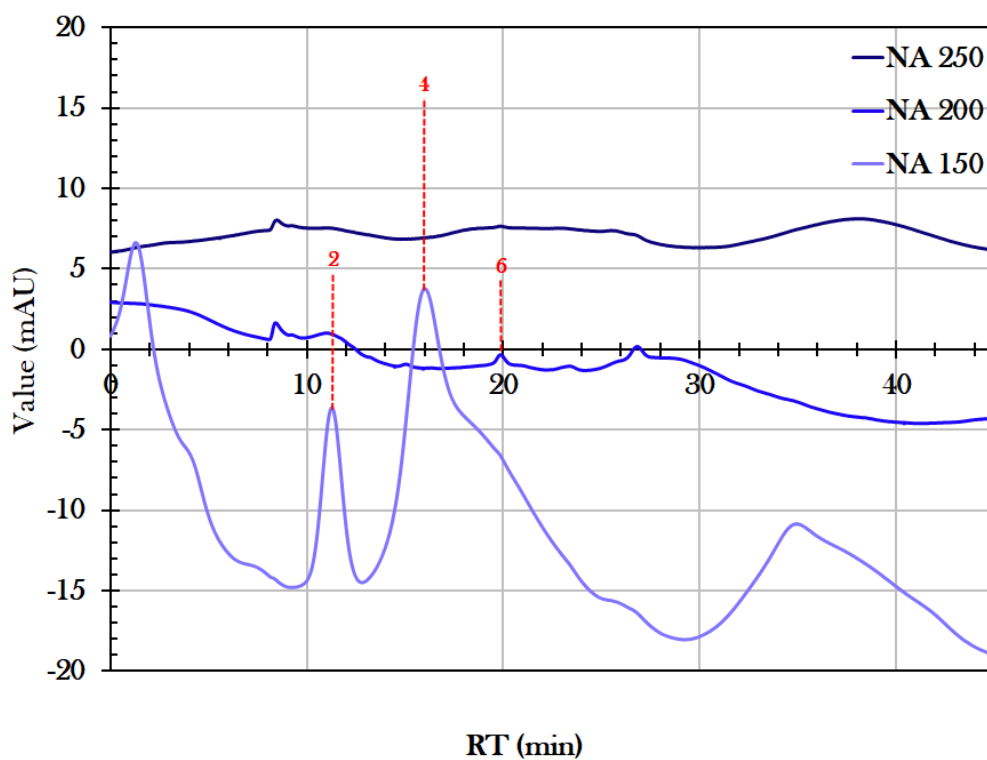


(b) Sodium Alginate, Cellulose and Lignin (ACL) blend VFAs

Fig. A.8 Stacked HPLC Chromatographs of the Sodium Alginate, Cellulose and Lignin (ACL) blend aqueous phase samples after HTC for Sugars (a) and VFAs (b).

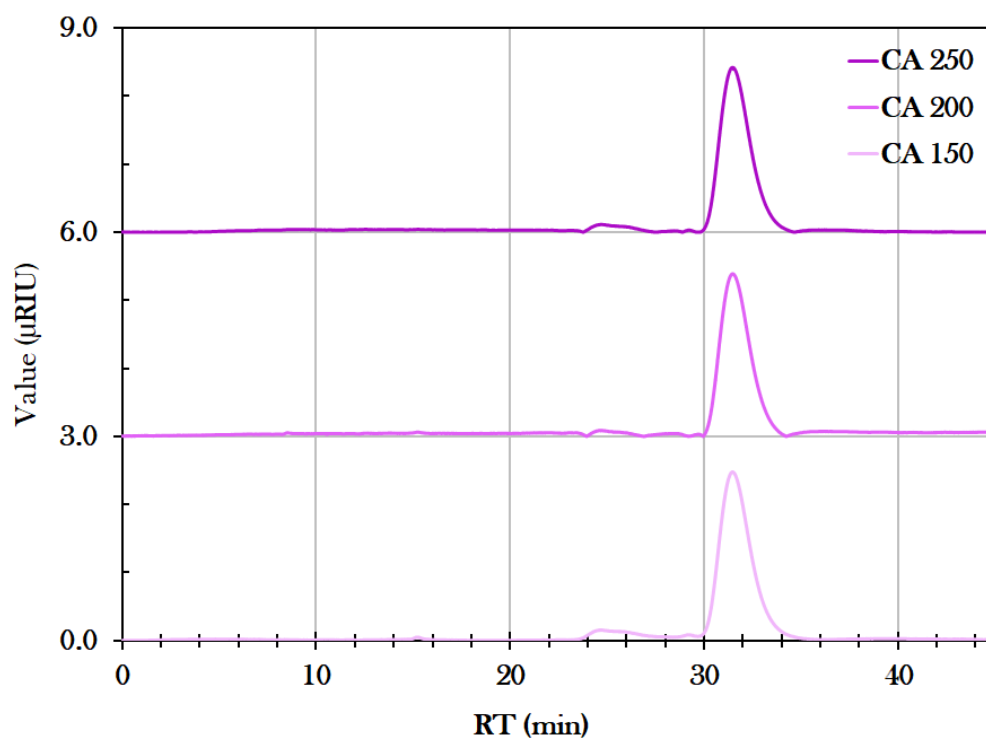


(a) Sodium Alginate Sugars

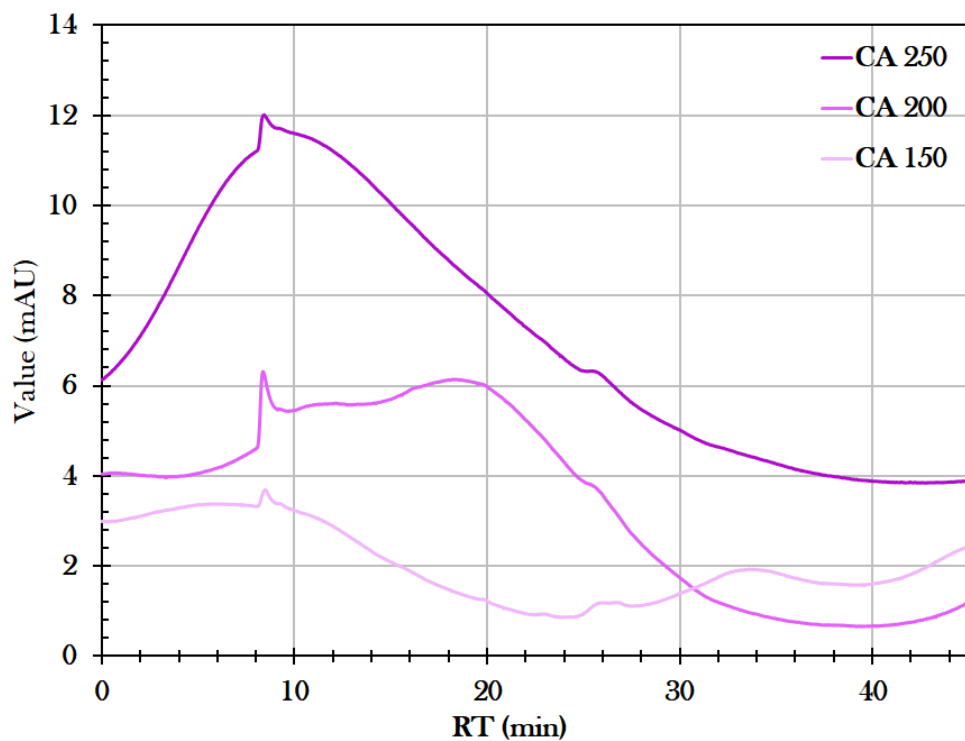


(b) Sodium Alginate VFAs

Fig. A.9 Stacked HPLC Chromatographs of the Sodium Alginate aqueous phase samples after HTC for Sugars (a) and VFAs (b).

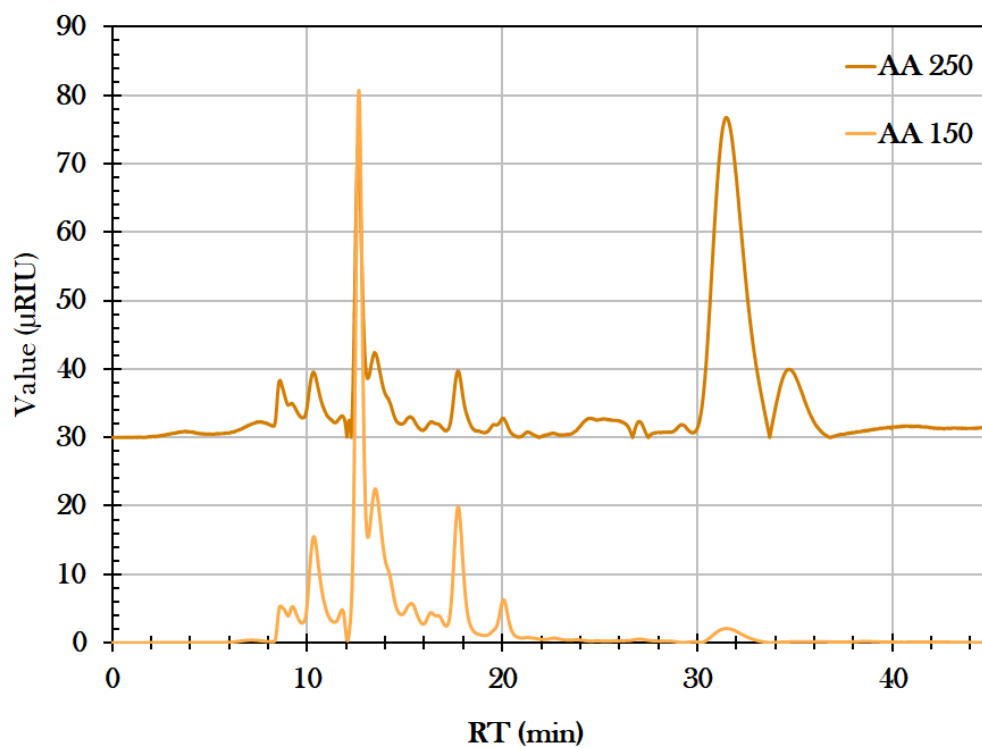


(a) Calcium Alginate Sugars

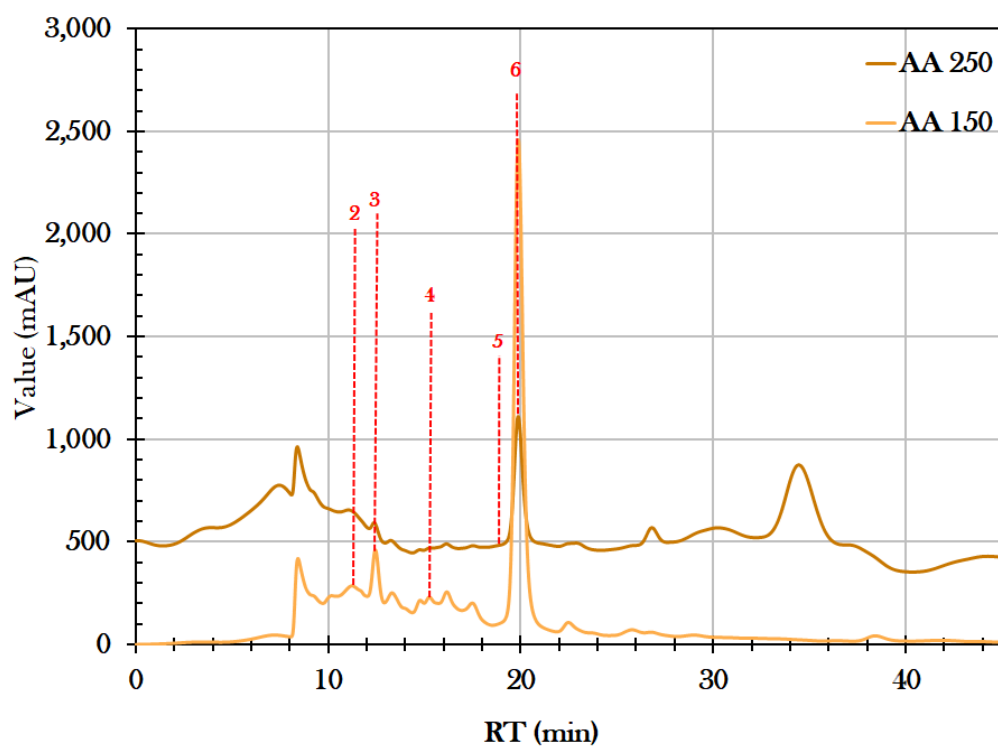


(b) Calcium Alginate VFAs

Fig. A.10 Stacked HPLC Chromatographs of the Calcium Alginate aqueous phase samples after HTC for Sugars (a) and VFAs (b).

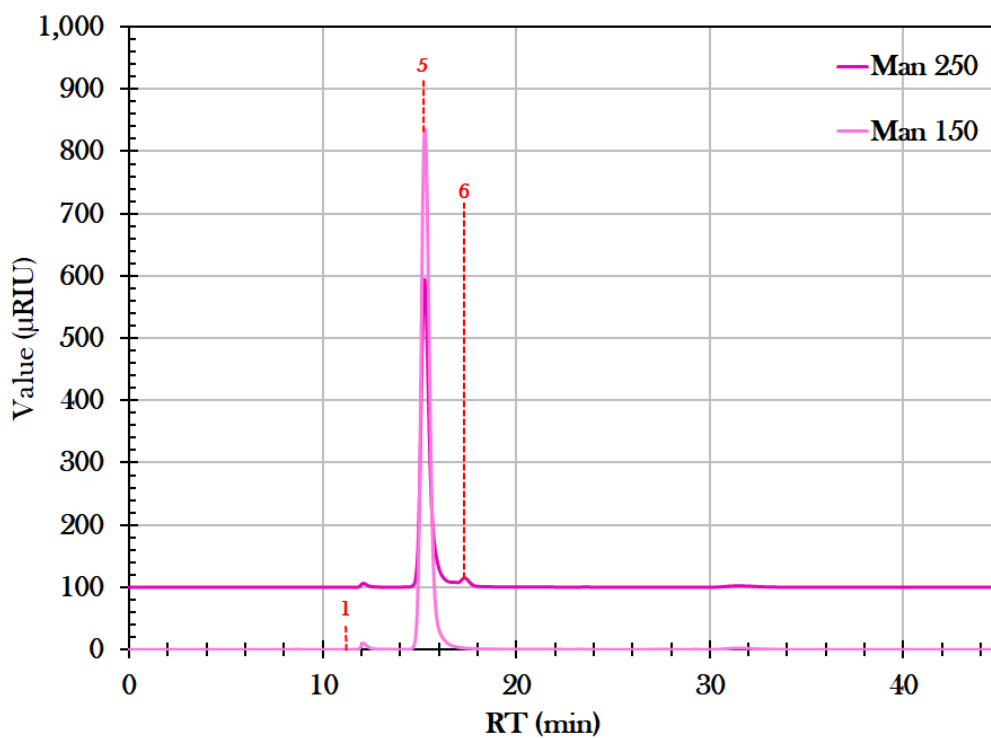


(a) Alginic Acid Sugars

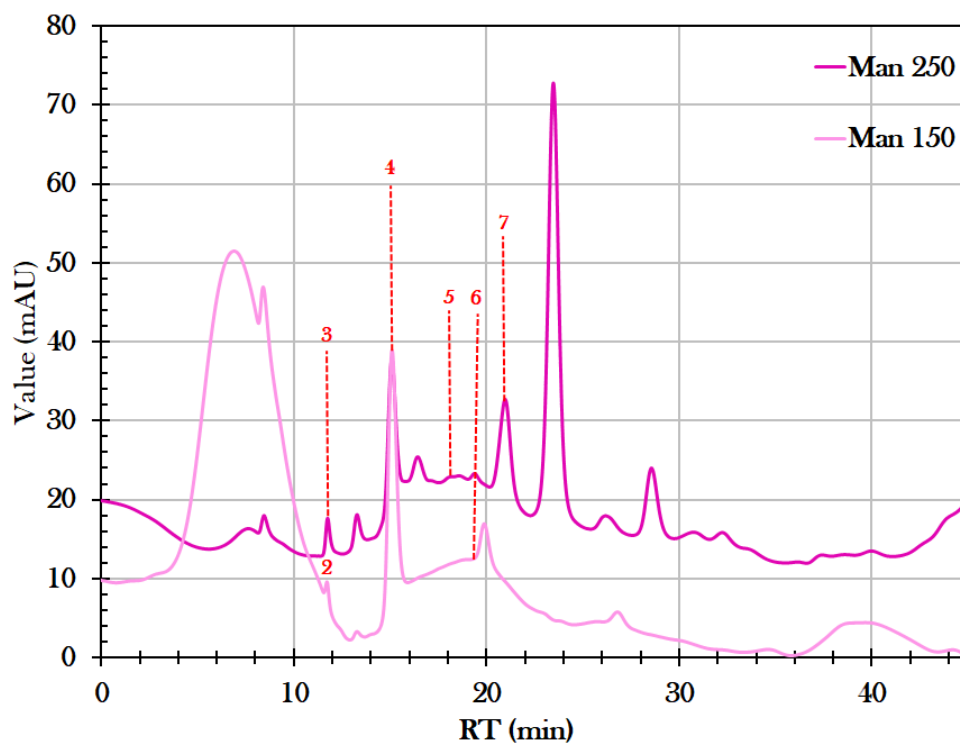


(b) Alginic Acid VFAs

Fig. A.11 Stacked HPLC Chromatographs of the Alginic Acid aqueous phase samples after HTC for Sugars (a) and VFAs (b).

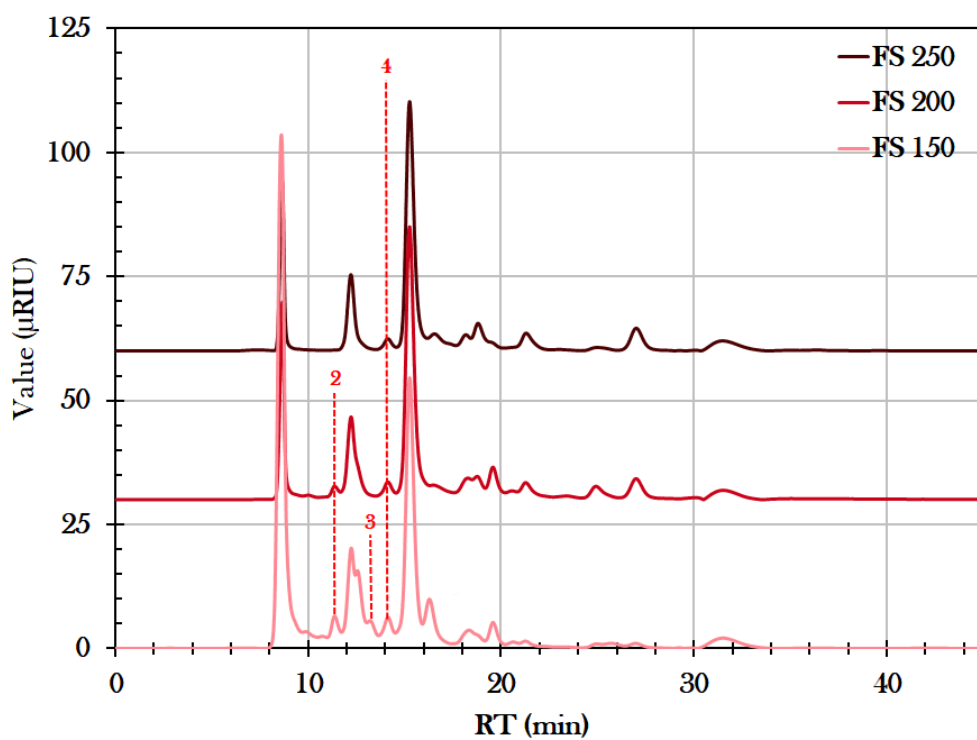


(a) Mannitol Sugars

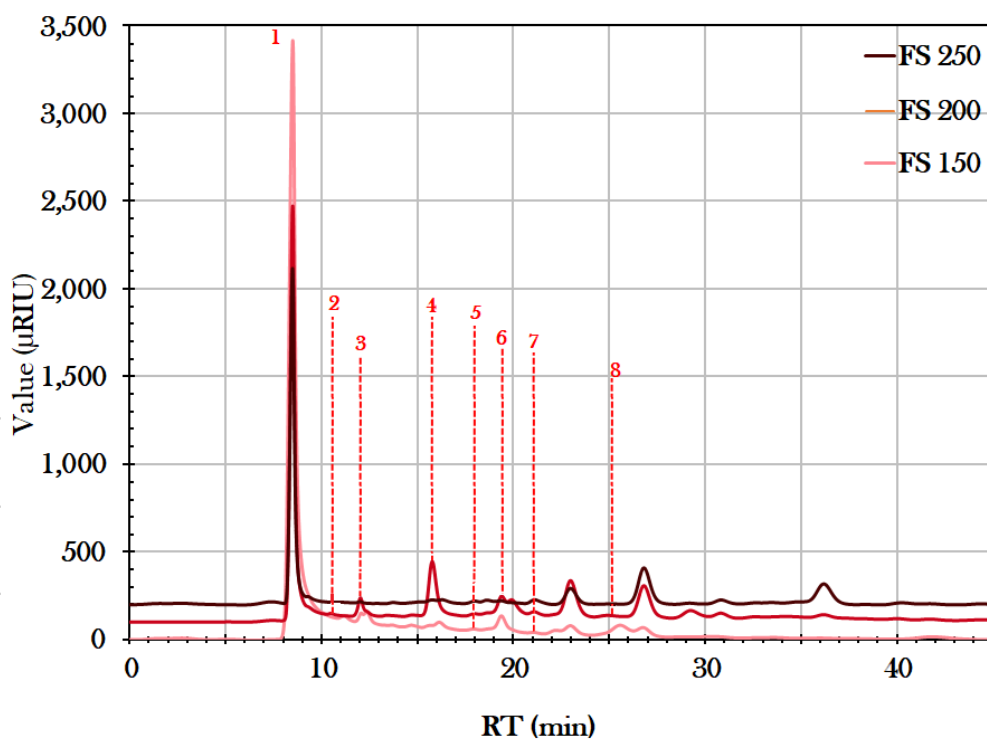


(b) Mannitol VFAs

Fig. A.12 Stacked HPLC Chromatographs of the Mannitol aqueous phase samples after HTC for Sugars (a) and VFAs (b).



(a) Fucus serratus Sugars



(b) Fucus serratus VFAs

Fig. A.13 Stacked HPLC Chromatographs of the Fucus serratus aqueous phase samples after HTC for Sugars (a) and VFAs (b).

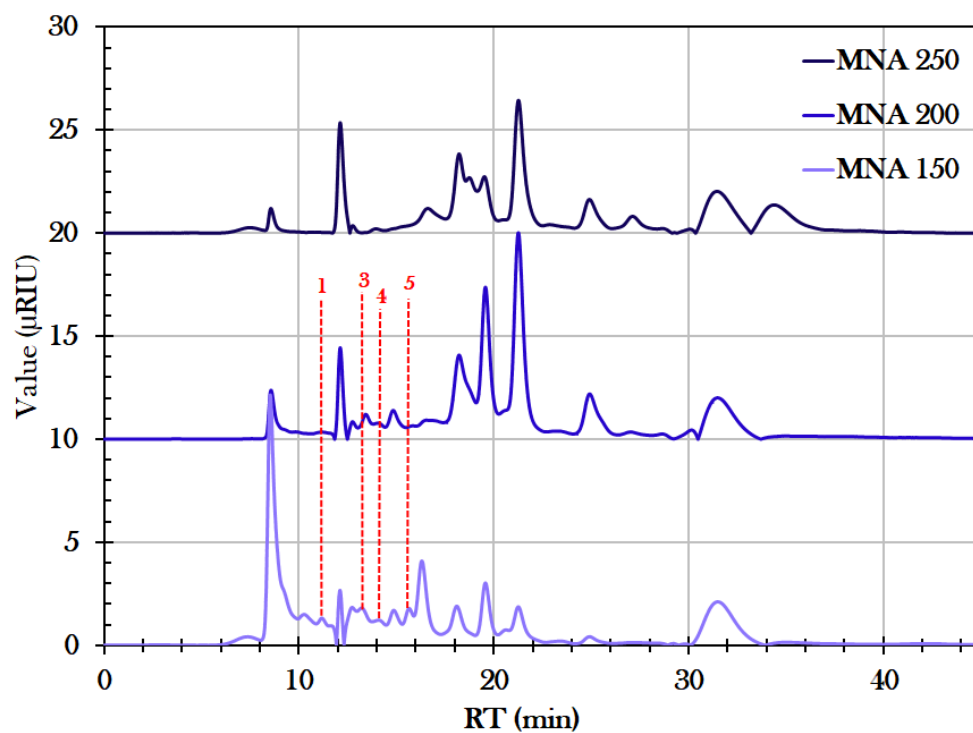
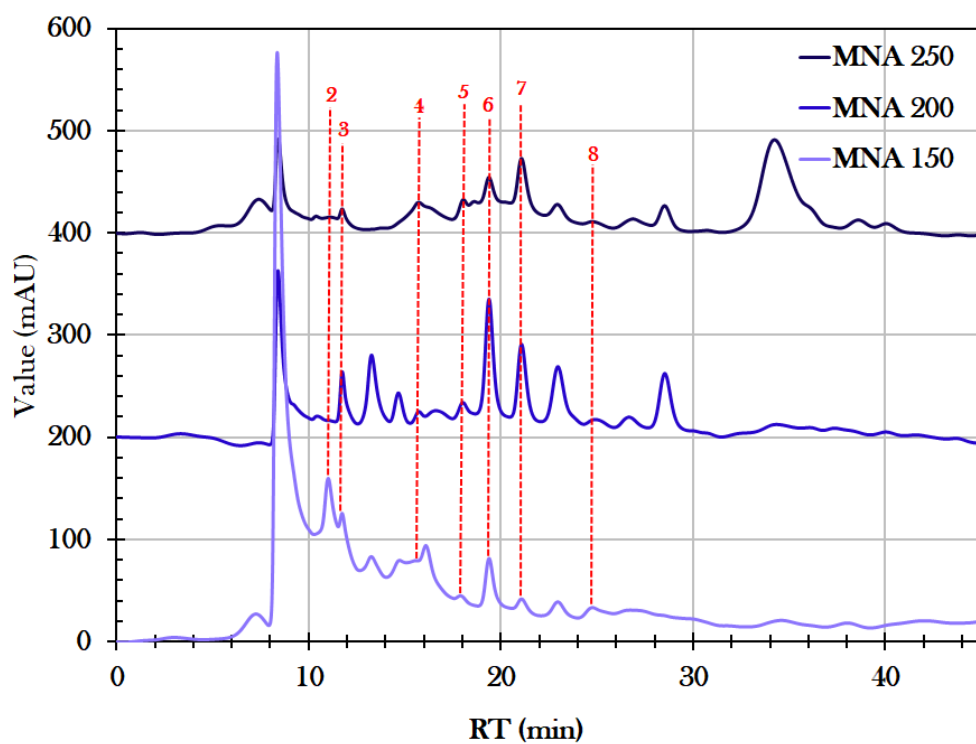
(a) *Miscanthus*:Sodium Alginate Sugars(b) *Miscanthus*:Sodium Alginate VFAs

Fig. A.14 Stacked HPLC Chromatographs of the *Miscanthus*:Sodium Alginate aqueous phase samples after HTC for Sugars (a) and VFAs (b).

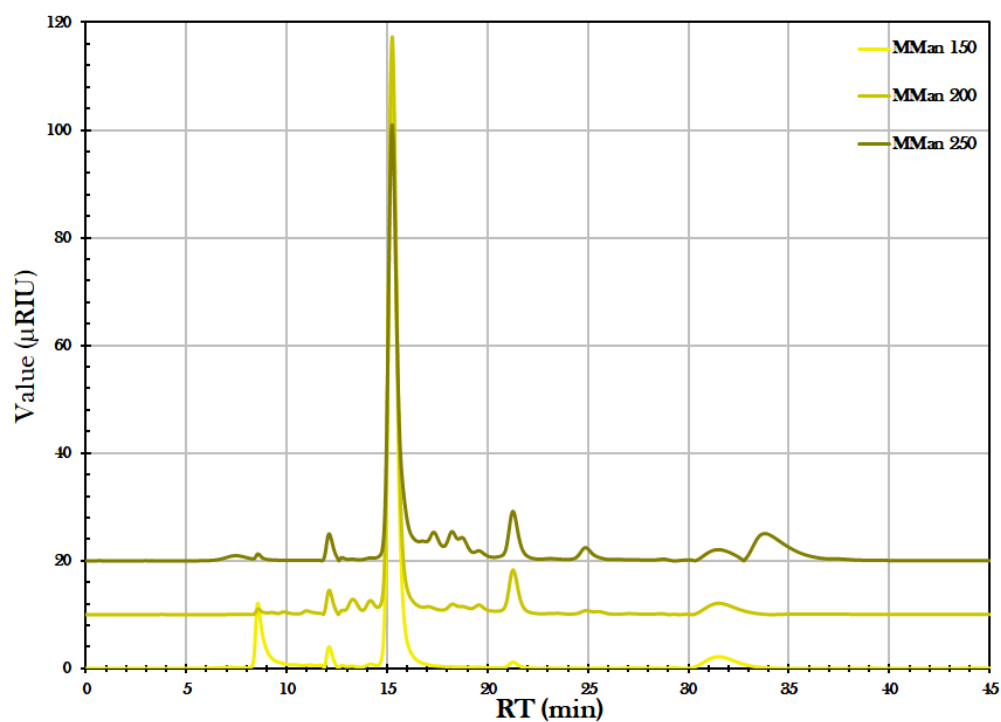
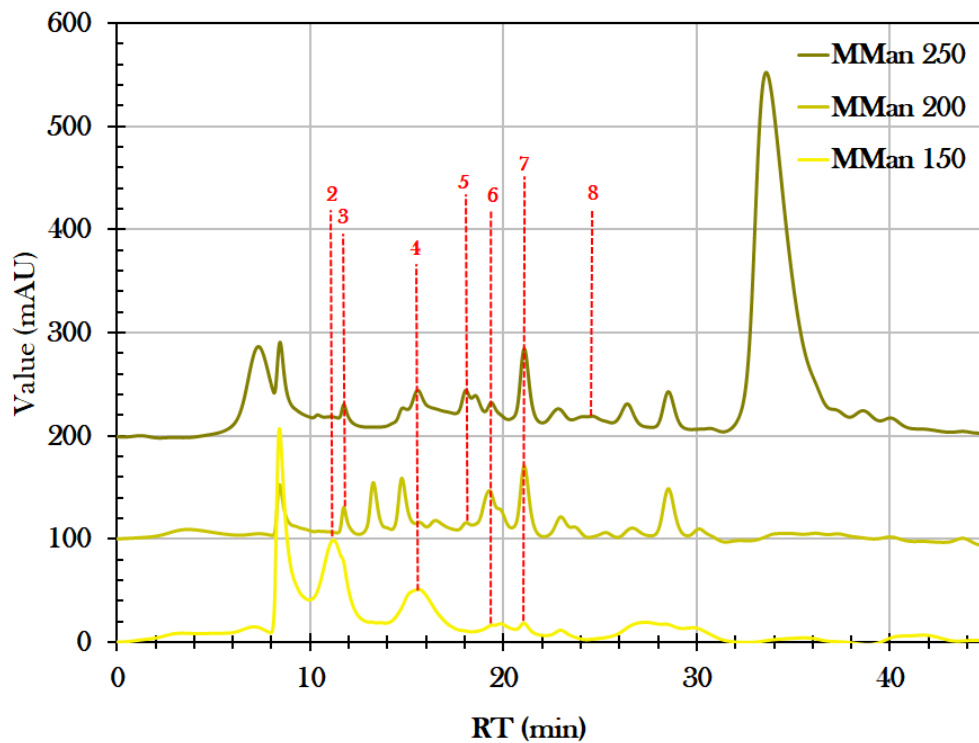
(a) *Miscanthus*:Mannitol Sugars(b) *Miscanthus*:Mannitol VFAs

Fig. A.15 Stacked HPLC Chromatographs of the *Miscanthus*:Mannitol aqueous phase samples after HTC for Sugars (a) and VFAs (b).